

8-2015

# Design of Cab Suspensions and Semi-Active Seat Damping Control Strategies for Tractor Semi-Trailers

Judhajit Roy  
*Clemson University*

Follow this and additional works at: [https://tigerprints.clemson.edu/all\\_dissertations](https://tigerprints.clemson.edu/all_dissertations)

 Part of the [Mechanical Engineering Commons](#)

---

## Recommended Citation

Roy, Judhajit, "Design of Cab Suspensions and Semi-Active Seat Damping Control Strategies for Tractor Semi-Trailers" (2015). *All Dissertations*. 2029.

[https://tigerprints.clemson.edu/all\\_dissertations/2029](https://tigerprints.clemson.edu/all_dissertations/2029)

This Dissertation is brought to you for free and open access by the Dissertations at TigerPrints. It has been accepted for inclusion in All Dissertations by an authorized administrator of TigerPrints. For more information, please contact [kokeefe@clemson.edu](mailto:kokeefe@clemson.edu).

DESIGN OF CAB SUSPENSIONS AND SEMI-ACTIVE SEAT DAMPING CONTROL  
STRATEGIES FOR TRACTOR SEMI-TRAILERS

---

A Dissertation  
Presented to  
the Graduate School of  
Clemson University

---

In Partial Fulfillment  
of the Requirements for the Degree  
Doctor of Philosophy  
Mechanical Engineering

---

by  
Judhajit Roy  
August 2015

---

Accepted by  
Dr. A. Vahidi, Committee Chair  
Dr. E. H. Law  
Dr. B. Ayalew  
Dr. J. Wagner

## ABSTRACT

This thesis uses a high fidelity vertical plane ride model of the tractor semi-trailer to study the effect of different cab design configurations and semi-active seat damper control strategies on the driver's ride comfort.

The secondary suspensions of a tractor have been an area of particular interest because of the considerable ride comfort improvements they provide. A gap exists in the current engineering domain of an easily configurable high fidelity low computational cost simulation tool to analyze the ride of a tractor semi-trailer. A 15 degree of freedom model of the tractor semi-trailer was used to develop a simulation tool in the Matlab/Simulink environment. The simulation tool developed was verified against TruckSim. The contributions of the different modes of vibration to the ride comfort were analyzed. It is shown in this work that the ride at the driver's seat can be significantly improved by relocating the cab mounts near the nodes of the 1st mode of bending of the tractor frame and by employing a full cab suspension. The developed simulation tool was used to quantify the improvements in the driver ride comfort.

To develop seat isolation systems, the truck seat was modeled as a base excited 1 d.o.f. system. It is shown in this work that two optimal solutions exist depending on the spatial characteristics of the base excitation. One of the optimal solutions can be physically realized in the form of a passive spring and a passive damper in parallel. The other optimal solution can be approximated by a passive spring and a continuously variable damper in parallel. A fuzzy logic based switch mechanism was developed to switch between two realizations of the optimal solutions. A recursive least square estimator was developed to estimate the seat load

and the stiffness of the spring using the same signals as the controller thus allowing universal application of the seat damper controller. The resultant controller is shown to provide the best ride comfort over various types of road surfaces.

A model predictive controller for the seat damper was also developed for this work. A novel method was developed to model the bounds on the seat suspension stroke as hard constraints of the optimization problem. An efficient scheme was developed to include the frequency weighted acceleration in the performance index of the optimization problem. It is shown in this work that the MPC based seat damper controller provides better ride comfort in some specific scenarios.

This work contributes towards the furthering the knowledge-base of the issues encompassing the ride quality of a tractor semi-trailer. The efficacy of the developed tractor semi-trailer ride simulation tool as a design and analysis tool is presented in this work.

## ACKNOWLEDGEMENTS

I would not have completed my pursuit of Doctor of Philosophy degree without the help of many people. I would like to take this opportunity to thank all of them. I express deep gratitude to my advisor, Dr. E. Harry Law for his constant support, guidance and encouragement which helped me strive for high levels of excellence. His enthusiasm for research is very infectious. I also would like to thank my dissertation chair, Dr. Ardalan Vahidi for his immense help and support especially in the development of the model predictive controller, and in teaching the controls courses. I would also like to thank my committee members, Dr. Beshah Ayalew and Dr. John Wagner for all their technical guidance.

I express my gratitude to my colleagues Mandar Hazare, Anup Khekare, Chinmay Pandit Norman Frey, David Wafer and Damon Delorenzis for lending me their time and sharing their technical knowledge. I am indebted to Nitendra. Nath, Shyam Panyam, Sriram Venkataraman, Raghu Ramachandran, Durlove Mohanty, Arghya Chakravorty and Monsur Islam for their help during my stay in Clemson. Finally, I would like thank my parents, Dr. Bhaskar Roy and Aparajita Roy. This dissertation would not have been possible without their patience, constant support and inspiration.

# TABLE OF CONTENTS

	Page
TITLE PAGE .....	i
ABSTRACT.....	ii
ACKNOWLEDGEMENTS .....	iv
LIST OF FIGURES.....	viii
LIST OF TABLES .....	xv
1. INTRODUCTION AND MOTIVATION.....	1
1.1 Motivation.....	1
1.2 Outline of the Thesis.....	2
2. LITERATURE REVIEW.....	5
2.1 Performance Metrics, Modeling and Ride Quality.....	5
2.2 Semi-active Suspensions and Control Strategies.....	11
3. TRACTOR SEMI-TRAILER MODEL AND VALIDATION .....	20
3.1 Model Description.....	20
3.2 Road Profile Generation.....	24
3.3 Performance Metrics .....	27
3.4 Model validation with TruckSim.....	30
4. CAB MOUNT AND FRAME FLEXIBILITY DESIGN STUDY .....	36

Table of Contents (Continued)

	Page
4.1 Baseline Results .....	36
4.2 Effect of Tractor Frame Beaming Frequencies .....	45
4.3 Full Cab Suspension .....	53
4.4 Effect of Cab Mount Location .....	58
4.5. Summary .....	68
5. CONTROL POLICIES FOR SEMI-ACTIVE SEAT DAMPERS .....	71
5.1 Optimal Policies for Seat Isolation .....	72
5.2 Skyhook Law Controller .....	78
5.3 Limitations of the Semi-Skyhook Policy .....	84
5.4 Fuzzy Switch .....	88
5.5 Estimation of the Seat Load and Suspension Stiffness .....	92
5.6 Ride Comfort with Semi-Active Seat damper on Different Road Surfaces .....	94
5.7 Semi-Active Seat Damper with Rear Cab Mounted at Optimum Position .....	100
5.8 Semi-Active Seat Damper with Full Cab at Optimum Mount Positons .....	103
5.9. Model Predictive Control with Excitation Preview .....	106
5.10. Quadrant Law Control.....	116
5.11. Conclusions: Semi-active Damper Control Strategies.....	124
6. SUMMARY AND CONCLUSIONS .....	126
APPENDICES.....	132
A: Baseline Truck Data, Eigenvalues and Eigenvectors .....	133
B: Equations of Motion .....	142

Table of Contents (Continued)

	Page
C: Sample Calculation for Tractor Beaming Frequency.....	164
D: Derivation of Optimal Policies for Seat Isolation .....	171
E: Derivation of the MPC Controllers .....	178
F: Derivation of the RLS Estimator.....	188
G: Model Validation TruckSim and Matlab Parameters .....	190
BIBLIOGRAPHY .....	202



## LIST OF FIGURES

	Page
Figure 2.1: Magneto-Rheological Seat Damper, Lord Corporation [25] .....	12
Figure 2.2: Hydropneumatic Semi-Active Spring Damper System [26].....	18
Figure 3.1: Side View Schematic of the 15 D.O.F. Tractor Semi- Trailer.....	21
Figure 3.2: PSD of Generated Road Profiles.....	27
Figure 3.3: Vertical (top) and Longitudinal (bottom) ISO Comfort Boundaries .....	28
Figure 3.4: Comparison of the Sprung Mass Dynamic Response .....	34
Figure 3.5: Comparison of the Axle Dynamic Response.....	35
Figure 4.1: Beaming Mode Shapes of Tractor and Trailer Frames.....	38
Figure 4.2: Mode #13 at 1.36 Hz.....	39
Figure 4.3: Mode #14 at 1.98 Hz.....	40
Figure 4.4: Mode #15 at 1.77 Hz.....	40
Figure 4.5: Seat RMS Acceleration on Smooth Highway @ 60mph, Baseline Truck.....	41
Figure 4.6: Seat RMS Acceleration for Different Roads .....	43
Figure 4.7: Seat and Rear Cab Suspension Deflections on Smooth Highway and Gravel Road .....	44
Figure 4.8: Representative Tractor Frame, Freightliner Trucks [51] .....	46
Figure 4.9: Typical Cross-section of Tractor Frame with Cross member.....	46
Figure 4.10: Chassis Frame Cross-section with Plates Mounted for additional Bending Stiffness.....	48
Figure 4.11: Plate Thickness vs. Frame Beaming Frequency .....	50
Figure 4.12: Tractor Frame Beaming Frequencies vs Mass per unit length of C-Channels for standard C-channel.....	51

List of Figures (Continued)

	Page
Figure 4.13: Effect of Frame Beaming Frequency on Seat RMS Acceleration.....	52
Figure 4.14: Effect of Beaming Frequency on Weighted RMS Acceleration.....	53
Figure 4.15: Variation of Total Weighted Normalized RMS Acceleration with Cab Damping over Smooth Highway @ 60 mph.....	54
Figure 4.16: Variation of Total Weighted Normalized RMS Acceleration with Cab Damping over Gravel Road @ 40 mph.....	55
Figure 4.17: Ride Comfort for Different Passive Cab Suspension Configurations,.....	56
Figure 4.18: Weighted RMS Acceleration for Different Passive Cab Suspension Configurations, Smooth Highway, 60 mph.....	57
Figure 4.19: Variation of Total Weighted RMS Acceleration with Cab Mount Location. ....	60
Figure 4.20: Baseline and Optimal Cab Mount Location for Rear Suspended Cab.....	60
Figure 4.21: Total Weighted RMS Seat Acceleration Comparison of Baseline vs. Optimal Cab Mount Positions, Rear Suspended Cab.....	61
Figure 4.22: RMS Seat Acceleration Comparison of Baseline vs. Optimal Cab Mount Positions, Rear Suspended Cab.....	62
Figure 4.23: Variation of Total Weighted RMS Acceleration with Cab Mount Locations, Fully Suspended Cab.....	64

List of Figures (Continued)

	Page
Figure 4.24: Baseline and Optimal Cab Mount Location, Fully Suspended Cab.....	65
Figure 4.25: Total Weighted RMS Seat Acceleration of Fully Suspended Cab over Smooth Highway at 60 mph (96.56 kph), Nominal vs Optimal Mount Positions. ....	65
Figure 4.26: RMS Seat Acceleration Comparison of Fully Suspended Cab, Nominal vs Optimal Cab Mount locations .....	66
Figure 5.1: A 1 d.o.f. system for developing the optimal control policies.....	72
Figure 5.2: PSD of Displacement at the seat mount, $S_E(\omega)$ .....	73
Figure 5.3: Physical realization of control policy 1 .....	76
Figure 5.4: Physical Realization of Control Policy 2.....	78
Figure 5.5: Semi-Active Realization of an Ideal Skyhook Damper .....	79
Figure 5.6: Ideal Skyhook Damper compared to Semi-Active Skyhook Damper for a 1 d.o.f. model.....	82
Figure 5.7: Semi-Active Skyhook Damper Compared to Passive system .....	83
Figure 5.8: Semi-Active Skyhook Seat Damper, Gravel Road, 40 mph (64.4 kph).....	84
Figure 5.9: Seat Suspension Stroke, Semi-Active Skyhook Damper .....	85
Figure 5.10: PSD of the Seat Mount Vertical Deflection, Gravel Road, 40 mph (64.4 kph).....	86
Figure 5.11: Acceleration/Stroke tradeoff for several damping ratios.....	87
Figure 5.12: Fuzzy Switch Scheme .....	89
Figure 5.13: ISO 2631-1 Vertical Acceleration Weighting Curve.....	90
Figure 5.14: Fuzzy Switch Output Surface.....	90
Figure 5.15: Fuzzy Switch Input Membership functions.....	91

List of Figures (Continued)

	Page
Figure 5.16: Estimator Signal Flow .....	92
Figure 5.17: Estimation of seat mass and stiffness .....	94
Figure 5.18: Estimator Controller Scheme.....	95
Figure 5.19: Driver RMS Vert. Acceleration Comparison for Different Control Strategies, Smooth Highway @ 60 mph.....	96
Figure 5.20: Weighted RMS Seat Acceleration Damper Controller Comparison, Smooth Highway @ 60 mph.....	97
Figure 5.21: Driver RMS Vert. Acceleration Comparison for Different Control Strategies, Gravel Road @ 40 mph.....	98
Figure 5.22: Weighted RMS Seat Acceleration Damper Controller Comparison, Gravel Road @ 40 mph.....	99
Figure 5.23: Seat RMS Acceleration, Baseline vs. Semi-Active Seat + Optimum Rear Cab Position, Smooth Highway @ 60 mph.....	101
Figure 5.24: Weighted RMS Seat Acceleration, Baseline vs. Semi- Active Seat + Optimum Rear Cab Position, Smooth Highway @ 60mph.....	102
Figure 5.25: Seat RMS Acceleration, Baseline vs. Semi-Active Seat + Optimum Full Cab Position, Smooth Highway @ 60 mph.....	104
Figure 5.26: Weighted RMS Seat Acceleration , Baseline vs. Semi- Active Seat + Optimum Full Cab Position, Smooth Highway @ 60 mph.....	105
Figure 5.27: Seat RMS Acceleration, MPC vs. Passive vs. Skyhook Law, Smooth highway @60mph .....	109

List of Figures (Continued)

	Page
Figure 5.28: Weighted RMS Seat Acceleration, MPC vs. Passive vs. Skyhook Law, Smooth Highway @60 mph.....	109
Figure 5.29: Seat RMS Acceleration, MPC vs. Passive vs. Skyhook Law, Gravel Road @ 40 mph .....	110
Figure 5.30: Weighted RMS Seat Acceleration, MPC vs. Passive vs. Skyhook Law, Gravel Road @ 40 mph.....	111
Figure 5.31: Seat RMS Acceleration, Weighted MPC vs. Passive vs. Skyhook Law, Smooth Highway @ 60 mph .....	113
Figure 5.32: Weighted RMS Seat Acceleration, Weighted MPC vs. Passive vs. Skyhook Law, Smooth Highway @60 mph.....	114
Figure 5.33: Seat RMS Acceleration, Weighted MPC vs. Passive vs. Skyhook Law, Gravel Road @ 40 mph.....	114
Figure 5.34: Weighted RMS Seat Acceleration, Weighted MPC vs. Passive vs. Skyhook Law, Gravel Road @ 40 mph.....	115
Figure 5.35: Working Principle of Semi-active Quadrant (Rakheja-Sankar [11]) Law.....	117
Figure 5.36: Response to Base Excitation: Passive vs. Semi-active Quadrant Damper, 1 d.o.f. ride model .....	119
Figure 5.37: Weighted RMS Seat Acceleration, Passive vs Skyhook vs Quadrant Seat Damper, Smooth Highway @ 60 mph .....	120
Figure 5.38: RMS Seat Vertical Acceleration, Passive vs Skyhook vs Quadrant Seat Damper, Smooth Highway@ 60 mph (96.56 kph).....	121
Figure 5.39: RMS Seat Vertical Acceleration, Passive vs Semi-active Quadrant Seat Damper, Gravel Road, 40 mph (64.4 kph).....	122

List of Figures (Continued)

	Page
Figure 5.40: Seat Suspension Stroke, Semi-Active Damper with Quadrant Law (Top), Passive Damper (Bottom), Highway with Gravel, 60 mph (96.56 kph).....	123
Figure B.1: Free Body Diagram of the Seat. ....	142
Figure B.2: Seat Spring Force vs. Deflection Curve .....	143
Figure B.3: Free Body Diagram of the Cab .....	144
Figure B.4: Free Body Diagram of the Engine.....	145
Figure B.5: Free Body Diagram of Steer Axle.....	151
Figure B.6: Free Body Diagram of 1 <sup>st</sup> Drive Axle.....	152
Figure B.7: Free Body Diagram of 2 <sup>nd</sup> Drive Axle.....	153
Figure B.8: Free Body Diagram of 1 <sup>st</sup> Trailer Axle .....	157
Figure B.9: Free body diagram of 2 <sup>nd</sup> Trailer Axle .....	158
Figure C.1: Typical Frame Chassis Cross-section .....	164
Figure C.2: Chassis Frame Cross-section with Plates Mounted for additional Bending Stiffness.....	168
Figure D 1: A 1 d.o.f. system for developing the optimal control policies.....	171
Figure E.1: Free body diagram of the 1 d.o.f system used for MPC controller derivation.....	178
Figure G.1: TruckSim Main Screen.....	190
Figure G.2: TruckSim Procedure Screen.....	191
Figure G.3: TruckSim Road Definition .....	191
Figure G.4: Driver Seat Sensor Location .....	192
Figure G.5: Tractor Main Screen .....	192
Figure G.6: Tractor Sprung Mass Definition.....	193
Figure G.7: Steer Axle Kinematics .....	193
Figure G.8: Steer Axle Kinematics .....	194

List of Figures (Continued)

	Page
Figure G.9: 1st Drive Axle Kinematics.....	194
Figure G.10: 1st Drive Compliance.....	195
Figure G.11: 2nd Drive Axle Kinematics.....	195
Figure G.12: 2nd Drive Axle Compliance.....	196
Figure G.13: Semi-Trailer Main Screen .....	196
Figure G.14: Semi-Trailer Sprung Mass Definition .....	197
Figure G.15: Trailer Axle Kinematics .....	197
Figure G.16: Trailer Axle Compliance .....	198
Figure G.17: Trailer Load Definition.....	198

## LIST OF TABLES

	Page
Table 3.1: Degrees of Freedom of Tractor Semi-Trailer .....	20
Table 3.2: Road Profiles, Wong [50] .....	25
Table 3.3: Values of $\mathcal{A}$ and $\mathcal{Q}$ for different road profiles.....	26
Table 3.4: ISO 2631 Weighted RMS Acceleration Comfort Levels .....	30
Table 3.5: TruckSim vs Matlab axle loads .....	32
Table 4.1: Natural Frequencies and Damping Ratios, Baseline Configuration .....	37
Table 4.2: Ride Characteristics for Baseline Configuration .....	45
Table 4.3: Driver's Seat Ride Comfort from all the Design Studies .....	68
Table 5.1: Fuzzy Logic Rules.....	91
Table 5.2: RLS Estimated Seat Values .....	93
Table 5.3: MPC Controller Parameters.....	108
Table 5.4: Driver Seat Ride Comparison for Different Damper Control Strategies, Nominal Rear Suspended Cab .....	116
Table 5.5: Driver's Seat Ride Comfort for Different Control Strategies and Cab Configurations .....	124
Table A.1: Dimensions of the Tractor Semi-Trailer Model.....	133
Table A.2: Inertial Properties .....	133
Table A.3: Vehicle Suspension Parameters .....	134
Table A.4: Seat Suspension Parameters .....	134
Table A.5: Cab Suspension Parameters .....	134
Table A.6: Natural Frequencies and Damping Ratios (Baseline).....	135
Table A.7: Eigenvectors of the Baseline Linearized Model.....	135
Table C.1: Tractor Frame Beaming frequencies with Standard C- channels.....	170



List of Tables (Continued)

	Page
Table G.1: Modified Matlab/Simulink Suspension and Beaming Frequency Values .....	199

# CHAPTER 1

## INTRODUCTION AND MOTIVATION

### 1.1 Motivation

It is well known that the ride quality of trucks is much harsher than that of automobiles. Additionally, truck drivers typically drive trucks for much longer duration (up to 16 hours per day) than automobile drivers. These two factors contribute to the fatigue that a truck driver typically experiences during long haul deliveries. Fatigue reduces driver alertness and increases reaction times, increasing the possibility of an accident. Due to the size of trucks, accidents involving trucks cause much more damage than automobiles. One may conclude that better ride quality contributes to a safer vehicle.

A study conducted by the Federal Motor Carrier Safety Administration [1] investigated 967 crashes between 2001 and 2004. The study found that truck driver fatigue directly contributed to the accidents in at least 13% of the accidents. Driver recognition and decision error which might be brought about partly by driver fatigue were the most cited critical reason (42%) for the accidents.

There are various factors that affect ride quality. Though lots of studies have been done to improve the ride quality in automobiles, considerably fewer studies have been performed on the ride analysis of trucks. The significant factors that contribute to ride quality of a truck are

- Axle Suspension,

- Frame flexibility,
- Tires,
- Road surface,
- Cab suspension, and
- Seat Suspension.

Most trucks in North America are designed as cab-over-frame. This means that the cab body is suspended over the truck frame. This is the main difference in the design of a truck and an automobile. The cab suspensions provide engineers with another parameter to improve the ride quality. Most trucks sold in North America have a rear cab suspension design. The front of the cab is mounted on the frame (with elastomers). Various suspension technologies are available for rear cab suspension. Most common among these are air springs and hydraulic dampers.

Recent advancements in variable hydraulic dampers and the emergence of variable rate magneto-rheological (MR) dampers provide a unique opportunity to improve ride quality of trucks.

## **1.2 Outline of the Thesis**

A brief overview of the subsequent chapters of the thesis is presented in this section.

In chapter 2 a general overview of the existing literature in the area of heavy truck ride is presented. The literature review covers three fundamental aspects related to the heavy truck

ride. The first aspect deals with the modeling of the tractor semi-trailer and the performance metrics used to quantify ride quality. The second aspect deals with the available tractor design choices to improve driver ride. The third aspect deals with the control strategies for semi-active suspensions. The chapter presents the state of the art on each of these aspects.

In chapter 3 the models used to analyze the ride of a tractor semi-trailer are described. The simulation tool developed in the Matlab/Simulink environment based on the model is also introduced. The road model and the road input generation tool is also described. The performance metrics used in this thesis to evaluate the driver ride quality is also described. Lastly the results of the validation against TruckSim, a commercially available truck dynamics simulation tool, of the developed model are discussed.

In chapter 4 improvements in driver ride quality due to cab and frame design choices are explored. The ride results of the baseline model are presented and an in depth analysis of the various modes contributing to the truck dynamics is performed. The effect of tractor frame beaming frequencies on driver ride comfort is analyzed. The benefits in ride comfort of the full cab suspension over a conventional cab with only rear suspensions are discussed. The hypothesis of placing the cab mounts close to beaming nodes is explored using the developed simulation tool. A methodology to find the optimum location of the cab mounts for both rear cab suspension and full cab suspension configurations is discussed.

In chapter 5 control strategies for a semi-active seat damper are discussed. The optimal policies for seat isolation for different spatial characteristics of the seat mount excitation are presented. The limitation of the Skyhook law for semi-active damper control is discussed. A novel semi-

active damper control strategy involving a fuzzy switch mechanism is developed. The driver ride improvements due to the new control strategy are presented. Two novel model predictive semi-active damper control strategies are developed. The strengths and weakness of the MPC based control strategies are discussed.

Finally chapter 6 summarizes the main conclusions of the thesis and makes recommendations for future research.

## CHAPTER 2

### LITERATURE REVIEW

#### 2.1 Performance Metrics, Modeling and Ride Quality

Ride analysis of tractor semi-trailers has been a subject of engineering study for almost five decades. A model of the vehicle that accurately represents the dynamics of the vehicle and that is not computationally costly is a very useful tool to analyze the vehicle ride. This section will introduce the main developments in the modeling of a heavy truck. Mathematical models and actual vehicles can then be used to identify the main components that affect the ride quality.

To evaluate the ride quality of a vehicle, various performance metrics have been developed. The most commonly used performance metric is the methodology laid out in ISO 2631[2,3]. ISO 2631 comfort levels are discussed in more detail in section 3.3. A procedure for evaluating exposure when high level shocks are involved is not laid out in ISO 2631. Paddan, et al. [4,5] suggest an alternative performance metric to evaluate ride comfort called vibration dose values (VDV). The VDV uses frequency weighted acceleration along each axis and the exposure duration.

$$VDV(m / s^{1.75}) = \left[ \int_0^T a(t)^4 dt \right]^{1/4}, \quad (2.1)$$

where  $a(t)$  is the frequency weighted acceleration time history.

This thesis uses the methodology laid out in ISO 2631:1774 and ISO 2631:1997 to evaluate the ride quality.

Heavy truck cab and seat suspensions have been an area of particular interest because of the considerable improvements they provide in ride comfort. Use of a cab suspension to improve truck ride has been studied since the late 1960s. Foster [6] studied the effect of a full-cab suspension for a cab-over-engine (COE) tractor using prototype vehicles. He concluded that the natural frequency of the cab suspensions should be lower than 3Hz to isolate the cab from the chassis modes. Flower [7] also assessed the ride quality of a COE tractor fitted with either a front or a rear cab suspension to study the effects of cab isolation system on ride. The study evaluated the ride using a planar 54 d.o.f model and also used four professional drivers to subjectively evaluate the cab isolation systems. The model included Euler-Bernoulli beam bending representations for both the tractor and the trailer frames. He modeled the tractor frame using three discrete beams connected end to end. The study found that the rear cab isolation was easier to install and provided some ride benefits due to decoupling of the cab motion from the frame bending. The front cab isolation system provided noticeably superior ride compared to the rear cab system or a cab without isolation system (standard configuration during 1978) though the installation of the front cab isolation system is more challenging. Tractors having rear cab isolation are now the industry standard.

Gross, et al. [8] studied the effect of a four-point air cab suspension for conventional U.S. trucks on driver ride comfort. The study employed a 32 d.o.f three dimensional model of the truck. Their study concluded that the full cab suspension provided significant improvement in the ride comfort. Field, et al. [9,10] used a finite element model of a conventional U.S. heavy

truck to assess the ride quality. They investigated the effects of the cab isolation system at the rear mount both with a computer model and by testing a prototype Department of Energy class 8 truck. Their study found about 20% improvement in ride with the use of a cab isolation system at the rear as compared to the cab hard mounted to the frame.

Another way to improve the ride quality is to optimize the suspension parameters for minimum vertical and horizontal acceleration at the driver's seat. Jain [11] studied the effect of various passive cab suspensions on ride comfort using an Adams model of a cab-over engine tractor-trailer. He used ISO-2631 [3] guidelines for target setting in numerical simulation. He found that for a conventional tractor setup, with the cab mounted to the truck frame at the front and suspended at the rear, the effect of tractor rear suspension stiffness on cabin ride was not significant. He achieved a significant improvement in ride through the application of a low frequency (1.8 Hz) suspension system at the front of the cab. Rajan, et al. [12] used a quarter car model of the truck to improve the ride comfort by optimizing the cab suspension with the spring and the damper as the tuning parameters. Their study showed the effectiveness of lumped mass modeling to analyze the ride of rigid trucks. Recently, Ksiazek, et al. [13] developed an optimization routine to find the values of the isolation components that minimize the driver's and the cargo ride discomfort. The method was applied to a 9 d.o.f. tractor semi-trailer model. By applying the method the authors observed significant reduction in the seat accelerations and relative displacements between the axles and frames.

Most studies on truck ride agree that the presence of the front cab suspension or a full cab suspension significantly improves the ride. However installing a front cab suspension provides many design challenges. Also due to the dominance of rear cab suspensions in the North



American market, retrofitting a full cab suspension to existing on-road trucks would be both time consuming and costly.

Bending of the frame has a large bearing on the ride quality of the truck. Among other aspects, Gillespie [14] studied the influence of frame stiffness on the transmission of road inputs to the cab of a cab-over-engine tractor. He identified the first vertical bending mode to occur in the 6-9 Hz range. Margolis, et al. [15] used the bond graph method to model a flexible frame which is supported by springs and dampers at its ends. Cao [16] used the commercial software NASTRAN to model the truck frame of a single drive axle, cab-over-engine truck and validated the model using the frequency response analysis method. He looked at three approaches to reduce truck beaming but did not consider many vehicle components. The study concluded that the most effective method to reduce beaming was to align the rear beaming node with the rear axle. Ibrahim, et al. [17] also looked at the effect of beaming on ride quality. They used finite element methods (FEM) to compute power spectra for truck models using both rigid frames and multi-element frames. The results confirmed previous work that found that frame flexibility strongly affects the accelerations of the truck as well as the occupants.

Vaduri [18] developed a linear 12 d.o.f. tractor semi-trailer model. He modeled the tractor frame as an Euler-Bernoulli beam with both the ends of the beam free. The first mode of bending of the frame was included in the ride model using the assumed mode method. A tractor frame with a natural beaming frequency of 18.9 Hz, which is considerably higher than the typical beaming frequency, was used for simulation. Two types of tire models, the point contact and the fixed footprint tire models, were used for the simulation. The thesis

investigated the effect of tire non-uniformities, a seat suspension and various cab suspensions on the driver's ride comfort. The study concluded that tractor frame beaming contributed significantly to the longitudinal acceleration at the driver's seat since the driver seat is at a considerable height above the frame. The study also found that the vehicle with a rear cab suspension had better vertical ride but worse longitudinal ride compared to a vehicle with no cab suspension and a front cab suspension provides better ride in both the longitudinal and vertical directions compared to a rear cab suspension. Law, et al. [19] used a version of Vaduri's model to compare the ride response of trucks fitted with conventional dual tires and wide-base tires. The study found that the less "stiff" wide-base tires provided better ride in the wheel hop range ( $\sim 9$  -13 Hz).

Trangsrud [20] built on the work of Vaduri and developed a 14 d.o.f. tractor semi-trailer model. Also, his model included beaming of the semi-trailer together with the engine heave with respect to the tractor chassis. Using frequency analysis methods the study investigated the effects on ride of (a) the new wide-base tires developed by Michelin, (b) tire non-uniformities, and (c) friction in the suspension system.

Spivey [21] built on the work of Trangsrud and Vaduri to develop a linear 15 d.o.f. model of the tractor semi-trailer. His model included the effects of the possible presence of a suspension at the fifth wheel joint. Euler-Bernoulli beams with "free-free" and "free-pinned (at the fifth wheel)" boundary conditions were used to represent the tractor and trailer frames in this study. He investigated the effects of cab and seat suspension on the isolation of the driver from the road inputs. Among the parameters he investigated were the cab and seat suspensions, tractor axle suspensions, fifth wheel suspension, frame bending vibrations, and tractor wheelbase. His

study concluded that inserting a fifth wheel vertical suspension system in a rear cab suspended truck was detrimental to the ride comfort of the driver.

Jiang, et al. [22] provide an in-depth literature survey on the evolution of tractor semi-trailer models. The study reviewed seven different tractor semi-trailer models and five driver seat models. Their study concluded that the cab suspensions and the seat suspension are the only components that can modify the ride comfort of a heavy vehicle without affecting the road holding capabilities of the vehicle. The study also showcased the importance of a driver/seat model to the ride analysis.

Patricio [23] compared the effects of two different cab suspensions and the effects of two different truck frames on ride comfort using a prototype tractor vehicle. His study found improvements in ride comfort with use of lightweight truck frames and a prototype rear cab suspension. Interestingly, though there was improvement in the vertical ride, the longitudinal ride comfort deteriorated with the use of prototype shocks.

An interesting approach to reduce the effect of frame beaming was explored by Anderson [24]. He developed and tested a tuned mass damper (TMD) to reduce the frame beaming vibration. The study found the ideal location to mount the TMD was at the tail of the tractor frame. The ideal mass for the damper was found to be  $1/20^{\text{th}}$  of the effective mass at the mounting location. The tuned absorber was effective in reducing the transmissibility from the rear drive tire to the B-pillar by about 60%. This approach provides an alternative route to reduce the effect of frame beaming on the ride quality.

The coupling of the frame beaming motion with the cab motion significantly affects the ride dynamics of a truck. Locating the cab suspension to minimize this coupling effect can be an effective way of improving the ride quality. A gap exists in the current literature on the effects of varying the cab mounting positions on the ride quality. Another important factor affecting the ride quality is the available design space for the various suspensions. In particular, the seat suspension design space is critical to the ride quality especially on rough road surfaces and at high speeds. This thesis includes a model of the bump stops for the seat suspension to accurately evaluate the ride at the driver's seat.

## **2.2 Semi-active Suspensions and Control Strategies**

Recently much study has been performed on semi-active suspensions for heavy vehicles. The concept of semi-active suspensions dates from 1970s. Recent developments in control theory and the development of variable valve dampers, and magnetorheological (MR) dampers have made semi-active suspensions feasible. MR dampers have been developed and implemented in production vehicles by Lord Corporation and Delphi (Magneride™).



**Figure 2.1: Magneto-Rheological Seat Damper, Lord Corporation [25]**

Semi-active suspensions allow variation of the viscous damping coefficient based on some control strategies using a small source of power. They differ from active suspensions in that they cannot provide positive energy to the suspension systems. Also, semi-active suspensions are inherently stable systems. Semi-active suspensions consume significantly less power compared to fully active suspension systems. Active seat suspension have been recently developed by Bose Corporations and successfully implemented on commercial trucks [26]. This section will provide the main developments in physical realization of semi-active suspension and strategies to control the semi-active suspension to provide the best ride comfort.

Bender [27] proposed the idea of using linear optimal control theory with quadratic performance index for the design of active vehicle suspensions. Karnopp, et al. [28] provided the basic groundwork for analyzing semi-active suspensions. The study showed that when

quadratic performance criteria involving the sprung mass acceleration and the relative displacement are used the optimal suspension system is a passive spring and an ideal “skyhook” damper. The concept of “skyhook” damper is explained in section 5.3. Based on the ideal “skyhook” damper the paper presented the skyhook law for a semi-active damper.

Alanoly and Sankar [29] and Jolly and Miller [30] independently developed a control strategy for a variable damper system to minimize the sprung mass acceleration. According to the suggested control strategy, the damping force is set to zero when the damping force and the spring force are in the same direction and the damping force is adjusted to balance the spring force when they act in the opposite direction. This control strategy has been called the Rakheja-Sankar (R-S) law or the quadrant law or relative control law. This law is discussed in more detail in section 5.10.

Margolis [31] used frequency analysis methods to study a semi-active system to control the heave and pitch motion using a 4 d.o.f system model. He concluded that semi-active isolation systems are far superior to a conventional system near its resonance frequency.

A majority of studies involving semi-active suspensions are for passenger vehicle axle suspensions which have different design requirements to secondary truck suspensions. Song [32] explored some of the issues concerning the practical implementation of a semi-active skyhook system to a seat suspension for heavy trucks. The skyhook control strategy requires relative and absolute velocities of the suspended object. He examined various continuous skyhook control strategies and analyzed the dynamic response of the semi-active system. The simulation results based on a non-parametric model of the MR damper revealed “jumps” in

seat acceleration concurrent with the switching of the dampers from the off to the on state. His analysis led to the formulation of two modified skyhook control strategies to mitigate this jerk: Continuous Skyhook Function control and No-jerk Skyhook control. These modified skyhook control strategies decreased the acceleration and jerk at the seat. However these strategies work over a fairly narrow bandwidth and thus would not be suitable for cab or axle suspensions. The effect of hitting the seat suspension bump stops were not explored in this study.

ElMadany has done extensive simulation work describing both fully active and semi-active cab suspension systems and comparing their performance with passive systems [33-36]. ElMadany used simulations to test a fully active cab suspension with a linear stochastic optimal controller with great success . These studies used a linear lumped parameter 10 d.o.f. tractor semi-trailer model.

Moline [37] proposed a controller for a two-state semi-active rear cab damper. The proposed controller was analyzed on a 12 d.o.f. tractor semi-trailer model. This model did not include frame beaming degrees of freedom. The study did not find any significant improvement in ride comfort. But the study also concluded that there can be significant improvement in ride comfort with other control strategies.

Iersel [38] used a 4 d.o.f. truck model to study various suspension concepts applied to the 4-point cabin suspension. A 4 point cab suspension is more typical in Europe. The work concluded that there was limited potential improvement of driver comfort with the existing concepts. The study also proposed a control strategy for semi-active cabin suspension based

on linear quadratic optimal control and linear parameter varying theory. The developed control strategy was found to improve the ride comfort by more than 12% compared to the baseline suspension within the suspension working space.

Marcu [39] implemented variations of the skyhook control policy for 4 point cab suspensions and described the benefits in ride comfort of the skyhook policy variations. The study also developed a Hierarchical SemiActive Control (HSAC) with the objectives of keeping the suspension from hitting the bump-stops, and to control the skyhook gain online for best ride comfort. The study found that the HSAC controller provided better ride in the sleeper portion of the cab compared to the baseline configuration.

Kok, et al. [40] suggested a preview based optimal control system using a Kalman filter for both active and semi-active suspension systems at the rear axle. They did not find any improvement in ride comfort with the use of the preview based optimal control strategy for a semi-active suspension. Ieluzzi, et al. [41] analyzed ride comfort and lateral dynamic characteristics of a cab-over-engine, single-drive axle tractor with semi-active axle suspensions. They used an Adams model of the truck to test the efficacy of the suspension control system. They developed a control strategy composed of three tasks. The first control task reduced the vibration of the frame. The second control task moderated the vehicle roll motion and the third task managed the pitch motion under braking maneuvers. To control the vehicle vertical motion, the controller used a linear combination of a skyhook damper and a passive damper (modal skyhook law). Their study found perceivable improvements in ride and lateral dynamic characteristics of the truck.



Recent advancement in computational power has seen the emergence of model predictive controller (MPC) for semi-active suspensions. The control problem in this case is reduced to an optimization problem at each time step. If the performance index is quadratic and the system and constraints are linear the MPC problem can be solved efficiently using quadratic programming (QP). The constraints imposed due to the dissipative nature of the semi-active damper are not a linear function of the states of the system. Canale, et al. [42] developed a “fast” MPC strategy for semi-active dampers in road vehicles. The developed control strategy was simulated using a 2 d.o.f. quarter car model. The study found reduction in the sprung mass acceleration and sprung mass relative displacement compared to the skyhook law. Cseko, et al.[43] developed an explicit MPC controller with Kalman filter for a road vehicle semi-active suspension. They used a quadratic performance index incorporating the sprung mass acceleration, suspension deflection and tire deflection. The control strategy was simulated using a 2 d.o.f quarter car model. The study found that the developed control strategy yielded a lower value of the performance index when compared to a full-state feedback controller.

Though MR dampers are the most popular semi-active damper, other types of semi-active suspension systems have also been developed in the last two decades. Eslaminasab [44] developed a semi-active twin-tube damper with an internal variable solenoid-actuated valve that generated four distinct linear damping rates (very high, high, low and very low damping coefficient) and evaluated the ride and rollover performance of the system when used at the axle suspensions. The study analyzed the performance with two different controllers for the semi-active dampers on a 2 d.o.f. quarter car ride model and on a 4 d.o.f roll-plane vehicle

lumped-mass model. The control algorithms used concepts of neural networks and fuzzy logic. Both skyhook and ground hook control theories were analyzed. He concluded that the proposed neuro-fuzzy based R-S controller for the developed semi-active suspension improved the ride comfort when compared to skyhook or two state R-S controllers.

Giliomee, et al. [45] developed a semi-active hydropneumatic spring and damper system for heavy off-road vehicles. This system is able to switch between a soft and hard stiffness as well low and high damping. He discusses the construction of the hydropneumatic spring-damper system. The system consists of a hydraulic actuator connected to two different sized accumulators through a hydraulic damper. The flow to the larger accumulator can be cut off or reduced using a solenoid valve. This arrangement allows two state spring stiffness. Also the fluid flow from the actuator to the accumulators can be achieved through a bypass valve. The damper and bypass valve arrangement allows a two-state damper system. The system is shown in the Figure 2.2.

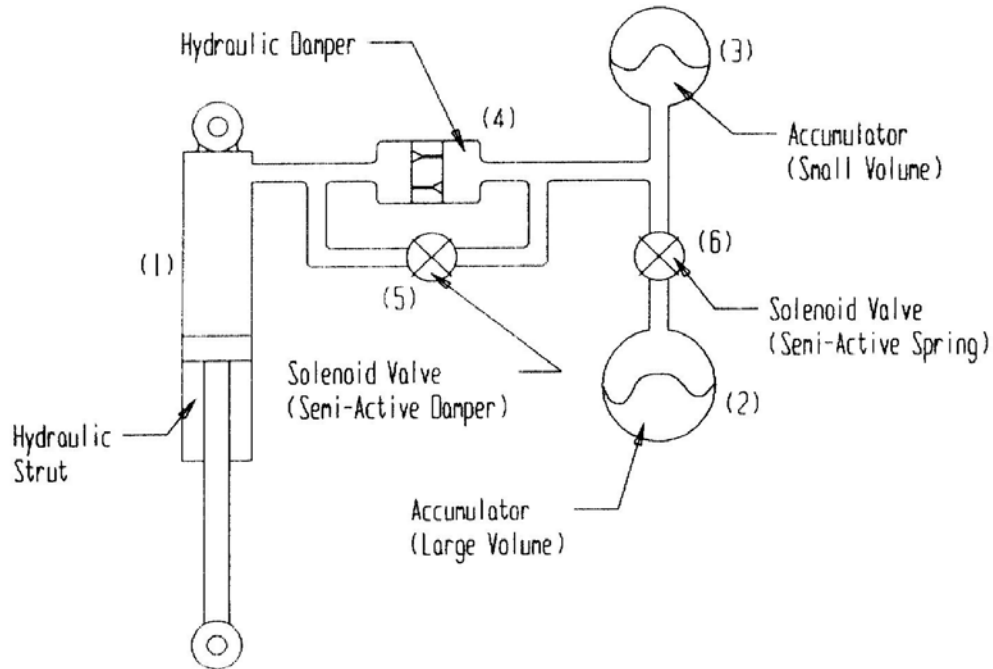


**Figure 2.2: Hydropneumatic Semi-Active Spring Damper System [26]**

Gilomee was able to achieve two distinctive spring stiffness values with the above system. The system shows a fairly linear response with each of these.. A maximum spring force of 50 kN was achieved with the system. By operating the bypass valve, two state damping was also achieved though in the 'off' state the damping rate was not equal to zero. This was due to various leakages and flow losses. The response of the damper in the “on” state is not linear with respect to the damper velocity. In the “on” state at high damper velocities the suspension system is less sensitive to change in velocities. The author found this to be a property of the hydropneumatic system. Solenoid valves were used for the system. The valve response time was between 70-170 milliseconds. Using the hydropneumatic suspension the authors demonstrated better ride comfort for a 1-d.o.f. system on a test rig.

Deprez, et al. [46] modeled and analyzed a semi-active hydropneumatic suspension for isolating the cabin of agricultural tractors. The modeled system gave results in close accordance to the experimental results with matched inputs. The passive system ('on' state for both damper and spring) was optimized using a goal function based on the objective comfort parameters as outlined in ISO 2631 [3] and BS 6841 [47]. For semi-active damping two modified skyhook laws were explored. Experimental results showed that the semi-active suspension improved the comfort values by 30% as compared to the optimized passive system.

Most control strategies developed for the seat suspension have been analyzed using a 1 d.o.f. ride model. Since the ride is greatly affected by the excitation to the system it is important to characterize the excitation correctly to have meaningful results. In this thesis the performance of the control strategy for the seat damper is analyzed using the full truck ride model. The control strategies developed for the semi-active suspension involve a trade-off in the sprung mass acceleration and the suspension stroke. A good control strategy must provide a good ride on all types of road surfaces and at all permissible vehicle speeds.

## CHAPTER 3

### TRACTOR SEMI-TRAILER MODEL AND VALIDATION

#### 3.1 Model Description

A cab-over-frame tractor with basic flatbed semi-trailer was modeled in this thesis. The tractor semi-trailer model contains 15 degrees of freedom (d.o.f.), 10 d.o.f. for the tractor and 5 d.o.f. for the trailer. The equations were derived using Newtonian and Lagrangian mechanics. The degrees of freedom describing the tractor semi-trailer model can be found in Table 3.1.

**Table 3.1: Degrees of Freedom of Tractor Semi-Trailer**

Sr. No	Description	Symbol
1	Vertical displacement of Driver's Seat	$z_s$
2	Vertical displacement of Cab	$z_c$
3	Pitch of Cab	$\theta_c$
4	Vertical displacement of Engine	$z_e$
5	Vertical displacement. of Tractor Frame	$z_t$
6	Pitch of Tractor Frame	$\theta_t$
7	Beaming of Tractor Frame	$q_t$
8	Vertical displacement of Trailer	$z_{tr}$
9	Pitch of Trailer	$\theta_{tr}$
10	Beaming of Trailer	$q_{tr}$
11	Vertical displacement of Axle #1	$z_1$
12	Vertical displacement of Axle #2	$z_2$
13	Vertical displacement of Axle #3	$z_3$
14	Vertical displacement of Axle #4	$z_4$
15	Vertical displacement of Axle #5	$z_5$

A schematic of the model can be found in Figure 3.1. All the displacements are measured from the static equilibrium. Data for the baseline model were obtained from a prototype class 8 model supplied by a major truck manufacturer. A detailed description of the geometric parameters, inertial properties and suspension parameters can be found in appendix A. Road inputs were assumed to be identical on the left and right sides of the vehicle.

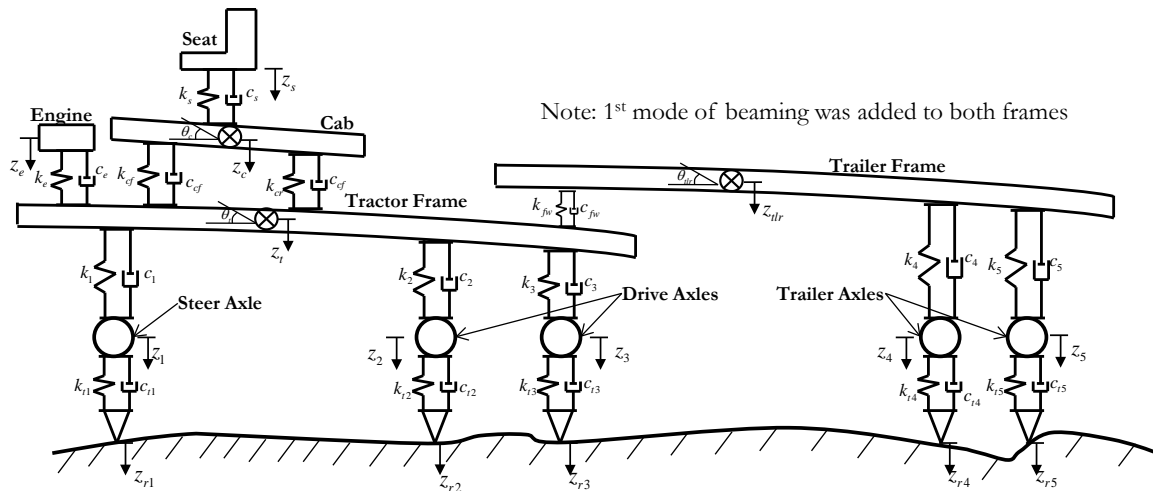


**Figure 3.1: Side View Schematic of the 15 D.O.F. Tractor Semi-Trailer**

All suspension elements in the model were represented by combinations of linear springs (except seat springs) and damping elements to approximate suspensions on an actual truck. The seat spring element is modeled with bump-stops. The seat spring behaves linearly in the normal operation regime of  $\pm 7.5$  cm from equilibrium. There is a smooth transition between the linear regime and the bump-stops. The cab was modeled with front and rear suspensions that permit both relative pitch and heave of the cab with respect to the tractor chassis. To simulate the effect of a rear suspended cab, the front cab suspension was made very stiff. Cab suspension parameters were tuned based on the resonance frequency of cab found in literature

[6, 14, 41]. The engine was modeled as a lumped mass suspended from the tractor frame. The stiffness and damping of the modeled engine suspension was the summation of the stiffness and damping coefficients of all the engine mounts. The fifth wheel joint was modeled as a parallel spring and damper system. To approximate a conventional fifth wheel joint the values of the fifth wheel suspension stiffness and damping were set very high.

The tractor and trailer frames consist of two parallel frame rails connected to each other with cross members. The tractor and trailer frames were modeled as Euler-Bernoulli beams. The first bending or “beaming mode” normally occurs between 6-9Hz [6, 7]. Only the first bending mode was considered for this research since it is normally the most important mode. Bending of the tractor frame affects both the longitudinal and vertical acceleration at the driver’s seat.

The equation of motion for a uniform Euler-Bernoulli beam is,

$$EI \frac{\partial^4 \eta(x,t)}{\partial x^4} + \rho A \frac{\partial^2 \eta(x,t)}{\partial t^2} = f(x,t) , \quad (3.1)$$

where  $E$  is the modulus of elasticity,  $I$  is the area moment of inertia of the beam about the transverse axis,  $\eta(x,t)$  is the vertical displacement of the beam at some distance  $x$  along the beam at time  $t$ ,  $\rho$  is the density of the material used for constructing beam, and  $A$  is the cross-sectional area of the beam [48]. For free vibration,  $f(x,t) = 0$ , and so the equation of motion becomes

$$EI \frac{\partial^4 \eta(x,t)}{\partial x^4} + \rho A \frac{\partial^2 \eta(x,t)}{\partial t^2} = 0 . \quad (3.2)$$

The solution is found using separation of variables as,

$$\eta_i(x, t) = X(x)q(t) \quad (3.3)$$

Equation (3.3) simplifies to two equations, describing deflection in  $x$  and with time  $t$  as,

$$\frac{d^4 X(x)}{d x^4} - \beta^4 X(x) = 0 \quad (3.4)$$

and,

$$\frac{d^2 q(t)}{d t^2} - \omega^2 q(t) = 0, \quad (3.5)$$

where

$$\beta^4 = \frac{\omega^2}{c^2} = \frac{\rho A \omega^2}{EI} . \quad (3.6)$$

The natural frequency of beaming is denoted by  $\omega$ . The temporal equation (3.5) was merged with the other equations of motion of the system using the assumed modes method [49].

The spatial solution of equation (3.4) can be expressed as

$$X(x) = C_1 \cos \beta x + C_2 \sin \beta x + C_3 \cosh \beta x + C_4 \sinh \beta x . \quad (3.7)$$

The constants  $C_1, C_2, C_3, C_4$ , are obtained by imposing the boundary conditions at the two ends. Since the two frames are pinned at the fifth wheel, a pinned (simply supported) boundary condition is applied at that point. The other ends of the frames are free to flex. Therefore, the



tractor frame is modeled as a free-pinned beam and the trailer frame is modeled as pinned-free beam. A pinned end causes zero deflection and zero bending moment at that end.

$$\text{Deflection} = X = 0, \quad \text{Bending Moment} = EI \frac{\partial^2 X}{\partial x^2} = 0. \quad (3.8)$$

A free end leads to zero bending moment and zero shear force at that end expressed as,

$$\text{Bending moment} = EI \frac{\partial^2 X}{\partial x^2} = 0, \quad \text{Shear Force} = EI \frac{\partial^3 X}{\partial x^3} = 0. \quad (3.9)$$

Imposing the boundary conditions on equation (3.8) yields the mode shapes for the tractor frame (free-pinned) and trailer frame (pinned-free):

$$X_t(x) = \cos \beta x + \cosh \beta x - \left( \frac{\cos \beta l + \cosh \beta l}{\sin \beta l + \sinh \beta l} \right) \sin \beta x + \sin h \beta x, \quad (3.10)$$

$$X_{tr}(x) = \sin \beta x + \left( \frac{\sin \beta l}{\sinh \beta l} \right) \sinh \beta x, \quad (3.11)$$

where for the first mode of beaming  $\beta l = 3.926602$ .

Detailed derivations of the equations of motion for the entire model can be found in appendix B.

### 3.2 Road Profile Generation

A simulated random road was generated to perform ride comfort frequency domain analysis.

The road profile can be characterized by its temporal power spectral density function [20],

$$S(\omega) = (2\pi \cdot V)^{N-1} \frac{C_{sp}}{\omega^N}, \quad (3.12)$$

where  $S(\omega)$  is the road PSD in  $\text{m}^2/(\text{rad/s})$ ,  $V$  is the speed of the vehicle in  $\text{m/s}$ ,  $\omega$  is the temporal frequency in  $\text{rad/s}$ , and  $C_{sp}$  and  $N$  are constants. The PSDs of a few common road profiles as described by Wong [20] are given in Table 3.2

**Table 3.2: Road Profiles, Wong [50]**

Road Type	$C_{sp}$ (SI units)	N
Smooth Runway	$4.3 \times 10^{-11}$	3.8
Rough Runway	$8.1 \times 10^{-6}$	2.1
Smooth Highway	$4.8 \times 10^{-7}$	2.1
Highway with Gravel	$4.4 \times 10^{-6}$	2.1

For this thesis, two primary road profiles were created corresponding to the PSDs of the smooth highway and highway with gravel. These two road profiles were chosen to represent the extreme conditions observed during long hauls typical for trucks.

To create the road profiles, an unpublished Matlab program, created by Marc Paradiso and David Moline, was modified. The road amplitude properties were set by multiplying each frequency by an amplitude,  $A$ , and raising each frequency  $f$  to a power,  $Q$ ,

$$a = A \cdot f^Q. \quad (3.13)$$

The value of  $A$  corresponds to the resulting value of  $C_{sp}$ , and the value of  $Q$  corresponds to the resulting value of  $N$  for the PSD of the created roadway. In creating the roadway,

sinusoidal waves were created with the sine wave generator in Simulink. The output of the wave generator is

$$\xi(t) = \frac{a}{2\pi f} \cdot \sin(2\pi f \cdot t + \Phi), \quad (3.14)$$

where  $\Phi$  is a random variable of same length as the  $f$ , drawn from a normal distribution with zero mean and unit standard deviation.

The simulation created a vector of sine waves corresponding to the length of the frequency vector. At each time-step the current values of the sine waves in the vector were added together yielding the random road profile.

Values of  $A$  and  $Q$  were iteratively altered till the PSD of the simulated road matched the PSD of smooth highway within the frequency region of 0.25 – 50 Hz. The values of  $A$  and  $Q$  for the two road profiles used in this thesis are given in Table 3.3

**Table 3.3: Values of  $A$  and  $Q$  for different road profiles**

Road Type	$A$	$Q$
Smooth Highway @ 60 mph	0.013282	-0.045
Gravel Road @ 40 mph	0.0402018	-0.045

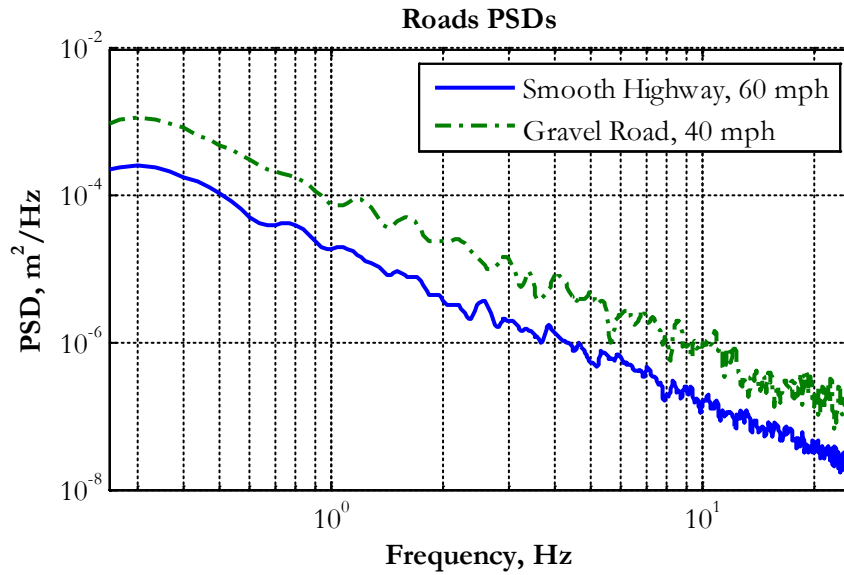


Figure 3.2: PSD of Generated Road Profiles

The PSDs of the two road profiles are shown in Figure 3.2.

### 3.3 Performance Metrics

The road profiles described in the previous section were used as input to the system. The time duration of the simulation run was 120 seconds. This duration allows sufficient road input power to be developed at low frequencies. The speed of the truck was maintained at 60 mph to simulate typical highway speeds.

Frequency response analysis allows results to be easily compared to ride quality standards set forth by the International Standard Organization, ISO 2631. The ISO 2631 standard is still regarded as a leading standard for quantifying ride quality. The ride comfort boundaries are defined for root mean square (RMS) vertical and longitudinal accelerations measured at the driver's seat over the frequency range from 0.1 to 50 Hz. In ISO 2631:1974 [2], the boundaries

in Figure 3.3 represent the amount of time the driver can sustain that particular acceleration before becoming uncomfortable. As one would expect, lower acceleration magnitudes can be tolerated as the driver operates the vehicle for longer periods of time.

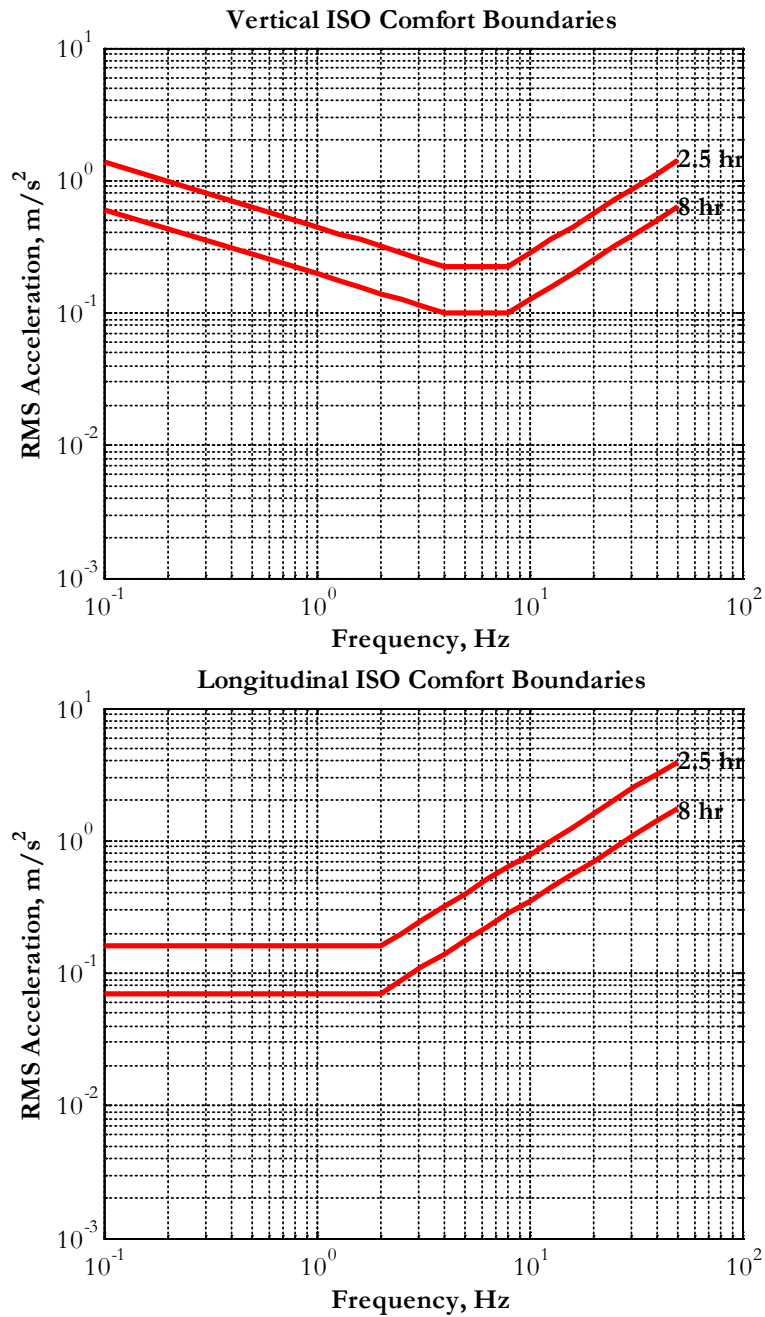


Figure 3.3: Vertical (top) and Longitudinal (bottom) ISO Comfort Boundaries

The Matlab function *pwelch* was used to obtain the frequency domain response from the time history results. ISO 2631 defines the low and high frequency corresponding to the center frequency of each 1/3 octave band as,

$$\begin{aligned}\omega_{\text{low}} &= 0.89 \times \omega_{\text{center}} \\ \omega_{\text{high}} &= 1.12 \times \omega_{\text{center}}\end{aligned}\quad (3.15)$$

The center frequencies are defined by ISO 2631. Based on ISO 2631 [2,3] the RMS of the vertical and the longitudinal acceleration at the driver's seat are calculated from the respective acceleration PSDs ( $S(\omega)$ ) at the driver's seat for various center frequencies using the following formula,

$$a_{\text{rms,seat}}(\omega) = \int_{\omega_{\text{low}}}^{\omega_{\text{high}}} S_{\text{seat}}(\omega) \cdot d\omega \quad (3.16)$$

The 1997 amended ISO 2631 dropped the dependency of the comfort criteria on time. ISO 2631:1997 [3] defines the calculation of a single weighted RMS acceleration number for measurement of ride comfort. In this thesis, the time dependent comfort boundaries are retained since they provide a good reference point. Plotting the RMS of the accelerations at the driver's seat against frequency of vibration helps in identifying the modes which are close to or above the time comfort boundaries. The vibration problem is then reduced to finding methods for better isolation at the driver's seat for the problem modes.

The single valued weighted RMS acceleration is calculated as,

$$a_{\text{rms,weighted}} = \left[ \sum (W(\omega) a_{\text{rms}}(\omega))^2 \right]^{0.5} \quad (3.17)$$

where  $W(\omega)$  is the weighting factor specified in ISO 2631:1997 [3] at each center frequency  $\omega_{center}$ .

The total weighted RMS acceleration due to vertical acceleration (z) and fore-aft acceleration (x) is defined as,

$$a_t = \sqrt{a_{rms,weighted}^2(x) + a_{rms,weighted}^2(z)} \quad (3.18)$$

Once the total weighted RMS acceleration at the driver seat has been calculated, it can be compared to the comfort levels specified in ISO 2631-1:1997

**Table 3.4: ISO 2631 Weighted RMS Acceleration Comfort Levels**

Overall Weighted Acceleration		ISO 2631 Comfort Level
m/s <sup>2</sup>	G	
<0.315	0.032	Not Uncomfortable
0.315 – 0.63	0.032 – 0.064	A Little Uncomfortable
0.5 – 1	0.051 – 0.102	Fairly Uncomfortable
0.8 – 1.6	0.082 – 0.163	Uncomfortable
1.25 – 2.5	0.125 – 0.255	Very Uncomfortable
2.5>	0.254>	Extremely Uncomfortable

### 3.4 Model validation with TruckSim

Ride data were not available for the prototype model. To validate the model, the simulation tool developed was validated against the commercially available truck dynamics simulator, TruckSim. TruckSim models the tractor and the trailer sprung masses as lumped rigid bodies

with 6 d.o.f. for each. TruckSim represents each axle suspension with 2 d.o.f. and each wheel with 1 spin d.o.f. TruckSim available for this work did not have the following d.o.f.: cab pitch and heave, seat heave, tractor and trailer frame bending, and engine heave. The developed 15 d.o.f. model has greater vertical ride dynamics fidelity compared to the TruckSim model due to the presence of tunable cab and seat suspensions as well as flexible tractor and trailer frames. To validate the model both the static axle loads and the dynamic response of the truck traversing a small bump were compared with those of the TruckSim simulation. The validation process was carried out by defining the same parameter values across the two models, and linearizing the TruckSim suspensions. Since TruckSim models the tractor sprung mass as a rigid lumped mass, the relative motion between the frame and the cab, and the cab and seat in the Matlab/Simulink model must be minimized. This was achieved by increasing the cab and seat stiffness in the Matlab/Simulink model by 5 orders of magnitude. Increasing the natural frequencies of the tractor and trailer frame beaming mode of the Matlab model to beyond 100 Hz effectively made the frames behave as rigid bodies in the frequencies of interest (<25 Hz). The detailed list of modifications to the Matlab model and the parameters specified in the TruckSim model can be found in appendix G.

#### ***3.4.1. Static Axle Loads***

The first step of the validation process was to compare the static axle loads between the Matlab and TruckSim models. The static axle loads for TruckSim were the observed steady state axle vertical loads for a constant velocity run.



With no axle suspensions, the static vertical equilibrium equations for the tractor are indeterminate. However, there are suspensions and if each axle is independent of the others, the system is determinate. There is also kinematic coupling of the tandem axles in TruckSim. These effects are included by means of two configurable parameters in TruckSim – Static load for rear axle of the tandem (tractor and trailer main screen in appendix G) that affects the static axle loads. These two parameters determine the amount of static load allocated to the rear axles of the tandem combinations. For example, a value of 0.25 was prescribed for the configurable parameter for the tractor drive axles. This ensured that the rear drive axle static load was 25% of the total drive axle static load. These two parameters in TruckSim were manually varied till the static axle loads for the Matlab and TruckSim models matched.

**Table 3.5: TruckSim vs Matlab axle loads**

Location	TruckSim (N)	Matlab (N)	% Difference
1st Axle	57749	58167.7	-0.7%
Drive Axle 1	68732	68520.2	0.3%
Drive Axle 2	60864	60586.0	0.4%
Trailer Axle 1	81321	81188.6	0.1%
Trailer Axle 2	65296	65584.7	-0.4%
Fifth Wheel	90527	90442.3	0.09%

A Matlab script was developed to determine the static axle loads and the static deflections. The frame deflection is neglected for static axle load calculations. Details of the equations used to determine the axle load can be found in appendix G.

Table 3.5 compares the static axle loads from the two models. The largest difference observed between the two models was less 1%. The differences in axle loads between the two models were insignificant.

### ***3.4.2 Time Histories Traversing a Bump***

To compare the dynamics of the two models the truck was simulated traversing a small bump at 60 mph. A half sine wave bump of height 1 cm and length 50 cm was chosen to allow smooth load variation. At a speed of 60 mph (26.8 m/s), the temporal frequency of the bump is 26.8 Hz. The input frequency of the bump is therefore much greater than any of the natural frequencies associated with the truck model. For comparison, the wheel hop frequencies are in the range of 8-12 Hz. Due to the short distance between the dual axles ( $\sim 1.3$  m) a wheelbase pitching effect might be observed when traversing a road bump of wavelength twice the axle wheelbase. When traversing such a road bump the two axles of the tandem axle travel 180 degrees out of phase leading to a wheelbase pitching effect. For a wheelbase of 1.3m at 60 mph the frequency associated with this mode is 20 Hz.

Figure 3.4 shows a comparison of the sprung mass dynamics. The convention used by TruckSim is upward vertical motion and nose down (counter-clockwise) pitch motion are positive. The outputs of the Matlab simulation were accordingly modified. The first plot is the road elevation as seen by the different axles. It was observed that there was almost perfect match between the sprung mass response of the TruckSim and Matlab models.

Figure 3.5 shows a comparison of the axle deflections. Positive axle deflection is under compression. It was again observed that there was almost perfect match between the axle deflections of the two models.

Since the static axle loads and dynamic response of the two models are very similar, one can conclude that the reduced order Matlab model matches the TruckSim model.

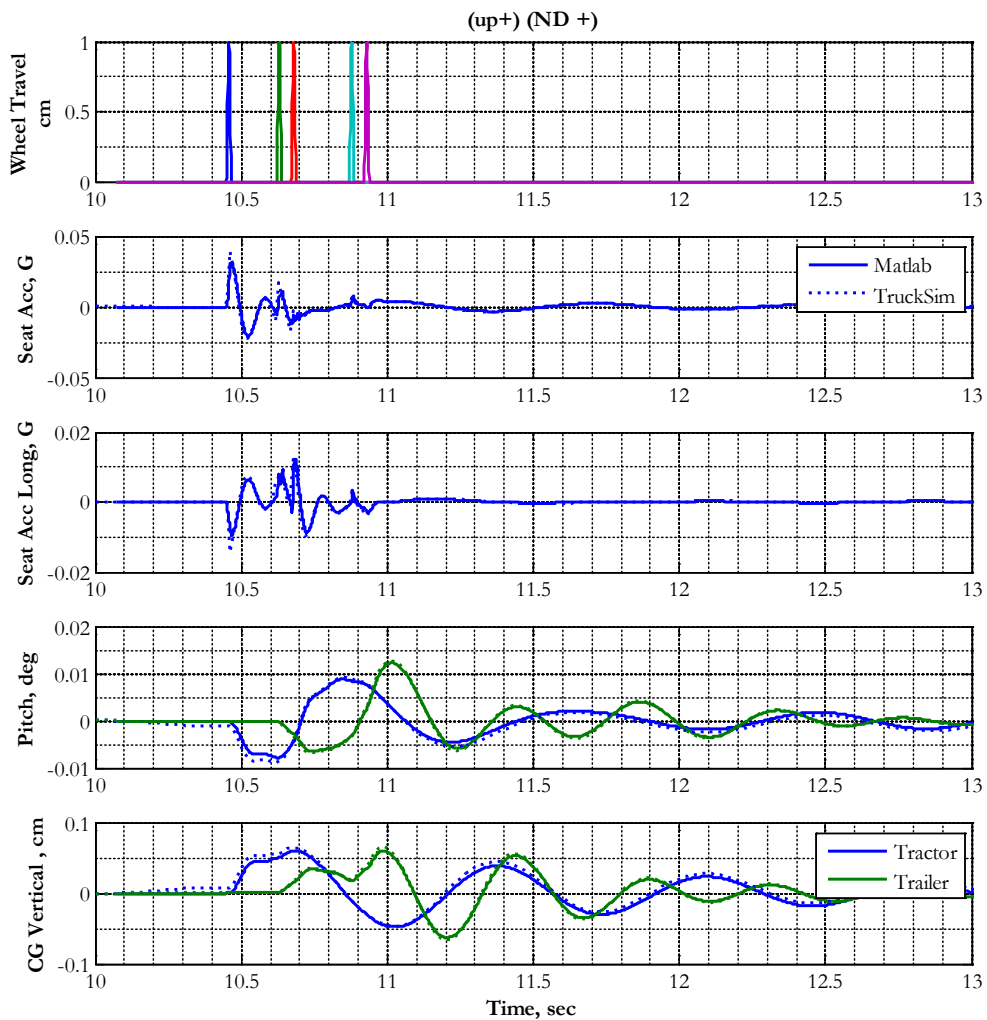


Figure 3.4: Comparison of the Sprung Mass Dynamic Response

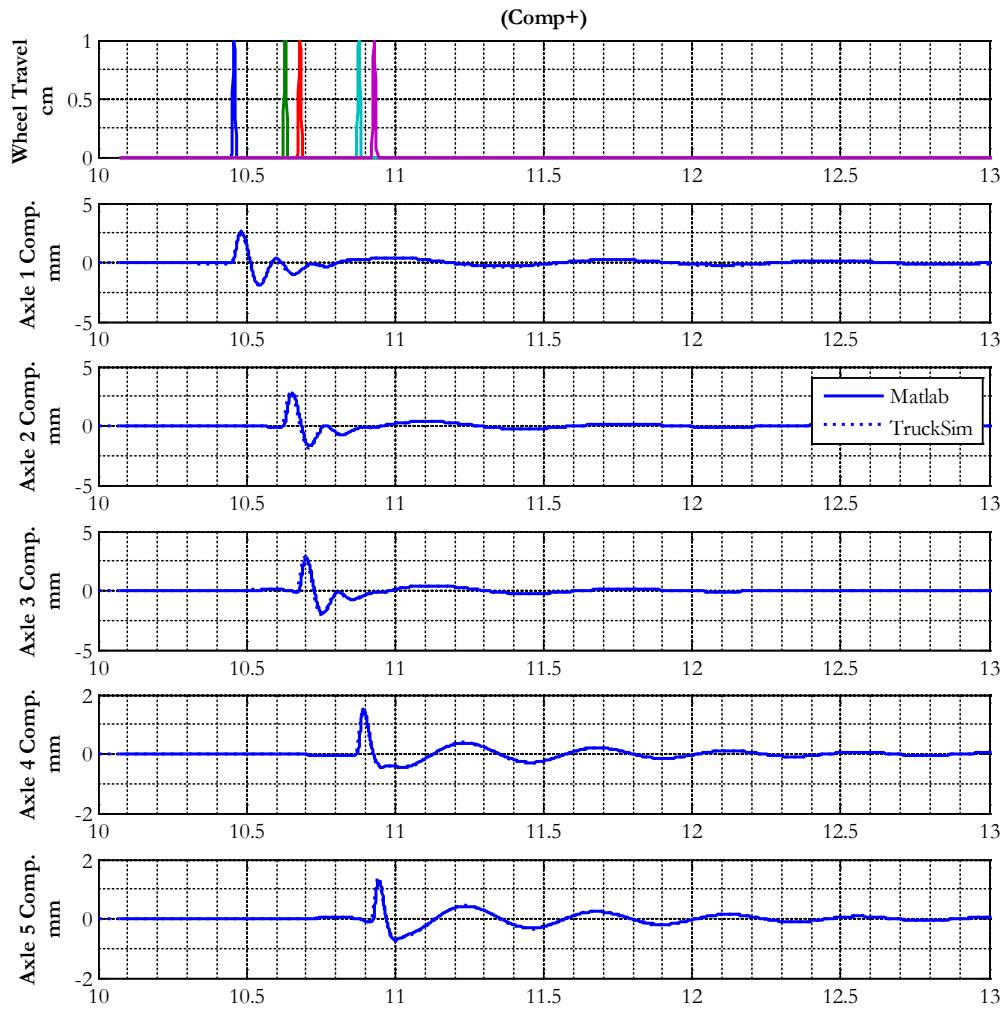


Figure 3.5: Comparison of the Axle Dynamic Response

## CHAPTER 4

### CAB MOUNT AND FRAME FLEXIBILITY DESIGN STUDY

#### 4.1 Baseline Results

The data for the baseline model was provided by a truck manufacturer. All suspensions were modeled as linear components except the seat spring. The standard configuration of the tractor in the USA has the cab mounted on a ladder frame. In the standard configuration, the front of the cab is hinged to the frame and the rear of the cab is suspended using steel springs or air springs. The natural frequency of the cab with rear air springs, a common configuration in the USA, lies in the range 1-1.4 Hz [23]. The natural frequency of the cab with steel springs lies in the range 1.8-3 Hz [6]. The stiffness values of the cab springs were tuned to achieve a cab mode frequency of 1.8 Hz since no force vs. deflection data were found for the cab springs. Nominally at the fifth wheel the tractor frame is effectively pinned to the trailer frame. The fifth wheel was modeled as a stiff suspension between the tractor frame and the trailer frame which provides more latitude for examining different configurations. Data for the dimensions of the truck and the values of various parameters are listed in appendix A. The natural frequencies and damping ratios of the 15 d.o.f. baseline model are listed in Table 4.1.

**Table 4.1: Natural Frequencies and Damping Ratios, Baseline Configuration**

Mode #	Frequency (Hz)	Damping Ratio	Mode Description (Most excited d.o.f.)
1	146.95	0.015	Out of phase heave motion of the frames
2	54.06	0.008	Cab Pitch about rear mount
3	13.74	0.073	Engine Heave
	11.92	0.677	First trailer axle suspension
5	11.51	0.582	Second trailer axle suspension
6	9.54	0.371	Third tractor axle suspension
7	8.96	0.271	Second tractor axle suspension
8	8.7	0.19	First tractor axle suspension
9	8.14	0.008	Trailer Frame Beaming
10	6.9	0.054	Tractor Frame Beaming
11	1.84	0.976	Cab pitch about front hinge
12	0.77	0.7	Seat heave
13	1.36	0.078	Tractor Sprung mass pitch about fifth wheel (Engine heave)
14	1.98	0.193	Counter pitch motion of tractor and trailer frames (Tractor frame heave)
15	1.77	0.078	Trailer sprung mass pitch about fifth wheel (Trailer frame heave)

A modal study was carried out using corresponding eigenvectors and animating the time simulation results. As discussed previously, the assumed modes method was used to approximate the tractor and trailer frame bending. The assumed mode shapes are the fundamental bending modes of an Euler-Bernoulli beam having the following boundary

conditions. The beaming mode shapes for free-pinned (tractor) and pinned-free (trailer) end conditions are shown in Figure 4.1. The first two high frequency modes observed in Table 4. are due to the stiff suspensions at the fifth wheel and at the front of the cab. An engine heave mode was observed around 13.68 Hz. Modes 4 through 8 are the wheel hop modes for the different axles. The wheel hop modes of the trailer axles are more damped than the tractor axles. The trailer frame beaming (mode #9) and the tractor frame beaming mode (#10) are both lightly damped.

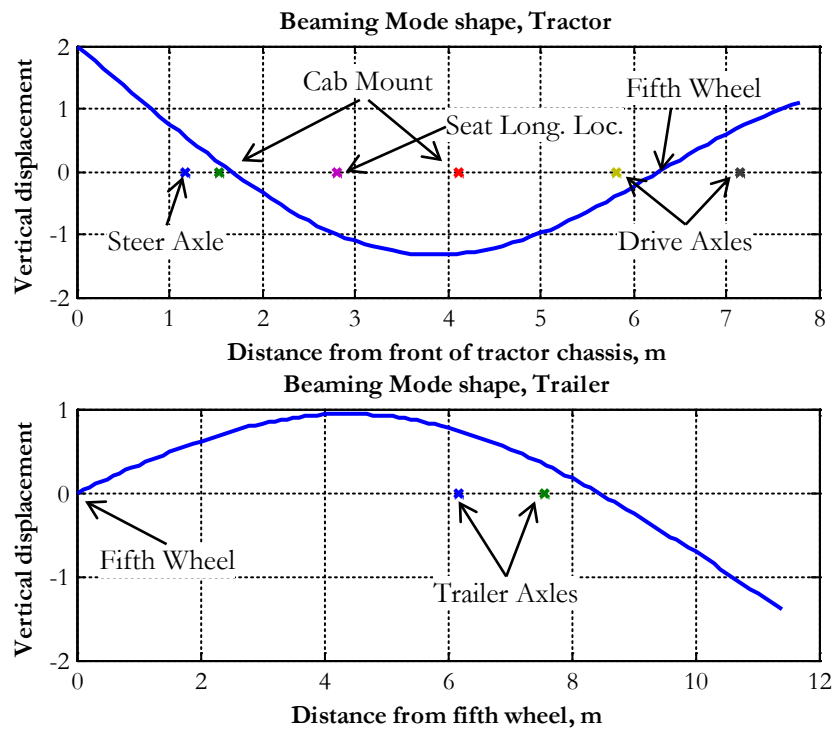


**Figure 4.1: Beaming Mode Shapes of Tractor and Trailer Frames**

Mode #11 is the mode associated with the tractor cab pitching about its hinge at the front cab mount. This mode is almost critically damped. Mode #12 is the seat heave mode. Modes #13 and #14 are of the greatest interest because they are both lightly damped modes and the seat

and cab d.o.f are significantly excited. Mode #13 can be termed as a tractor pitch mode. In this mode the entire tractor sprung mass pitches about the fifth wheel. As shown in Figure 4.2, the trailer frame and axles are not excited in this mode. Tractor frame heave, first (steer) axle heave and cab heave are also significantly excited in this mode.

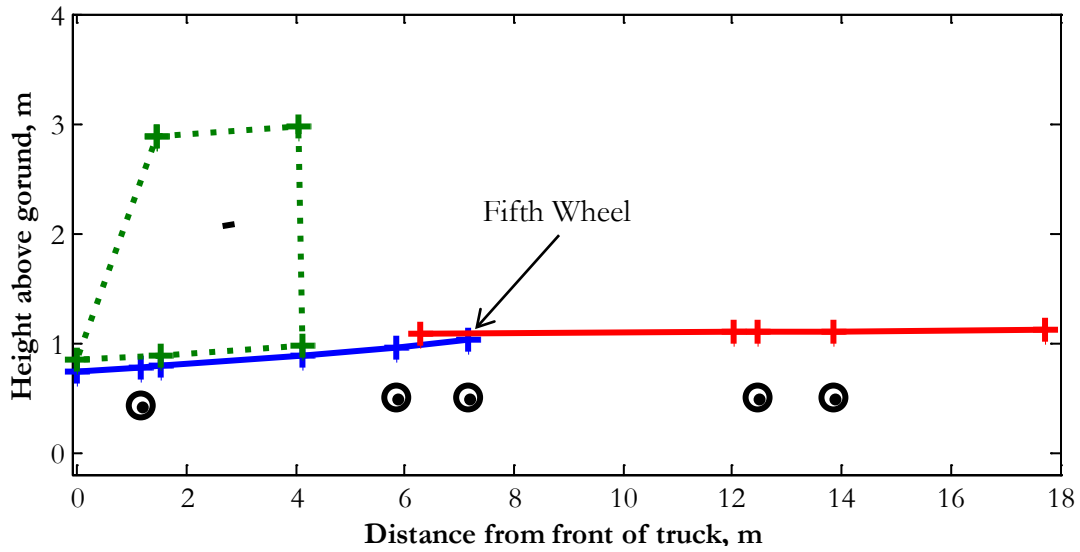


Figure 4.2: Mode #13 at 1.36 Hz

Mode #14 can be described as a counter pitch mode. In this mode, the tractor frame heave and pitch, drive axle heave, cab heave and pitch, seat, and trailer frame heave are the d.o.f. that are significantly excited. It was observed that the tractor and trailer pitch are out-of-phase in this mode. The counter pitching motion of the frames can be clearly seen in Figure 4.3



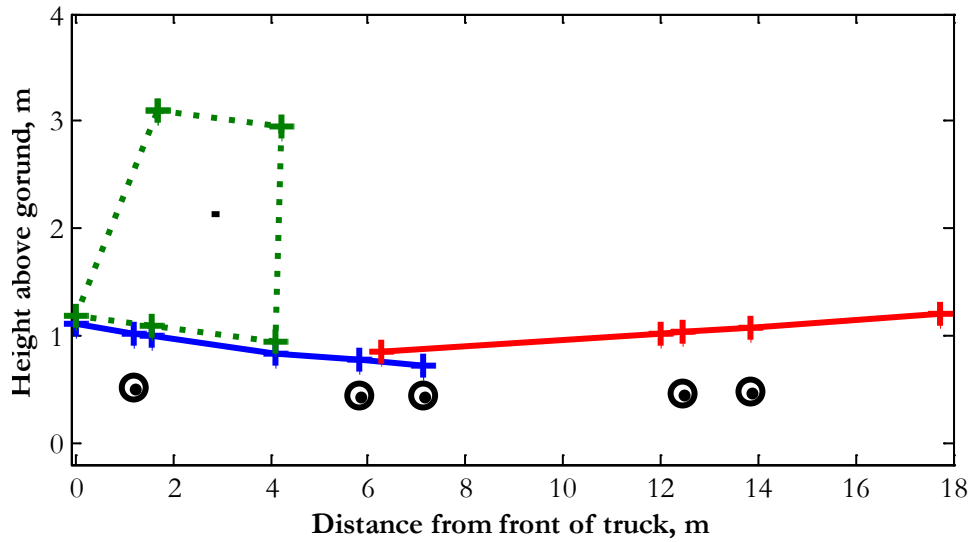


Figure 4.3: Mode #14 at 1.98 Hz

Mode #15 describes the trailer pitch mode. The trailer sprung mass pitches about the fifth wheel in this mode. The trailer axles and pitch motion about the c.g. of the trailer frame are the most excited d.o.f. in this mode. The tractor frame, the cab heave and pitch, and the seat heave are also significantly excited (13-20% of trailer c.g. heave) in this mode.

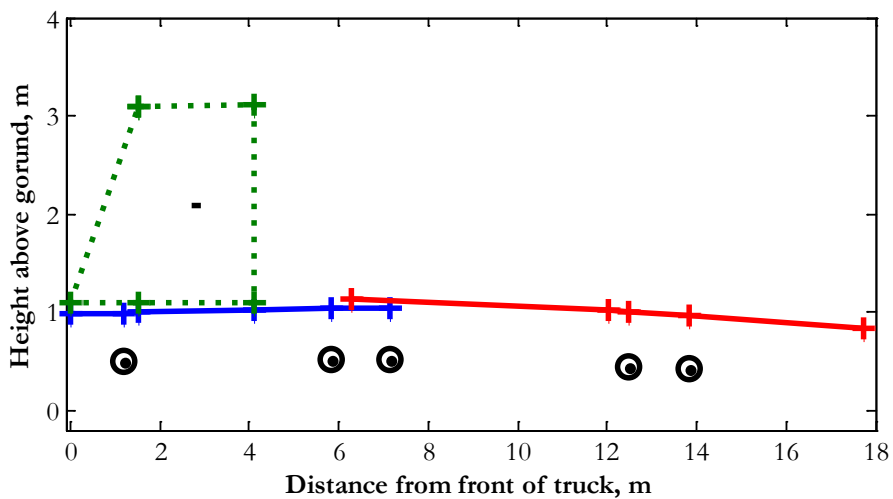


Figure 4.4: Mode #15 at 1.77 Hz

The RMS acceleration at the seat when the tractor semi-trailer was simulated traversing a smooth highway is shown in Figure 4.5. The four lightly damped modes can be clearly observed.

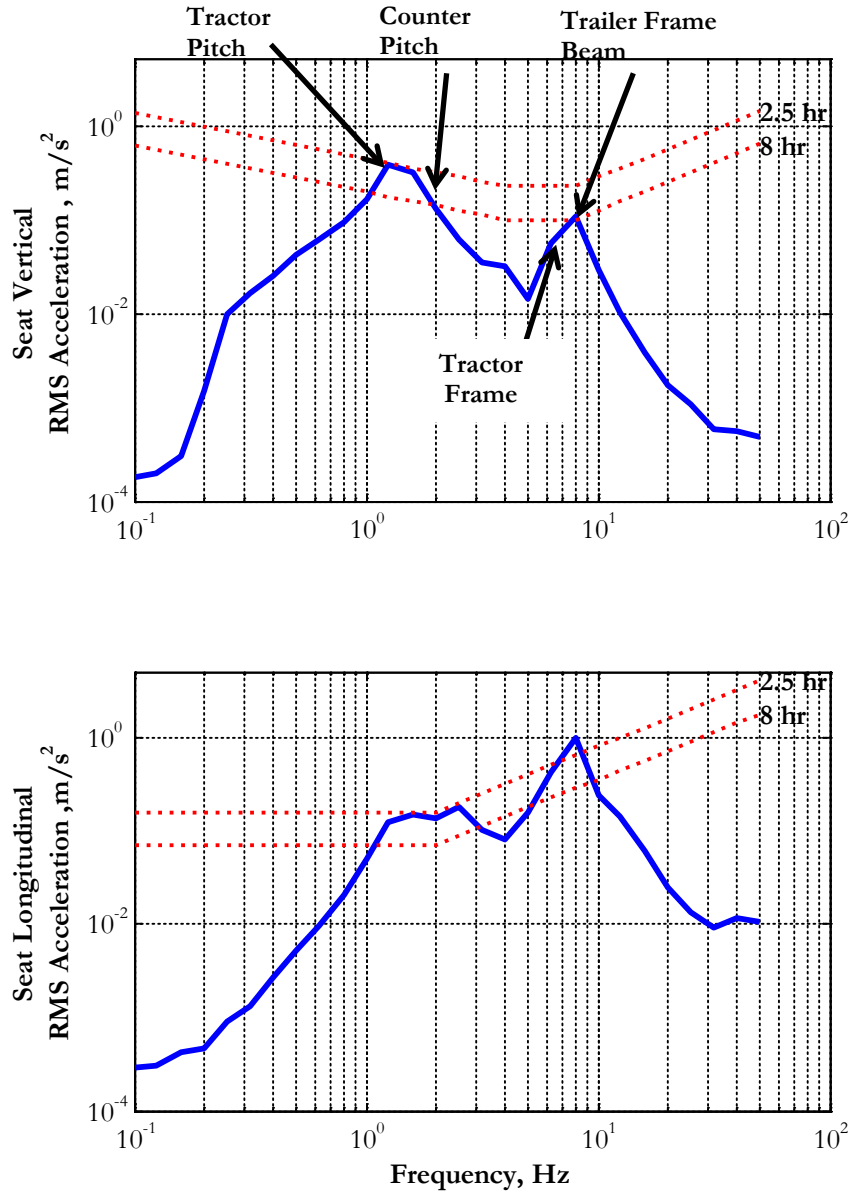
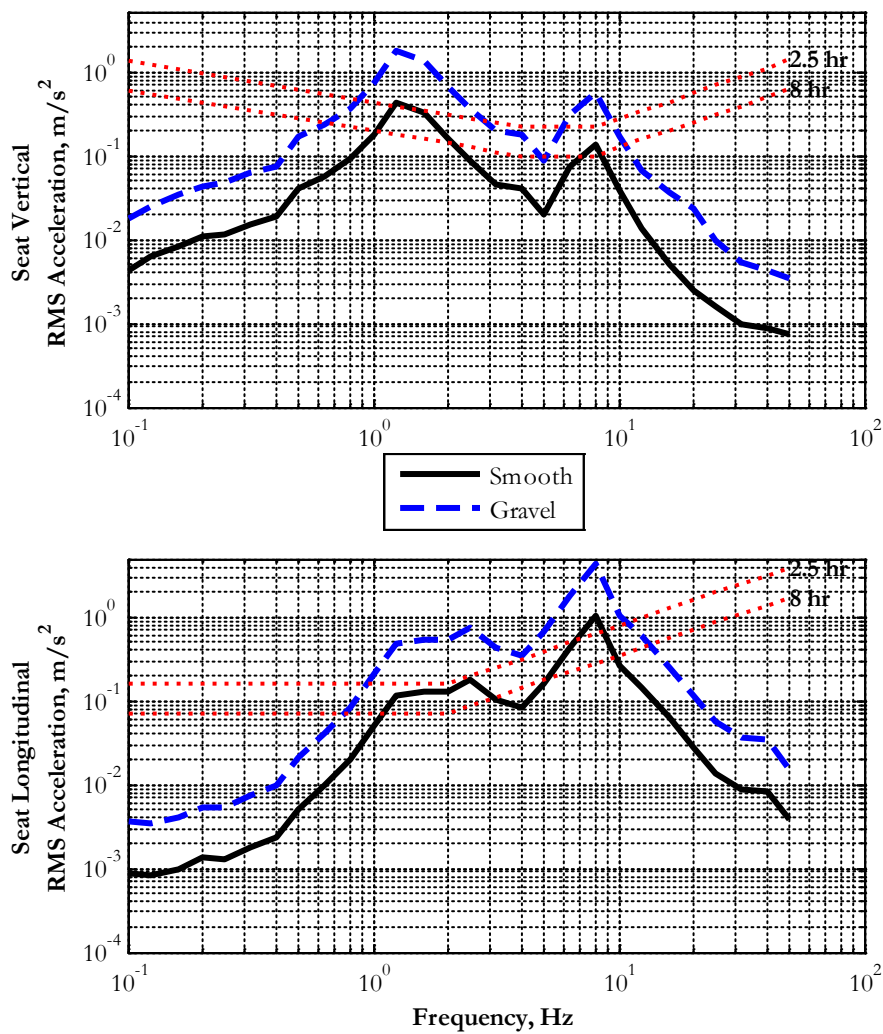


Figure 4.5: Seat RMS Acceleration on Smooth Highway @ 60mph, Baseline Truck

The 2.5 hour and 8 hour comfort boundaries as specified by ISO 2631:1974 for vertical and longitudinal acceleration are superimposed on the RMS acceleration plots. On a smooth highway, the baseline configuration seat acceleration exceeds the vertical 8 hour comfort boundary in the frequency band of 1-2 Hz. Longitudinal seat acceleration exceeds the 8 hour comfort boundary between the frequency bands 1-3 Hz and 6-9 Hz. The lightly damped beaming and tractor pitch modes are the main causes of these vibrations. The seat was constrained with respect to the cab floor longitudinally. Since the seat was located at a significant height above the cab center of gravity, the pitch motion of the cab contributes to longitudinal motion at the driver's seat.



**Figure 4.6: Seat RMS Acceleration for Different Roads**

Figure 4.6 shows the RMS seat accelerations while traversing a smooth highway at 60 mph and a gravel road at 40 mph.

Based on the simulation on the gravel road at 40 mph, the RMS vertical and longitudinal accelerations at the seat exceed the 8 hour comfort boundary in the frequency band of 0.6-

12.5 Hz. The 2.5 hour comfort boundary was also exceeded in the frequency bands 0.9-3 Hz and 6-10 Hz.

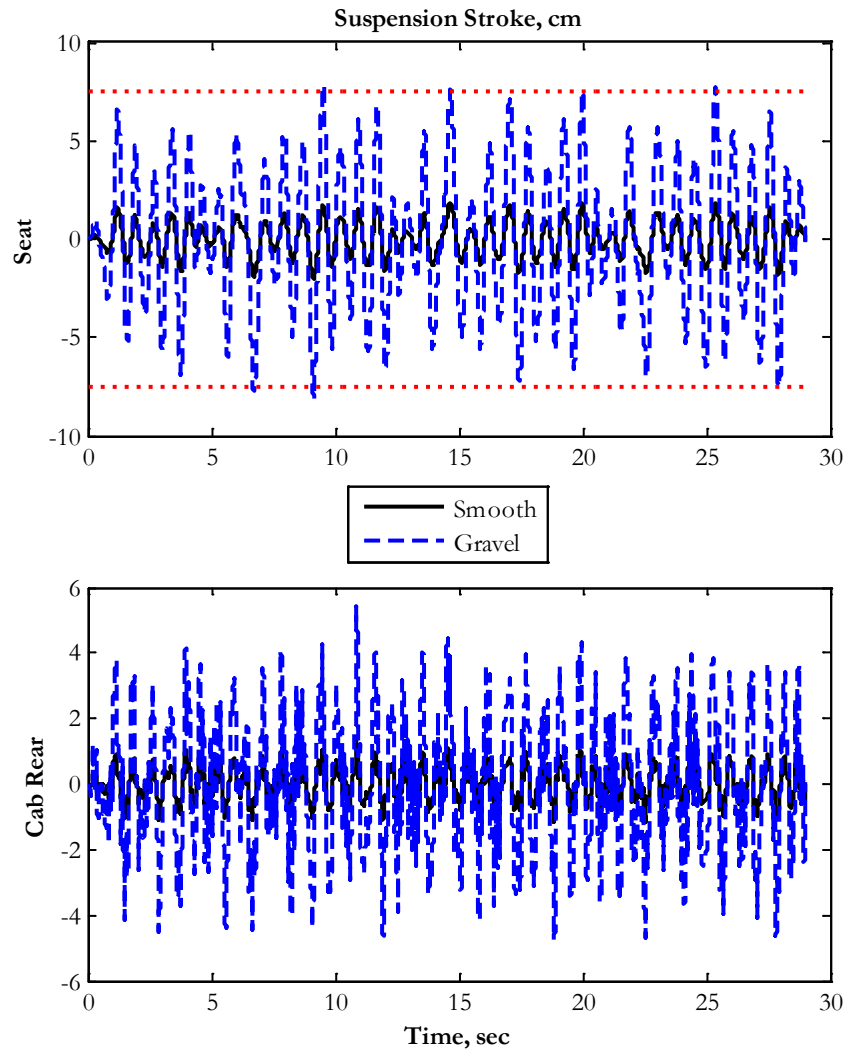


**Figure 4.7: Seat and Rear Cab Suspension Deflections on Smooth Highway and Gravel Road**

The strokes of the cab rear suspension and the seat suspension are shown in Figure 4.7. The red dashed lines represent the bump-stops on the seat suspension. While traversing a gravel road the seat suspension touches the bump-stops on 8 occasions in 30 seconds. A prime

objective of any damper development should be to minimize striking the bump stops. The weighted RMS acceleration and maximum seat suspension strokes are tabulated in Table 4.2.

**Table 4.2: Ride Characteristics for Baseline Configuration**

Measure	Smooth Highway	Gravel Road	units
Weighted Vertical RMS Acceleration	0.031	0.074	G
Weighted Longitudinal RMS Acceleration	0.042	0.099	G
Weighted Total RMS Acceleration	0.052	0.12	G
Maximum Seat Suspension Stroke	3.5	7.9	cm

On a smooth highway at 60 mph the ride at the driver’s seat is “fairly uncomfortable” as per ISO 2631:1997. On a gravel road at 40 mph the ride is “uncomfortable”.

#### **4.2 Effect of Tractor Frame Beaming Frequencies**

The flexibility of the frame structure affects the transmitted vibration to the driver’s seat which can lead to ride discomfort [17]. The fundamental frequency of bending vibration is in the range of 6-9 Hz [14,17]. This frequency range overlaps with the 4-8 Hz frequency band in vertical acceleration where drivers are most sensitive to ride discomfort. One of the ways to decrease vibrational input into the cab is to increase the fundamental frequency of the lightly damped bending mode beyond the 4-8Hz band.

A typical tractor frame is shown in Figure 4.8. The tractor and the trailer chassis frames are composed of two parallel C-channel beams interconnected by cross members to form a ladder like structure when viewed from the top. Various components like the battery, the fuel tank, the fifth wheel assembly, the axle suspensions, etc. are bolted on to the frame. The locations of these components vary depending on the specific truck.

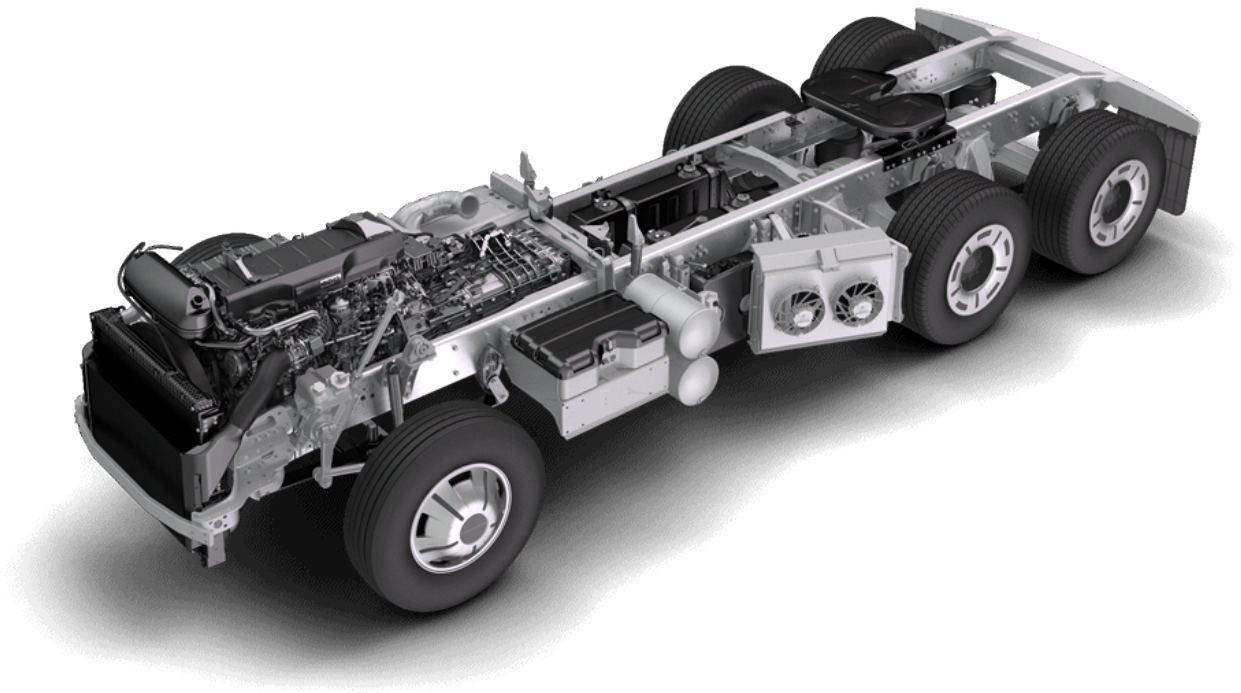


Figure 4.8: Representative Tractor Frame, Freightliner Trucks [51]

The tractor and trailer frames were modeled as Euler-Bernoulli beams. A typical cross-section of tractor frame is shown in Figure 4.9.

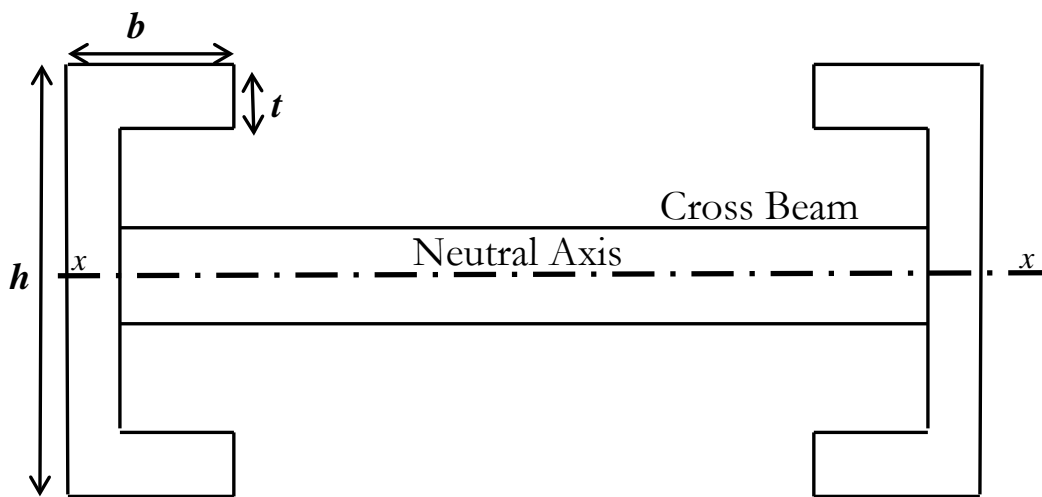


Figure 4.9: Typical Cross-section of Tractor Frame with Cross member

The fundamental beaming frequency of vibration for a beam is given by:

$$\omega_{\text{beam}} = \frac{(\beta l)^2}{l^2} \sqrt{\frac{EI_{xx}}{\rho A + \mu_{\text{comp}}}}, \quad (4.1)$$

where

- $\rho$ , is the density of the material, kg/m<sup>3</sup>,
- $E$ , the modulus of elasticity, Pa,
- $I$ , the cross-section area moment of inertia of the c-channels about the x-axis, m<sup>4</sup>,
- $A$ , the cross-section area of the c-channels, m<sup>2</sup>,
- $l$ , the length of the beam, m,
- $\mu_{\text{comp}}$ , the mass per unit length due additional components and cross-structures, kg/m, and
- $(\beta l)$ , is a constant determined from the boundary conditions

The first two parameters,  $\rho$  and  $E$ , are material properties and the next three are determined by the geometry of the beam. The choice of components bolted onto the frame determines the sixth parameter,  $\mu_{\text{comp}}$ .

Once the material for frame is chosen, the length of the frame is determined according to the function of the truck. The parameters that can be designed are the area moments of inertia and cross-sectional areas of the c-channels. The fundamental frequency of vibration is therefore,



$$\omega_{\text{beam}} \propto \sqrt{\frac{I_{xx}}{\rho A + \mu_{\text{comp}}}} . \quad (4.2)$$

We can see from equation (4.2) that the beaming frequency is a square root function of the area moment of inertia of the c-channels. Mass added to the frame farthest from the x-axis has the greatest influence on the moment of inertia. A study was carried out to find the effect on tractor frame beaming frequency of rigidly mounting steel plates along the top and the bottom of the flanges of the C-channel. The plates are of thickness,  $t_{\text{add}}$ , and are of the same width as the flange of the C-channels. This configuration is illustrated in Figure 4.10.

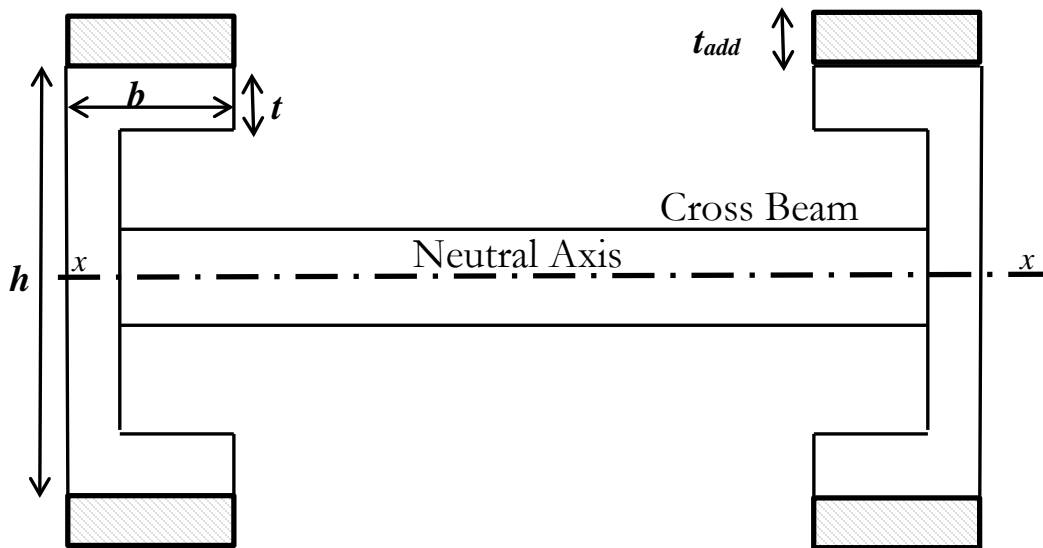


**Figure 4.10: Chassis Frame Cross-section with Plates Mounted for additional Bending Stiffness.**

Since the beaming frequency is a function of the area moment of inertia and the cross-sectional area, the beaming frequency of the frame with the added plates can be calculated as

$$\omega_n = \omega_{\text{nom}} \left( \frac{(I_{x-x,\text{nom}} + I_{x-x,\text{plates}}) \frac{\rho A_{\text{nom}} + \mu_{\text{comp.}}}{I_{x-x,\text{nom}}}}{(\rho A_{\text{nom}} + \mu_{\text{comp.}} + A_{\text{plates}})} \right)^{0.5}, \quad (4.3)$$

where  $I_{x-x,\text{nom}}$  is the total area moment of inertia of the nominal C-channels about the x-axis and  $A_{\text{nom}}$  is the total cross-section area of the nominal C-channels,  $I_{x-x,\text{plates}}$  is the additional moment of inertia due to the plates and  $A_{\text{plates}}$  is the additional cross-section area due the plates, and  $\omega_{\text{nom}}$  is fundamental bending mode frequency of the frame with nominal C-channels. The dimensions of the nominal C-channels are  $b = 300$  mm,  $b = 75$  mm, and  $t = 7$  mm. The American Standard C-channel C12x20 most closely approximates these dimensions. Note that the flange thickness of a standard C-channel is greater than its web thickness. Typical C-channels used for truck frames have a uniform thickness across the web and the flanges. Sample calculations for calculating the beaming natural frequencies can be found in Appendix C.

Adding plates to the C-channel has the effect of increasing the area moment of inertia of the structure but it also adds to the mass of the system. The beaming frequency of the tractor frame with the nominal C-channel is  $\sim 7$  Hz.

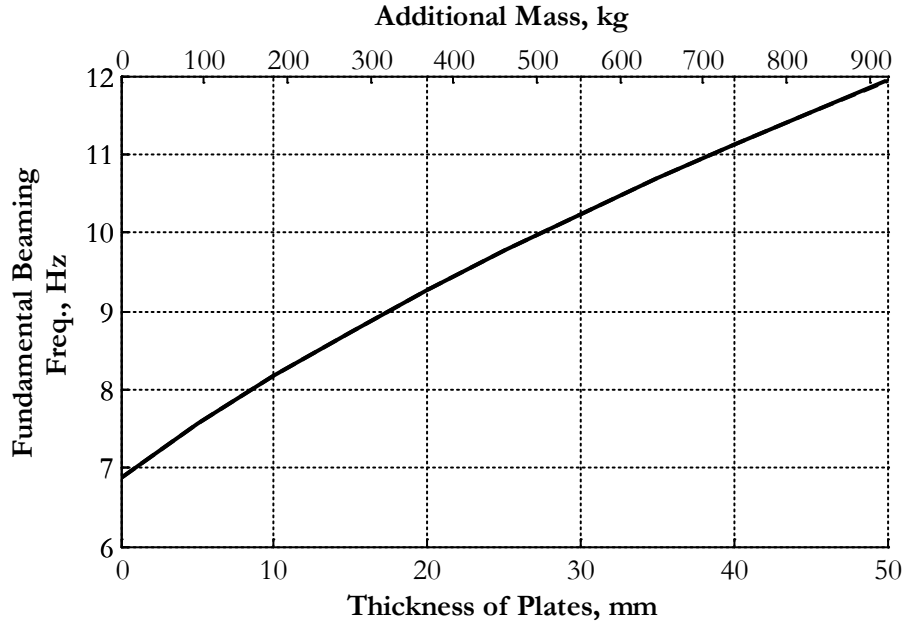


**Figure 4.11: Plate Thickness vs. Frame Beaming Frequency**

The lower x-axis of Figure 4.11 displays thickness of the plates and the upper x-axis shows the additional mass due to the plates. To increase the beaming natural frequency of the frame by 50% (~10.5 Hz), plates with an additional mass of ~625 kg must be added to the tractor frame. The total mass of the nominal frame is 3783 kg. The mass of the plates represents an additional 16% mass. Any addition of dry mass adversely affects the fuel economy of truck.

Another case study was carried out where the C-channels of the nominal tractor frame were replaced by a few American standard C-channels whose dimensions are close to those of the nominal C-channels. Specifically the C10, the C12 and the C15 standard C-channels were considered for this study. Figure 4.12 plots the beaming frequency of the tractor frame versus the mass per unit length of the C-channel for various standard C-channels. Table C.1 in appendix C provides the data used to calculate the beaming frequency.

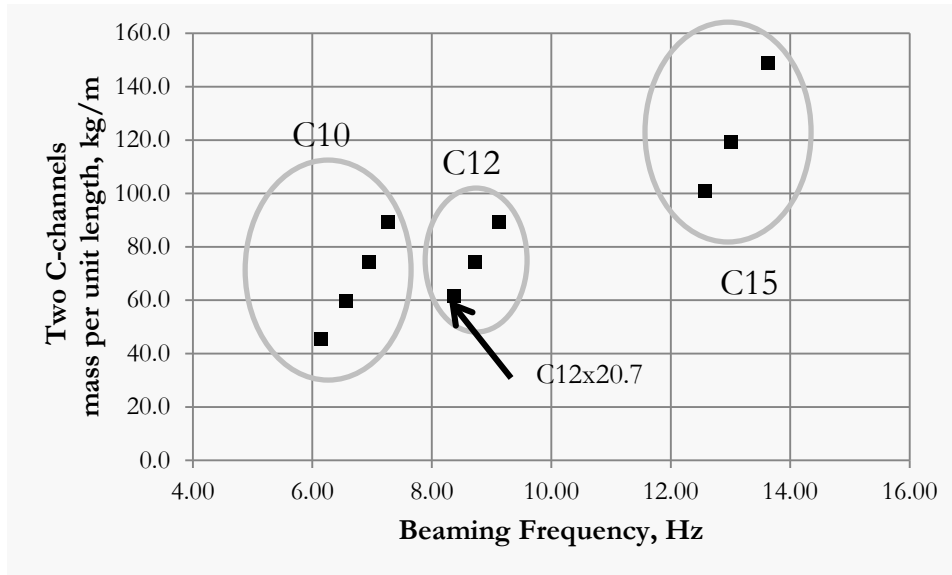


**Figure 4.12: Tractor Frame Beaming Frequencies vs Mass per unit length of C-Channels for standard C-channel**

The frame beaming frequency ( $\sim 8$  Hz) and the corresponding mass per unit length ( $\sim 60$  kg/m) of the 2 C-channels when C12x20.7 (12 inch web depth, 20.7 lb/ft mass density) C-channels are shown in Figure 4.12. To increase the frame beaming frequency by 50%, C15 C-channels need to be used. The lightest of the C15 C-channels (C15x33.9) has a mass per unit length of  $\sim 100$  kg/m. Over a span of 7.87 m this corresponds to an increase of 315 kg. This represents an increase in the dry mass of the tractor frame by about 8.3%.

Figure 4.13 shows the effect of increasing the beaming frequency on ride comfort. Changes in tractor frame beaming frequency did not affect the low frequency ( $<4$  Hz) and high frequency ( $>10$  Hz) responses. However, the RMS acceleration at the driver seat in mid-range frequency (4-8 Hz) changes significantly. Note that wheel hop modes are typically in the 8-12 Hz range.

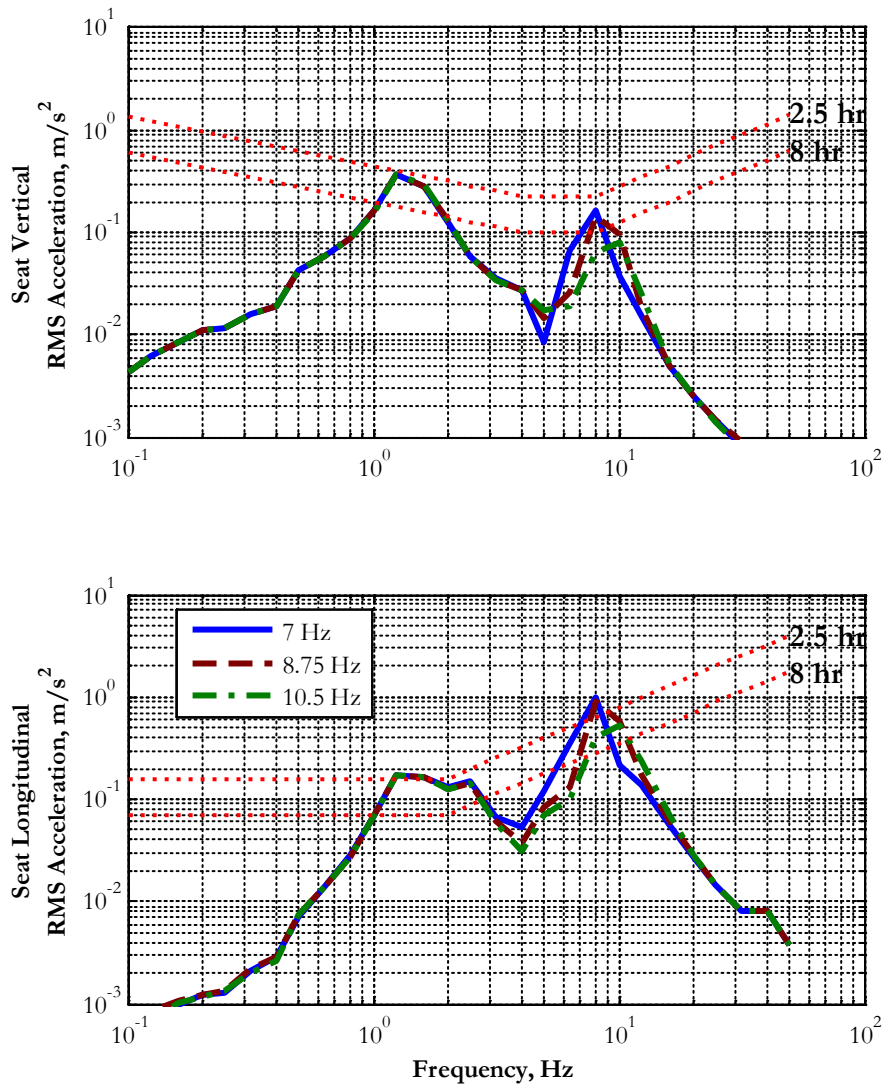
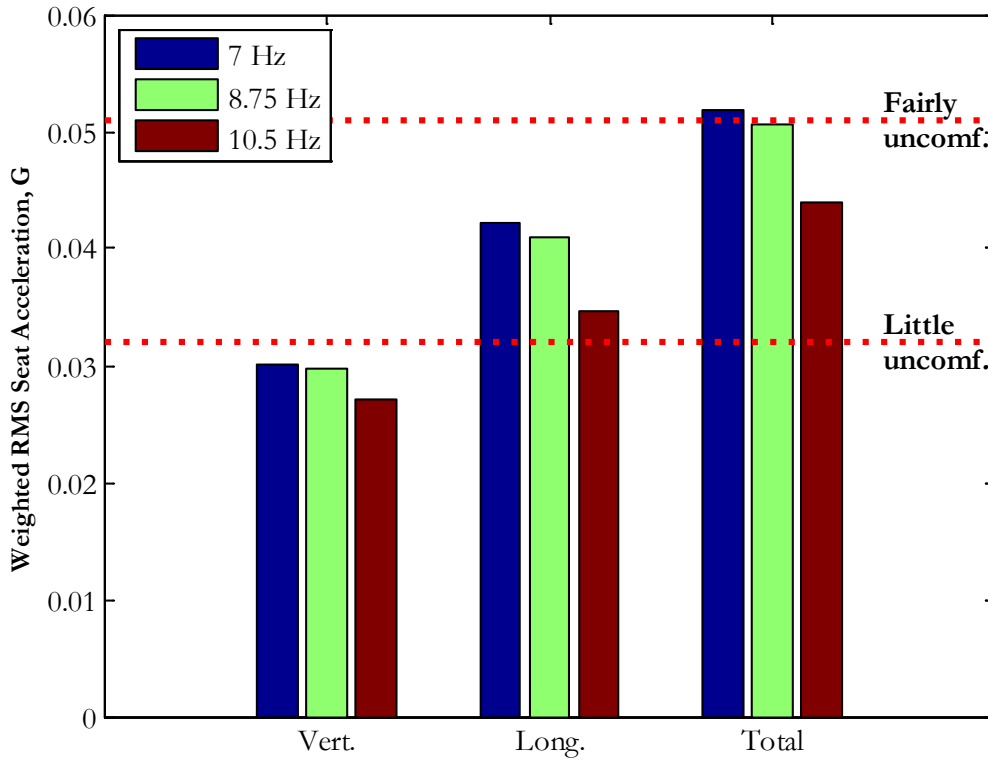


Figure 4.13: Effect of Frame Beaming Frequency on Seat RMS Acceleration.

Figure 4.14 shows the effect of increasing the beaming frequency on the weighted RMS acceleration. Increasing the frame beaming frequency by adding plates on top of the flanges of the channels improves ride comfort by 15% but increases the mass by 16%.



**Figure 4.14: Effect of Beaming Frequency on Weighted RMS Acceleration**

There will obviously be a trade-off of between the improved ride comfort and the decreased fuel economy due to the added mass. This trade-off will have to be evaluated by the truck manufacturers and operators.

### 4.3 Full Cab Suspension

Nominal configurations of tractor semi-trailers in the USA have the front of the cab hinged and the rear suspended. In Europe, fully suspended cabs are more common. A study was conducted to explore the benefits of a fully suspended cab over a rear suspended cab. As a starting point, the rear cab suspension parameters were replicated at the front of the cab.

To find the optimum damping at the front and rear cab suspensions, the damping coefficients of the front and rear cab suspensions were varied. The total weighted RMS acceleration at the driver seat was used as the performance metric. Simulations were carried out on both a smooth highway at 60 mph and a gravel road at 40 mph. Figures 4.15 and 4.16 show the normalized total weighted RMS acceleration at the seat for smooth highway and highway with gravel road profiles when the cab damping coefficients are varied.

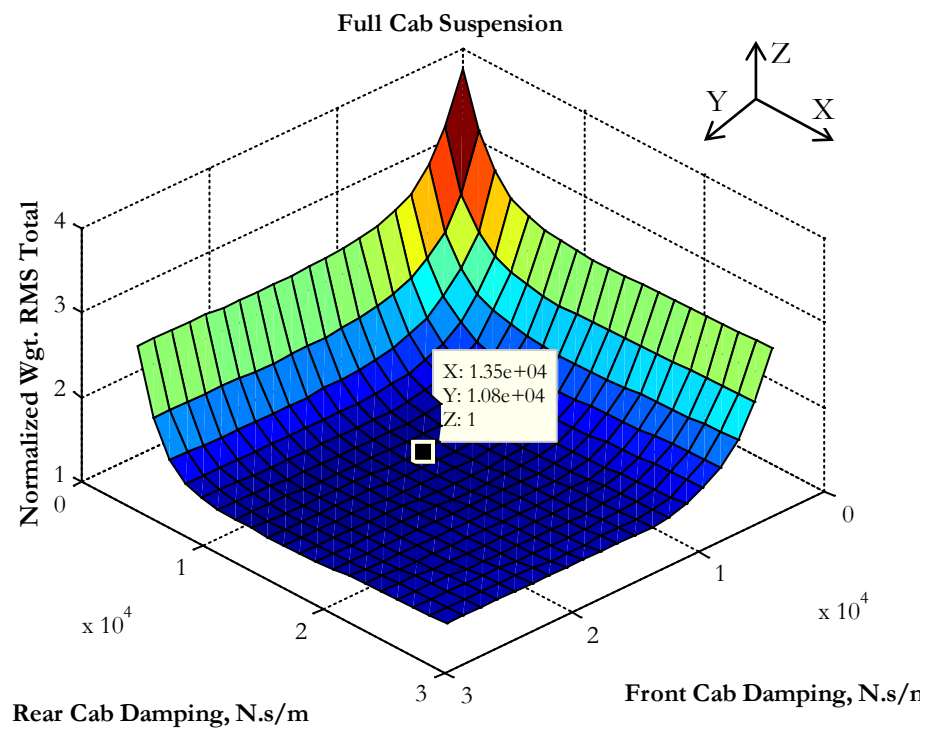


**Figure 4.15: Variation of Total Weighted Normalized RMS Acceleration with Cab Damping over Smooth Highway @ 60 mph**

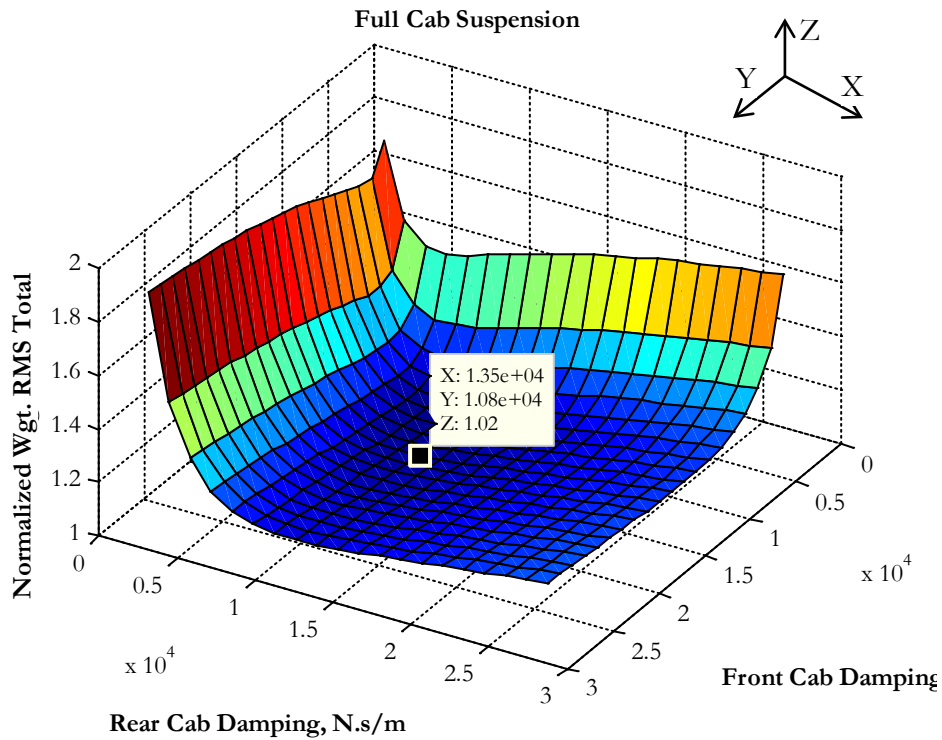


**Figure 4.16: Variation of Total Weighted Normalized RMS Acceleration with Cab Damping over Gravel Road @ 40 mph**

The optimum damping coefficients were found to be 13500 N.s/m for the front cab suspension and 10800 N.s/m for the rear cab suspension. These values of damping coefficient gave the smallest weighted RMS acceleration at the driver’s seat when traversing a gravel road. Smaller cab suspension damping coefficients lead to excessive cab motion which caused the seat suspension to hit the bump-stops. The ride comfort of the baseline configuration over a smooth highway was compared with that of the fully suspended cab having the same suspension at both ends, and with the fully suspended cab with optimized damping parameters in Figure 4.17.



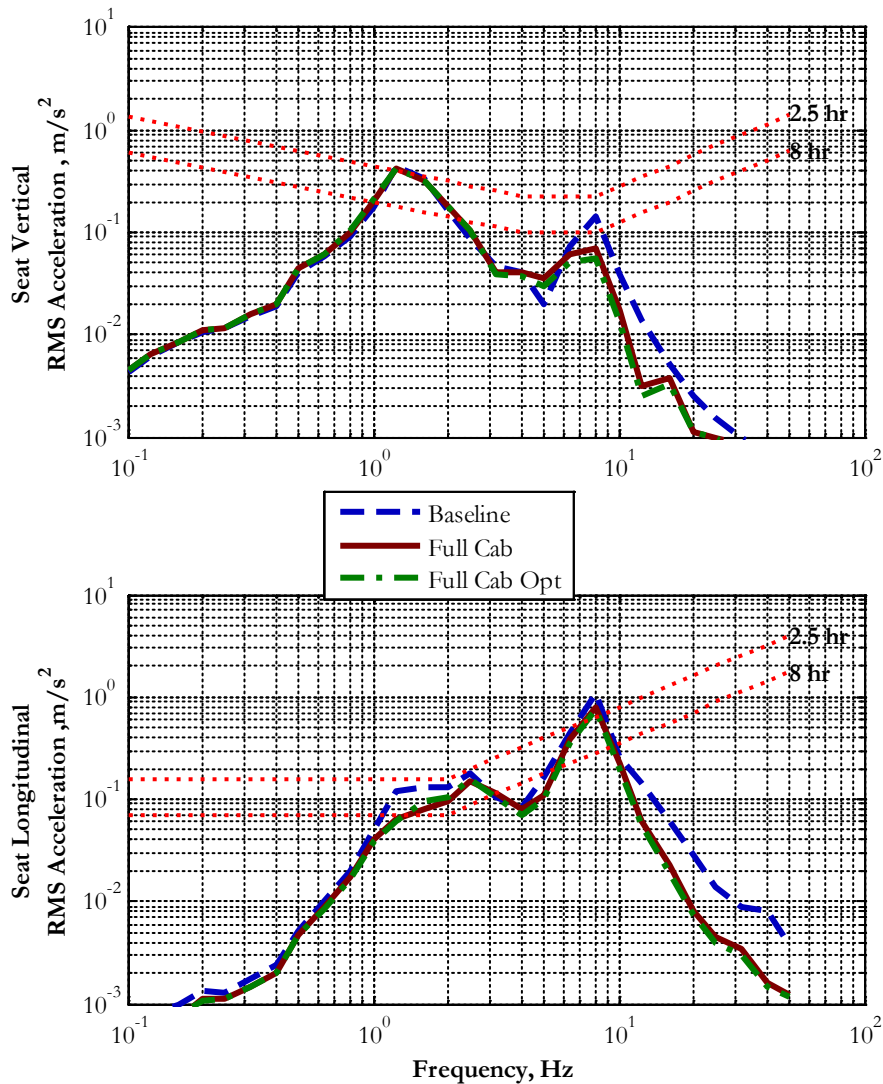


**Figure 4.17: Ride Comfort for Different Passive Cab Suspension Configurations,  
Smooth Highway, 60mph**

The fully suspended cab provided better isolation at higher frequencies. A fully suspended cab was better able to decouple the cab from the tractor frame. The tractor pitch mode (~1.3 Hz) was a lightly damped mode where the tractor frame pitches about the fifth wheel. The

additional damping provided by the front cab suspension increased the damping of the tractor pitch mode.

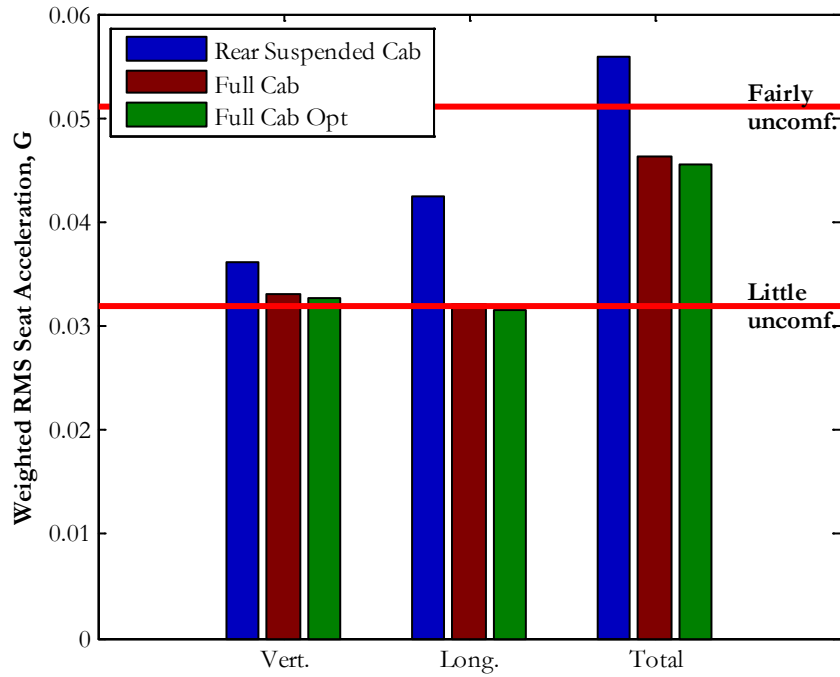


**Figure 4.18: Weighted RMS Acceleration for Different Passive Cab Suspension Configurations, Smooth Highway, 60 mph**

The weighted RMS acceleration values of the three cab configurations are compared in Figure 4.18. Compared to the baseline configuration the fully suspended cab exhibits an 18% reduction in the total weighted RMS acceleration at the seat and up to a 26% reduction in the longitudinal weighted RMS acceleration.

#### **4.4 Effect of Cab Mount Location**

The bending of the tractor frame introduces ride vibration near its resonance frequencies. The most significant bending mode is normally the first mode as it occurs at the lowest frequency and causes the largest displacement. An effective method to prevent this vibration being transmitted to the cab is to locate the cab mounts near the nodal points of the first bending mode. As observed earlier, the beaming mode of the tractor frame has two nodes: one located at the fifth wheel and the other located near the steer axle. Current practice in the industry is to locate the front (hinge) of the cab near the front node. The rear cab suspension is located midway between the two nodes. This presents great challenges in designing the rear suspension. Human beings are most sensitive to longitudinal vibration below 2 Hz. Thus the cab pitch frequency should ideally be designed to be higher than 2 Hz. On the other hand, a lower cab frequency improves vibration isolation. Therefore, choosing the rear cab suspension is always a compromise. It was hypothesized that locating the cab mounts as close to the nodes of the beaming mode as possible would reduce seat vibration.

A study was undertaken to evaluate the effect of cab mount location on ride comfort. Truck ride was simulated over a smooth highway at 60 mph. Both a rear suspended cab design and a fully suspended cab design were evaluated. The total weighted RMS seat acceleration was used to evaluate the effectiveness of varying the mount positions.

##### ***4.4.1 Rear suspended cab***

To find the optimum location for the cab mounts for a rear suspended cab, the mount locations were varied iteratively. Changing the distance between the cab mounts affects the

natural frequency of the cab mode. To counter this effect the cab suspension stiffness and damping were modified so that the cab rigid body mode frequency was close to the baseline cab mode frequency of 1.8 Hz. This was achieved by calculating the rear suspension stiffness and damping using the following formulae,

$$(q+r)^2 k_{cr} = (\hat{q} + \hat{r})^2 \hat{k}_{cr} \quad (4.4)$$

$$(q+r)^2 c_{cr} = (\hat{q} + \hat{r})^2 \hat{c}_{cr}. \quad (4.5)$$

where  $q$  and  $r$  are the modified distances of the cab mounts from the cab CG,  $k_{cr}$  and  $c_{cr}$  are the spring stiffness and damping coefficient to be calculated for the modified cab,  $\hat{q}$  and  $\hat{r}$  are the distances of the cab mounts from the cab CG in the baseline model, and  $\hat{k}_{cr}$  and  $\hat{c}_{cr}$  are rear suspension parameters for the baseline model.

Figure 4.19 shows the total weighted RMS seat acceleration normalized to the minimum calculated. The cab mount positions are displayed as distances from the tractor frame CG. The location of the cab mounts that minimized total weighted RMS seat acceleration are shown in Figure 4.20.

It was observed that the optimum cab mount locations are close to the beaming mode nodal points. Also, the optimum locations are on the ‘inside’ of the frame nodal points. This ensures that the forces through the mounts due to bending are in phase.

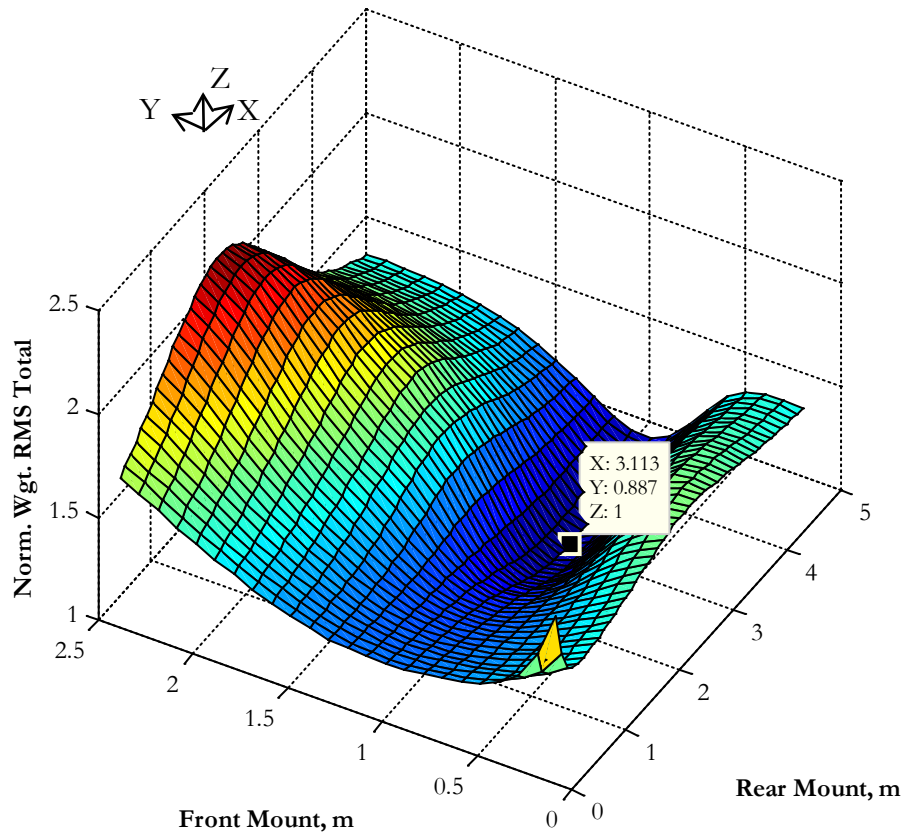


Figure 4.19: Variation of Total Weighted RMS Acceleration with Cab Mount Location.

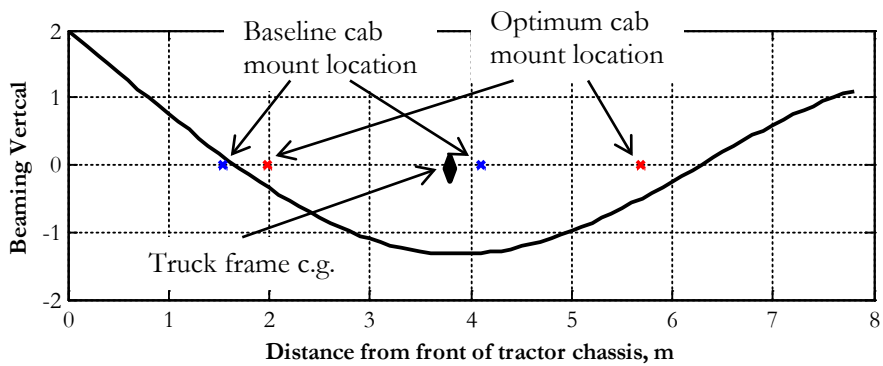
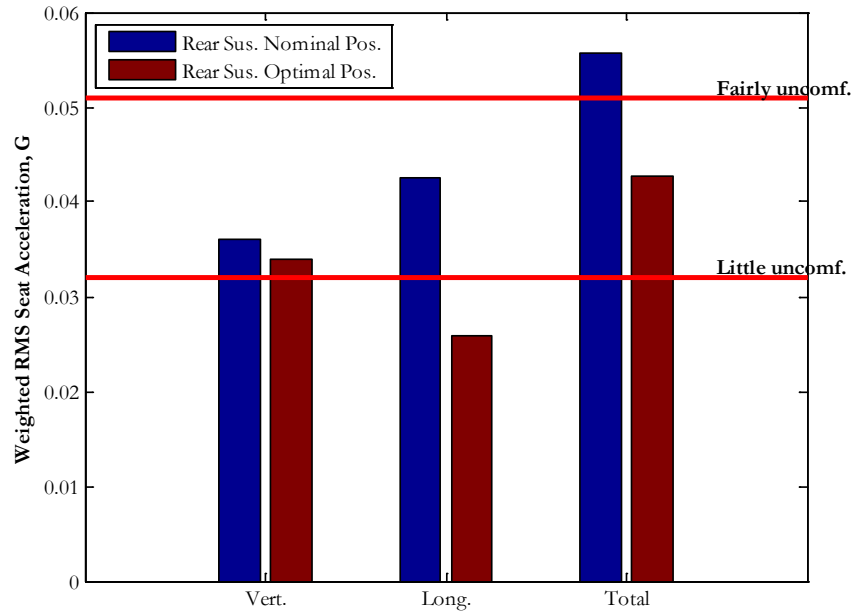
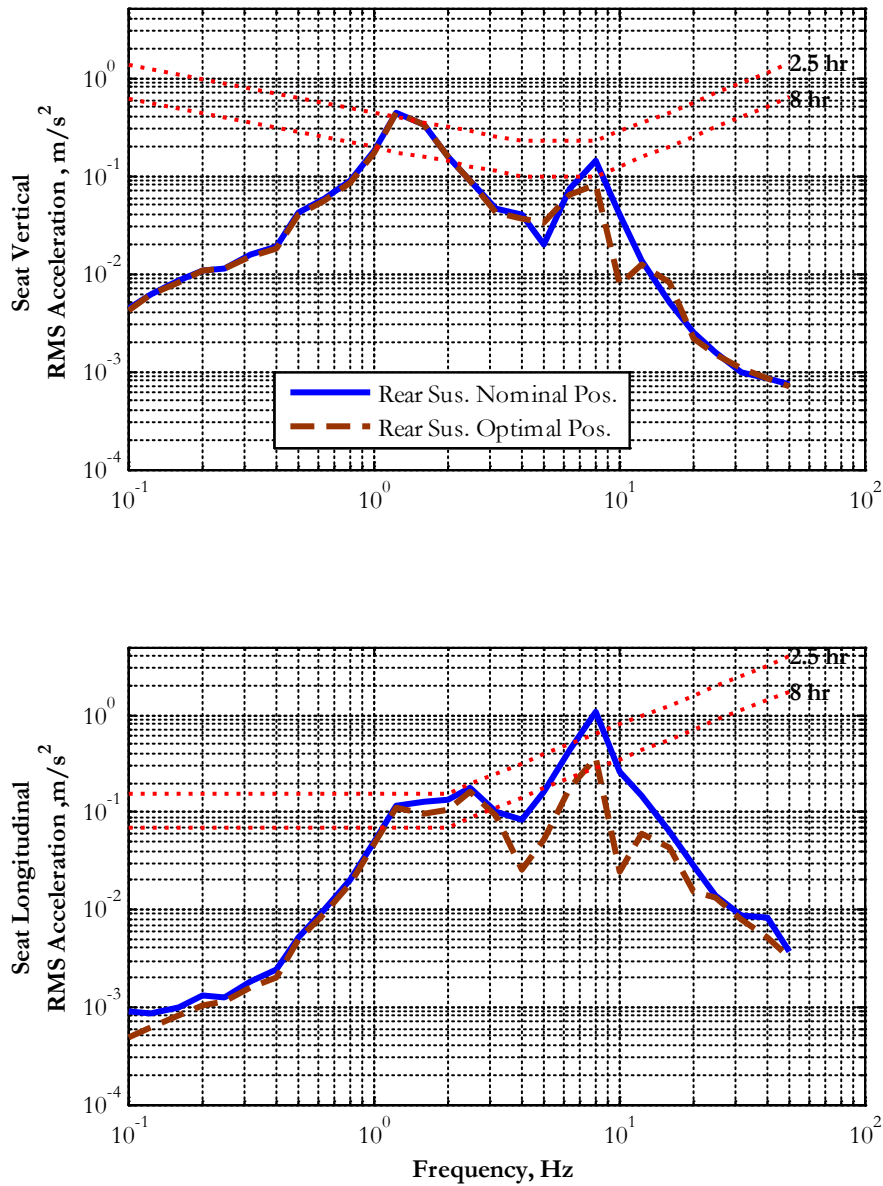


Figure 4.20: Baseline and Optimal Cab Mount Location for Rear Suspended Cab.



**Figure 4.21: Total Weighted RMS Seat Acceleration Comparison of Baseline vs. Optimal Cab Mount Positions, Rear Suspended Cab.**

In Figure 4.21 we observe that by locating the cab mounts close to the nodal points of beaming, the weighted RMS longitudinal seat acceleration was reduced by 39% and the total weighted RMS acceleration at the seat was reduced by 24%.



**Figure 4.22: RMS Seat Acceleration Comparison of Baseline vs. Optimal Cab Mount Positions, Rear Suspended Cab**

A comparison of ride comfort at the seat for the baseline configuration and the optimal cab mount positions is shown in Figure 4.22. The frame bending translates to cab pitch motion. Due to the height of the driver’s seat above the frame, cab pitch motion translates to

longitudinal motion at the driver's seat. Longitudinal ride comfort near 7 Hz was significantly improved by locating the cab suspensions optimally near the nodes.

#### ***4.4.2 Fully suspended cab***

A similar process was adopted to find the optimum suspension locations for the fully suspended cab. The mount locations were varied iteratively. A fully suspended cab has two rigid body modes associated with it. To ensure the rigid body mode frequencies were close to the baseline frequencies as the mount positions were varied, the following equations were solved simultaneously to determine the cab suspension stiffness values.

$$k_{cf} + k_{cr} = \hat{k}_{cf} + \hat{k}_{cr} \quad (4.6)$$

$$q^2 k_{cf} + r^2 k_{cr} = \hat{q}^2 \hat{k}_{cf} + \hat{r}^2 \hat{k}_{cr}. \quad (4.7)$$

$q$  and  $r$  are the modified distances of the cab mounts from the cab CG,  $k_{cf}$  and  $k_{cr}$  are the cab spring stiffness values to be calculated,  $\hat{q}$  and  $\hat{r}$  are the distances of the cab mounts from the cab CG in the baseline model, and  $\hat{k}_{cf}$  and  $\hat{k}_{cr}$  are cab spring rates of the baseline full cab mode. The cab suspension damping coefficients were similarly calculated. Solutions to equations (4.5) and (4.6) which yield negative stiffness values were ignored.



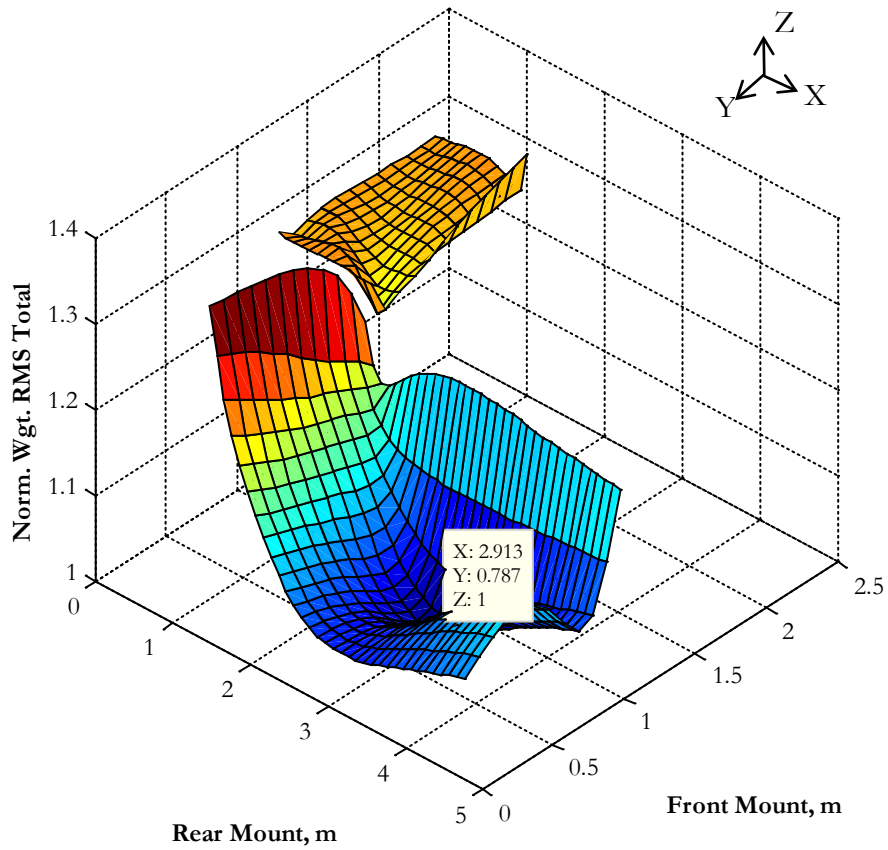


**Figure 4.23: Variation of Total Weighted RMS Acceleration with Cab Mount Locations, Fully Suspended Cab**

Figure 4.23 shows the total weighted RMS seat acceleration normalized to the minimum calculated for the fully suspended cab. The cab mount positions are displayed as distances from the tractor frame CG. The location of the cab mounts for a fully suspended cab that minimized total weighted RMS seat acceleration are shown in Figure 4.24.

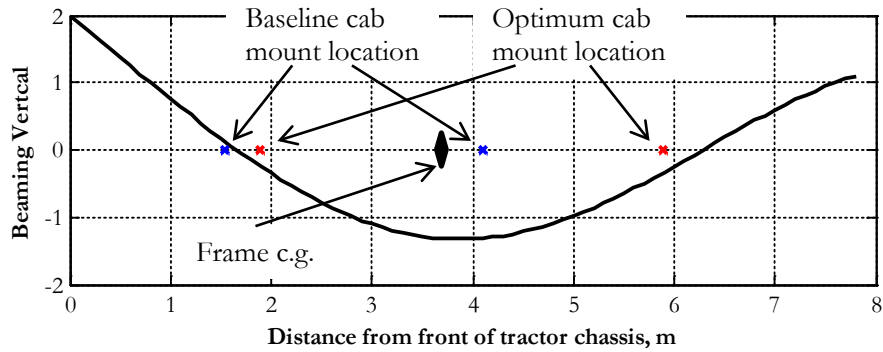


Figure 4.24: Baseline and Optimal Cab Mount Location, Fully Suspended Cab.

As was the case with rear cab suspension, the optimum cab mount locations are “inside” and close to the bending nodes.

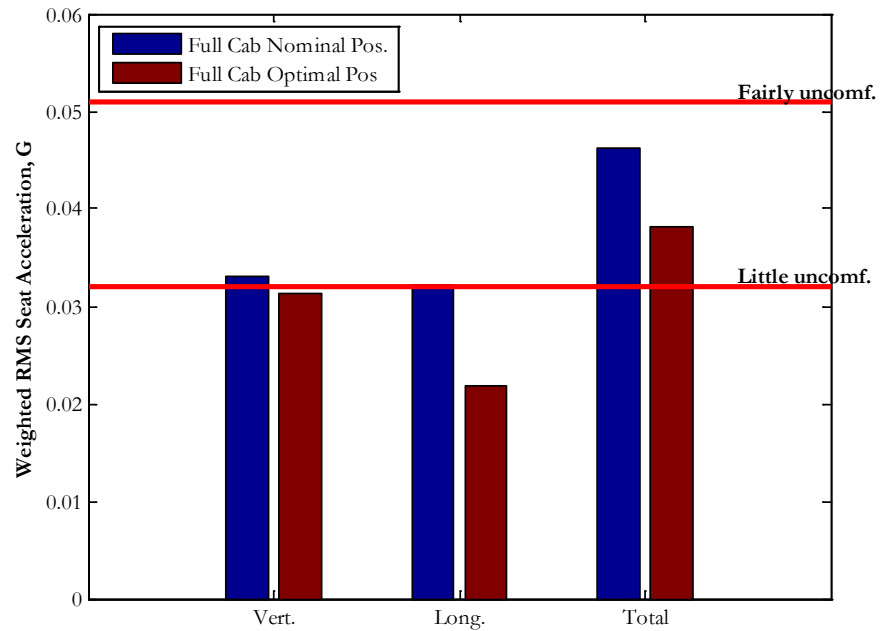
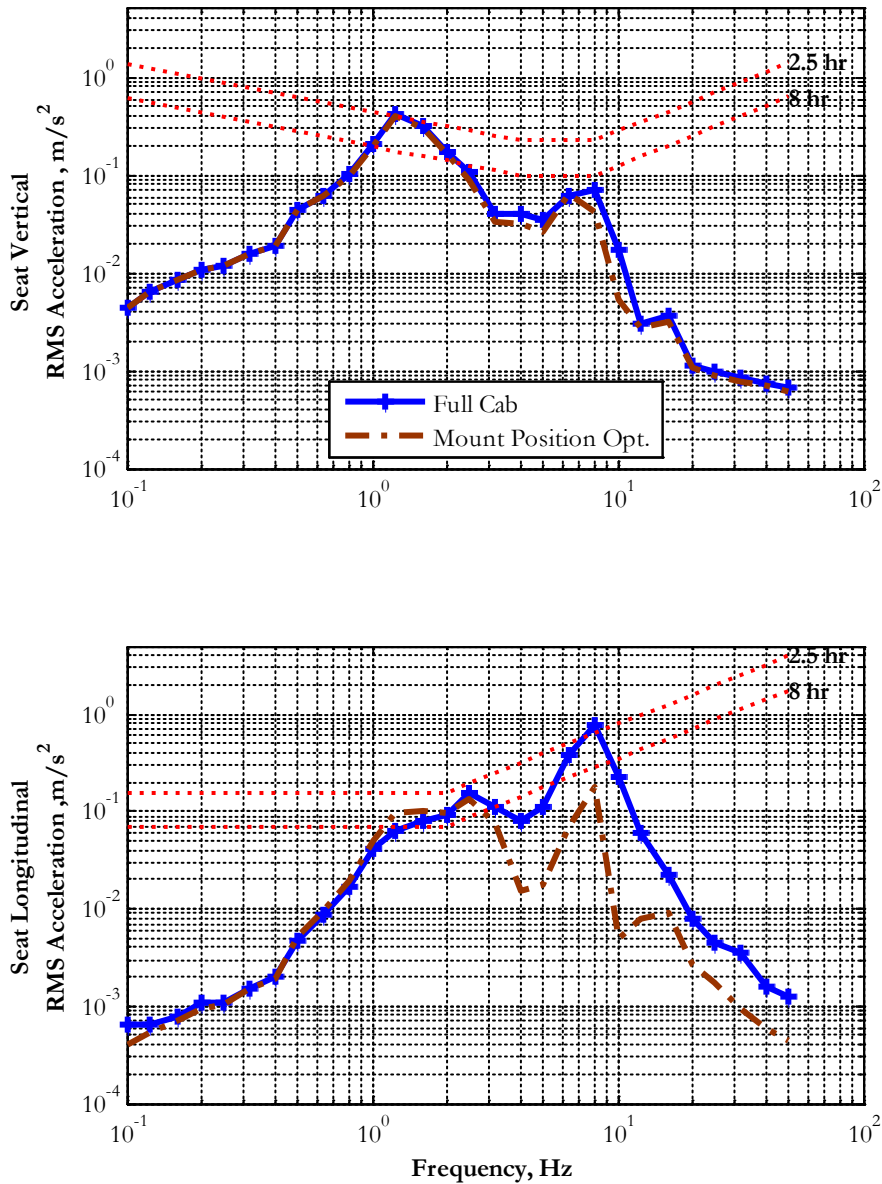


Figure 4.25: Total Weighted RMS Seat Acceleration of Fully Suspended Cab over Smooth Highway at 60 mph (96.56 kph), Nominal vs Optimal Mount Positions.



**Figure 4.26: RMS Seat Acceleration Comparison of Fully Suspended Cab, Nominal vs Optimal Cab Mount locations**

The RMS accelerations at the seat of the nominal full cab configuration and the full cab configuration with the optimal mount locations are shown in Figure 4.26. The optimal mount locations were quite effective in reducing the cab pitch vibrations higher than 3 Hz. By locating

the cab mounts close to the nodal points of beaming, the weighted RMS longitudinal seat acceleration was reduced by 32% and the total weighted RMS acceleration was reduced by 17% (Figure 4.25). By locating the cab mounts of the fully suspended cab at their optimal location (near the beaming nodal points) the weighted RMS longitudinal seat acceleration was reduced by 48% and the total weighted RMS acceleration by 31% when compared to the baseline model (rear suspended cab).

#### 4.5. Summary

**Table 4.3: Driver's Seat Ride Comfort from all the Design Studies**

<b>Controller/Configuration</b>	<b>Weighted total RMS acceleration, G</b>	<b>% Ride Improvement</b>	<b>ISO 2631:1997 Ride Classification</b>
<b>Smooth Highway at 60 mph</b>			
Baseline (Rear Suspended Cab, Tractor Frame 7Hz)	0.052		Fairly Uncomfortable
Tractor Frame 10.5 Hz	0.045	14%	A Little Uncomfortable
Rear Suspended Cab, Optimal Cab Mount Positons	0.04	24%	A Little Uncomfortable
Fully Suspended Cab	0.043	18%	A Little Uncomfortable
Fully Suspended Cab, Optimal Cab Mount Positions	0.036	31%	A Little Uncomfortable
<b>Gravel Road at 40 mph</b>			
Baseline (Rear Suspended Cab, Tractor Frame 7Hz)	0.12		Uncomfortable
Tractor Frame 10.5 Hz	0.11	8.3%	Uncomfortable
Rear Suspended Cab, Optimal Cab Mount Positons	0.095	21%	Fairly Uncomfortable
Fully Suspended Cab	0.1	17%	Uncomfortable
Fully Suspended Cab, Optimal Cab Mount Positions	0.087	28%	Fairly Uncomfortable

From Table 4.3 we can observe that none of the configurations makes the ride “comfortable” on smooth highway at 60 mph. A fully suspended cab with the cab mount located at the most optimal location come closest to making the ride at the driver’s seat comfortable. This

configuration reduces the total weighted RMS acceleration at the driver's seat by 31% compared to the baseline configuration. On a smooth highway the ride is "a little uncomfortable". Adding suspensions at the front cab mount to the baseline configuration, the total weighted RMS acceleration at the seat can be reduced by 18% compared to the baseline configuration on a smooth highway. Though a full cab suspension significantly improves the ride at the driver's seat, designing suspensions for the front mount of the cab is a challenging problem. Also, retro-fitting the existing trucks in U.S.A. with fully suspended cabs will be costly.

For a rear suspended cab with the cab mounts close to the nodal points of beaming, the weighted RMS longitudinal seat acceleration on smooth highway at 60 mph is reduced by 39% and the total weighted RMS acceleration at the seat is reduced by 24%. Even over gravel roads at 40 mph the ride is improved by 21%. The optimal locations for the cab mounts are near the nodes of the beaming mode. Locating the rear cab mount near the fifth wheel pin (a beaming mode nodal point) is a challenging design problem due to the limited available longitudinal design space. If properly designed, locating the cab mounts near the beaming mode nodal points could be a fairly cheap retro-fitting exercise that leads to significantly improved ride.

Increasing the beaming mode frequency by increasing the bending stiffness of the frame also improved the ride at the driver's seat. Increasing the beaming mode frequency by 50% compared to a nominal frame improved the ride at the driver's seat by 14% on a smooth highway at 60 mph. However to increase the stiffness of the frame, 15% more mass needs to

be added to the frame. The additional mass will adversely affect the fuel economy of the truck.

This might not be an acceptable trade-off for most truck operators.

## CHAPTER 5

### CONTROL POLICIES FOR SEMI-ACTIVE SEAT DAMPERS

The development of the 15 d.o.f. truck model in Simulink allows for addition of non-linear elements to the model. In view of the emergence and implementation of semi-active dampers in commercial vehicles, a study was carried out to evaluate the application of various control strategies for a semi-active damper at the seat. The latest development in damper technologies like magneto-rheological (MR) dampers and variable orifice hydraulic dampers allow for continuously variable damping rates. Therefore the dampers were modeled to be continuously variable from a minimum to a maximum damping rate.

In this study two novel semi-active damper control policies were explored. When traversing rough roads, the suspension travel limitations play an important role in the driver ride quality. It is obvious that for better ride it is preferable that the suspensions do not hit the bump stops. The two control policies developed in this work help to mitigate this occurrence on rough roads while providing ride improvements on smooth roads when compared to passive seat dampers. This study shows the existence of two possible optimal control force policies based on the spatial characteristics of the seat mount excitation when seat acceleration and suspension stroke are penalized in the performance index. A novel fuzzy logic based switch mechanism was developed to switch between the two optimal policies. An estimator was developed to estimate the seat load and spring stiffness to compliment the developed semi-active damper controller. Thus the system adapts to different seat loads and seat mount excitation.



A novel model predictive controller was also developed incorporating seat excitation preview information and frequency based weighting filters on the seat acceleration. The developed controller solves a nonlinear optimization problem online to determine the optimum damping rate at each time step.

### 5.1 Optimal Policies for Seat Isolation

The seat (with the driver) can be dynamically modeled as a base excited 1 d.o.f. system as shown in Figure 5.. The force acting on the sprung mass,  $u$ , is the control force. The isolation problem is therefore treated in a more general context without any initial assumptions regarding the passivity of the forcing elements. Since the road input to the truck can be assumed to be Gaussian in nature [1], the excitation at the seat mount,  $z_u$ , and the sprung mass deflection,  $z_s$ , are also Gaussian in the linear regime (not hitting the bump-stops).

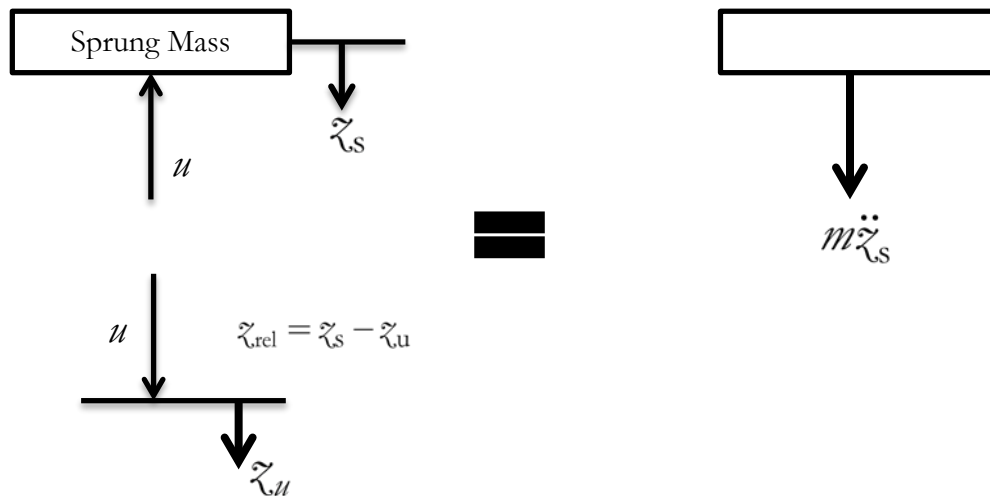


Figure 5.1: A 1 d.o.f. system for developing the optimal control policies

The 1 d.o.f. system can be modeled as:

$$m\ddot{z}_s + u = 0 \quad (5.1)$$

Figure 5.2 shows the power spectral density (PSD) of the deflection at the base of the seat mount when the truck model traverses a gravel road at 40 mph. The PSD of the seat mount deflection is a function of the frequency,  $\omega$  and can be approximated in a power law form as

$$S_e = \frac{K_{psd}}{\omega^N}, \quad (5.2)$$

where  $K_{psd}$  and  $N$  determine the amplitude at 1 rad/s and slope of the road PSD on a log scale respectively.

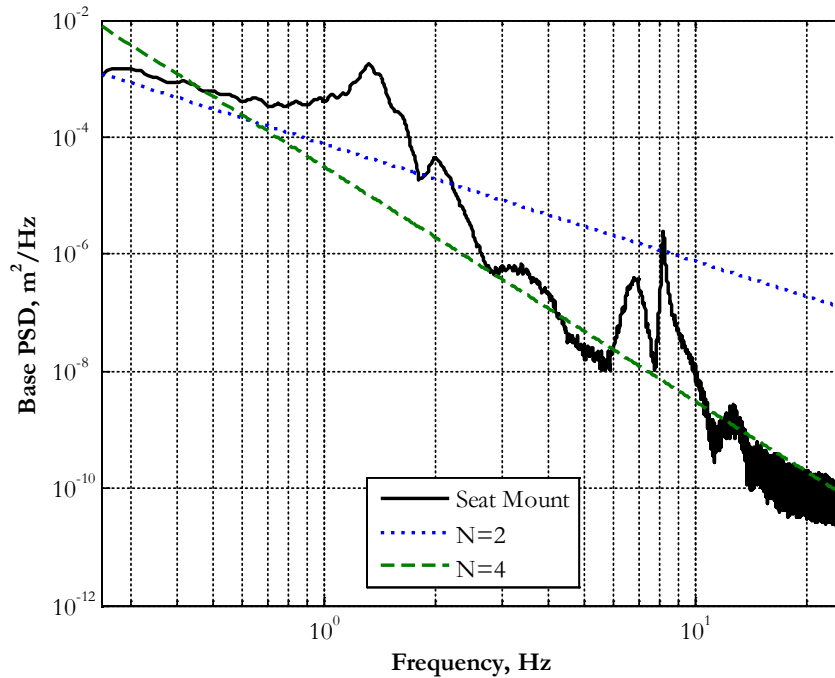


Figure 5.2: PSD of Displacement at the seat mount,  $S_E(\omega)$

The best fits of the seat mount PSDs for different two different  $N$  values are superimposed on the actual seat mount PSDs in Figure 5.2. For  $N = 2$ , there is good fit with the seat mount excitation in the low frequency range ( $< 2$  Hz). The PSD of the velocity of the excitation for this approximation can be derived as

$$S_{\dot{E}} = |(j\omega)|^2 S_E = |(j\omega)|^2 \frac{A}{\omega^2} = A \quad (5.3)$$

Therefore in the low frequency range, the seat mount excitation velocity PSD is a Gaussian white noise.

For  $N = 4$ , there is a good fit with the seat mount excitation in the frequency range of 3 - 20 Hz. The PSD of the acceleration of the excitation for this approximation can be derived as

$$S_{\ddot{E}} = |(j\omega)^2|^2 S_E = |(j\omega)^2|^2 \frac{A}{\omega^4} = A \quad (5.4)$$

Therefore one can conclude that in the frequency range of 3-20 Hz, the seat mount excitation acceleration PSD behaves like Gaussian white noise. It will be shown in the following section that the choice of approximation used leads to different optimal solutions.

Optimal policy 1 was developed by treating the base input velocity,  $\dot{\chi}_u$ , as Gaussian white noise disturbance to the system for the low frequency range ( $< 3$  Hz). The state equations can be written as,

$$\begin{aligned} \dot{x}_1 &= \dot{\chi}_s - \dot{\chi}_u = \dot{\chi}_r = x_2 - v \\ \dot{x}_2 &= \ddot{\chi}_s = \frac{u}{m} \end{aligned} \quad , \quad (5.5)$$

where the state vector is defined as  $x = [\tilde{z}_s - \tilde{z}_u \quad \dot{\tilde{z}}_s]'$ .

The PSD of the base excitation can be expressed as

$$S_e = \frac{A}{\omega^2}. \quad (5.6)$$

Let the performance index be defined as a quadratic function of the relative displacement (stroke) and the sprung mass acceleration.

$$P.I. = \lim_{T \rightarrow \infty} \frac{1}{2} E \left[ \int_0^T (\tilde{z}_r^2 + r \ddot{\tilde{z}}_s^2) dt \right] \quad (5.7)$$

The optimal control policy can be found by minimizing the performance index with respect to the control input  $u$ . Since the system is linear and the performance index is quadratic in nature, the analytical solution to the linear quadratic Gaussian system is feasible. The derivation of the optimal control law can be found in Appendix D. The optimal control law for the system is

$$\text{Policy 1: } u^* = -k_s^* \tilde{z}_r - c_{sky}^* \dot{\tilde{z}}_s \quad (5.8)$$

One can observe that the optimal feedback control is a combination of passive spring and a hypothetical skyhook damper. A physical realization of the optimal control policy is shown in Figure 5.3

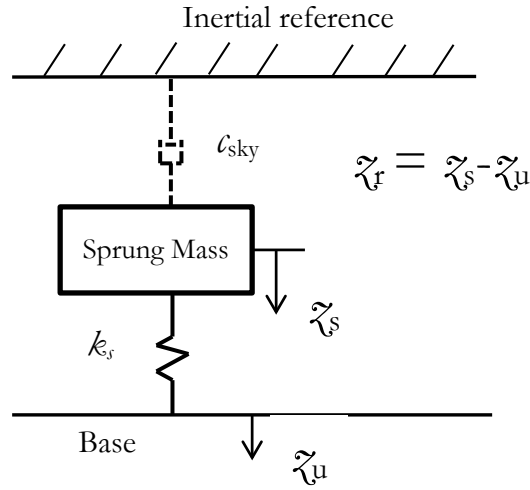


Figure 5.3: Physical realization of control policy 1

In this configuration a passive damper is placed between the sprung mass and an imaginary “sky” reference frame. This damper configuration is widely known as the ideal “skyhook” damper. The idea of the skyhook damper has existed since the early 1970s [2]. The concept was initially developed for automobile primary suspensions. The force generated by this conceptual configuration is a weighted sum of the forces which are proportional to the relative displacement and the absolute velocity of the sprung mass.

Optimal policy 2 was developed by treating the base input acceleration,  $\ddot{z}_u$ , as Gaussian white noise disturbance to the system. The PSD of the base excitation can be expressed as

$$S_e = \frac{A}{w^4}. \quad (5.9)$$

The state equations can be written as

$$\begin{aligned}\dot{x}_1 &= \dot{z}_s - \dot{z}_u = \dot{z}_r = x_2 \\ \dot{x}_2 &= \ddot{z}_s - \ddot{z}_u = \frac{u}{m} - v \quad ,\end{aligned}\tag{5.10}$$

where the state vector is defined as  $x = [z_s - z_u \quad \dot{z}_s - \dot{z}_u]'$ .

If the performance index is defined as in equation (5.7), the optimal control policy to minimize the performance index with respect to the input,  $u$ , can be found analytically. The derivation of the control policy can be found in Appendix D. The optimal control policy 2 for this process is

$$\text{Policy 2: } u^* = -k_s z_r - c_s \dot{z}_r.\tag{5.11}$$

*Remark 1:* The optimal damping value is a constant as defined by equation (5.12). It is the same for both the optimal policies if the sprung mass and the tuning value in the performance index,  $r$ , are kept the same. Since the spring stiffness  $k_s$  is a function of sprung mass and  $r$ , the same values of sprung mass and  $r$  imply the same  $k_s$  value.

$$c_{\text{sky}} = c_s = c_{\text{optimal}} = \sqrt{2mk_s}.\tag{5.12}$$

In this case, the optimal control policy is the well known parallel combination of a passive spring and a passive damper.

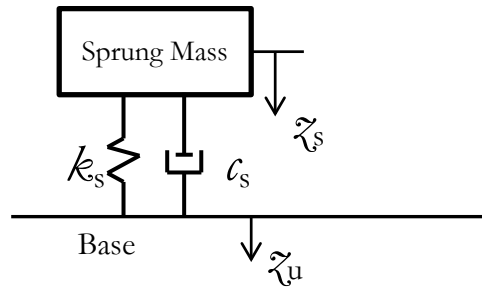


**Figure 5.4: Physical Realization of Control Policy 2**

A physical realization of the optimal control policy 2 is shown in Figure 5.4. The passive spring-damper system is essentially a special closed loop feedback system which generates a force which is weighted sum of the forces proportional to the relative position and the relative velocity of the sprung mass.

Therefore, there are the two possible optimal policies based on the spatial characteristics of the base excitation. The following sections will compare the seat acceleration and suspension stroke response due to the two policies for a truck traversing various roads. The strength and weakness of each policy will be discussed in more detail.

## 5.2 Skyhook Law Controller

As seen in the previous section, one of the optimal isolation systems involves a skyhook damper. The ideal skyhook damper is a hypothetical concept. The ideal skyhook damper can be realized in either of two ways. One way to develop the skyhook damping force is by using active force generators. This results in complex systems requiring significant amount of power input. Another approach is to approximate the ideal skyhook damper with a semi-active

damper. The damping coefficient of the semi-active damper can be varied continuously between a minimum and a maximum. Semi-active dampers are configured similar to passive dampers, i.e. they are located between the sprung mass and the base. The damping force generated by the damper can be expressed as,

$$f_{semi} = c_{semi} v_{relative} \quad (5.13)$$

where  $c_{semi}$  is the variable damping coefficient.

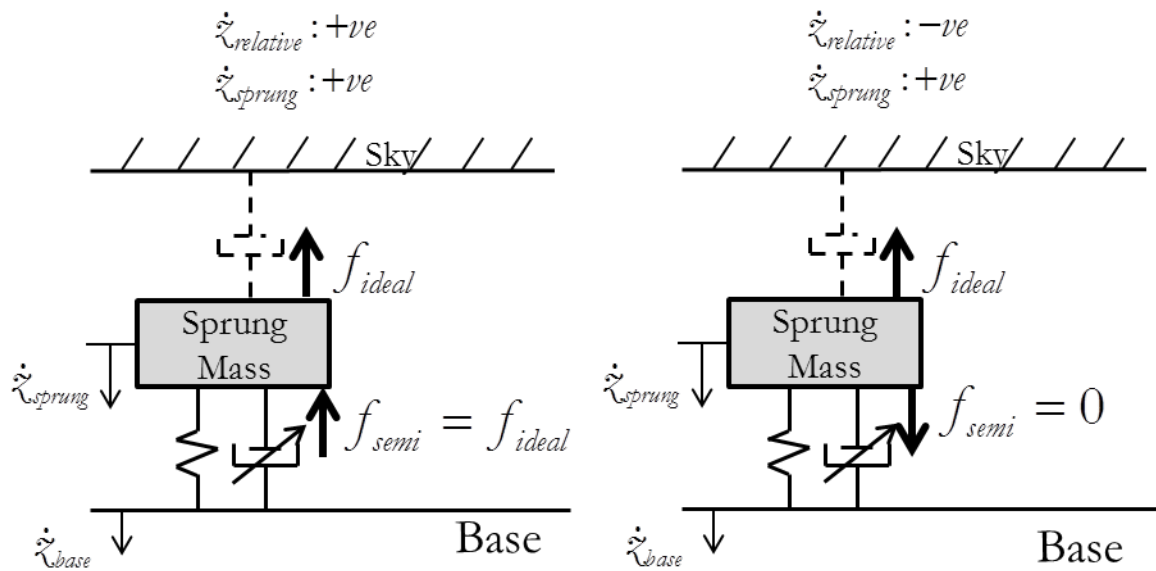


Figure 5.5: Semi-Active Realization of an Ideal Skyhook Damper

The objective of the skyhook law applied to semi-active dampers is to exert a damping force equal to the force exerted by the hypothetical ideal skyhook damper on the sprung mass. Consider the case where the sprung mass is travelling downwards and the suspension is undergoing compression. In this case, the forces  $f_{ideal,skyhook}$  and  $f_{semi,skyhook}$  exerted on the sprung mass are both directed upwards as shown in Figure 5.5 (left) and thus they may be equated.



A similar case can be made when the sprung mass is travelling upwards and the suspension is under tension. The right hand side of equation (5.13) can be equated to the force exerted by the ideal skyhook damper on the sprung mass to determine the desired damping coefficient when the ideal and semi-active skyhook damping forces (and therefore the sprung mass and relative velocities) are in the same direction.

$$c_{\text{semi,desired}} v_{\text{relative}} = c_{\text{sky}} v_{\text{sprung}}, \quad \frac{v_{\text{sprung}}}{v_{\text{relative}}} > 0. \quad (5.14)$$

The absolute velocity of the sprung mass,  $v_{\text{sprung}}$ , needs to be estimated to determine the semi-active damping coefficient using the Skyhook law. Theoretically it can be obtained by integrating the acceleration of the sprung mass and then detrending the resulting signal to remove the DC offset. Song [3] suggested the use of a 2<sup>nd</sup> order integral filter. Shen, et al. [4] proposed the use of jerk (derivative of the acceleration) of the sprung mass in place of sprung mass velocity. This approach amplifies the noise that is usually observed when collecting acceleration data.

By rearranging the terms in equation (5.14) the desired damping coefficient can be defined as,

$$c_{\text{semi,desired}} = c_{\text{sky}} \frac{v_{\text{sprung}}}{v_{\text{relative}}}, \quad \frac{v_{\text{sprung}}}{v_{\text{relative}}} > 0 \quad (5.15)$$

Now consider the case where the sprung mass is travelling downwards and the suspension is in tension. In this case, the forces  $f_{\text{ideal,skyhook}}$  and  $f_{\text{semi}}$  exerted on the sprung mass are in opposite directions, as shown in Figure 5.5 (right). In this scenario the best that can be achieved by a semi-active damper to emulate the ideal skyhook damping force is to exert no damping force.

This can be achieved by setting the desired damping coefficient of the semi-active damper to zero.

$$c_{\text{semi,desired}} = 0, \frac{v_{\text{sprung}}}{v_{\text{relative}}} < 0 \quad (5.16)$$

In practice the maximum,  $c_{\text{max}}$ , and minimum damping coefficients,  $c_{\text{min}}$ , that the semi-active damper can attain are determined by its design. Therefore the demanded damping coefficient of the semi-active damper can be expressed as,

$$c_{\text{semi,skyhook}} = \begin{cases} c_{\text{max}} & , c_{\text{semi,desired}} > c_{\text{max}} \\ c_{\text{semi,desired}} & , c_{\text{min}} < c_{\text{semi,desired}} < c_{\text{max}} \\ c_{\text{min}} & , 0 < c_{\text{semi,desired}} \leq c_{\text{min}} \end{cases} \quad (5.17)$$

The typical range of damping coefficients suggested by Ahmadian and Blanchard [5] is,

$$\begin{aligned} c_{\text{max}} &= 2c_{\text{passive}} \\ c_{\text{min}} &= 0.1c_{\text{passive}} \end{aligned} \quad (5.18)$$

The linear damping coefficient of the passive seat damper was chosen to be 730 N.s/m for the following simulations. Accordingly, the maximum and minimum damping coefficients for the seat semi-active damper were,

$$\begin{aligned} c_{\text{max}} &= 1460 \text{ N.s/m} \\ c_{\text{min}} &= 73 \text{ N.s/m} \end{aligned} \quad (5.19)$$

Figure 5.6 compares the responses to base excitation of the 1 d.o.f. systems with the ideal skyhook damper and with the semi-active skyhook damper. The deflection of the base of the system was the input to the system and was described as,

$$\tilde{z}_{\text{base}} = 0.04 \sin(\omega_e t), \text{ m}, \quad (5.20)$$

where  $\omega_e$  was the frequency of the base excitation. The sprung mass acceleration of the semi-active damper system was marginally greater than that of the ideal skyhook damper system. The sprung mass displacement and suspension stroke of the semi-active system are good approximations of the ideal skyhook system for excitation frequencies greater than the natural frequency.

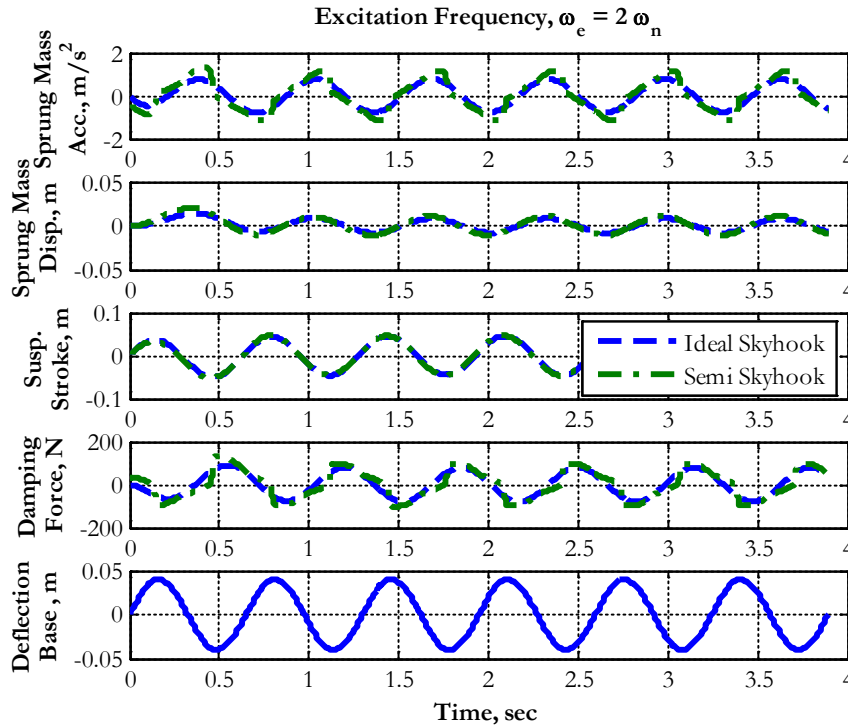


Figure 5.6: Ideal Skyhook Damper compared to Semi-Active Skyhook Damper for a 1 d.o.f.

model

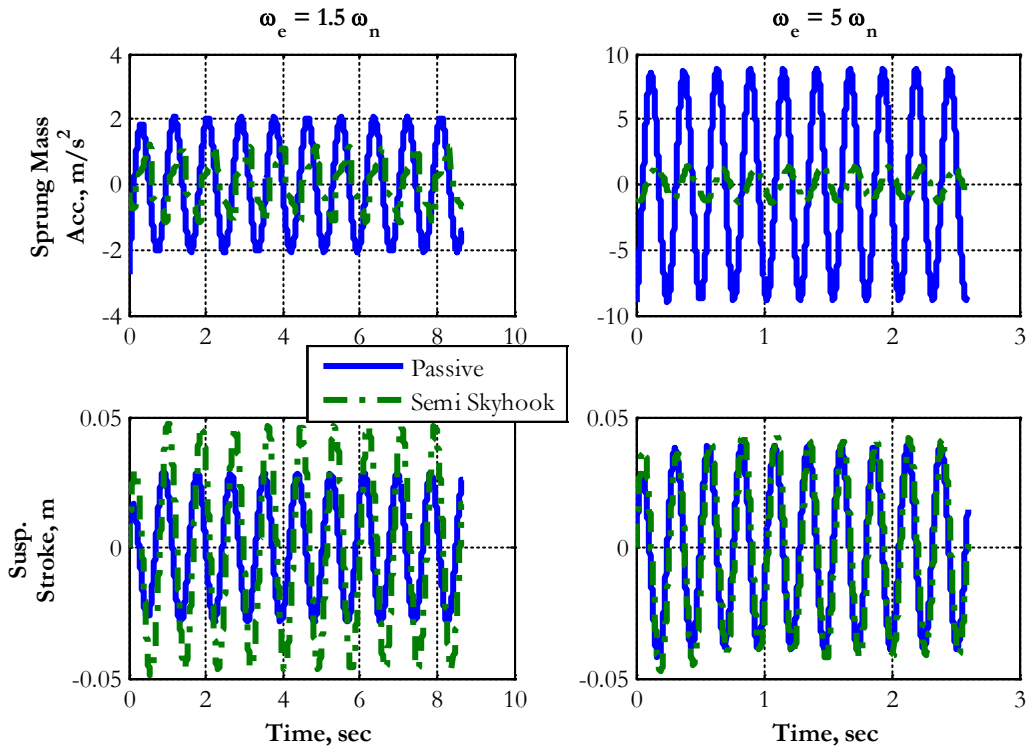


Figure 5.7: Semi-Active Skyhook Damper Compared to Passive system

Figure 5.7 compares the sprung mass acceleration and the suspension stroke of the semi-active skyhook damper to that of the passive system for the base excited 1 d.o.f system at two different excitation frequencies, one close to (1.5x) the natural frequency and the other five times the natural frequency. When the excitation frequency was close to the natural frequency ( $1.5\omega_n$ ), the amplitude of the suspension stroke of the semi-active system was larger than that of the passive system and was also greater than the amplitude of the base excitation. If there are design constraints on the suspension stroke and the base excitation frequency is close to the system natural frequency, the performance benefits of semi-active skyhook damper may be compromised. For excitation frequencies higher than the natural frequency, the sprung

mass acceleration due to the semi-active skyhook damper is much smaller than that of the passive system while the suspension strokes are comparable. The semi-active skyhook system is preferable over the passive system if the excitation frequencies are much higher than the natural frequency or if there are no constraints on the suspension stroke.

### 5.3 Limitations of the Semi-Skyhook Policy

The ride at the driver’s seat was analyzed by replacing the nominal passive damper with a semi-active skyhook damper. The skyhook damping rate,  $c_{sky}$ , can be used as a tuning to achieve the best ride comfort. For this study the skyhook damping rate was set to its optimal value of  $(2 * k_s * m_s)^{0.5} = 730 \text{ N.s/m}$ .

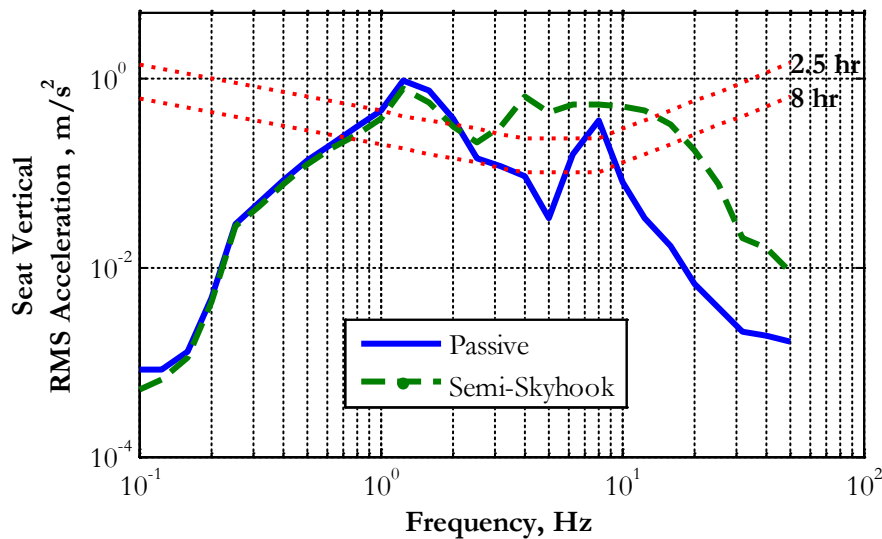
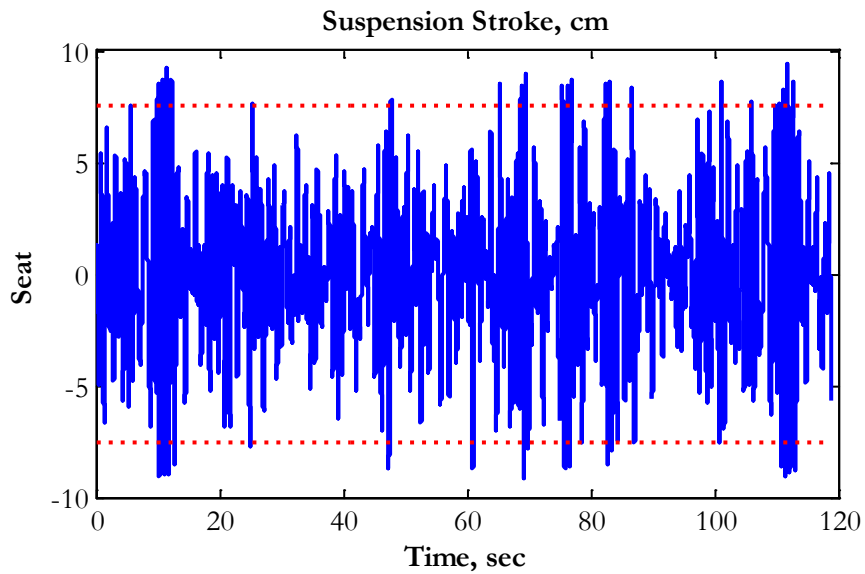


Figure 5.8: Semi-Active Skyhook Seat Damper, Gravel Road, 40 mph (64.4 kph).

The RMS vertical acceleration responses of the two systems traversing over a gravel road are plotted in Figure 5.8. In this scenario, the semi-active skyhook damper (approximation of

optimal policy 1) performed significantly worse than the passive suspension (optimal policy 2).

To understand the cause of the poor performance of the skyhook semi-active suspension, the seat suspension deflection was analyzed.



**Figure 5.9: Seat Suspension Stroke, Semi-Active Skyhook Damper**

The time history of the seat suspension stroke for the semi-active skyhook damper is plotted in Figure 5.9. It was observed that the seat suspension hits the bump-stops multiple times. When the suspension hits the bump-stops the sprung mass (i.e. the seat and the driver) experiences a sharp increase in acceleration which is harmful to the driver's health.

A closer look at the PSD of the base displacement of the seat suspension (seat mount) provides a understanding of the cause for the large suspension strokes for the semi-active skyhook damper system.

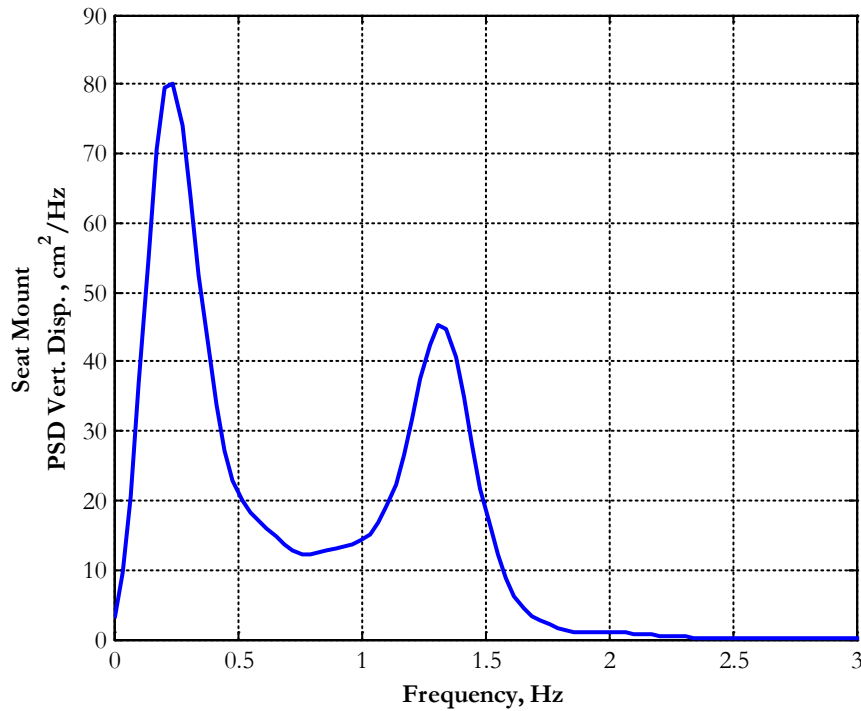


**Figure 5.10: PSD of the Seat Mount Vertical Deflection, Gravel Road, 40 mph (64.4 kph)**

On a gravel road, the seat mount experiences large amplitude excitation between 1.1 Hz and 1.5 Hz as observed from the PSD of the seat mount vertical displacement in Figure 5.10. The seat mount excitation is a function of the cab floor vertical deflection and the cab floor pitch motion. Road excitation around 1.3 Hz excites the tractor pitch mode (as discussed in section 4.1) which is a poorly damped mode. Since the cab mode is  $\sim 1.8$  Hz, the tractor pitch mode is not filtered by the cab suspension. The natural frequency associated with the seat heave mode for a passive damper was 0.79 Hz (Table 4.1). As discussed earlier, for base excitation frequencies close to the natural frequency, the suspension stroke of the semi-active skyhook system was greater than that of the passive system. The seat suspension stroke range was limited by the bump-stops ( $\pm 7.5$  cm). On a gravel road, the passive seat suspension utilizes

the entire range of the seat suspension stroke. Replacing the passive damper with the semi-active skyhook damper at the seat suspension leads to even greater suspension strokes. Therefore the semi-active skyhook damper suspension hits the bump-stops multiple times on a gravel road. This is a limitation of the application of skyhook controller to semi-active seat dampers.

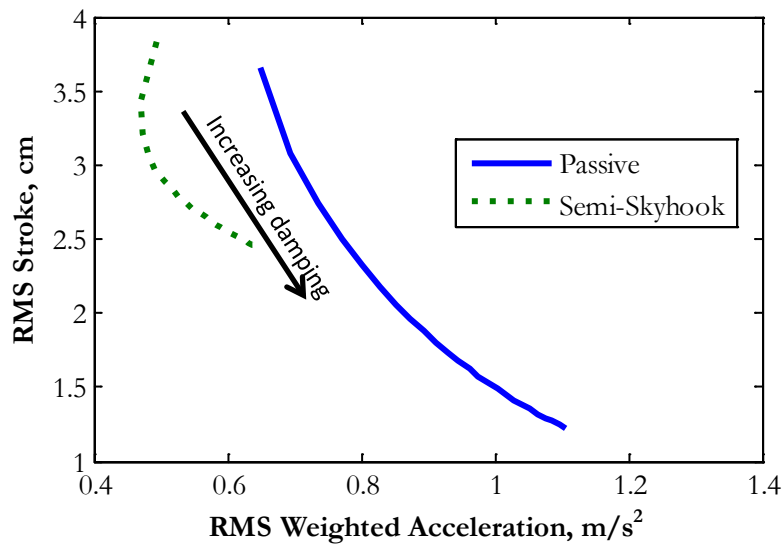


**Figure 5.11: Acceleration/Stroke tradeoff for several damping ratios**

The suspension stroke of the semi-active skyhook seat damper on the gravel road can be reduced by increasing the skyhook damping rate,  $\zeta_{\text{sky}}$ . The tradeoff in the suspension stroke vs sprung mass acceleration for increasing values of  $\zeta_{\text{sky}}$  and  $\zeta_{\text{passive}}$  of the seat suspension when traversing a gravel road at 40 mph are shown in Figure 5.11. It is observed that for the same root mean square (RMS) suspension stroke the semi-skyhook damper produces much smaller RMS weighted sprung mass acceleration. The RMS stroke corresponding to the maximum  $\zeta_{\text{sky}}$  value for the semi-active skyhook damper is much larger than that for maximum passive



damping,  $c_{\text{passive}}$ . If the magnitude of the road excitation demands a greater emphasis on limiting the suspension stroke to avoid hitting the suspension bump stops, the passive damper is a better solution. Choosing the value of the  $c_{\text{sky}}$  is therefore a tradeoff between seat suspension stroke and seat vertical acceleration. For this study the value of  $c_{\text{sky}}$  and  $c_{\text{passive}}$  were held at their optimum value of  $(2k_s m_s)^{0.5}$  as derived in appendix D and stated in equation (5.12).

#### 5.4 Fuzzy Switch

A fuzzy logic based algorithm was developed to enable the transition between the passive policy and skyhook policy for both seat suspensions.

The inputs to the fuzzy logic algorithm were the RMS of weighted sprung mass acceleration and the RMS of seat relative stroke. A frequency based weighting filter for vertical acceleration, designed as per the ISO 8041 standard, was applied to the acceleration signal. The weighted acceleration provides a more realistic input to the fuzzy switch. The root mean squares (RMS) over a moving window of 2s were calculated for both the input signals. This time duration allow enough time for the lowest frequencies of interest ( $\sim 0.5$  Hz) to complete one cycle.

The output of the fuzzy logic was a number between 0 and 1. An output of 0 made the suspension behave as semi-skyhook suspension whereas an output of 1 made the suspension behave as a passive suspension (pseudo-passive).

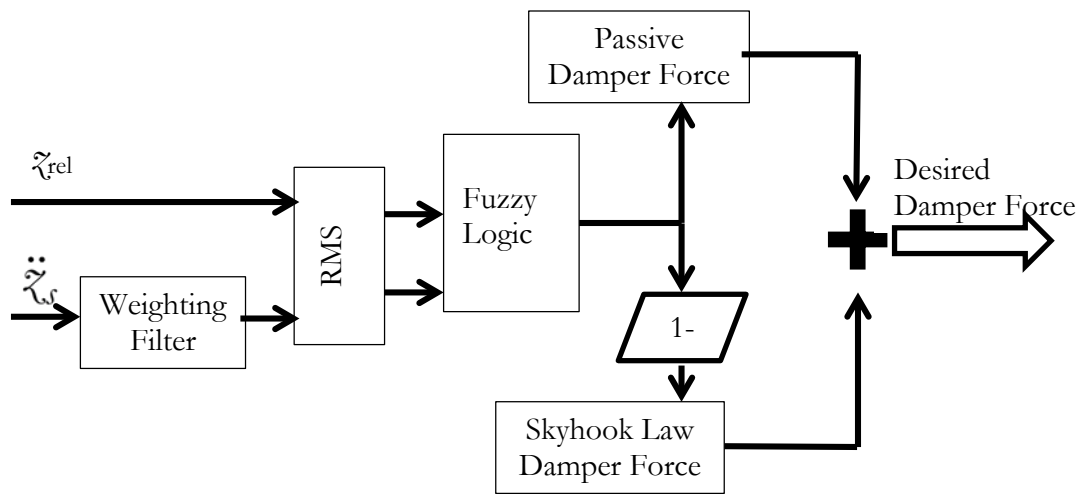


**Figure 5.12: Fuzzy Switch Scheme**

The vertical acceleration at the seat was weighted using a weighting filter. The frequency weightings for vertical acceleration are described in ISO 2631-1:1997 and ISO 8041:2005 [6,7]. A transfer function developed by Rimell and Mansfield [8] to describe the frequency weightings was used as the weighting filter. Applying the frequency weightings to the vertical acceleration allows the acceleration membership function of the fuzzy logic to be developed as per ISO 2631-1:1997 comfort boundaries. The filter profile is shown in Figure 5.13.

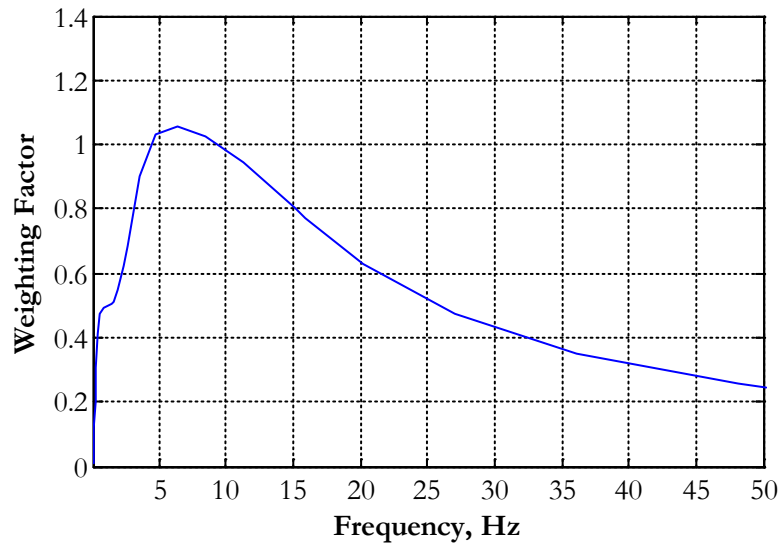


Figure 5.13: ISO 2631-1 Vertical Acceleration Weighting Curve

The Fuzzy Switch input membership functions are shown Figure 5.15. The resultant surface of the fuzzy output is shown in the Figure 5.14.

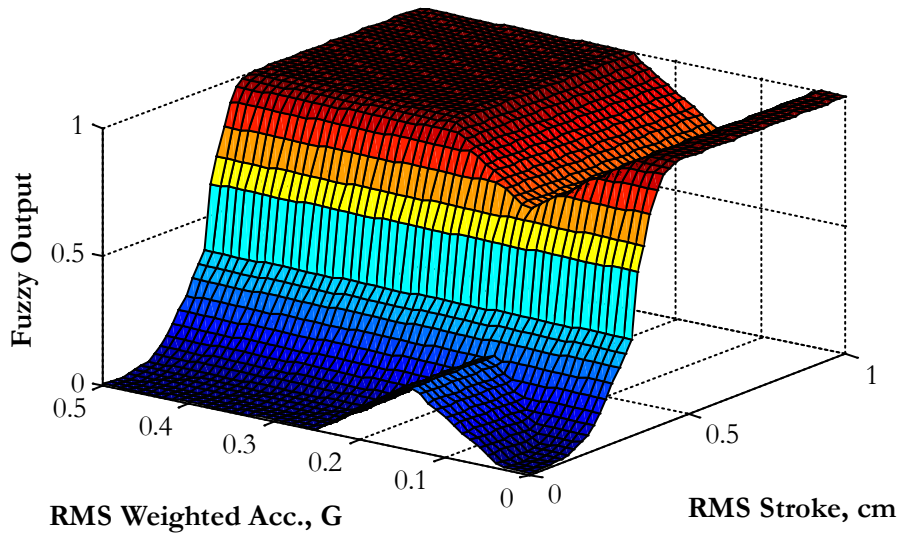


Figure 5.14: Fuzzy Switch Output Surface

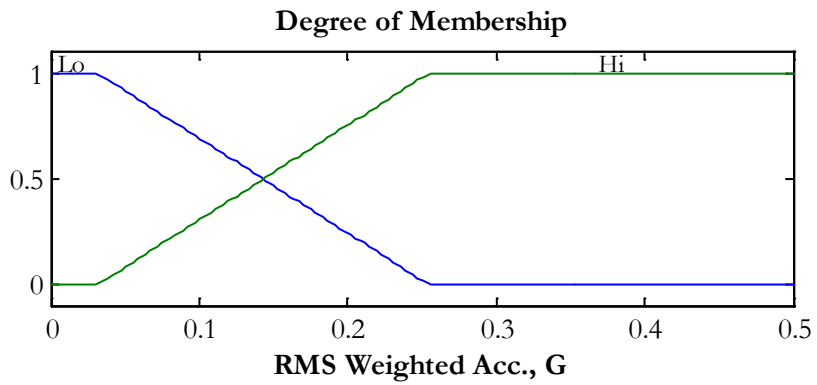
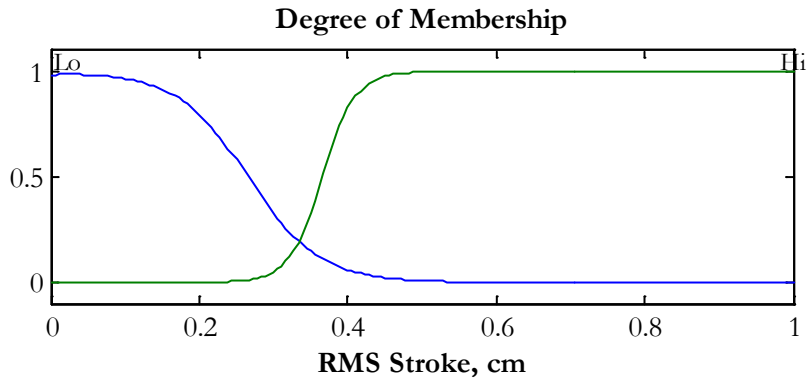


Figure 5.15: Fuzzy Switch Input Membership functions

The verbal rules used for the fuzzy logic block-set are shown in Table 5.1.

Table 5.1: Fuzzy Logic Rules

Weighted Vert. Seat Acc.	Seat Suspension Stroke	Fuzzy Output
High	Low	Low
High	High	High
Low	Low	Low
Low	High	High

## 5.5 Estimation of the Seat Load and Suspension Stiffness

For the seat suspension, the mass of the seat + driver was used for calculation. Since the mass of the driver varies from driver to driver and the stiffness of the suspension might change due to operational wear and tear, estimating the mass and the stiffness leads to more accurate optimal damping calculation.

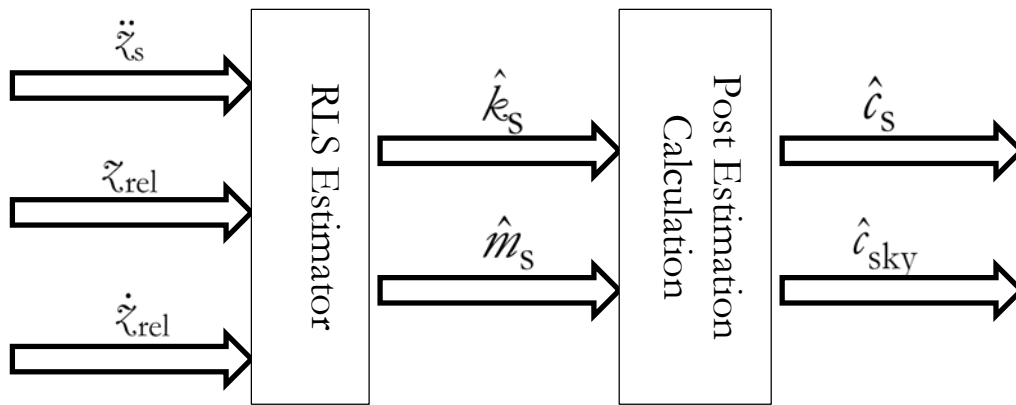


Figure 5.16: Estimator Signal Flow

The seat suspension stroke and the acceleration at the seat can be easily measured. These were the input signals to the estimator. The velocity of the damper was obtained by differentiating the suspension stroke. The following model was used for estimating the mass and the stiffness:

$$-c_s \dot{z}_{rel} = m_s \ddot{z}_s + k_s z_{rel} , \quad (5.21)$$

where  $m_s$  and  $k_s$  are the sprung mass and stiffness to be estimated respectively,  $c_s$  was the known damping value applied to the system during the duration of the estimator operation. To minimize the memory requirement, a recursive least square (RLS) algorithm was adopted for parameter estimation. The derivation of the RLS estimator can be found in appendix F.

The seat estimator is run for 30 seconds. The sampling rate for the input signals was 200 Hz. Noise was added to the input signals (SNR = 50) to replicate practical scenarios. A forgetting factor of 0.98 was chosen for good convergence. The final estimated values of mass and stiffness are used by the damper control policy. Figure 5.17 shows the estimated values when the system is simulated over smooth highway. During the duration of estimation the seat damping is set to its lowest value, i.e. the semi-active damper is turned ‘off’ .

**Table 5.2: RLS Estimated Seat Values**

<b>Parameters</b>	<b>Simulation Value</b>	<b>Estimated Value</b>	<b>% Difference</b>
<b>Seat Mass</b>	106.9	106.3	0.56%
<b>Seat Spring Stiffness</b>	2500	2456	1.76%

Table 5.2 shows the results of the RLS estimator. The estimated mass is within 1% of the actual value and the estimated spring stiffness is within 2% of the actual value.

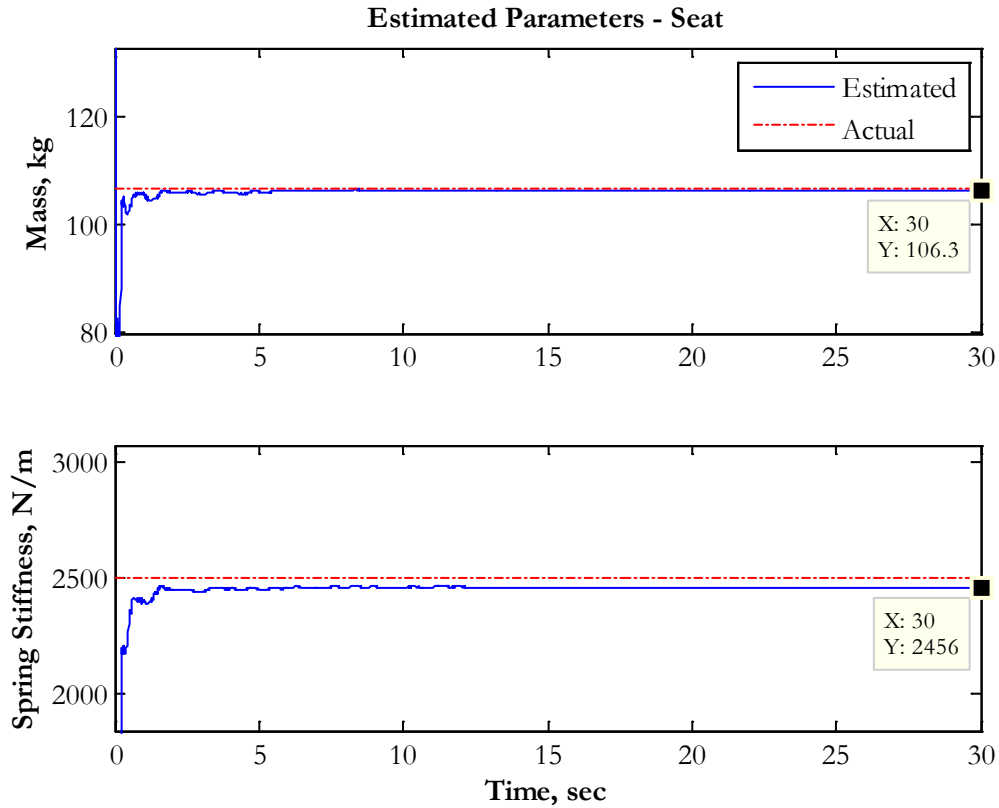


Figure 5.17: Estimation of seat mass and stiffness

### 5.6 Ride Comfort with Semi-Active Seat damper on Different Road Surfaces

The RLS estimator was run for 30 seconds to estimate the sprung mass and the seat spring stiffness values. Based on the final estimated values, the  $c_{sky}$  value for the Skyhook law and  $c_s$  value for the pseudo-passive damper in the Fuzzy Switch Control law were calculated based on equation (5.12). The second simulation run was conducted to analyze the ride with these estimated values used in the controllers. Since the difference in the estimated values and the actual values are less than 2%, the results in the following sections hold for both cases. The scheme used is shown in Figure 5.18.

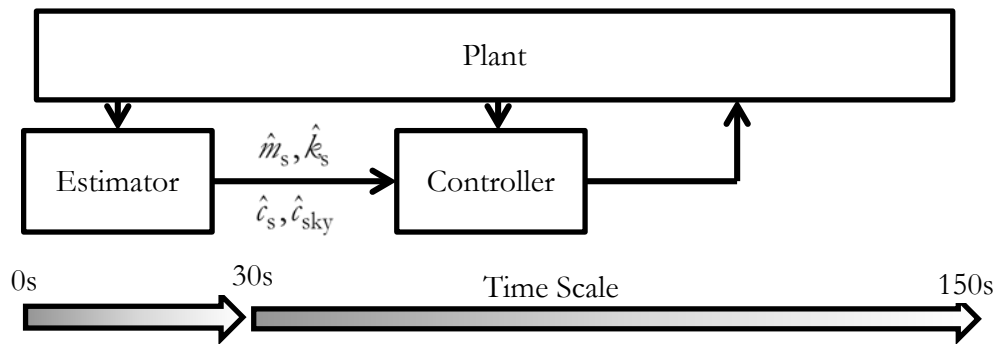


Figure 5.18: Estimator Controller Scheme

### 5.6.1 Smooth Highway at 60 mph

A study was carried out to analyze the ride at the driver's seat by replacing the seat passive damper with a semi-active damper using the Skyhook law and Fuzzy Switch Optimal law.

Figure 5.19 compares the RMS vertical accelerations at the seat between the passive system and the semi-active damper systems on the smooth highway traversed at 60 mph.



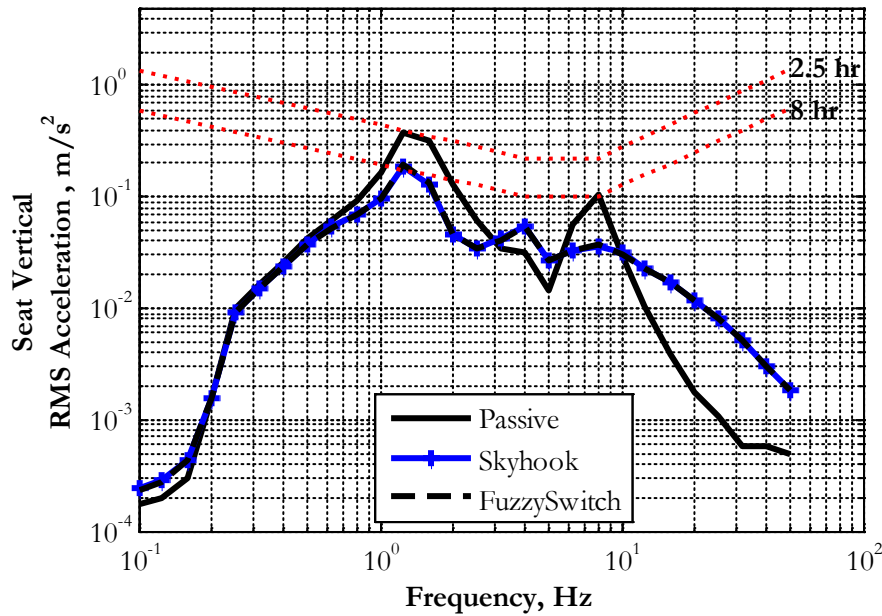


**Figure 5.19: Driver RMS Vert. Acceleration Comparison for Different Control Strategies,  
Smooth Highway @ 60 mph**

The semi-active damper provides better isolation in the (0.8-3) Hz range as well as in the 6-9 Hz compared to the passive system. Observe that over the smooth highway the Fuzzy Switch Optimum law behaves mostly like the Skyhook law. The switching nature of the Skyhook law introduces some high frequency vibration in the sprung mass acceleration. Modified skyhook laws have been studied to reduce the switching effect [9, 10].

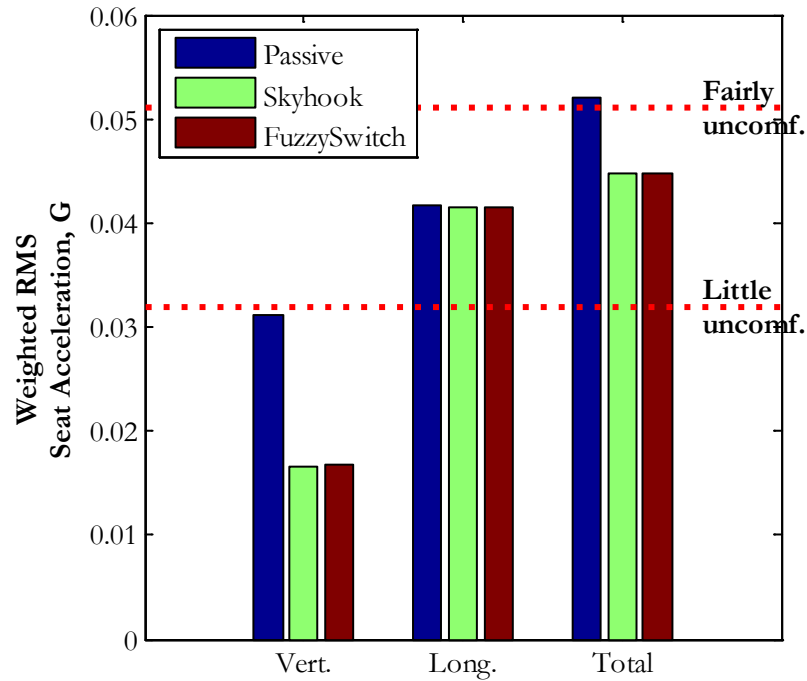


**Figure 5.20: Weighted RMS Seat Acceleration Damper Controller Comparison, Smooth Highway @ 60 mph**

The weighted RMS vertical acceleration at the seat was reduced by 45% by employing a Skyhook law or Fuzzy Switch Optimum law controller as shown in Figure 5.20. As one would expect the longitudinal RMS acceleration is not affected by the seat suspension. The total weighted acceleration at the seat is reduced by 14%.

### ***5.6.2 Gravel Road at 40 mph***

Figure 5.21 compares the RMS vertical accelerations at the seat between the passive system and the semi-active damper systems on a gravel road traversed at 40 mph. Similar to the

results on the smooth highway, the semi-active dampers provide better isolation in the (0.8-3) Hz.

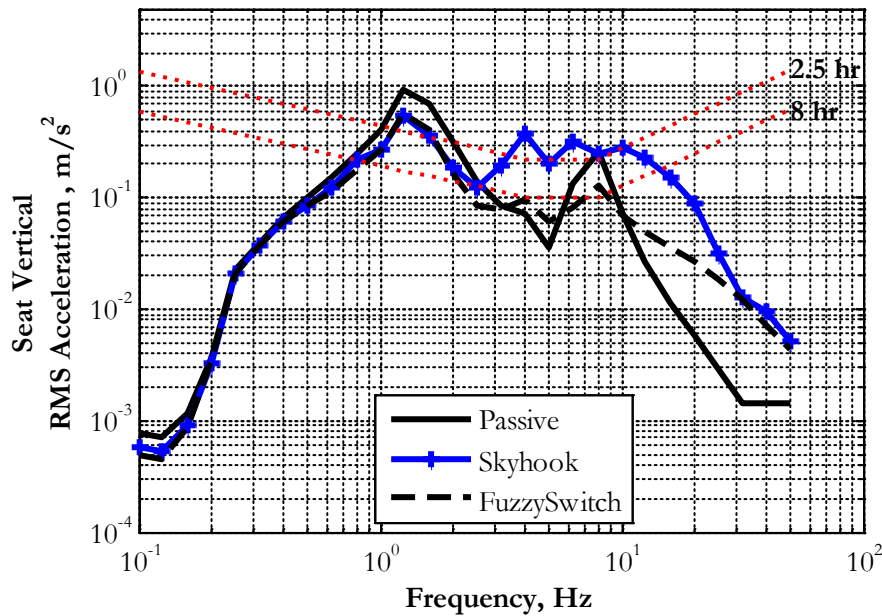


**Figure 5.21: Driver RMS Vert. Acceleration Comparison for Different Control Strategies, Gravel Road @ 40 mph**

As discussed in section 5.3, the Skyhook law leads to large suspension deflection when the base excitation magnitude is large. This causes the suspension to hit the bump stops which contributes to the degradation of ride quality due to increased sprung mass acceleration. This is clearly observed for the Skyhook law for frequencies above 3 Hz. The Fuzzy Switch optimum law provides much better isolation to the sprung mass than the Skyhook law above

3 Hz. Even at frame beaming resonant frequencies ( $\sim 7$  Hz), the Fuzzy Switch Optimal law provides better isolation compared to the passive damper.

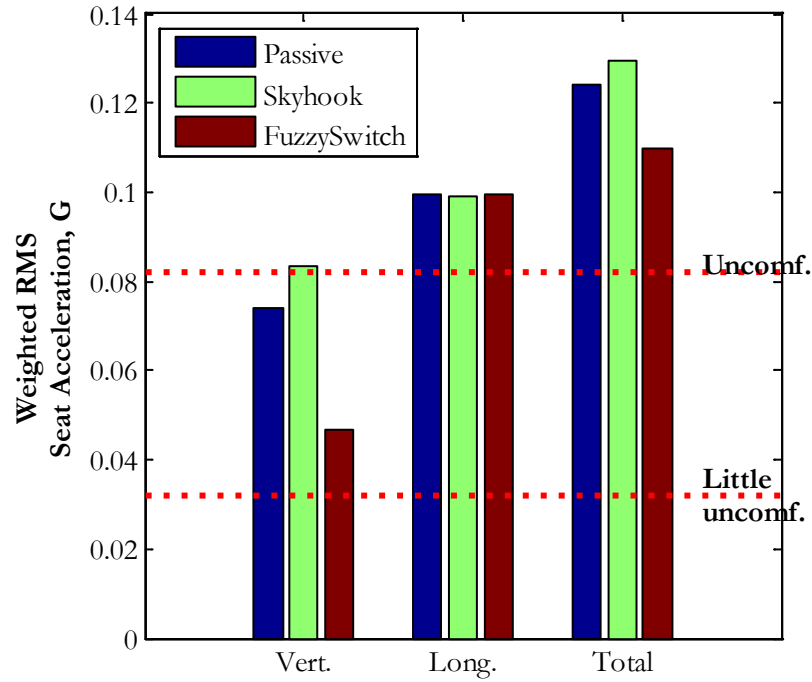


**Figure 5.22: Weighted RMS Seat Acceleration Damper Controller Comparison, Gravel Road @ 40 mph**

On a gravel road traversed at 40 mph, the weighted RMS vertical acceleration at the seat increased by 14% by employing a Skyhook law and was reduced by 36% with the Fuzzy Switch Optimum law controller as shown in Figure 5.22. The total weighted acceleration at the seat increased by 8% for the Skyhook law damper and reduced by 8% for with the Fuzzy Switch Optimum law controller. The contribution of the longitudinal acceleration to the total acceleration at the driver’s seat is greater than that of the vertical acceleration.

## 5.7 Semi-Active Seat Damper with Rear Cab Mounted at Optimum Position

In chapter 4 it was observed that by placing the rear cab mounts near the beaming mode nodes, both the longitudinal and the vertical accelerations at the seat near the tractor frame beaming mode frequency ( $\sim 7\text{Hz}$ ) were significantly reduced. Significant gains in ride comfort (both longitudinal and vertical) are expected by combining the effects of the semi-active seat damper and that of the optimal cab mount Positions. A study was carried out to quantify the ride comfort gains at the driver's seat by replacing the seat passive damper with a semi-active damper using the Fuzzy Switch Optimal law as well as placing the rear cab mounts in their optimal position. For ease of writing let us term this configuration as the FSO1 configuration.

Figure 5.23 compares the driver seat RMS accelerations of the baseline configuration against the FSO1 configuration. As expected the Fuzzy Switch Optimal law provides good isolation to the seat vertical motion and the effect of the optimum cab mount locations is seen in the lower longitudinal acceleration.

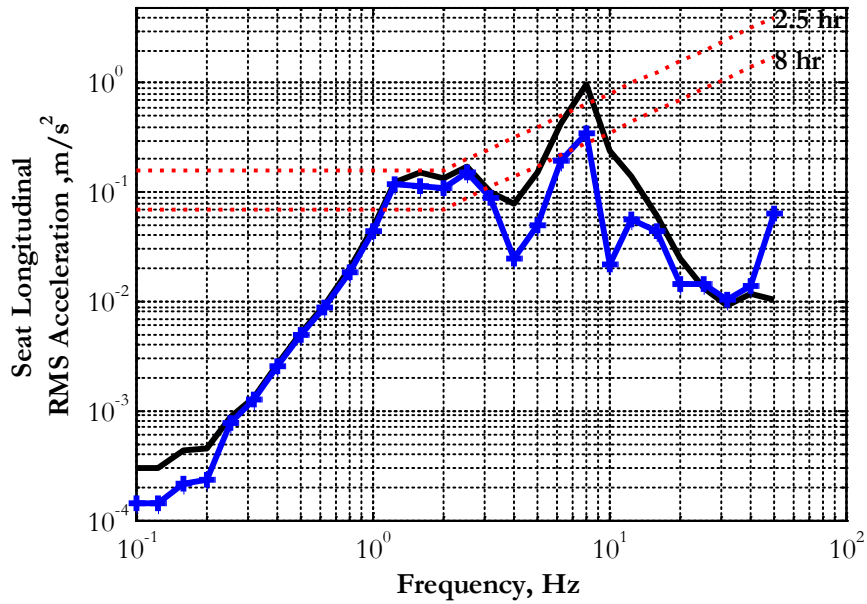
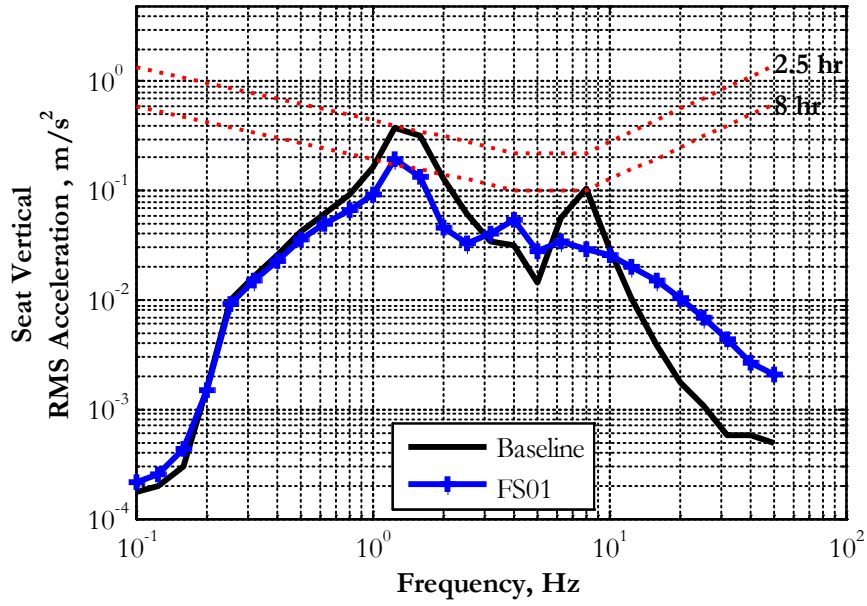
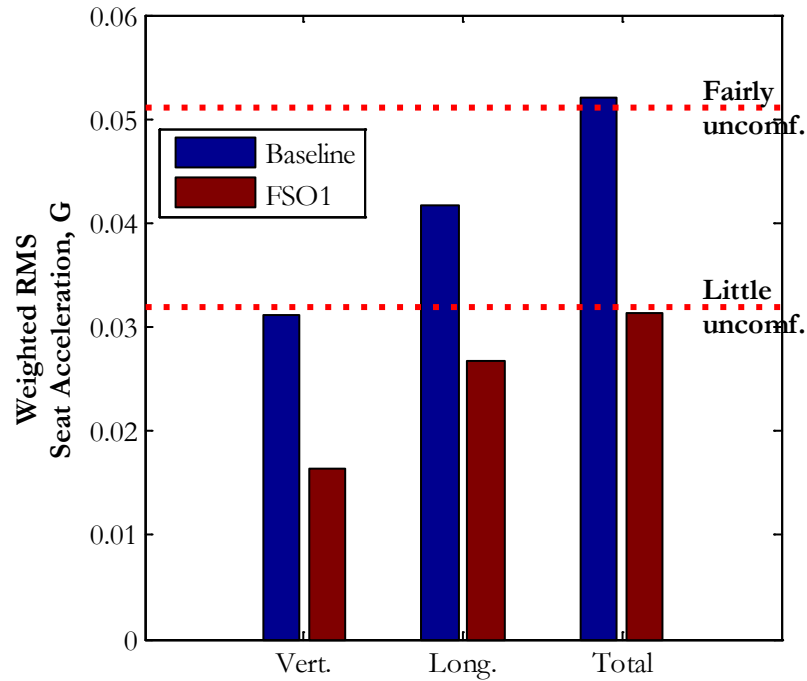


Figure 5.23: Seat RMS Acceleration, Baseline vs. Semi-Active Seat + Optimum Rear Cab Position, Smooth Highway @ 60 mph



**Figure 5.24: Weighted RMS Seat Acceleration, Baseline vs. Semi-Active Seat + Optimum  
Rear Cab Position, Smooth Highway @ 60mph**

On a smooth highway traversed at 60 mph, the weighted RMS vertical acceleration at the seat was reduced by 48% by employing the FSO1 configuration as shown in Figure 5.24. The weighted RMS longitudinal acceleration at the seat was reduced by 36% and the total weighted acceleration at the seat is reduced by 40%. In fact as per the ISO 2761:1997 classification the ride with the FSO1 configuration can be termed as “not uncomfortable”. Similar improvements in ride comfort can be expected on the other road surfaces.

## 5.8 Semi-Active Seat Damper with Full Cab at Optimum Mount Positons

In chapter 4 it was observed that by employing a fully suspended cab and placing the cab mounts near the beaming mode nodes, the longitudinal and the vertical accelerations at the seat were significantly reduced. The added ride benefit of the “full cab” should be observed in the low frequency longitudinal acceleration since the cab and frame pitch motions would be better damped. A study was carried out to quantify the ride comfort gains at the driver’s seat by replacing the seat passive damper with a semi-active damper using the Fuzzy Switch Optimal law as well as placing the cab mounts in their optimal positon for a fully suspended cab. Let us term this configuration as the FSO2 configuration.

Figure 5.25 compares the driver seat RMS accelerations of the baseline configuration against the FSO2 configuration. As expected the Fuzzy Switch Optimal law provides good isolation to the seat vertical motion and the effect of the optimum cab mount locations in seen in the decreased longitudinal acceleration.



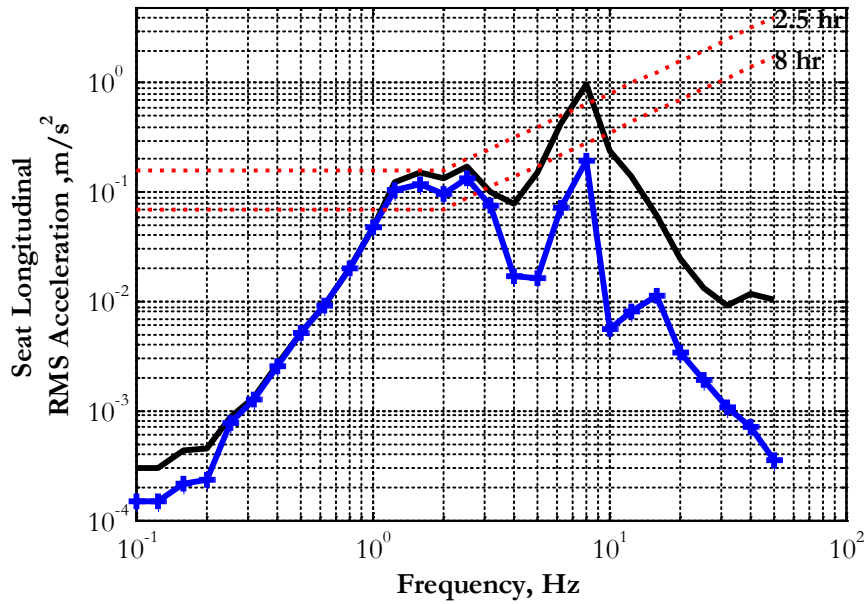
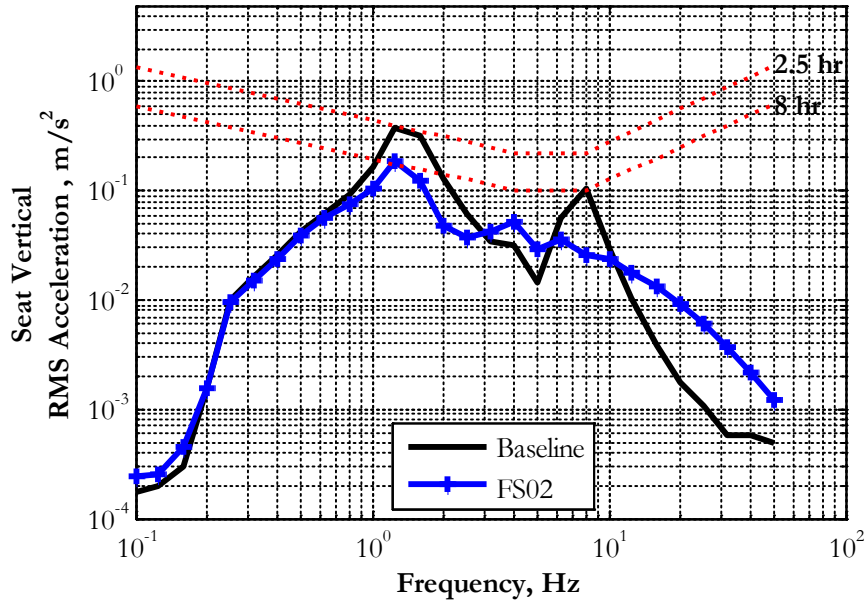
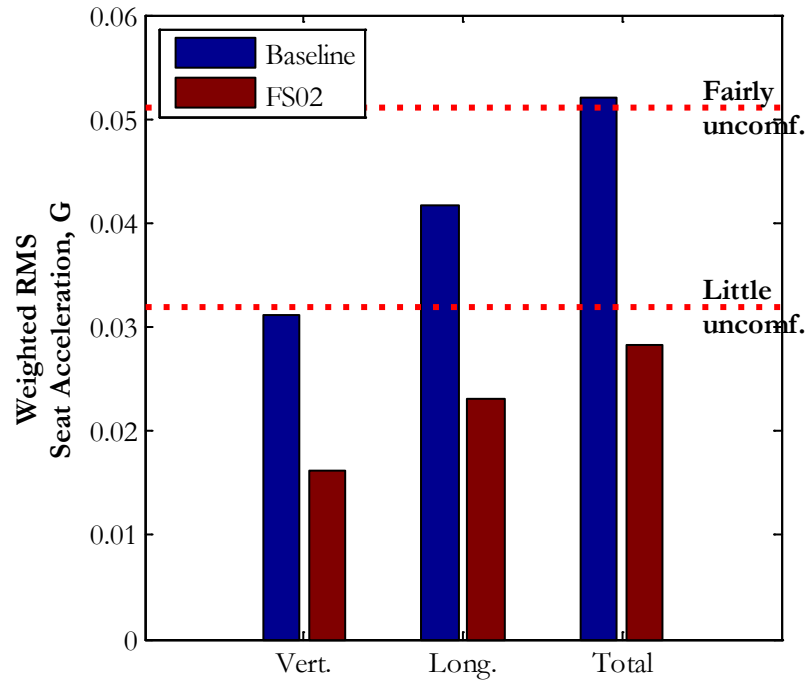


Figure 5.25: Seat RMS Acceleration, Baseline vs. Semi-Active Seat + Optimum Full Cab

Position, Smooth Highway @ 60 mph



**Figure 5.26: Weighted RMS Seat Acceleration , Baseline vs. Semi-Active Seat + Optimum  
 Full Cab Position, Smooth Highway @ 60 mph**

On a smooth highway traversed at 60 mph, the weighted RMS vertical acceleration at the seat was reduced by 48% by employing the FSO2 configuration as shown in Figure 5.26. The weighted RMS longitudinal acceleration at the seat was reduced by 45% and the total weighted acceleration at the seat is reduced by 46%. As per the ISO 2761:1997 classification the ride with the FSO2 configuration can also be termed as “not uncomfortable”. The FSO2 configuration improves the ride by 10% compared to the FSO1 configuration.

Two additional control strategies for semi-active seat damper were explored in this work. Each of these control strategies provides some benefit over the Skyhook law but at some cost. The benefits provided by these control strategies and the penalties of them will be discussed in more detail in the following sub-sections.

### 5.9. Model Predictive Control with Excitation Preview

The previous formulation of optimal control policy looked at developing the optimal policy for the isolation system of a 1 d.o.f. system where the stroke of the suspension is penalized in the performance index. An alternative approach to developing the optimal policy was explored in this work where the limits of the suspension stroke (dictated by the bump stop-bump stop range) are incorporated in the constraints of the optimization problem. To test the efficacy of this approach a model predictive controller (MPC) was developed. The evolution of fast computing has opened the possibility of applying MPC policy to systems with relatively fast dynamics like a suspension system. Consider the 1 d.o.f. problem shown in Figure 5.

The corresponding equation of motion of the system in the discrete state space form is

$$x(i+1) = \mathbf{A}_d x(i) + \mathbf{B}_d u(i) + \mathbf{B}_{md} w(i) \quad (5.22)$$

where  $x = [\tilde{z}_{\text{rel}} \quad \dot{\tilde{z}}_{\text{rel}}]'$  is the state vector,  $\tilde{z}_{\text{rel}}$  and  $\dot{\tilde{z}}_{\text{rel}}$  are the relative sprung mass displacement and velocity respectively. The control force  $u$  dictates the sprung mass acceleration as:

$$u = m \ddot{\tilde{z}}_s \quad (5.23)$$

Since the control force is realized by a spring and a semi-active damper, the allowable force is described by

$$u = k_s \tilde{z}_{\text{rel}} + c(t) \dot{\tilde{z}}_{\text{rel}} \quad (5.24)$$

The base acceleration is modeled as disturbance to the system. For this study it is assumed that accurate preview of the base acceleration is available. For this study the base acceleration was recorded using the 15 d.o.f model traversing different roads.

$$w = a_{\text{base}} = \ddot{\tilde{x}}_{\text{base}} \quad (5.25)$$

Let the performance index be

$$J = \sum_{i=1}^{n-1} [\ddot{\tilde{z}}_s^2(i)] \quad (5.26)$$

where  $n$  is the prediction horizon. For this work the preview horizon and the prediction horizon are assumed to be the same. If  $c_{\text{max}}$  and  $c_{\text{min}}$  are the limits of the damping rate of the variable semi-active damper, the dissipativity constraints on the control force are

$$\begin{aligned} -|u - k_s \tilde{z}_{\text{rel}}| + c_{\text{min}} |\dot{\tilde{z}}_{\text{rel}}| &\leq 0 \\ |u - k_s \tilde{z}_{\text{rel}}| - c_{\text{max}} |\dot{\tilde{z}}_{\text{rel}}| &\leq 0 \\ \text{sgn}(u - k_s \tilde{z}_{\text{rel}}) - \text{sgn}(\dot{\tilde{z}}_{\text{rel}}) &= 0 \end{aligned} \quad (5.27)$$

To avoid the suspensions hitting the bump stops, an additional constraint on the relative displacement of the sprung mass is

$$|\tilde{z}_{\text{rel}}| \leq \tilde{z}_{\text{lim}} \quad (5.28)$$

The objective of the problem is to minimize the performance index described in equation (5.26) subject to the system dynamics described in equation (5.22) and the constraints described by the equations (5.27) and (5.28). The optimal control problem can be solved by using a finite optimization horizon and obtaining the sequence of optimal control inputs over the horizon. Only the first in the sequence of inputs is applied at each time step. The complete derivation of the MPC policy can be found in appendix E. The parameters used for the MPC policy are stated in Table 5.3. The constraints are non-linear and therefore optimization at each time step was computed using the *fmincon* function in the Matlab environment.

**Table 5.3: MPC Controller Parameters**

Discrete time step	Preview time	Preview distance	
		@ 60 mph	@ 40 mph
0.01s	0.1s	2.7m	1.8m

Figure 5.27 compares the seat RMS acceleration for the different control strategies when the vehicle traverses a smooth highway at 60 mph. It was observed that the MPC policy improves the ride comfort when compared to the passive damper in the 0.8-3 Hz and the 6-9 Hz range. It must be noted that the Skyhook law performs better than the MPC policy. This indicates that the optimal control sequence computed at each time step is probably not the global optimum.

On a smooth highway traversed at 60 mph, the weighted RMS vertical acceleration at the seat was reduced by 39% by employing the MPC policy as compared to the passive damper as shown in Figure 5.28.

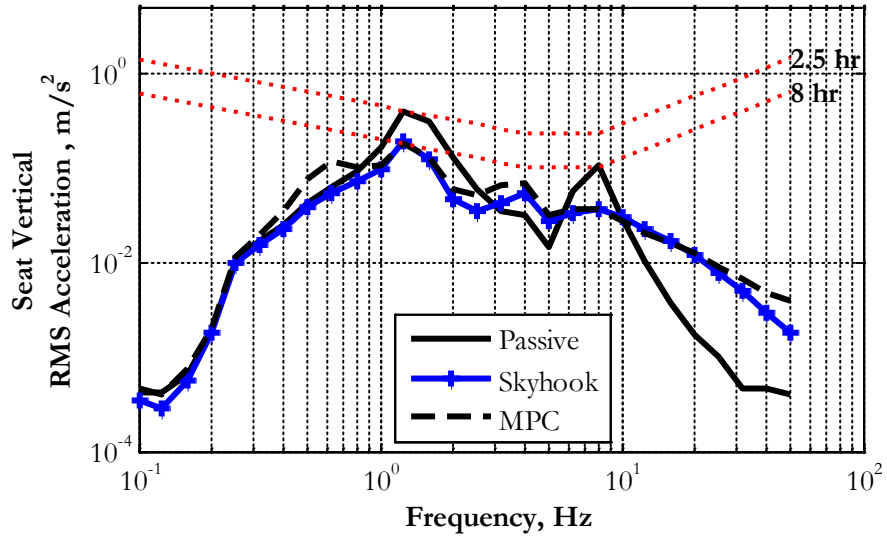


Figure 5.27: Seat RMS Acceleration, MPC vs. Passive vs. Skyhook Law, Smooth highway @60mph

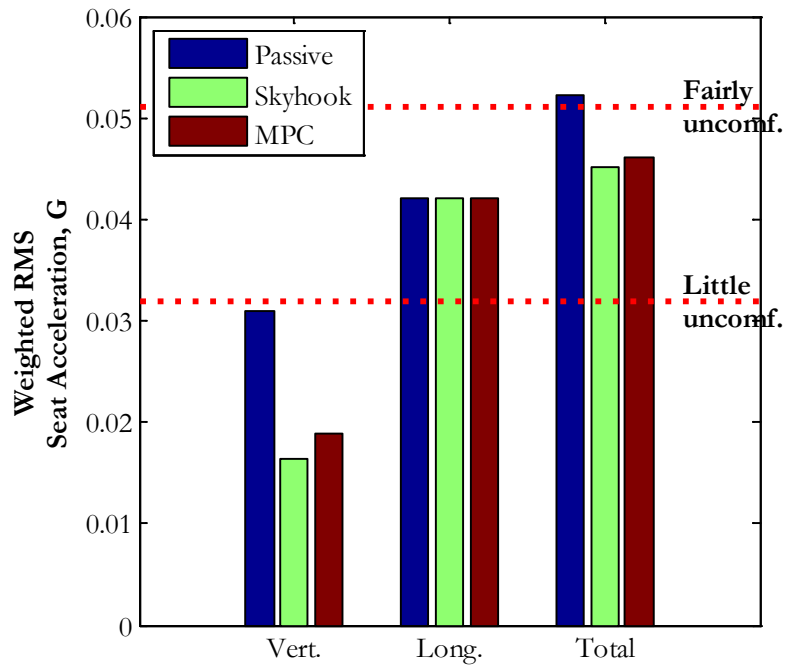


Figure 5.28: Weighted RMS Seat Acceleration, MPC vs. Passive vs. Skyhook Law, Smooth Highway @60 mph

Figure 5.29 compares the seat RMS acceleration for the different control strategies when the vehicle traverses a gravel road at 40 mph. The seat acceleration is marginally improved by the use of the MPC controller compared to a Skyhook law controller. The MPC controller is able to maintain the suspension stroke within the bounds of the bump-stop limits (Table 5.4). Compared to the passive damper, the MPC controller provides better ride in the 1-3 Hz range but is significantly worse in the 3-6 Hz range and above 10 Hz.

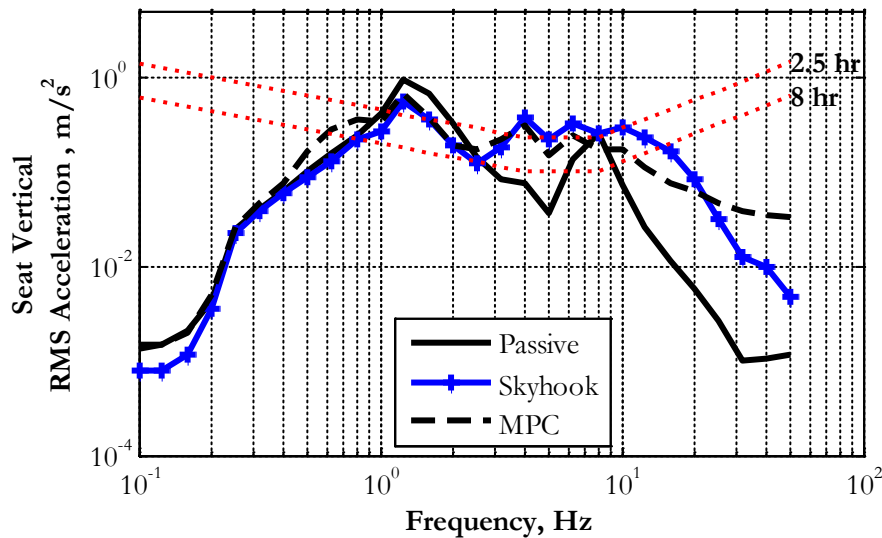
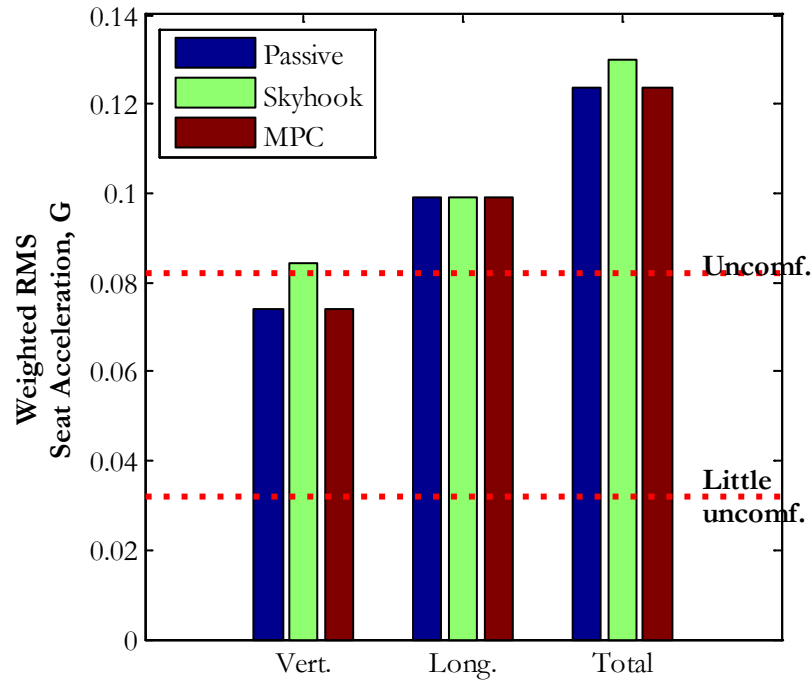


Figure 5.29: Seat RMS Acceleration, MPC vs. Passive vs. Skyhook Law, Gravel Road @ 40 mph



**Figure 5.30: Weighted RMS Seat Acceleration, MPC vs. Passive vs. Skyhook Law, Gravel Road @ 40 mph**

On the gravel road the weighted RMS vertical acceleration at the seat was the same for both the passive and the MPC policy as shown in Figure 5.30. The MPC policy provides better ride than the Skyhook law. The ride was “uncomfortable” for all three cases.

In the previous formulation of the MPC controller, the seat acceleration was penalized. Human sensitivity to vertical acceleration varies with the frequency of the acceleration. Specifically, human beings are more sensitive to vertical acceleration in 4-8 Hz band. The ISO 2631:1997 and ISO 8041 [6, 7] specify a frequency based weighting filter for vertical and horizontal acceleration which accounts for this factor. A study was carried out to explore the benefits of penalizing the frequency weighted seat vertical acceleration. The performance



index can be reformulated from equation (5.26) to include the effect of frequency weighting as:

$$J = \sum_{i=1}^{n-1} [\ddot{x}_{s,w}^2(i)] \quad (5.29)$$

where  $a_w$  is the frequency weighted sprung mass accelerations. The transfer function relating the frequency weighted acceleration to the acceleration is defined as:

$$a_w(s) = W_k(s)a(s) \quad (5.30)$$

where  $W_k(s)$  is the weighting filter in the s-domain as specified by [7]. The objective of the optimization problem at each time step of the frequency weighted model predictive controller (weighted MPC) is to minimize the performance index as specified by equation (5.29) subject to the system dynamics described in equation (5.22) and the constraints described by the equations (5.27) and (5.28). The complete formulation of the performance index and the constraints in predictive form can be found in appendix E. The parameters used for the weighted MPC policy were kept the same as the MPC policy and are stated in Table 5.3.

Figure 5.31 compares the seat RMS acceleration for the weighted MPC control strategies against the Skyhook law and passive seat damper when the vehicle traverses a smooth highway at 60 mph. It was observed that the weighted MPC policy improves the ride comfort when compared to the passive damper in the 0.8-3 Hz and the 6-9 Hz range. Even with the weighting filter applied to the predicted acceleration, the Skyhook law provides the best ride. Further

study needs to be carried out to ascertain whether the global optimum of the optimization problem is found at each time step.

On a smooth highway traversed at 60 mph, the weighted RMS vertical acceleration at the seat was reduced by 42% by employing the weighted MPC policy as compared to the passive damper as shown in Figure 5.32.

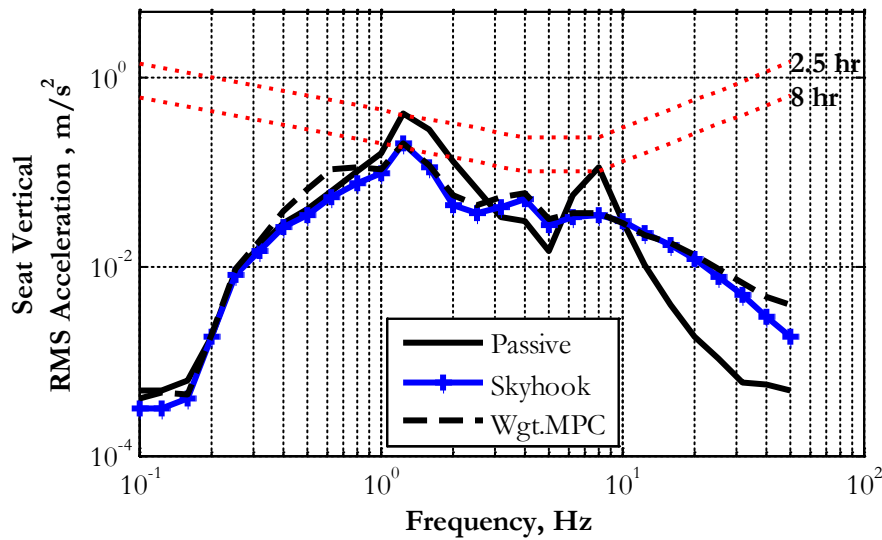


Figure 5.31: Seat RMS Acceleration, Weighted MPC vs. Passive vs. Skyhook Law, Smooth Highway @ 60 mph

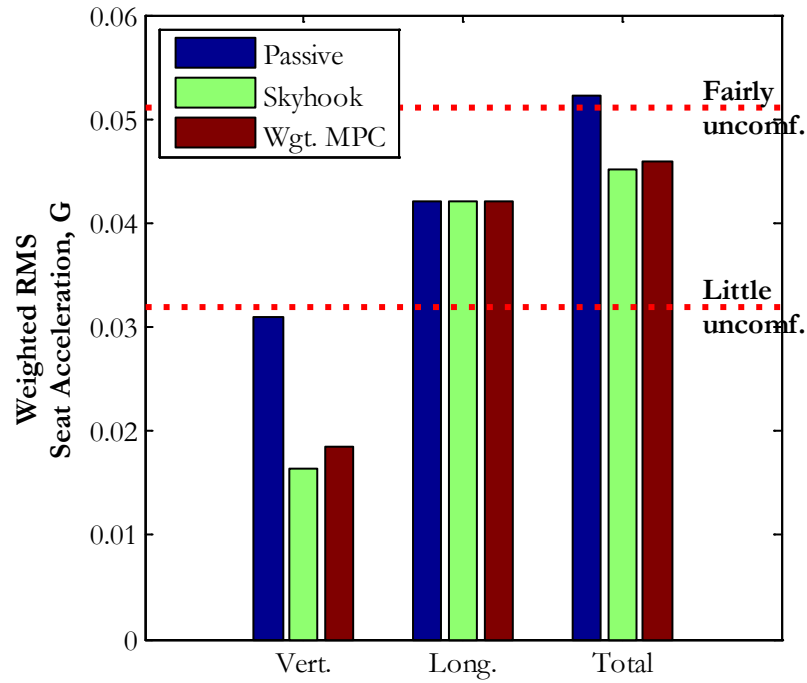


Figure 5.32: Weighted RMS Seat Acceleration, Weighted MPC vs. Passive vs. Skyhook Law, Smooth Highway @60 mph

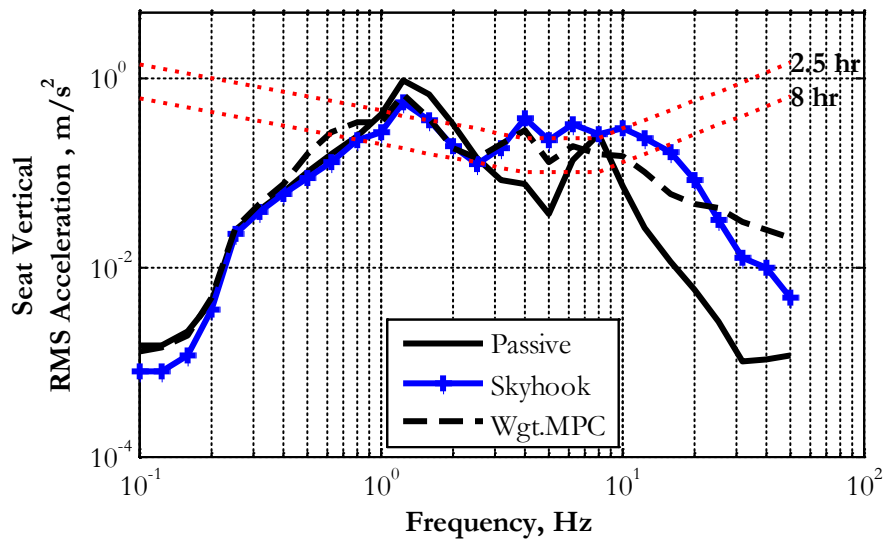
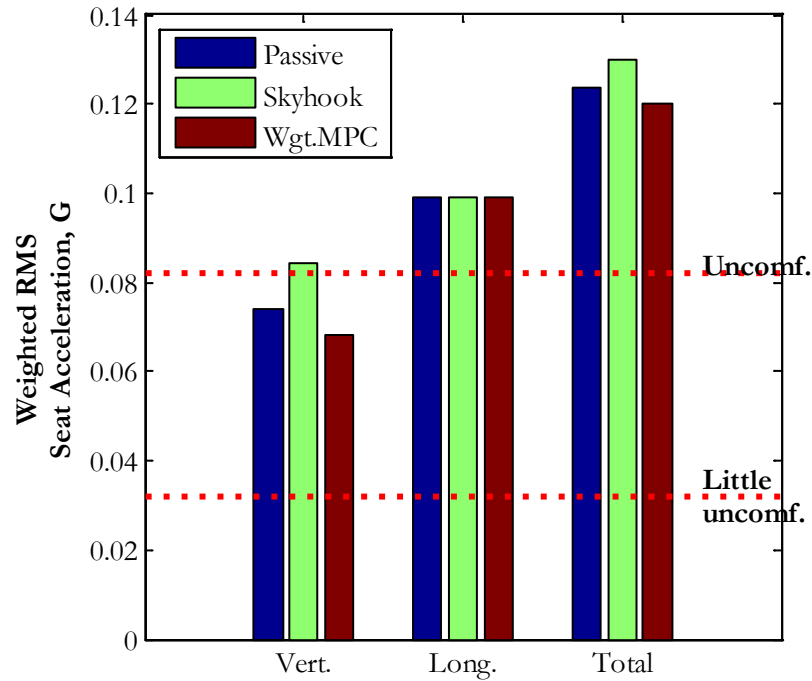


Figure 5.33: Seat RMS Acceleration, Weighted MPC vs. Passive vs. Skyhook Law, Gravel Road @ 40 mph



**Figure 5.34: Weighted RMS Seat Acceleration, Weighted MPC vs. Passive vs. Skyhook Law, Gravel Road @ 40 mph**

Figures 5.33 and 5.34 compare the seat acceleration for the different control strategies when the vehicle traverses a gravel road at 40 mph. The driver ride is marginally improved with the use of the weighted MPC policy compared to the MPC policy.

Table 5.4 compares the passive damper against the skyhook law, the MPC and the weighted MPC policies. The weighted MPC policy improves the ride significantly on the smooth highway and marginally over the gravel road. The computational costs of the MPC and weighted policies are order of magnitude greater than the Skyhook law based on the time required to complete the simulation runs.

**Table 5.4: Driver Seat Ride Comparison for Different Damper Control Strategies, Nominal Rear Suspended Cab**

Damper Type	Weighted Vertical RMS acceleration, G	% Ride Improvement	Max Stroke, cm	Time to simulate 120 seconds, s
<b>Smooth Highway @ 60 mph</b>				
Passive	0.031		3.4	13
Skyhook law	0.016	48%	5	15
MPC	0.019	39%	5.6	400
MPC with weighted acc.	0.018	42%	5.6	400
<b>Gravel Road at 40 mph</b>				
Passive	0.074		7.9	13
Skyhook law	0.084	-18%	9.3	15
MPC	0.074	0.03%	7.9	552
MPC with weighted acc.	0.068	8%	7.8	552

### 5.10. Quadrant Law Control

A closed form controller for semi-active damper based on the Quadrant law was developed in the 1980s by Rakheja and Sankar [11] as an alternative to the Skyhook law specifically for semi-active damper. The objective of the Quadrant law is to minimize the acceleration of the sprung mass. Figure 5.35 shows the working principle of Quadrant law applied to a semi-active damper. This thesis compared the performance of a semi-active quadrant damper with a semi-active skyhook damper and a passive damper.

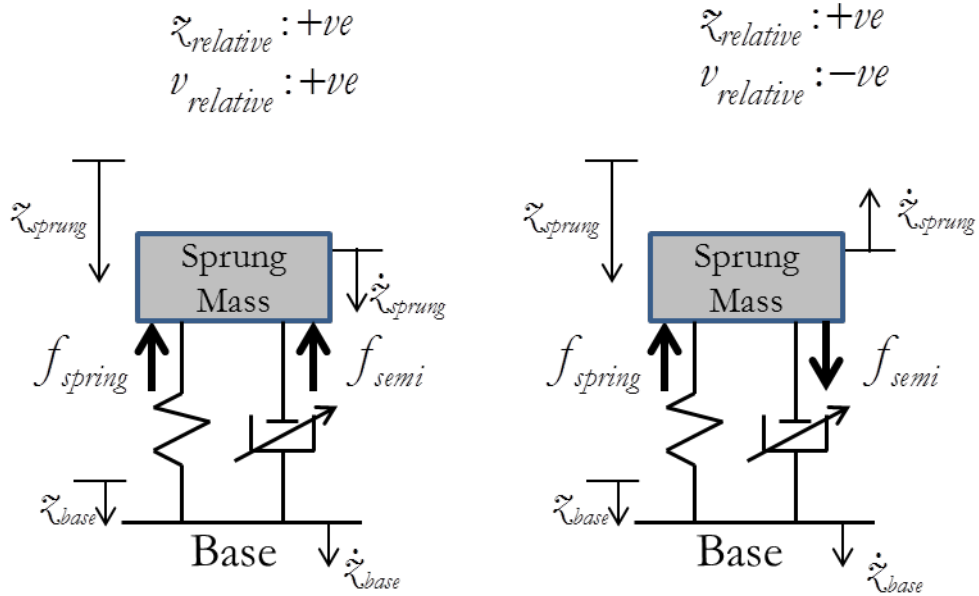


**Figure 5.35: Working Principle of Semi-active Quadrant (Rakheja-Sankar [11]) Law**

Rakheja and Sankar [11] observed that for a passive damper when the spring force,  $f_{spring}$ , and the damping force,  $f_{semi}$ , exerted on the sprung mass are in the same direction, as shown in Figure 5.35 (left), they add up to produce the sprung mass acceleration.

$$a_{sprung} = \ddot{z}_{sprung} = \frac{-(f_{spring} + f_{semi})}{m_{sprung}}, \frac{z_{relative}}{v_{relative}} > 0, \quad (5.31)$$

where  $z_{relative}$  and  $v_{relative}$  are the relative displacement and velocity between sprung mass and the base. In this scenario, an ideal semi-active damper should exert no damping force to minimize the sprung mass acceleration. This can be achieved by setting the damping coefficient of the semi-active damper to zero.

$$c_{desired,quadrant} = 0, \frac{z_{relative}}{v_{relative}} > 0 \quad (5.32)$$

When the spring and the damping forces exerted on the sprung mass are in opposite directions as shown in Figure 5.35 (right), their difference causes the sprung mass acceleration.

$$a_{\text{sprung}} = \ddot{x}_{\text{sprung}} = \frac{-(f_{\text{spring}} - f_{\text{semi}})}{m_{\text{sprung}}}, \frac{\dot{x}_{\text{relative}}}{v_{\text{relative}}} < 0 \quad (5.33)$$

In this scenario to minimize the sprung mass acceleration, the Quadrant law prescribes a damping force equal in magnitude and opposite in direction of the spring force to the sprung mass. Accordingly, the desired damping force exerted by the semi-active Quadrant damper on the sprung mass should be,

$$f_{\text{semi}} = c_{\text{desired,quadrant}} v_{\text{relative}} = -k_{\text{spring}} \dot{x}_{\text{relative}}, \frac{\dot{x}_{\text{relative}}}{v_{\text{relative}}} < 0. \quad (5.34)$$

After rearranging the terms in equation (42), the damping coefficient can be expressed as,

$$c_{\text{desired,quadrant}} = \frac{-k_{\text{spring}} \dot{x}_{\text{relative}}}{v_{\text{relative}}}, \frac{\dot{x}_{\text{relative}}}{v_{\text{relative}}} < 0 \quad (5.35)$$

In practice, the maximum,  $c_{\text{max}}$ , and the minimum,  $c_{\text{min}}$ , damping coefficient that the semi-active damper can attain is determined by its design. The demanded damping coefficient of the semi-active Quadrant damper can be expressed as,

$$c_{\text{semi,quadrant}} = \begin{cases} c_{\text{max}} & , c_{\text{desired,quadrant}} \geq c_{\text{max}} \\ c_{\text{desired,quadrant}} & , c_{\text{min}} < c_{\text{desired,quadrant}} < c_{\text{max}} \\ c_{\text{min}} & , 0 < c_{\text{desired,quadrant}} \leq c_{\text{min}} \end{cases} \quad (5.36)$$

The response of a 1 d.o.f. system using a semi-active quadrant damper is compared to that of a passive system in Figure 5.36. The excitation frequency of the base was twice the system natural frequency. The semi-active quadrant damper system reduces the sprung mass acceleration. Observe that the suspension stroke was somewhat greater for the semi-active system.

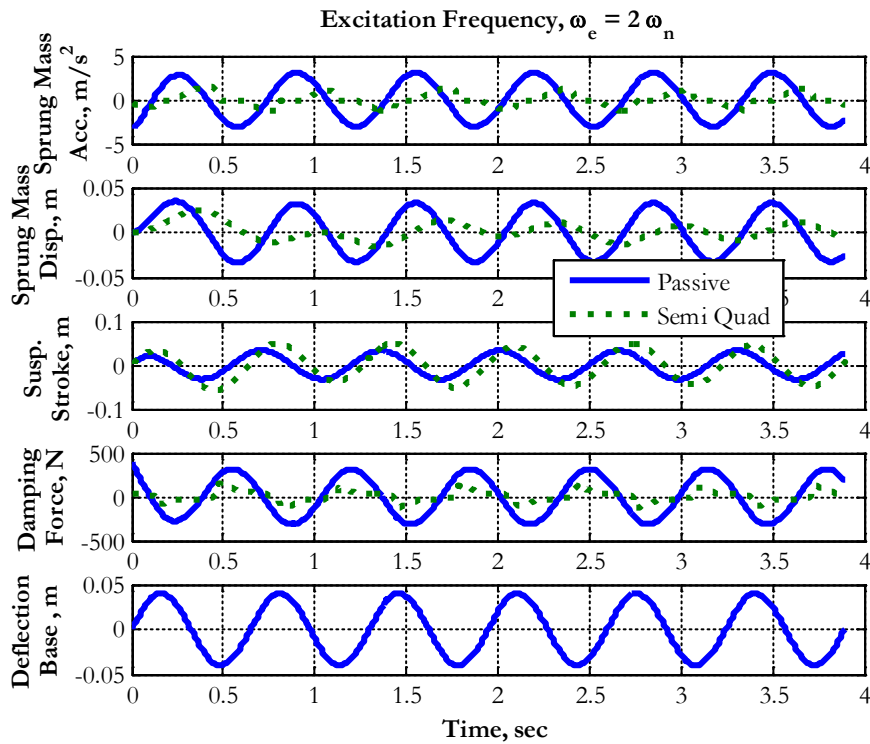


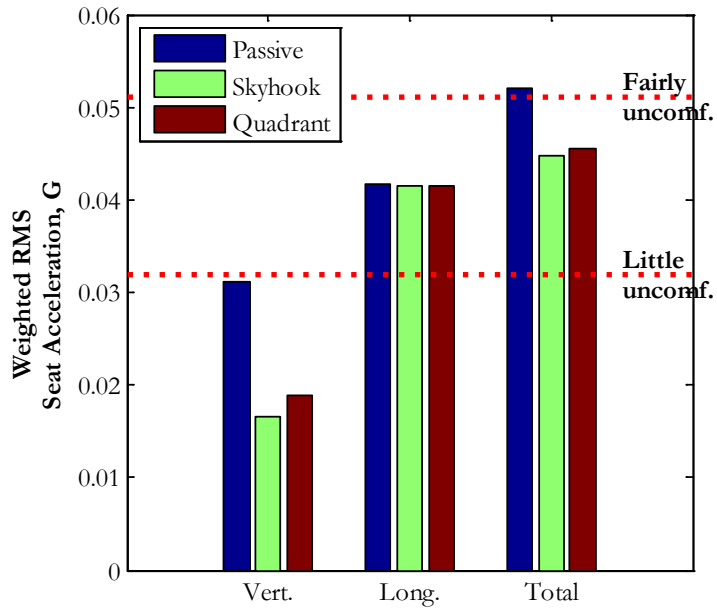
Figure 5.36: Response to Base Excitation: Passive vs. Semi-active Quadrant Damper, 1 d.o.f.

#### ride model

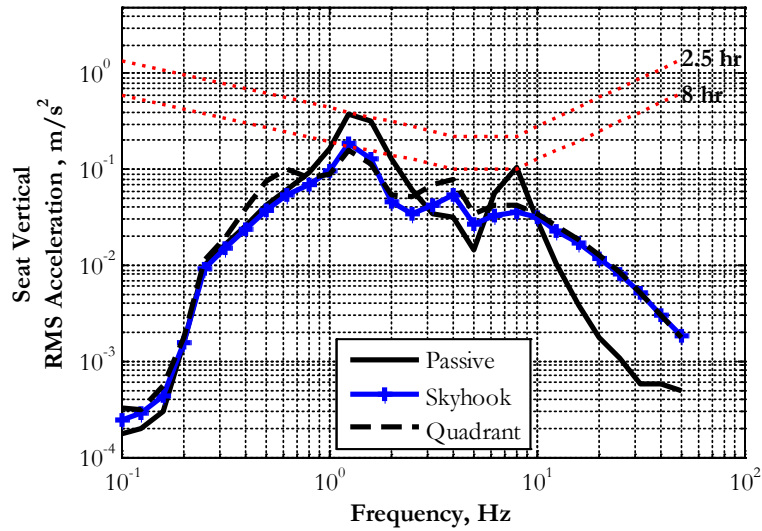
A study was carried out to analyze the ride at the driver's seat by replacing the seat passive damper with a semi-active damper using the Quadrant law. Figure 5.38 compares the RMS vertical accelerations at the seat between the passive system and the semi-active Quadrant damper system on the smooth highway. The weighted RMS vertical acceleration at the seat



was reduced by 42% by employing a quadrant law controller (Figure 5.37). However, the reduction in the weighted RMS vertical acceleration was less than that achieved by skyhook law controller.

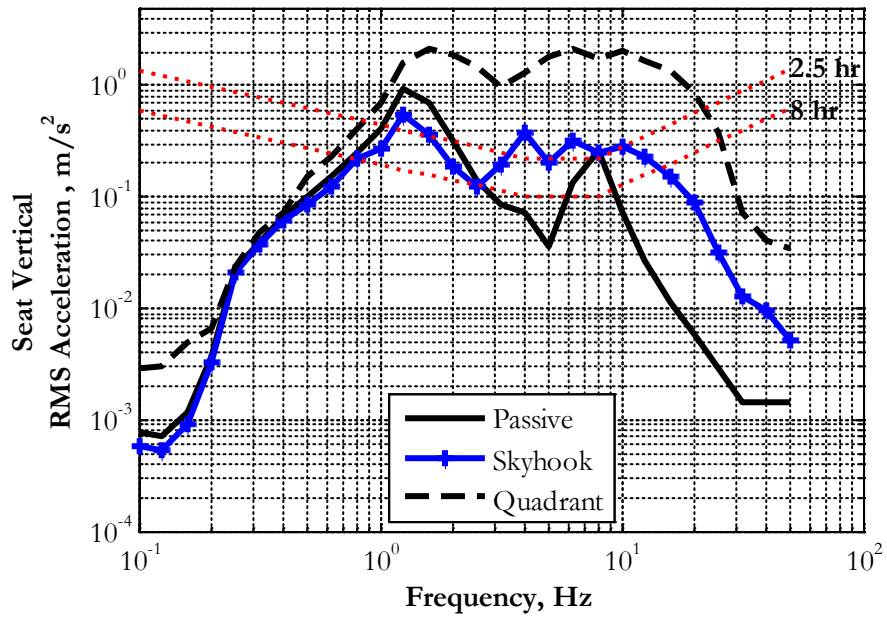


**Figure 5.37: Weighted RMS Seat Acceleration, Passive vs Skyhook vs Quadrant Seat Damper, Smooth Highway @ 60 mph**



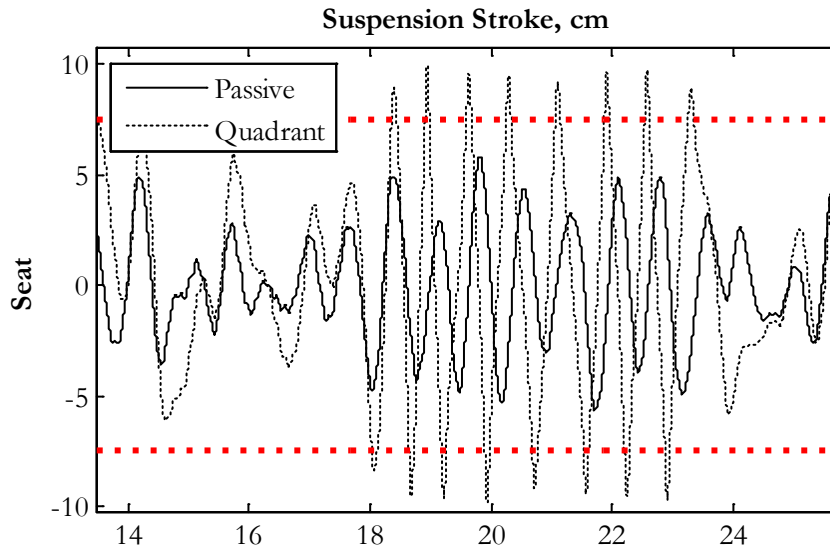
**Figure 5.38: RMS Seat Vertical Acceleration, Passive vs Skyhook vs Quadrant Seat Damper, Smooth Highway@ 60 mph (96.56 kph).**

Figure 5.39 shows the response of each system on a gravel road at 40 mph (64.4 kph). The semi-active Quadrant damper performed worst on this type of road.



**Figure 5.39: RMS Seat Vertical Acceleration, Passive vs Semi-active Quadrant Seat Damper, Gravel Road, 40 mph (64.4 kph).**

Figure 5.40 compares the seat suspension stroke of a semi-active Quadrant damper system and a passive damper traversing a gravel road at 40 mph. For the semi-active Quadrant damper, the suspension hits the bump-stops multiple times.



**Figure 5.40: Seat Suspension Stroke, Semi-Active Damper with Quadrant Law (Top), Passive Damper (Bottom), Highway with Gravel, 60 mph (96.56 kph).**

The Quadrant law prescribes the damping force based on the suspension deflection. The damping force is high at the beginning of the compression and expansion strokes since the exerted spring force and the damping force are in opposite directions (Figure 5.35 (right)). When the suspension is approaching the bump-stops the damping is set to a minimum since the spring force and the damping force exerted on the sprung mass are in the same direction (Figure 5.35 (left)). When approaching the bump-stops the semi-active Quadrant damper dissipates less energy than the passive damper leading to greater suspension strokes. Therefore the seat suspension with the semi-active Quadrant damper was observed to hit the bump-stops frequently. Hitting the bump stops significantly reduces the efficacy of the skyhook and quadrant law dampers on rougher roads.

## 5.11. Conclusions: Semi-active Damper Control Strategies

**Table 5.5: Driver's Seat Ride Comfort for Different Control Strategies and Cab Configurations**

Controller/Configuration	Weighted total RMS acceleration, G	% Ride Improvement	ISO 2631:1997 Ride Classification
<b>Smooth Highway @ 60 mph</b>			
Passive with rear cab	0.052		Fairly Uncomfortable
Fuzzy Switch with rear cab	0.045	14%	A Little Uncomfortable
Weighted MPC with rear cab	0.046	12%	A Little Uncomfortable
Quadrant with rear cab	0.046	12%	A Little Uncomfortable
FS01 (Fuzzy with rear cab, optimum position)	0.031	40%	Not Uncomfortable
FS02 (Fuzzy with full cab, optimum position)	0.028	46%	Not Uncomfortable
<b>Gravel Road at 40 mph</b>			
Passive with rear cab	0.12		Uncomfortable
Fuzzy Switch with rear cab	0.11	8.3%	Uncomfortable
Weighted MPC with rear cab	0.12	3.2%	Uncomfortable
Quadrant with rear cab	0.53	-341%	Extremely Uncomfortable
FS01 (Fuzzy with rear cab, optimum position)	0.079	34%	Fairly Uncomfortable
FS02 (Fuzzy with full cab, optimum position)	0.071	40%	Fairly Uncomfortable

Table 5.5 compares the performance of the control strategies for the seat semi-active damper along with different cab configurations. Among the control strategies for the seat semi-active dampers, the control strategy employing the fuzzy switch mechanism provides the best ride on both a smooth highway and a gravel road. The ride at the driver's seat is "fairly uncomfortable" on a smooth highway employing a passive damper. All the control strategies studied in this thesis manage to make the ride "a little uncomfortable" on the smooth highway which is an improvement over the passive damper. Improvement in ride on a gravel road is much more difficult to achieve due to the suspension design space constraint. The ride is "uncomfortable" with a passive damper. Employing a fuzzy switch or a weighted MPC control strategy, the driver's seat ride on a gravel road can be marginally improved but it is still "uncomfortable". The Quadrant law control strategy provides an "extremely uncomfortable" ride on gravel road. It must also be commented that the weighted MPC controller is computationally very expensive and is probably not implementable in real time.

A large improvement in driver ride comfort is achievable by employing a semi-active damper at the seat with the fuzzy switch mechanism and locating the cab mounts near the beaming nodes. For a rear suspended cab, the ride on a smooth highway is "not uncomfortable" and that on a gravel road is "fairly uncomfortable". This would be the author's recommended configuration as it significantly improves the ride on both roads and would not involve substantial redesign of the tractor. A fully suspended cab mounted on the frame near the nodal points with semi-active seat damper provides the best ride. The ride improvements compared to passive damper is 40% or more. For truck manufacturers seeking to offer the best possible ride, this configuration offers the best promise.

## CHAPTER 6

### SUMMARY AND CONCLUSIONS

#### 6.1 Model Validation

The truck vertical ride dynamics simulation tool used in this thesis was developed based on a 15 vertical plane d.o.f. model of the tractor semi-trailer. The simulated response of the developed (reduced order) model was compared to that of the commercially available simulation software, TruckSim.

The following conclusions were drawn from the validation process

- The largest difference observed between the static axle loads of the two models was less 1%. The difference between the two model's axle loads was insignificant.
- Comparison of the dynamic response of the two models traversing a smooth small road bump at 60 mph revealed similar sprung mass and axle deflection response.
- Since the static axle loads and dynamic response of the two models are very similar, one can conclude that the reduced order Matlab model matches the TruckSim model.

#### 6.2 Design Study Results

The following conclusions were drawn from the frame flexibility and cab design studies.

- Increasing the frame beaming frequency by 50% improves ride comfort by 15% but also increases the dry mass by 14%. The trade-off between improved ride comfort and reduced fuel economy needs to be evaluated by the truck fleet operators.

- The fully suspended cab compared to the baseline configuration provides up to 18% reduction in the total weighted RMS acceleration at the seat and up to 26% reduction in the longitudinal weighted RMS acceleration. The cost of designing a front cab suspension and retrofitting it to the existing trucks might be financially unappealing to the truck manufacturers.
- For a rear suspended cab with the cab mounts re-located close to the nodal points of the beaming mode, the weighted RMS longitudinal seat acceleration is reduced by 39% and the total weighted RMS acceleration at the seat is reduced by 24%. If properly designed, locating the cab mounts near the beaming mode nodal points could be a fairly cheap retro-fitting process that leads to significantly improved ride.
- Compared to the baseline model, a 48 % reduction in the weighted RMS longitudinal seat acceleration and 31 % reduction in total weighted RMS seat acceleration is achieved by locating the mounting positions of a fully suspended cab near the nodes of the beaming mode.

### **6.3 Semi-active Damper Study Results**

Various control strategies for a semi-active seat damper were explored in this work .The following conclusions were drawn from the study of the semi-active seat damper control study as applied to a tractor semi-trailer with rear suspended cab.

- There are two possible optimal policies for the seat isolation system based on the spatial characteristics of the base excitation.



- The optimal damping value is a constant and is the same for both the optimal policies if the sprung mass and the spring stiffness are kept the same.
- The weighted RMS vertical acceleration at the seat when the truck is traversing a smooth highway at 60 mph was reduced by 45% by employing a Skyhook law or Fuzzy Switch Optimum law controller compared to a passive damper.
- On a gravel road traversed at 40 mph, the weighted RMS vertical acceleration at the seat was reduced by increased by 14% by employing a Skyhook law and was reduced by 36% with the Fuzzy Switch Optimum law controller. The drawbacks of the Skyhook Law to large excitation levels are clearly manifested on this road and at this velocity.
- On a smooth highway traversed at 60 mph, the weighted RMS vertical acceleration at the seat was reduced by 48% by employing the Fuzzy Switch Optimal semi-active seat damper and locating the rear cab mounts near the beaming nodes of the tractor frame. In this configuration, the weighted RMS fore-aft acceleration at the seat was reduced by 36% and the total weighted acceleration at the seat is reduced by 40%. In fact, as per the ISO 2761:1997 classification the ride with this configuration can be termed as “not uncomfortable”. This is the most promising avenue to improve the ride comfort at the driver seat.
- On a smooth highway traversed at 60 mph, the weighted RMS vertical acceleration at the seat was reduced by 48% by employing the Fuzzy Switch Optimal semi-active seat damper, suspending the front and rear of the cab from the frame and locating the cab

mounts near the beaming nodes of the tractor frame. The weighted RMS fore-aft acceleration at the seat was reduced by 45% and the total weighted acceleration at the seat is reduced by 46%. As per the ISO 2761:1997 classification the ride with this configuration can also be termed as “not uncomfortable”. This configuration provides the greatest benefit to driver seat ride comfort. However a financial design study needs to be carried out to find if the cost of employing a fully suspended cab justifies the additional cost.

- The novel MPC based semi-active damper reduces the weighted RMS vertical acceleration by up to 42% and 8% when compared to a passive damper when traversing a smooth highway and a gravel road at 60 mph respectively. The improvement in ride comfort when traversing a gravel road is significant when compared to the passive seat damper. It must be commented that the computational requirements of the developed MPC controller are much greater than any of the other semi-active damper controllers and is probably infeasible to implement in real time.

#### **6.4 Future Work**

Some possible avenues for future work to further develop the tractor semi-trailer model and the control strategies for semi-active cab damper.

- Correlating the simulated data with physical test data would lend more credibility to the model. This study shows the importance of locating the nodal points of the tractor frame bending modes to the proper design of the cab mount locations. Test data which

sheds more light on the mode shapes with appropriate boundary conditions on the frame would greatly add to the understanding of the ride dynamics of the truck.

- Developing a three dimensional truck ride model that includes the longitudinal sprung mass velocity, the cab roll motion and the frame twist. This model can be used to accurately evaluate the ride comfort due to asymmetric road excitation.
- This study only includes the first bending mode of the frames. The “assumed mode” method lends itself to easy addition of higher frequency modes with if the mode shapes are known analytically or can be approximated. A finite element analysis of the frame can be used to determine the mode shapes of the frame bending modes in the frequencies of interest (<25 Hz).
- This study shows the possibility of greatly improving the ride at the driver’s seat by employing a semi-active seat damper with an appropriate control strategy. A possibility exists of further improving the driver’s seat ride by developing control strategies for semi-active cab dampers (for a rear suspended cab or a fully suspended cab).
- A recursive least square estimator to estimate the seat load and the seat suspension stiffness was developed in this thesis. The development of the estimator assumes constant longitudinal velocity of the truck. The estimated values are then fed to the seat semi-active damper control strategy. A more realistic scenario would be to estimate the values when the vehicle is accelerating (e.g. starting from stand still).

- It is the belief of this author that the relative poor performance of the MPC scheme when applied to the semi-active seat damper is because of the failure of the optimization routine to find the global minimum of the design performance index. Further study to improve the MPC scheme should focus on this aspect.

## APPENDICES

## Appendix A

### Baseline Truck Data, Eigenvalues and Eigenvectors

**Table A.1: Dimensions of the Tractor Semi-Trailer Model**

Symbol	Description	Generic	Unit
$a$	Distance from 1 <sup>st</sup> Tractor Axle to Tractor CG	2.210	m
$b$	Distance from 2 <sup>nd</sup> Tractor Axle to Tractor CG	2.440	m
$d$	Distance from 3 <sup>rd</sup> Tractor Axle to Tractor CG	3.760	m
$e$	Distance from 1 <sup>st</sup> Trailer Axle to Trailer CG	0.460	m
$f$	Distance from 2 <sup>nd</sup> Trailer Axle to Trailer CG	1.83	m
$j$	Distance from Tractor CG to 5 <sup>th</sup> Wheel mount	2.900	m
$l$	Distance from 5 <sup>th</sup> Wheel mount to Trailer CG	5.725	m
$u$	Distance from front cab mount to Tractor CG	1.825	m
$h$	Distance from engine mount to Tractor CG	1.400	m
$i$	Distance from rear cab mount to Tractor CG	0.725	m
$n$	Height of Tractor CG above Horizontal 5 <sup>th</sup> Wheel mount	0.025	m
$p$	Height of Trailer CG above the Tractor CG	0.845	m
$q$	Distance from front cab mount to cab CG	1.232	m
$r$	Distance from rear cab mount to cab CG	1.338	m
$s$	Distance from cab CG to seat mount	0.032	m
$w$	Distance from cab CG to tractor CG	0.613	m
$y$	Distance from tractor CG to seat mount	-0.419	m
$ds$	Height of driver seat over cab CG	1.0 <sup>+</sup>	m
$b_{a1}$	Front end of the tractor to axle #1	1.175	m
$L_t$	Length of Tractor	7.870	m
$L_{trl}$	Length of Trailer	11.450	m
$r_{ire}$	Nominal Tire Radius	0.48	m

**Table A.2: Inertial Properties**

Symbol	Description	Generic	Unit
$m_t$	Tractor Mass	3783	kg
$I_t$	Tractor Frame Moment of Inertia	46590.9	kg m <sup>2</sup>
$m_{tr}$	Trailer Mass	10800	kg
$I_{tr}$	Trailer Moment of Inertia	200000	kg m <sup>2</sup>
$m_l$	Trailer Load Mass	11367	kg
$m_c$	Cab Mass	1471	kg
$I_c$	Cab Moment of Inertia $I_{yy}$	2250	kg m <sup>2</sup>

$m_s$	mass of driver's seat + 200lb driver	106.7	kg
$m_e$	Mass of engine	2030	kg
$m_{i1}$	Tractor Steer Axle mass with tires	635	kg
$m_{i2}$	1 <sup>st</sup> Tractor Drive axle mass with tires (conv./wide-base)	988	kg
$m_{i3}$	2 <sup>nd</sup> Tractor Drive axle mass with tires (conv./wide-base)	857	kg
$m_{i4}$	1 <sup>st</sup> Trailer axle mass with tires (conv./wide-base)	1007	kg
$m_{i5}$	2 <sup>nd</sup> Trailer axle mass with tires (conv./wide-base)	1007	kg

**Table A.3: Vehicle Suspension Parameters**

Symbol	Description	Generic	Unit
$k_1$	1 <sup>st</sup> tractor axle spring coefficient	540000	N/m
$k_2$	2 <sup>nd</sup> tractor axle spring coefficient	675000	N/m
$k_3$	3 <sup>rd</sup> tractor axle spring coefficient	630000	N/m
$k_4$	1 <sup>st</sup> trailer axle spring coefficient	2764000	N/m
$k_5$	2 <sup>nd</sup> trailer axle spring coefficient	2764000	N/m
$c_1$	1 <sup>st</sup> tractor axle damping coefficient	11270	N.s/m
$c_2$	2 <sup>nd</sup> tractor axle damping coefficient	27500	N.s/m
$c_3$	3 <sup>rd</sup> tractor axle damping coefficient	27500	N.s/m
$c_4$	1 <sup>st</sup> trailer axle damping coefficient	83300	N.s/m
$c_5$	2 <sup>nd</sup> trailer axle damping coefficient	83300	N.s/m
$k_e$	Engine Mount Spring coefficient <sup>@</sup>	10050000	N/m
$c_e$	Engine Mount Damping coefficient	13300	N.s/m

**Table A.4: Seat Suspension Parameters**

Symbol	Description	Generic	Unit
$k_s$	Driver's seat spring coefficient	2500	N/m
$c_s$	Driver's seat damping coefficient	730	N.s/m

**Table A.5: Cab Suspension Parameters**

Symbol	Description	Rear Suspended	Fully Suspended	Units
$k_{sf}$	Front spring stiffness	68880000	80000	N/m
$k_{sr}$	Rear spring stiffness	80000	80000	N/m
$c_{sf}$	Front damping	227000	13500	N.s/m
$c_{sr}$	Rear damping	13800	13500	N.s/m

*Note: No seat and cab suspension data available. The cab suspensions were designed for natural frequency of*

*~ 1.8Hz and damping ratio,  $\xi \sim 1$*

<sup>@</sup> For our calculations we combine all the suspensions on the engine to arrive at a total value –  $k_e = 10050 \times 10^3$  N/m and  $c_e = 13300$

**Table A.6: Natural Frequencies and Damping Ratios (Baseline)**

Mode #	Frequency (Hz)	Damping Ratio	Mode Description
1	146.95	0.015	Body Heave (out of phase)
2	54.06	0.008	Cab
3	13.74	0.073	Engine Heave
4	11.92	0.677	First trailer axle suspension
5	11.51	0.582	Second trailer axle suspension
6	9.54	0.371	Third tractor axle suspension
7	8.96	0.271	Second tractor axle suspension
8	8.7	0.19	First tractor axle suspension
9	8.14	0.008	Trailer Frame Beaming
10	6.9	0.054	Tractor Frame Beaming
11	1.84	0.976	Cab mode
12	0.98	0.695	Seat heave
13	1.36	0.078	Tractor Pitch (Engine heave)
14	1.98	0.193	Counter Pitch (Tractor Frame Mode)
15	1.77	0.078	Trailer Pitch (Trailer frame heave)

**Table A.7: Eigenvectors of the Baseline Linearized Model**

Natural Frequency = 146.95 Hz, Damping Ratio = 0.015		
DOF	Magnitude	Phase
$z_s$	0	95
$z_c$	0.04	-175
$\theta_c$	0.03	-5
$z_e$	0	-130
$z_t$	1	0
$\theta_t$	0.23	0
$q_t$	0.62	1
$z_{tr}$	0.2	177
$\theta_{tr}$	0.13	-2
$q_{tr}$	0.48	-2
$z_1$	0.02	-92
$z_2$	0.04	-91
$z_3$	0.08	-90
$z_4$	0.02	-89
$z_5$	0.02	-89
Natural Frequency = 54.06 Hz, Damping Ratio = 0.008		
DOF	Magnitude	Phase
$z_s$	0.02	-90
$z_c$	1	0
$\theta_c$	0.81	180
$z_e$	0.02	26
$z_t$	0.31	-179



$\theta_t$	0.08	1
$q_t$	0.09	-179
$z_{thr}$	0.03	-178
$\theta_{thr}$	0.02	3
$q_{thr}$	0.07	4
$z_1$	0.03	86
$z_2$	0.01	93
$z_3$	0.01	95
$z_4$	0.01	-76
$z_5$	0.01	-76
<b>Natural Frequency = 13.74 Hz, Damping Ratio = 0.073</b>		
<b>DOF</b>	<b>Magnitude</b>	<b>Phase</b>
$z_s$	0.02	76
$z_c$	0.25	168
$\theta_c$	0.18	21
$z_e$	1	0
$z_t$	0.31	-176
$\theta_t$	0.08	4
$q_t$	0.26	12
$z_{thr}$	0.02	-179
$\theta_{thr}$	0.01	4
$q_{thr}$	0.05	3
$z_1$	0.13	71
$z_2$	0.12	103
$z_3$	0.11	-64
$z_4$	0.03	-36
$z_5$	0.02	-34
<b>Natural Frequency = 11.92 Hz, Damping Ratio = 0.677</b>		
<b>DOF</b>	<b>Magnitude</b>	<b>Phase</b>
$z_s$	0	-143
$z_c$	0.02	-12
$\theta_c$	0.01	177
$z_e$	0.01	52
$z_t$	0.05	-3
$\theta_t$	0.02	3
$q_t$	0.04	-12
$z_{thr}$	0.06	-144
$\theta_{thr}$	0.03	-166
$q_{thr}$	0.23	-179
$z_1$	0.01	151
$z_2$	0.03	-170
$z_3$	0.07	-178
$z_4$	1	0

$z_5$	0.76	5
<b>Natural Frequency = 11.51 Hz, Damping Ratio = 0.582</b>		
<b>DOF</b>	<b>Magnitude</b>	<b>Phase</b>
$z_s$	0	-62
$z_c$	0	61
$\theta_c$	0	-123
$z_e$	0	122
$z_t$	0	65
$\theta_t$	0	73
$q_t$	0	59
$z_{thr}$	0.02	-167
$\theta_{thr}$	0	-148
$q_{thr}$	0.04	18
$z_1$	0	-136
$z_2$	0	-98
$z_3$	0.01	-106
$z_4$	0.75	-174
$z_5$	1	0
<b>Natural Frequency = 9.54 Hz, Damping Ratio = 0.371</b>		
<b>DOF</b>	<b>Magnitude</b>	<b>Phase</b>
$z_s$	0.01	131
$z_c$	0.08	-121
$\theta_c$	0.04	-29
$z_e$	0.05	47
$z_t$	0.1	-149
$\theta_t$	0.03	-143
$q_t$	0.3	-161
$z_{thr}$	0.04	-145
$\theta_{thr}$	0.02	34
$q_{thr}$	0.11	2
$z_1$	0.16	0
$z_2$	0.11	61
$z_3$	1	0
$z_4$	0.12	-8
$z_5$	0.08	8
<b>Natural Frequency = 8.96 Hz, Damping Ratio = 0.271</b>		
<b>DOF</b>	<b>Magnitude</b>	<b>Phase</b>
$z_s$	0	20
$z_c$	0.03	122
$\theta_c$	0.02	154
$z_e$	0.06	-113
$z_t$	0.02	-162
$\theta_t$	0.01	-136

$q_t$	0.09	50
$z_{thr}$	0.01	-144
$\theta_{thr}$	0.01	34
$q_{thr}$	0.05	0
$z_1$	0.1	-143
$z_2$	1	0
$z_3$	0.07	-134
$z_4$	0.04	-8
$z_5$	0.02	4
<b>Natural Frequency = 8.7 Hz, Damping Ratio = 0.19</b>		
<b>DOF</b>	<b>Magnitude</b>	<b>Phase</b>
$z_s$	0.01	119
$z_c$	0.05	-145
$\theta_c$	0.03	-21
$z_e$	0.05	-110
$z_t$	0.04	178
$\theta_t$	0.01	49
$q_t$	0.11	172
$z_{thr}$	0.01	133
$\theta_{thr}$	0	-48
$q_{thr}$	0.03	-81
$z_1$	1	0
$z_2$	0.08	42
$z_3$	0.22	-178
$z_4$	0.03	-88
$z_5$	0.02	-79
<b>Natural Frequency = 8.14 Hz, Damping Ratio = 0.008</b>		
<b>DOF</b>	<b>Magnitude</b>	<b>Phase</b>
$z_s$	0.01	151
$z_c$	0.1	-125
$\theta_c$	0.13	-16
$z_e$	0.07	47
$z_t$	0.28	-176
$\theta_t$	0.08	-180
$q_t$	0.59	-166
$z_{thr}$	0.11	-178
$\theta_{thr}$	0.07	2
$q_{thr}$	1	0
$z_1$	0.56	166
$z_2$	0.26	170
$z_3$	0.92	-165
$z_4$	0.67	-2
$z_5$	0.36	-1

<b>Natural Frequency = 6.9 Hz, Damping Ratio = 0.054</b>		
<b>DOF</b>	<b>Magnitude</b>	<b>Phase</b>
$z_s$	0.04	-10
$z_c$	0.24	77
$\theta_c$	0.29	130
$z_e$	0.32	-166
$z_t$	0.13	-25
$\theta_t$	0.02	-152
$q_t$	1	0
$z_{thr}$	0.03	-36
$\theta_{thr}$	0.01	132
$q_{thr}$	0.41	18
$z_1$	0.68	9
$z_2$	0.26	-143
$z_3$	0.56	23
$z_4$	0.3	23
$z_5$	0.14	26
<b>Natural Frequency = 1.84 Hz, Damping Ratio = 0.976</b>		
<b>DOF</b>	<b>Magnitude</b>	<b>Phase</b>
$z_s$	0.74	-167
$z_c$	1	0
$\theta_c$	0.88	-1
$z_e$	0.1	169
$z_t$	0.09	169
$\theta_t$	0	2
$q_t$	0.04	-22
$z_{thr}$	0.02	165
$\theta_{thr}$	0.01	-13
$q_{thr}$	0	-33
$z_1$	0.02	177
$z_2$	0.01	176
$z_3$	0.01	-178
$z_4$	0	173
$z_5$	0	-6
<b>Natural Frequency = 0.77 Hz, Damping Ratio = 0.7</b>		
<b>DOF</b>	<b>Magnitude</b>	<b>Phase</b>
$z_s$	1	0
$z_c$	0.02	61
$\theta_c$	0.01	45
$z_e$	0	109
$z_t$	0	109
$\theta_t$	0	-69
$q_t$	0	-72

$Z_{thr}$	0	102
$\theta_{thr}$	0	-74
$q_{thr}$	0	-123
$Z_1$	0	113
$Z_2$	0	114
$Z_3$	0	101
$Z_4$	0	106
$Z_5$	0	-64
<b>Natural Frequency = 1.36 Hz, Damping Ratio = 0.078</b>		
<b>DOF</b>	<b>Magnitude</b>	<b>Phase</b>
$Z_s$	0.75	-76
$Z_c$	0.88	-9
$\theta_c$	0.19	-144
$Z_c$	1	0
$Z_t$	0.68	-1
$\theta_t$	0.21	-179
$q_t$	0.04	179
$Z_{thr}$	0.01	-17
$\theta_{thr}$	0.01	169
$q_{thr}$	0	0
$Z_1$	0.34	7
$Z_2$	0.04	11
$Z_3$	0.03	-154
$Z_4$	0	-13
$Z_5$	0.01	179
<b>Natural Frequency = 1.98 Hz, Damping Ratio = 0.193</b>		
<b>DOF</b>	<b>Magnitude</b>	<b>Phase</b>
$Z_s$	0.6	-117
$Z_c$	0.96	-33
$\theta_c$	0.82	-39
$Z_c$	0.38	18
$Z_t$	1	0
$\theta_t$	0.52	-7
$q_t$	0.22	-166
$Z_{thr}$	0.85	-24
$\theta_{thr}$	0.3	-175
$q_{thr}$	0.07	72
$Z_1$	0.08	166
$Z_2$	0.55	20
$Z_3$	0.62	19
$Z_4$	0.4	-14
$Z_5$	0.24	-47
<b>Natural Frequency = 1.77 Hz, Damping Ratio = 0.078</b>		

<b>DOF</b>	<b>Magnitude</b>	<b>Phase</b>
$z_s$	0.13	25
$z_c$	0.19	99
$\theta_c$	0.18	104
$z_e$	0.04	133
$z_t$	0.22	131
$\theta_t$	0.13	131
$q_t$	0.04	-39
$z_{tir}$	1	0
$\theta_{tir}$	0.26	-18
$q_{tir}$	0.18	-180
$z_1$	0.03	-37
$z_2$	0.13	151
$z_3$	0.16	151
$z_4$	0.54	7
$z_5$	0.77	3

## Appendix B

### Equations of Motion

The equations of motion for the fifteen degree-of-freedom tractor semi-trailer are derived in this appendix using Newtonian and Lagrangian approaches. Except the frames, all other equations of motion were derived using Newtonian mechanics.

For simplicity only spring forces are shown in the free body diagrams. As the spring and dampers are in parallel, the derivation of force is same for both elements.

#### Equation of Motion of Driver Seat

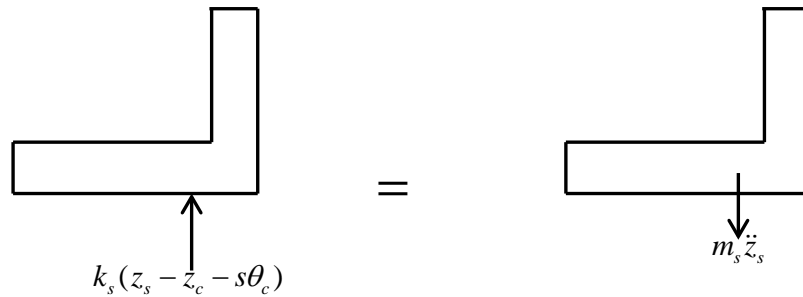


**Figure B.1: Free Body Diagram of the Seat.**

Summing forces in vertical direction, we have

$$+\uparrow \Sigma F : k_s(\dot{z}_s - \dot{z}_c - s\dot{\theta}_c) + c_s(\ddot{z}_s - \ddot{z}_c - s\ddot{\theta}_c) = -m_s \ddot{z}_s \quad (\text{B.1})$$

Bump-stops were introduced to the seat stiffness curve. The seat spring element behaves linearly in the normal operation regime of  $\pm 7.5$  cm. There is a smooth transition between the linear regime and the bump-stop. Figure B.2 shows the variation of spring force versus deflection for the seat suspension

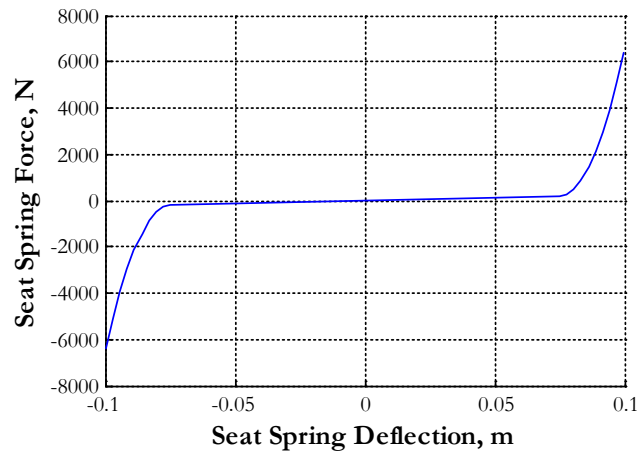
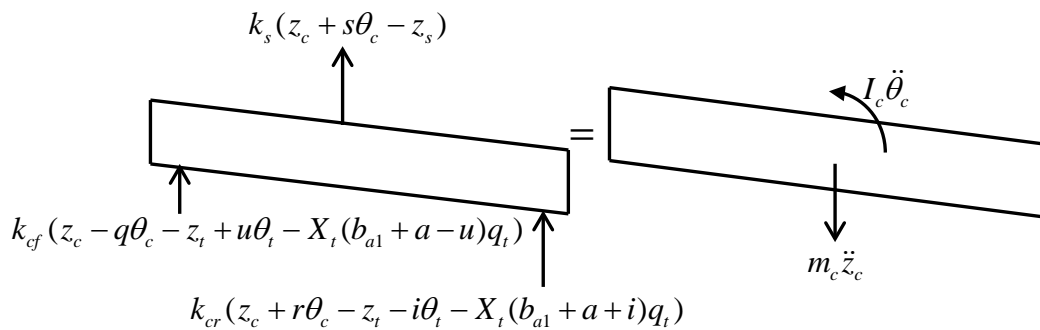


Figure B.2: Seat Spring Force vs. Deflection Curve

### Equation of Motion of Cab





**Figure B.3: Free Body Diagram of the Cab**

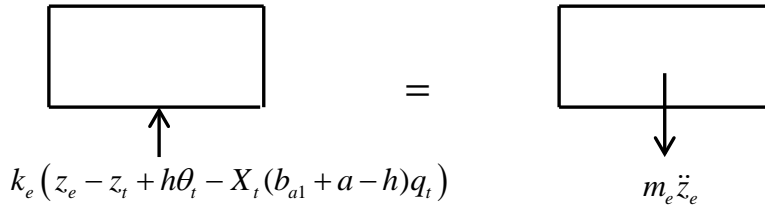
Summing forces vertically, we have,

$$\begin{aligned}
 & + \uparrow \Sigma F : \\
 & k_s(\tilde{x}_c + s\theta_c - \tilde{x}_s) + c_s(\dot{\tilde{x}}_c + s\dot{\theta}_c - \dot{\tilde{x}}_s) \\
 & + k_{cf}(\tilde{x}_c - q\theta_c - \tilde{x}_t + u\theta_t - X_t(b_{a1} + a - u)q_t) \\
 & + c_{cf}(\dot{\tilde{x}}_c - q\dot{\theta}_c - \dot{\tilde{x}}_t + u\dot{\theta}_t - X_t(b_{a1} + a - u)\dot{q}_t) \\
 & + k_{cr}(\tilde{x}_c + r\theta_c - \tilde{x}_t - i\theta_t - X_t(b_{a1} + a + i)q_t) \\
 & + c_{cr}(\dot{\tilde{x}}_c + r\dot{\theta}_c - \dot{\tilde{x}}_t - i\dot{\theta}_t - X_t(b_{a1} + a + i)\dot{q}_t) \\
 & = -m_c \ddot{\tilde{x}}_c
 \end{aligned} \tag{B.2}$$

Summing moments about cab CG , we have,

$$\begin{aligned}
 & \overleftarrow{+} \Sigma M : \\
 & + s k_s(\tilde{x}_c + s\theta_c - \tilde{x}_s) + s c_s(\dot{\tilde{x}}_c + s\dot{\theta}_c - \dot{\tilde{x}}_s) \\
 & - q k_{cf}(\tilde{x}_c - q\theta_c - \tilde{x}_t + u\theta_t - X_t(b_{a1} + a - u)q_t) \\
 & - q c_{cf}(\dot{\tilde{x}}_c - q\dot{\theta}_c - \dot{\tilde{x}}_t + u\dot{\theta}_t - X_t(b_{a1} + a - u)\dot{q}_t) \\
 & + r k_{cr}(\tilde{x}_c + r\theta_c - \tilde{x}_t - i\theta_t - X_t(b_{a1} + a + i)q_t) \\
 & + r c_{cr}(\dot{\tilde{x}}_c + r\dot{\theta}_c - \dot{\tilde{x}}_t - i\dot{\theta}_t - X_t(b_{a1} + a + i)\dot{q}_t) \\
 & = -I_c \ddot{\theta}_c
 \end{aligned} \tag{B.3}$$

### Equation of Motion of Engine



The diagram shows a rectangular box representing the engine. An upward-pointing arrow from the bottom center of the box is labeled with the spring force expression  $k_e(z_e - z_t + h\theta_t - X_t(b_{a1} + a - h)q_t)$ . To the right of the box is an equals sign. To the right of the equals sign is another rectangular box. A downward-pointing arrow from the bottom center of this second box is labeled with the weight force expression  $m_e \ddot{z}_e$ .

**Figure B.4: Free Body Diagram of the Engine**

Summing forces vertically, we have,

$$\begin{aligned} & k_e (\tilde{z}_e - \tilde{z}_t + b\theta_t - X_t(b_{a1} + a - b)q_t) \\ & + c_e (\dot{\tilde{z}}_e - \dot{\tilde{z}}_t + b\dot{\theta}_t - X_t(b_{a1} + a - b)\dot{q}_t) \\ & = -m_e \ddot{\tilde{z}}_e \end{aligned} \tag{B.4}$$

## Equations of Motion of Tractor Frame

The tractor frame has 3 d.o.f.: frame heave, frame pitch and 1<sup>st</sup> mode of beaming. The beaming mode is simplified using separation of variables

$$\eta_t(x, t) = E_t(x)q_t(t) \quad (\text{B.5})$$

The frame equations of motion are derived using Lagrangian method. Let the mass density of the frame per unit length be  $\mu_t$ . This includes the mass of the components bolted onto the C-channels as well as the C-channels themselves. It is assume that the mass of the components is uniformly distributed along the length of the tractor frame. Therefore,

$$\mu_t = \rho_{cc}A_{cc} + \mu_{\text{comp}}, \quad (\text{B.6})$$

where  $\rho_{cc}$  is the density (per unit volume) of the material used to manufacture the C-channels and  $A_{cc}$  is the cross-sectional area of the C-channels.  $\mu_{\text{comp}}$  is the mass per unit length of the additional components on the frame (obtained by dividing the mass of all the components on the frame by the total length of the frame).

The generalized coordinates for the tractor frame motion are

$$\xi_j = [z_t, \theta_t, q_t] \quad (\text{B.7})$$

The Lagrangian method uses kinetic ( $T$ ) and potential energy ( $V$ ) of the system, along with generalized forces ( $\Xi$ ), which are determined from the virtual work done by the external forces.

$$L = T - V \quad (\text{B.8})$$

For the tractor frame, the kinetic energy is derived as,

$$T = \int_0^{L_t} \frac{1}{2} \mu_t \left( \dot{z}_t - (b_{cg} - x) \dot{\theta}_t + X_t(x) \dot{q}_t \right)^2 dx, \quad (\text{B.9})$$

and the potential energy of the system is defined as,

$$\begin{aligned} V = & \frac{1}{2} EI_{t,cc} q_t^2 \int_0^{L_t} \left( X_t''(x) \right)^2 dx \\ & + \frac{1}{2} k_{cf} \left( z_c - q\theta_c - z_t + u\theta_t - X_t(b_{a1} + a - u)q_t \right)^2 \\ & + \frac{1}{2} k_{cr} \left( z_c + r\theta_c - z_t - i\theta_t - X_t(b_{a1} + a + i)q_t \right)^2 \\ & + \frac{1}{2} k_e \left( z_d - b\theta_t + X_t(b_{a1} + a - b)q_t - z_e \right)^2 \\ & + \frac{1}{2} k_1 \left( z_d - a\theta_t + X_t(b_{a1})q_t - z_1 \right)^2 \\ & + \frac{1}{2} k_2 \left( z_d + b\theta_t + X_t(b_{a1} + a + b)q_t - z_2 \right)^2 \\ & + \frac{1}{2} k_3 \left( z_d + d\theta_t + X_t(b_{a1} + a + d)q_t - z_3 \right)^2 \\ & + \frac{1}{2} k_v \left( z_t + j\theta_t + X_t(b_{a1} + a + j)q_t - z_{tr} + l\theta_{tr} - X_{tr}(0)q_{tr} \right)^2 \\ & + \text{damping energies} \end{aligned} \quad (\text{B.10})$$

Note that only the C-channels contribute to the strain energy of the system. The mass due to additional components that are bolted on to the frame are treated as rigid nodal mass points which do not undergo any strain (infinite Young's modulus).

It may be shown using Hamilton's principle that the variation of the Lagrangian is equal to the generalized forces,

$$\frac{d}{dt} \left( \frac{\delta L}{\delta \dot{\xi}_j} \right) - \frac{\delta L}{\delta \xi_j} = \Xi \quad (\text{B.11})$$

For tractor the external force do not perform any work thus  $\Xi = 0$ .

For  $\xi_1 = z_t$

$$\begin{aligned}
& -k_{cf} (z_c - q\theta_c - z_t + u\theta_t - X_t(b_{a1} + a - u)q_t) \\
& -c_{cf} (\dot{z}_c - q\dot{\theta}_c - \dot{z}_t + u\dot{\theta}_t - X_t(b_{a1} + a - u)\dot{q}_t) \\
& -k_{cr} (z_c + r\theta_c - z_t - i\theta_t - X_t(b_{a1} + a + i)q_t) \\
& -c_{cr} (\dot{z}_c + r\dot{\theta}_c - \dot{z}_t - i\dot{\theta}_t - X_t(b_{a1} + a + i)\dot{q}_t) \\
& +k_e (z_t - b\theta_t + X_t(b_{a1} + a - b)q_t - z_e) \\
& +c_e (\dot{z}_t - b\dot{\theta}_t + X_t(b_{a1} + a - b)\dot{q}_t - \dot{z}_e) \\
& +k_1 (z_t - a\theta_t + X_t(b_{a1})q_t - z_1) \\
& +c_1 (\dot{z}_t - a\dot{\theta}_t + X_t(b_{a1})\dot{q}_t - \dot{z}_1) \\
& +k_2 (z_t + b\theta_t + X_t(b_{a1} + a + b)q_t - z_2) \\
& +c_2 (\dot{z}_t + b\dot{\theta}_t + X_t(b_{a1} + a + b)\dot{q}_t - \dot{z}_2) \\
& +k_3 (z_t + d\theta_t + X_t(b_{a1} + a + d)q_t - z_3) \\
& +c_3 (\dot{z}_t + d\dot{\theta}_t + X_t(b_{a1} + a + d)\dot{q}_t - \dot{z}_3) \\
& +k_v (z_t + j\theta_t + X_t(b_{a1} + a + j)q_t - z_{thr} + l\theta_{thr} - X_{thr}(0)q_{thr}) \\
& +c_v (\dot{z}_t + j\dot{\theta}_t + X_t(b_{a1} + a + j)\dot{q}_t - \dot{z}_{thr} + l\dot{\theta}_{thr} - X_{thr}(0)\dot{q}_{thr}) \\
& = -m_t \ddot{z}_t + \mu_t \ddot{\theta}_t \int_0^{L_t} (b_{zg} - x) dx - \mu_t \dot{q}_t \int_0^{L_t} X_t(x) dx
\end{aligned} \quad (\text{B.12})$$

For  $\xi_2 = \theta_t$

$$\begin{aligned}
& +uk_{gf}(\dot{z}_c - q\dot{\theta}_c - \dot{z}_t + u\dot{\theta}_t - X_t(b_{a1} + a - u)q_t) \\
& +uc_{gf}(\dot{z}_c - q\dot{\theta}_c - \dot{z}_t + u\dot{\theta}_t - X_t(b_{a1} + a - u)\dot{q}_t) \\
& -ik_{cr}(\dot{z}_c + r\dot{\theta}_c - \dot{z}_t - i\dot{\theta}_t - X_t(b_{a1} + a + i)q_t) \\
& -ic_{cr}(\dot{z}_c + r\dot{\theta}_c - \dot{z}_t - i\dot{\theta}_t - X_t(b_{a1} + a + i)\dot{q}_t) \\
& -bk_e(\dot{z}_t - b\dot{\theta}_t + X_t(b_{a1} + a - b)q_t - \dot{z}_e) - bc_e(\dot{z}_t - b\dot{\theta}_t + X_t(b_{a1} + a - b)\dot{q}_t - \dot{z}_e) \\
& -ak_1(\dot{z}_t - a\dot{\theta}_t + X_t(b_{a1})q_t - \dot{z}_1) - ac_1(\dot{z}_t - a\dot{\theta}_t + X_t(b_{a1})\dot{q}_t - \dot{z}_1) \\
& +bk_2(\dot{z}_t + b\dot{\theta}_t + X_t(b_{a1} + a + b)q_t - \dot{z}_2) + bc_2(\dot{z}_t + b\dot{\theta}_t + X_t(b_{a1} + a + b)\dot{q}_t - \dot{z}_2) \\
& +dk_3(\dot{z}_t + d\dot{\theta}_t + X_t(b_{a1} + a + d)q_t - \dot{z}_3) + dc_3(\dot{z}_t + d\dot{\theta}_t + X_t(b_{a1} + a + d)\dot{q}_t - \dot{z}_3) \\
& +jk_v(\dot{z}_t + j\dot{\theta}_t + X_t(b_{a1} + a + j)q_t - \dot{z}_{thr} + l\dot{\theta}_{thr} - X_{thr}(0)q_{thr}) \\
& +jc_v(\dot{z}_t + j\dot{\theta}_t + X_t(b_{a1} + a + j)\dot{q}_t - \dot{z}_{thr} + l\dot{\theta}_{thr} - X_{thr}(0)\dot{q}_{thr}) \\
& = +\ddot{z}_t \mu_t \int_0^{L_t} (b_{g_t} - x) dx - I_t \ddot{\theta}_t + \mu_t \ddot{q}_t \int_0^{L_t} X_t(x) (b_{g_t} - x) dx
\end{aligned} \tag{B.13}$$

For  $\xi_3 = q_t$

$$\begin{aligned}
& -X_t(b_{a1} + a - u)k_{gf}(\dot{z}_c - q\dot{\theta}_c - \dot{z}_t + u\dot{\theta}_t - X_t(b_{a1} + a - u)q_t) \\
& -X_t(b_{a1} + a - u)c_{gf}(\dot{z}_c - q\dot{\theta}_c - \dot{z}_t + u\dot{\theta}_t - X_t(b_{a1} + a - u)\dot{q}_t) \\
& -X_t(b_{a1} + a + i)k_{cr}(\dot{z}_c + r\dot{\theta}_c - \dot{z}_t - i\dot{\theta}_t - X_t(b_{a1} + a + i)q_t) \\
& -X_t(b_{a1} + a + i)c_{cr}(\dot{z}_c + r\dot{\theta}_c - \dot{z}_t - i\dot{\theta}_t - X_t(b_{a1} + a + i)\dot{q}_t) \\
& +X_t(b_{a1} + a - b)k_e(z_t - b\theta_t + X_t(b_{a1} + a - b)q_t - z_e) \\
& +X_t(b_{a1} + a - b)c_e(\dot{z}_t - b\dot{\theta}_t + X_t(b_{a1} + a - b)\dot{q}_t - \dot{z}_e) \\
& +X_t(b_{a1})k_1(z_t - a\theta_t + X_t(b_{a1})q_t - z_1) + X_t(b_{a1})c_1(\dot{z}_t - a\dot{\theta}_t + X_t(b_{a1})\dot{q}_t - \dot{z}_1) \\
& +X_t(b_{a1} + a + b)k_2(z_t + b\theta_t + X_t(b_{a1} + a + b)q_t - z_2) \\
& +X_t(b_{a1} + a + b)c_2(\dot{z}_t + b\dot{\theta}_t + X_t(b_{a1} + a + b)\dot{q}_t - \dot{z}_2) \\
& +X_t(b_{a1} + a + d)k_3(z_t + d\theta_t + X_t(b_{a1} + a + d)q_t - z_3) \\
& +X_t(b_{a1} + a + d)c_3(\dot{z}_t + d\dot{\theta}_t + X_t(b_{a1} + a + d)\dot{q}_t - \dot{z}_3) \\
& +X_t(b_{a1} + a + j)k_v(z_t + j\theta_t + X_t(b_{a1} + a + j)q_t - z_{thr} + l\theta_{thr} - X_{thr}(0)q_{thr}) \\
& +X_t(b_{a1} + a + j)c_v(\dot{z}_t + j\dot{\theta}_t + X_t(b_{a1} + a + j)\dot{q}_t - \dot{z}_{thr} + l\dot{\theta}_{thr} - X_{thr}(0)\dot{q}_{thr}) \\
& +EI_{t,\alpha}q_t \int_0^{L_t} (X_t''(x))^2 dx \\
& = -\ddot{z}_t \mu_t \int_0^{L_t} X_t(x) dx + \mu_t \ddot{\theta}_t \int_0^{L_t} X_t(x) (b_g - x) dx - \mu_t \ddot{q}_t \int_0^{L_t} (X_t(x))^2 dx
\end{aligned} \tag{B.14}$$

### Equation of Motion of Steer Axle: Axle 1

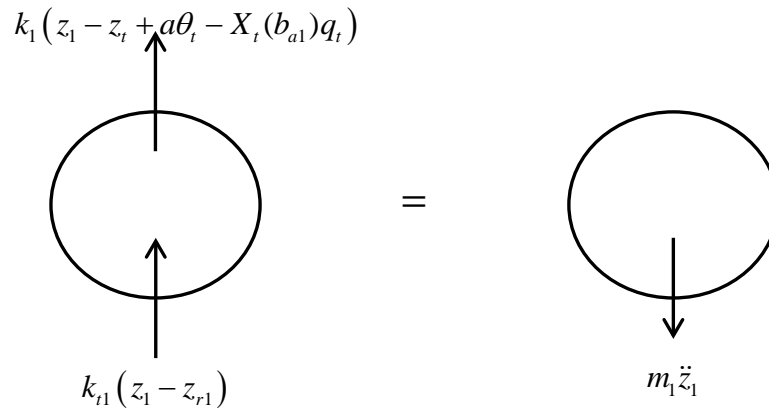


Figure B.5: Free Body Diagram of Steer Axle

Summing forces vertically, we have,

$$\begin{aligned}
 & k_1(z_1 - z_t + a\theta_t - X_t(b_{a1})q_t) + k_{t1}(z_1 - z_{r1}) \\
 & + c_{t1}(\dot{z}_1 - \dot{z}_{r1}) + c_1(\dot{z}_1 - \dot{z}_t + a\dot{\theta}_t - X_t(b_{a1})\dot{q}_t) = -m_1\ddot{z}_1
 \end{aligned}
 \tag{B.15}$$



### Equation of Motion of 1<sup>st</sup> Drive Axle: Axle 2

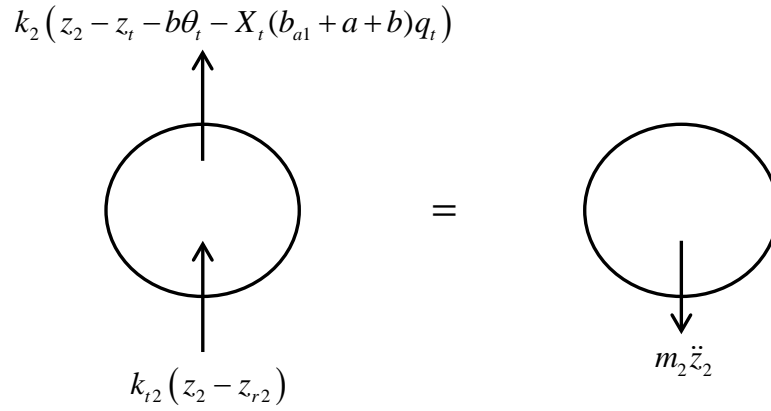
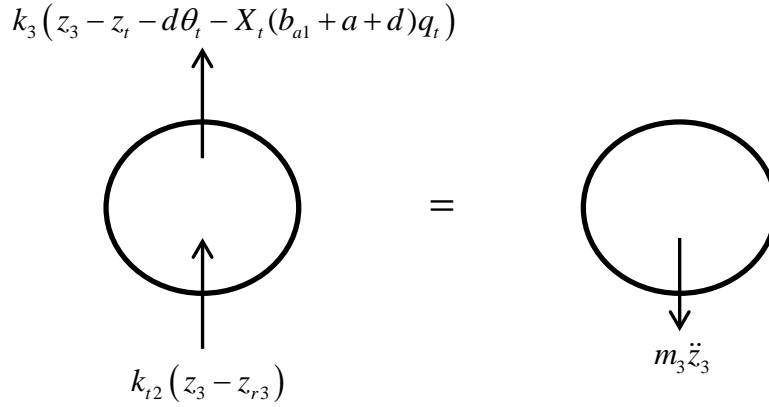


Figure B.6: Free Body Diagram of 1<sup>st</sup> Drive Axle

Summing forces vertically, we have,

$$\begin{aligned}
 & k_2(\tilde{z}_2 - \tilde{z}_t - b\dot{\theta}_t - X_t(b_{a1} + a + b)q_t) + k_{t2}(\tilde{z}_2 - \tilde{z}_{r2}) \\
 & + c_{t2}(\dot{\tilde{z}}_2 - \dot{\tilde{z}}_{r2}) + c_2(\dot{\tilde{z}}_2 - \dot{\tilde{z}}_t - b\dot{\theta}_t - X_t(b_{a1} + a + b)\dot{q}_t) = -m_2\ddot{\tilde{z}}_2
 \end{aligned}
 \tag{B.16}$$

### Equation of Motion of 2<sup>nd</sup> Drive Axle: Axle 3



**Figure B.7: Free Body Diagram of 2<sup>nd</sup> Drive Axle**

Summing forces vertically, we have,

$$\begin{aligned}
 & k_3(z_3 - z_t - d\theta_t - X_t(b_{a1} + a + d)q_t) + k_{t3}(z_3 - z_{r3}) \\
 & + c_{t3}(\dot{z}_3 - \dot{z}_{r3}) + c_3(\dot{z}_3 - \dot{z}_t - d\dot{\theta}_t - X_t(b_{a1} + a + d)\dot{q}_t) = -m_3\ddot{z}_3
 \end{aligned} \tag{B.17}$$

### Equations of Motion Trailer Frame

The equations of motion for the trailer beam are also developed using Lagrangian method. If the mass per unit length of the trailer is

$$\mu_{\text{tr}} = \rho_{\text{cc}}A_{\text{cc}} + \mu_{\text{comp,tr}}, \tag{B.18}$$

where  $\rho_c$  is the density (per unit volume) of the material used to manufacture the C-channels of the frame and  $A_c$  is the cross-sectional area of the C-channels.  $\mu_{\text{comp,tr}}$  is the mass per unit length of the additional structural elements on the frame.

The beaming mode is simplified using separation of variables.

$$\eta_{\text{tr}}(x, t) = X_{\text{tr}}(x)q_{\text{tr}}(t) \quad (\text{B.19})$$

The generalized coordinates for the trailer frame motion are

$$\xi_j = [z_{\text{tr}}, \theta_{\text{tr}}, q_{\text{tr}}] \quad (\text{B.20})$$

For the trailer frame, the kinetic energy is derived as,

$$T = \int_0^{L_{\text{tr}}} \frac{1}{2} \mu_{\text{tr}} \left( \dot{z}_{\text{tr}} - (l-x)\dot{\theta}_{\text{tr}} + X_{\text{tr}}(x)\dot{q}_{\text{tr}} \right)^2 dx, \quad (\text{B.21})$$

and, the potential energy in the system is,

$$\begin{aligned} V = & \frac{1}{2} EI_{\text{tr,cc}} q_{\text{tr}}^2 \int_0^{L_{\text{tr}}} \left( X_{\text{tr}}''(x) \right)^2 dx \\ & + \frac{1}{2} k_4 \left( z_{\text{tr}} - e\theta_{\text{tr}} + X_{\text{tr}}(l+e)q_{\text{tr}} - z_4 \right)^2 \\ & + \frac{1}{2} k_5 \left( z_{\text{tr}} + f\theta_{\text{tr}} + X_{\text{tr}}(l+f)q_{\text{tr}} - z_5 \right)^2 \\ & + \frac{1}{2} k_v \left( z_{\text{t}} + j\theta_{\text{t}} + X_{\text{t}}(b_{a1} + a + j)q_{\text{t}} - z_{\text{tr}} + l\theta_{\text{tr}} - X_{\text{tr}}(0)q_{\text{tr}} \right)^2 \\ & + \text{damping energies} \end{aligned} \quad (\text{B.22})$$

Note that only the C-channels contribute to the strain energy of the system. The mass due to additional components that are bolted on to the frame are treated as rigid nodal mass points which do not undergo any strain (infinite Young's modulus).

It may be shown using Hamilton's principle that the variation of the Lagrangian is equal to the generalized forces,

$$\frac{d}{dt} \left( \frac{\delta L}{\delta \dot{\xi}_j} \right) - \frac{\delta L}{\delta \xi_j} = \Xi \quad (\text{B.23})$$

For tractor the external force do not perform any work thus  $\Xi = 0$ .

For  $\xi_1 = z_{\text{tr}}$

$$\begin{aligned} & +k_4 (z_{\text{tr}} - e\theta_{\text{tr}} + X_{\text{tr}}(l+e)q_{\text{tr}} - z_4) \\ & +c_4 (\dot{z}_{\text{tr}} - e\dot{\theta}_{\text{tr}} + X_{\text{tr}}(l+e)\dot{q}_{\text{tr}} - \dot{z}_4) \\ & +k_5 (z_{\text{tr}} + f\theta_{\text{tr}} + X_{\text{tr}}(l+f)q_{\text{tr}} - z_5) \\ & +c_5 (\dot{z}_{\text{tr}} + f\dot{\theta}_{\text{tr}} + X_{\text{tr}}(l+f)\dot{q}_{\text{tr}} - \dot{z}_5) \\ & -k_v (z_{\text{t}} + j\theta_{\text{t}} + X_{\text{t}}(b_{a1} + a + j)q_{\text{t}} - z_{\text{tr}} + l\theta_{\text{tr}} - X_{\text{tr}}(0)q_{\text{tr}}) \\ & -c_v (\dot{z}_{\text{t}} + j\dot{\theta}_{\text{t}} + X_{\text{t}}(b_{a1} + a + j)\dot{q}_{\text{t}} - \dot{z}_{\text{tr}} + l\dot{\theta}_{\text{tr}} - X_{\text{tr}}(0)\dot{q}_{\text{tr}}) \\ & = -m_{\text{tr}}\ddot{z}_{\text{tr}} + \mu_{\text{tr}}\ddot{\theta}_{\text{tr}} \int_0^{L_{\text{tr}}} (l-x) dx - \mu_{\text{tr}}\ddot{q}_{\text{tr}} \int_0^{L_{\text{tr}}} X_{\text{tr}}(x) dx \end{aligned} \quad (\text{B.24})$$

For  $\xi_2 = \theta_{\text{tr}}$

$$\begin{aligned}
& -ek_4(\tilde{z}_{\text{tr}} - e\theta_{\text{tr}} + X_{\text{tr}}(l+e)q_{\text{tr}} - \tilde{z}_4) \\
& -ec_4(\dot{\tilde{z}}_{\text{tr}} - e\dot{\theta}_{\text{tr}} + X_{\text{tr}}(l+e)\dot{q}_{\text{tr}} - \dot{\tilde{z}}_4) \\
& +fk_5(\tilde{z}_{\text{tr}} + f\theta_{\text{tr}} + X_{\text{tr}}(l+f)q_{\text{tr}} - \tilde{z}_5) \\
& +fc_5(\dot{\tilde{z}}_{\text{tr}} + f\dot{\theta}_{\text{tr}} + X_{\text{tr}}(l+f)\dot{q}_{\text{tr}} - \dot{\tilde{z}}_5) \\
& +lk_v(\tilde{z}_t + j\theta_t + X_t(b_{a1} + a + j)q_t - \tilde{z}_{\text{tr}} + l\theta_{\text{tr}} - X_{\text{tr}}(0)q_{\text{tr}}) \\
& +lc_v(\dot{\tilde{z}}_t + j\dot{\theta}_t + X_t(b_{a1} + a + j)\dot{q}_t - \dot{\tilde{z}}_{\text{tr}} + l\dot{\theta}_{\text{tr}} - X_{\text{tr}}(0)\dot{q}_{\text{tr}}) \\
& = +\ddot{\tilde{z}}_t \rho_{\text{tr}} \mathcal{A}_{\text{tr}} \int_0^{L_{\text{tr}}} (l-x) dx - I_{\text{tr}} \ddot{\theta}_{\text{tr}} + \mu_{\text{tr}} \ddot{q}_{\text{tr}} \int_0^{L_{\text{tr}}} X_{\text{tr}}(x)(l-x) dx
\end{aligned} \tag{B.25}$$

For  $\xi_3 = q_{\text{tr}}$

$$\begin{aligned}
& +X_{\text{tr}}(l+e)k_4(\tilde{z}_{\text{tr}} - e\theta_{\text{tr}} + X_{\text{tr}}(l+e)q_{\text{tr}} - \tilde{z}_4) \\
& +X_{\text{tr}}(l+e)c_4(\dot{\tilde{z}}_{\text{tr}} - e\dot{\theta}_{\text{tr}} + X_{\text{tr}}(l+e)\dot{q}_{\text{tr}} - \dot{\tilde{z}}_4) \\
& +X_{\text{tr}}(l+f)k_5(\tilde{z}_{\text{tr}} + f\theta_{\text{tr}} + X_{\text{tr}}(l+f)q_{\text{tr}} - \tilde{z}_5) \\
& +X_{\text{tr}}(l+f)c_5(\dot{\tilde{z}}_{\text{tr}} + f\dot{\theta}_{\text{tr}} + X_{\text{tr}}(l+f)\dot{q}_{\text{tr}} - \dot{\tilde{z}}_5) \\
& -X_{\text{tr}}(0)k_v(\tilde{z}_t + j\theta_t + X_t(b_{a1} + a + j)q_t - \tilde{z}_{\text{tr}} + l\theta_{\text{tr}} - X_{\text{tr}}(0)q_{\text{tr}}) \\
& -X_{\text{tr}}(0)c_v(\dot{\tilde{z}}_t + j\dot{\theta}_t + X_t(b_{a1} + a + j)\dot{q}_t - \dot{\tilde{z}}_{\text{tr}} + l\dot{\theta}_{\text{tr}} - X_{\text{tr}}(0)\dot{q}_{\text{tr}}) \\
& +EI_{\text{tr},\text{cc}}q_{\text{tr}} \int_0^{L_{\text{tr}}} (X_{\text{tr}}''(x))^2 dx \\
& = -\ddot{\tilde{z}}_{\text{tr}} \mu_{\text{tr}} \int_0^{L_{\text{tr}}} X_{\text{tr}}(x) dx + \mu_{\text{tr}} \ddot{\theta}_{\text{tr}} \int_0^{L_{\text{tr}}} X_{\text{tr}}(x)(l-x) dx \\
& -\mu_{\text{tr}} \ddot{q}_{\text{tr}} \int_0^{L_{\text{tr}}} X_{\text{tr}}(x)^2 dx
\end{aligned} \tag{B.26}$$

### Equation of Motion of Axle 4: Trailer Axle 1

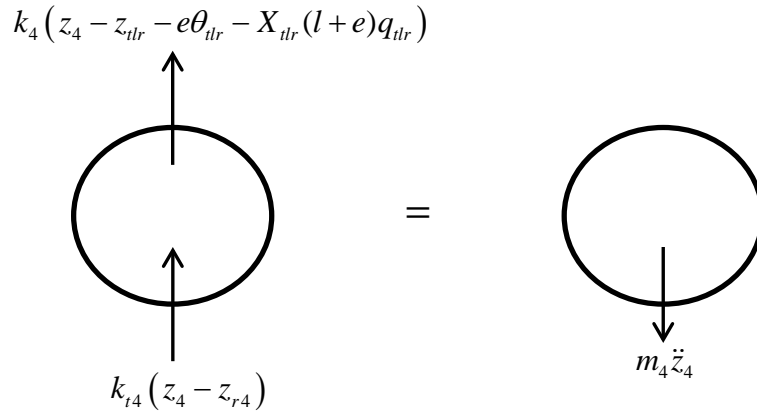


Figure B.8: Free Body Diagram of 1<sup>st</sup> Trailer Axle

Summing forces vertically, we have,

$$\begin{aligned}
 & k_4(\tilde{z}_4 - \tilde{z}_{tr} - e\dot{\theta}_{tr} - X_{tr}(l+e)q_{tr}) + k_{r4}(\tilde{z}_4 - \tilde{z}_{r4}) \\
 & + c_{t4}(\dot{\tilde{z}}_4 - \dot{\tilde{z}}_{r4}) + c_4(\dot{\tilde{z}}_4 - \dot{\tilde{z}}_{tr} - e\dot{\theta}_{tr} - X_{tr}(l+e)\dot{q}_{tr}) = -m_4\ddot{\tilde{z}}_4
 \end{aligned} \tag{B.27}$$

### Equation of Motion of Axle 5: Trailer Axle 2

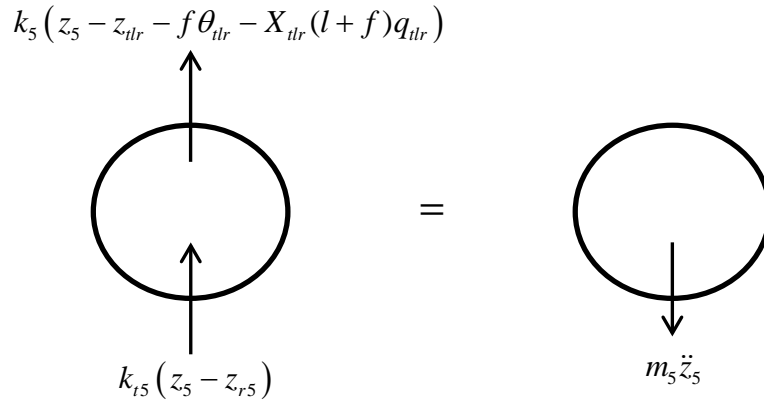


Figure B.9: Free body diagram of 2<sup>nd</sup> Trailer Axle

Summing forces vertically, we have,

$$\begin{aligned}
 & k_5(\tilde{z}_5 - \tilde{z}_{tr} - f\theta_{tr} - X_{tr}(l+f)q_{tr}) + k_{r5}(\tilde{z}_5 - \tilde{z}_{r5}) \\
 & + c_{t5}(\dot{\tilde{z}}_5 - \dot{\tilde{z}}_{r5}) + c_5(\dot{\tilde{z}}_5 - \dot{\tilde{z}}_{tr} - f\dot{\theta}_{tr} - X_{tr}(l+f)\dot{q}_{tr}) = -m_5\ddot{\tilde{z}}_5
 \end{aligned} \tag{B.28}$$

### Tractor and Trailer Frame Equations of Motion: Alternate Formulation.

For this thesis it was assumed that the mass of the components bolted onto the tractor and trailer frames is uniformly distributed over the length of the frame. One can alternatively assume that the masses of the components are concentrated at certain points along the length of the frame. Let components of mass,  $m_{\text{comp}_i}$ , and inertia,  $I_{\text{comp}_i}$ , be located at  $x_i$  from the c.g. of the frame. For the tractor frame, the kinetic energy is,

$$T = \left( \frac{1}{2} \sum I_{\text{comp}_i} \dot{\theta}_t^2 + \frac{1}{2} \sum \left( m_{\text{comp}_i} \left( \dot{x}_t - (b_{\text{cg}} - x_i) \dot{\theta}_t + X_t(x_i) \dot{q}_t \right)^2 \right) \right) + \int_0^{L_t} \frac{1}{2} \mu_{\text{cc}} \left( \dot{x}_t - (b_{\text{cg}} - x) \dot{\theta}_t + X_t(x) \dot{q}_t \right) dx \quad (\text{B.29})$$

Similarly for the trailer frame, the kinetic energy is derived as, ( $x_i$  is distance from trailer frame cg)

$$T = \left( \frac{1}{2} \sum I_{\text{comp,tr}_i} \dot{\theta}_{\text{tr}}^2 + \frac{1}{2} \sum \left( m_{\text{comp,tr}_i} \left( \dot{x}_{\text{tr}} - (l - x_i) \dot{\theta}_{\text{tr}} + X_{\text{tr}}(x_i) \dot{q}_{\text{tr}} \right)^2 \right) \right) + \int_0^{L_{\text{tr}}} \frac{1}{2} \mu_{\text{tr}} \left( \dot{x}_{\text{tr}} - (l - x) \dot{\theta}_{\text{tr}} + X_{\text{tr}}(x) \dot{q}_{\text{tr}} \right) dx \quad (\text{B.30})$$

Since the mass components on the frame do not contribute towards the strain energy of the system, the total potential energy in the system is as stated in equations (B.10) and (B.22). The spatial deflections  $X_t(\cdot)$  and  $X_{\text{tr}}(\cdot)$  are determined by the assumed mode shapes of the flexible structures. The assumed mode shapes should satisfy the boundary conditions. A approximate mode shape can be determined from the finite element model of the channels with the components attached. Since the potential energy is the same as in the previous method, the



stiffness and the damping matrices remain the same. The kinetic energy of the systems determines the mass matrix. Solving for each of the generalized coordinates as in the previous method, we get the following

For  $\xi_1 = \tilde{x}_t$

$$\begin{aligned} \frac{d}{dt} \left( \frac{\partial T}{\partial \dot{\tilde{x}}_t} \right) &= \sum m_{\text{comp},i} \left( \ddot{\tilde{x}}_t - (b_{\text{cg}} - x_i) \ddot{\theta}_t + X_t(x_i) \ddot{q}_t \right) \\ &+ \mu_{\text{cx}} \int_0^{L_i} \left( \ddot{\tilde{x}}_t - (b_{\text{cg}} - x) \ddot{\theta}_t + X_t(x) \ddot{q}_t \right) dx \end{aligned} \quad (\text{B.31})$$

Rearranging the terms,

$$\begin{aligned} \frac{d}{dt} \left( \frac{\partial T}{\partial \dot{\tilde{x}}_t} \right) &= \ddot{\tilde{x}}_t \left( \sum m_{\text{comp},i} + \mu_{\text{cx}} \int_0^{L_i} dx \right) + \\ &\ddot{\theta}_t \left( -\sum m_{\text{comp},i} (b_{\text{cg}} - x_i) - \mu_{\text{cx}} \int_0^{L_i} (b_{\text{cg}} - x) dx \right) + \\ &\ddot{q}_t \left( \sum m_{\text{comp},i} X_t(x_i) + \mu_{\text{cx}} \int_0^{L_i} X_t(x) dx \right) \end{aligned} \quad (\text{B.32})$$

For  $\xi_2 = \theta_t$

$$\begin{aligned} \frac{d}{dt} \left( \frac{\partial T}{\partial \dot{\theta}_t} \right) &= I_{\text{comp}} \ddot{\theta}_t - \sum m_{\text{comp},i} (b_{\text{cg}} - x_i) \left( \ddot{\tilde{x}}_t - (b_{\text{cg}} - x_i) \ddot{\theta}_t + X_t(x_i) \ddot{q}_t \right) \\ &+ \mu_{\text{cx}} \int_0^{L_i} \left( -(b_{\text{cg}} - x) \right) \left( \ddot{\tilde{x}}_t - (b_{\text{cg}} - x) \ddot{\theta}_t + X_t(x) \ddot{q}_t \right) dx \end{aligned} \quad (\text{B.33})$$

Rearranging the terms we have,

$$\begin{aligned}
\frac{d}{dt} \left( \frac{\partial T}{\partial \dot{\theta}_t} \right) &= \ddot{\xi}_t \left( -\sum m_{\text{comp}_i} (b_{\text{cg}} - x_i) - \mu_{\omega} \int_0^{L_i} (b_{\text{cg}} - x) dx \right) + \\
&\ddot{\theta}_t \left( I_{\text{comp}} + \sum m_{\text{comp}_i} (b_{\text{cg}} - x_i)^2 + \mu_{\omega} \int_0^{L_i} (b_{\text{cg}} - x)^2 dx \right) + \\
&\ddot{q}_t \left( -\sum m_{\text{comp}_i} X_t(x_i) (b_{\text{cg}} - x_i) - \mu_{\omega} \int_0^{L_i} X_t(x) (b_{\text{cg}} - x) dx \right)
\end{aligned} \tag{B.34}$$

For  $\xi_3 = q_t$

$$\begin{aligned}
\frac{d}{dt} \left( \frac{\partial T}{\partial \dot{q}_t} \right) &= \sum m_{\text{comp}_i} X_t(x_i) \left( \ddot{\xi}_t - (b_{\text{cg}} - x_i) \ddot{\theta}_t + X_t(x_i) \ddot{q}_t \right) \\
&+ \mu_{\omega} \int_0^{L_i} X_t(x) \left( \ddot{\xi}_t - (b_{\text{cg}} - x) \ddot{\theta}_t + X_t(x) \ddot{q}_t \right) dx
\end{aligned} \tag{B.35}$$

Rearranging the terms we have,

$$\begin{aligned}
\frac{d}{dt} \left( \frac{\partial T}{\partial \dot{q}_t} \right) &= \ddot{\xi}_t \left( \sum m_{\text{comp}_i} X_t(x_i) + \mu_{\omega} \int_0^{L_i} X_t(x) dx \right) + \\
&\ddot{\theta}_t \left( \sum m_{\text{comp}_i} (b_{\text{cg}} - x_i) X_t(x_i) + \mu_{\omega} \int_0^{L_i} X_t(x) (b_{\text{cg}} - x) dx \right) + \\
&\ddot{q}_t \left( \sum m_{\text{comp}_i} X_t^2(x_i) + \mu_{\omega} \int_0^{L_i} X_t^2(x) dx \right)
\end{aligned} \tag{B.36}$$

Let the total mass of the tractor frame including the components be  $m_t$  and the total mass inertia of the frame including the components about the frame c.g. be  $I_t$ . Therefore

$$m_t = \sum m_{\text{comp}_i} + \mu_{\alpha} \int_0^{L_j} dx, \quad (\text{B.37})$$

and,

$$I_t = I_{\text{comp}} + \sum m_{\text{comp}_i} (b_{\text{cg}} - x_i)^2 + \mu_{\alpha} \int_0^{L_j} (b_{\text{cg}} - x)^2 dx \quad (\text{B.38})$$

The modified mass matrix for the tractor frame is

$$M_{\text{tractor}} = \begin{pmatrix} m_t & -\sum m_{\text{comp}_i} (b_{\text{cg}} - x_i) & \sum m_{\text{comp}_i} X_i(x_i) + \mu_{\alpha} \int_0^{L_j} X_i(x) dx \\ -\sum m_{\text{comp}_i} (b_{\text{cg}} - x_i) & I_t & -\sum m_{\text{comp}_i} X_i(x_i)(b_{\text{cg}} - x_i) - \mu_{\alpha} \int_0^{L_j} X_i(x)(b_{\text{cg}} - x) dx \\ \sum m_{\text{comp}_i} X_i(x_i) + \mu_{\alpha} \int_0^{L_j} X_i(x) dx & -\sum m_{\text{comp}_i} X_i(x_i)(b_{\text{cg}} - x_i) - \mu_{\alpha} \int_0^{L_j} X_i(x)(b_{\text{cg}} - x) dx & \sum m_{\text{comp}_i} X_i^2(x_i) + \mu_{\alpha} \int_0^{L_j} X_i^2(x) dx \end{pmatrix} \quad (\text{B.39})$$

This mass matrix operates on the state vector  $\begin{bmatrix} \ddot{\chi}_t & \ddot{\theta}_t & \ddot{q}_t \end{bmatrix}'$ .

Similarly, if the total mass of the trailer frame including the components is  $m_{\text{tr}}$  and the total mass inertia of the trailer frame including the components about the frame c.g. is  $I_{\text{tr}}$ , the mass matrix for the trailer frame is,

$$M_{\text{tr}} = \begin{bmatrix} m_{\text{tr}} & -\sum m_{\text{comp, tr}}(l-x_i) & \sum m_{\text{comp, tr}} X_{\text{tr}}(x_i) + \mu_{\alpha, \text{tr}} \int_0^{L_{\text{tr}}} X_{\text{tr}}(x) dx \\ -\sum m_{\text{comp, tr}}(l-x_i) & I_{\text{tr}} & -\sum m_{\text{comp, tr}} X_{\text{tr}}(x_i)(l-x_i) - \mu_{\alpha} \int_0^{L_{\text{tr}}} X_{\text{tr}}(x)(l-x) dx \\ \sum m_{\text{comp, tr}} X_{\text{tr}}(x_i) + \mu_{\alpha, \text{tr}} \int_0^{L_{\text{tr}}} X_{\text{tr}}(x) dx & -\sum m_{\text{comp, tr}} X_{\text{tr}}(x_i)(l-x_i) - \mu_{\alpha} \int_0^{L_{\text{tr}}} X_{\text{tr}}(x)(l-x) dx & \sum m_{\text{comp, tr}} X_{\text{tr}}^2(x_i) + \mu_{\alpha, \text{tr}} \int_0^{L_{\text{tr}}} X_{\text{tr}}^2(x) dx \end{bmatrix} \quad (\text{B.40})$$

The state vector for the trailer frame mass matrix is  $\left[ \ddot{\alpha}_{\text{tr}} \quad \ddot{\theta}_{\text{tr}} \quad \ddot{q}_{\text{tr}} \right]^T$ ,

## Appendix C

### Sample Calculation for Tractor Beaming Frequency

A typical cross-section of a truck frame chassis is shown in Figure C.1

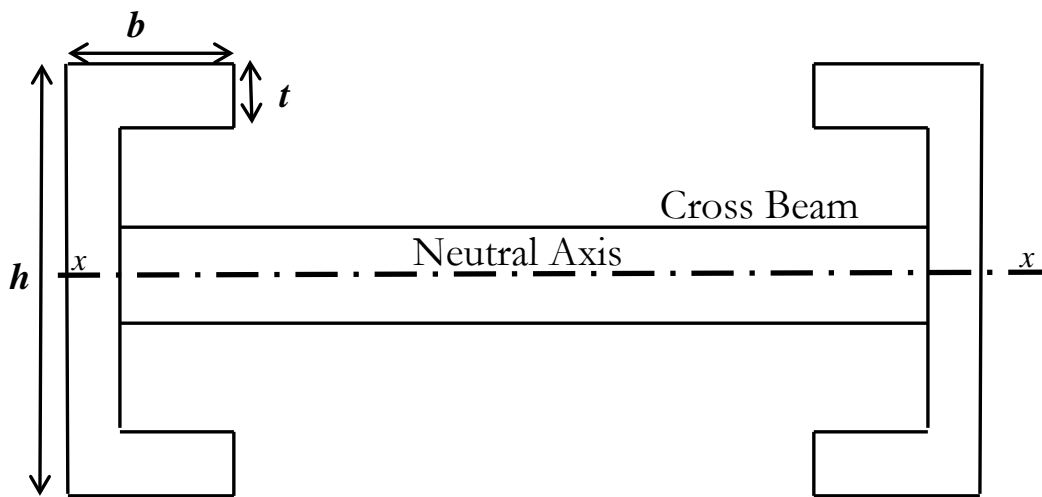


Figure C.1: Typical Frame Chassis Cross-section

If the tractor frame is modeled as an Euler-Bernoulli beam, the natural frequency of beaming is given by,

$$\omega_{\text{beam}} = \frac{(\beta l)^2}{l^2} \sqrt{\frac{EI_{xx}}{\rho A + \mu_{\text{comp}}}} \quad (\text{C.1})$$

where

- $\rho$ , is the density of the material, kg/m<sup>3</sup>,
- $E$ , the modulus of elasticity, Pa,
- $I$ , the cross-section area moment of inertia of the c-channels about the x-axis, m<sup>4</sup>,
- $A$ , the cross-section area of the c-channels, m<sup>2</sup>,
- $l$ , the length of the beam, m,
- $\mu_{\text{comp}}$ , the mass per unit length due additional components and cross-structures, kg/m, and
- $(\beta l)$ , is a constant determined from the boundary conditions

A typical tractor beam can be modeled as a steel beam pinned at the fifth wheel and free at the other end. Tractor beams are constructed of two C-channels connected by horizontal cross members called ladders. Typical dimensions of a C-channel are used for sample calculation below.

For a steel beam,

$$E = 200 \times 10^9 \text{ N/m}^2,$$

$$\rho = 7800 \text{ kg/m}^3,$$

For the C-Channel,

$$I_{c,x-x} = \frac{bh^3 - (b-t) \times (b-2 \times t)^3}{12}, \quad (\text{C.2})$$

A typical C channel dimension would be

$$b = 75 \text{ mm}, b = 300 \text{ mm and } t = 7 \text{ mm}$$

Therefore,

$$I_{c,x-x} = \frac{75 \times 300^3 - (68) \times (284)^3}{12}, \quad (\text{C.3})$$

$$I_{c,x-x} = 36.19 \times 10^6 \text{ mm}^4 = 3.619 \times 10^{-5} \text{ m}^4 \quad (\text{C.4})$$

Since the two C-channels are parallel to each other, the total area moment of inertia can be calculated summing the area moment of inertia of each C-channel. Therefore,

$$I_{xx} = 2I_{cc} = 7.237 \times 10^{-5} \text{ m}^4. \quad (\text{C.5})$$

The area of a C-channel cross-section is,

$$A_c = bh - (b-t)(b-2t) = 75 \times 300 - 68 \times 286, \quad (\text{C.6})$$

$$A_c = 3.05 \times 10^3 \text{ mm}^2 = 3.05 \times 10^{-3} \text{ m}^2. \quad (\text{C.7})$$

The total cross-sectional area can be calculated as the addition of the 2 C-channels.

Therefore,

$$A = 2A_c = 6.1 \times 10^{-3} \text{ m}^2. \quad (\text{C.8})$$

The length of the tractor beam is  $l = 7.87 \text{ m}$ . The total mass of the components bolted onto the tractor frame is  $m = 3408 \text{ kg}$ . Therefore the mass per unit length due to the additional

components is  $\mu_{\text{comp}} = 433 \text{ kg/m}$ . Using the values calculated for area moment of inertia and cross-sectional area, we can calculate the natural frequency of vibration as,

$$\omega_n = \frac{(\beta l)^2}{7.87^2} \sqrt{\frac{200 \times 10^9 \times 7.237 \times 10^{-5}}{7800 \times 6.1 \times 10^{-3} + 433}} , \quad (\text{C.9})$$

$$\omega_n = (\beta l)^2 \times 2.81 . \quad (\text{C.10})$$

For a free-pinned beam, for the first mode of vibration, the constant

$$\beta l = 3.923 . \quad (\text{C.11})$$

Therefore for a tractor beam modeled as an Euler-Bernoulli beam, the fundamental frequency of vibration is,

$$\omega_n = 3.923^2 \times 2.81 \text{ rad/s}, \quad (\text{C.12})$$

$$\omega_n = 6.89 \text{ Hz}. \quad (\text{C.13})$$

The natural frequency thus calculated matches closely with those found experimentally.



**Case Study: Adding plates on the top and the bottom of the flanges**

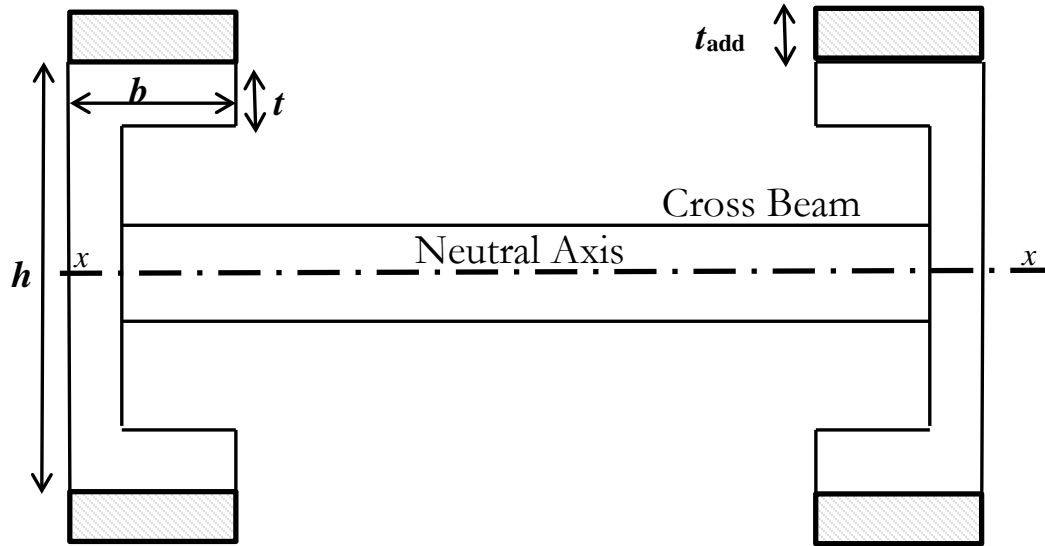


**Figure C.2: Chassis Frame Cross-section with Plates Mounted for additional Bending Stiffness.**

Consider the case where plates of thickness,  $t_{add} = 50$  mm, are rigidly mounted on the flanges of the C-channels. The width and the length of the plates are same as that of the flanges of C-channel.

The total cross sectional area of the plates is:

$$A_{plates} = 4bt_{add} = 4 \times 75 \times 50 = 15000 \text{ mm}^2 = 0.015 \text{ m}^2 \quad (\text{C.14})$$

The total area moment of inertia of the plates is:

$$I_{x-x,plates} = 4b \frac{\left(\frac{b+t_{add}}{2}\right)^3 - \left(\frac{b}{2}\right)^3}{3} = 4 \times 75 \times \frac{(350)^3 - (300)^3}{24} = 198.4 \times 10^6 \text{ mm}^4 \quad (\text{C.15})$$

$$I_{x-x,plates} = 198.4 \times 10^{-6} \text{ m}^4 \quad (\text{C.16})$$

The natural beaming frequency can be calculated as,

$$\begin{aligned} \omega_{\text{beam}} &= \frac{(\beta l)^2}{l^2} \sqrt{\frac{E(I_{xx} + I_{x-x,plates})}{\rho(A + A_{\text{plates}}) + \mu_{\text{comp}}}} \\ &= \frac{3.9266^2}{7.87^2} \sqrt{\frac{2 \times 10^{11} (0.7237 + 198.4) \times 10^{-6}}{7800(6.1 + 15) \times 10^{-3} + 433}} \end{aligned}$$

$$\omega_{\text{beam}} = 74.97 \text{ rad/s} = 11.93 \text{ Hz} \quad (\text{C.17})$$

Table C.1: Tractor Frame Beaming frequencies with Standard C-channels

Designation	Dimensions			Web Thickness s (in)	Sectional Area (in <sup>2</sup> )	Weight (lb/ft)	Weight 2 channels (kg/m)	Static Parameters Moment of Inertia		Beaming (Hz)	Mass (kg)	Mass Total (kg)
	h (in)	b (in)	t (in)					I <sub>x</sub> (in <sup>4</sup> )	I <sub>x</sub> (m <sup>4</sup> )			
C 15 x 50	15	3.716	0.716	14.7	50	148.8	404	1.7E-04	13.63	1171	4471	
C 15 x 40	15	3.52	0.52	11.8	40	119.1	349	1.5E-04	13.02	937	4237	
C 15 x 33.9	15	3.4	0.4	9.96	33.9	100.9	315	1.3E-04	12.58	794	4094	
C 12 x 30	12	3.17	0.51	8.82	30	89.3	162	6.7E-05	9.12	703	4003	
C 12 x 25	12	3.047	0.387	7.35	25	74.4	144	6.0E-05	8.73	586	3886	
C 12 x 20.7	12	2.942	0.282	6.09	20.7	61.6	129	5.4E-05	8.37	485	3785	
C 10 x 30	10	3.033	0.673	8.82	30	89.3	103	4.3E-05	7.27	703	4003	
C 10 x 25	10	2.886	0.526	7.35	25	74.4	91.2	3.8E-05	6.95	586	3886	
C 10 x 20	10	2.739	0.379	5.88	20	59.5	78.9	3.3E-05	6.56	468	3768	
C 10 x 15.3	10	2.6	0.24	4.49	15.3	45.5	67.4	2.8E-05	6.16	358	3658	
Tractor	Steel			Components								
	E			Density		Total Mass						
Length of Frame	(beta*I)			(kg/m <sup>3</sup> )		per unit length						
	7.87 m	3.926602	2.0E+11	7800	3300	419.3						

## Appendix D

### Derivation of Optimal Policies for Seat Isolation

The optimal policy for an isolation system is developed for a 1 d.o.f. system in this Appendix.

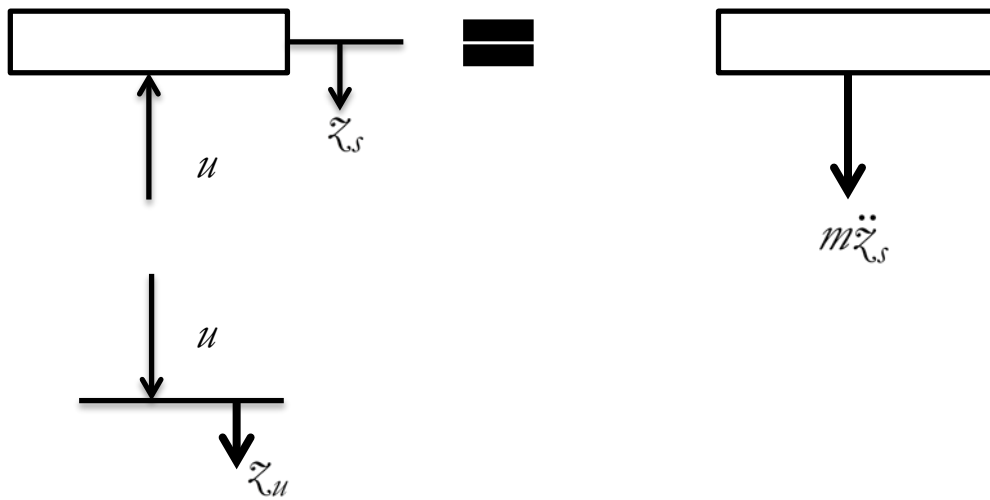


Figure D 1: A 1 d.o.f. system for developing the optimal control policies

#### Case 1: Base velocity as white noise disturbance

Consider the 1 d.o.f. system with sprung mass,  $m$ . The dynamic equation of the system is

$$m\ddot{z}_s + u = 0 \quad , \quad (D.1)$$

where  $u$  is the control input. Let the state vector be defined as

$$x = \begin{bmatrix} \tilde{x}_s - \tilde{x}_u \\ \dot{\tilde{x}}_s \end{bmatrix}. \quad (\text{D.2})$$

If the base input velocity,  $\dot{\tilde{x}}_r$ , is treated as white noise disturbance to the system, the state equations are,

$$\begin{aligned} \dot{x}_1 &= \dot{\tilde{x}}_s - \dot{\tilde{x}}_u = \dot{\tilde{x}}_r = x_2 - v \\ \dot{x}_2 &= \ddot{\tilde{x}}_s = \frac{u}{m} \end{aligned} \quad (\text{D.3})$$

Equation can be represented in state space form as below,

$$\dot{x} = \mathbf{A}x + \mathbf{B}u + \mathbf{L}v \quad (\text{D.4})$$

where,

$$\mathbf{A} = \begin{bmatrix} 0 & 1 \\ 0 & 0 \end{bmatrix} \quad (\text{D.5})$$

$$\mathbf{B} = \begin{bmatrix} 0 \\ 1/m \end{bmatrix} \quad (\text{D.6})$$

$$\mathbf{L} = \begin{bmatrix} -1 \\ 0 \end{bmatrix} \quad (\text{D.7})$$

If we assume that all the states are observed and include the process noise in the performance index, a Linear Quadratic Gaussian controller can be developed as shown below. The performance index to be minimized is a quadratic function of the suspension stroke and sprung mass acceleration,

$$P.I. = \lim_{T \rightarrow \infty} \frac{1}{2} E \left[ \int_0^T \left( x^T \mathbf{Q} x + r \ddot{x}_s^2 \right) dt \right] \quad (\text{D.8})$$

From equation (D.8) the acceleration term can be rewritten as the system input,

$$P.I. = \lim_{T \rightarrow \infty} \frac{1}{2} E \left[ \int_0^T \left( x^T \mathbf{Q} x + r \left( \frac{u}{m} \right)^2 \right) dt \right] \quad (\text{D.9})$$

where,

$$\mathbf{Q} = \begin{bmatrix} 1 & 0 \\ 0 & 0 \end{bmatrix}, \quad (\text{D.10})$$

and  $r$  is the weighting on the sprung mass acceleration. The weighting factor,  $r$ , can be used as a tuning factor to

Since the system is a linear system and the performance index is quadratic, using calculus of variation [52], the optimal solution for the infinite horizon case can be analytically found [53] and is a full state feedback control policy.

$$u^* = -\mathbf{K}x \quad (\text{D.11})$$

where  $\mathbf{K}$  is the optimal steady state feedback gain matrix,

$$\mathbf{K} = \frac{m^2 \mathbf{B}' \mathbf{P}}{r} \quad (\text{D.12})$$

and  $\mathbf{P}$  is the solution of the following algebraic Riccati equation (ARE)

$$\mathbf{A}'\mathbf{P} + \mathbf{P}\mathbf{A} - \frac{\mathbf{P}\mathbf{B}\mathbf{B}'\mathbf{P}}{r} + \mathbf{Q} = 0 \quad (\text{D.13})$$

Also, we know that  $\mathbf{P}$  is symmetric

$$\mathbf{P} = \begin{bmatrix} p_1 & p_2 \\ p_2 & p_3 \end{bmatrix} \quad (\text{D.14})$$

Solving the ARE we have

$$\begin{bmatrix} 0 & p_1 \\ p_1 & 2p_2 \end{bmatrix} - \frac{1}{r} \begin{bmatrix} p_2^2 & p_2 p_3 \\ p_2 p_3 & p_3^2 \end{bmatrix} + \begin{bmatrix} 1 & 0 \\ 0 & 0 \end{bmatrix} = \mathbf{0} \quad (\text{D.15})$$

Thus,

$$p_2 = r^{1/2}, p_3 = \sqrt{2}r^{3/4} \quad (\text{D.16})$$

The feedback gain matrix is

$$\mathbf{K} = \frac{\mathbf{B}'\mathbf{P}}{r} = \begin{bmatrix} 0 & 1/m \end{bmatrix} \begin{bmatrix} p_1 & p_2 \\ p_2 & p_3 \end{bmatrix} \frac{m^2}{r} \quad (\text{D.17})$$

$$\mathbf{K} = \frac{\mathbf{B}'\mathbf{P}}{r} = \begin{bmatrix} mr^{-1/2} & m\sqrt{2}r^{-1/4} \end{bmatrix} \quad (\text{D.18})$$

This leads to the formulation of the optimal control policy 1

$$u^* = -mr^{-1/2}x_1 - m\sqrt{2}r^{-1/4}x_2 \quad (\text{D.19})$$

Rewriting the controller in terms of the physical

$$u^* = -mr^{-1/2}\ddot{z}_r - m\sqrt{2}r^{-1/4}\dot{z}_s \quad (\text{D.20})$$

One can observe that the optimal feedback control is a combination of passive spring and a hypothetical skyhook damper.

$$u^* = -k_s^* z_r - c_{sky}^* \dot{z}_s \quad (\text{D.21})$$

The optimal spring stiffness and damping coefficient are function of the tuning factor  $r$ . It is interesting to note that the optimal damping ratio  $\xi$  is a constant

$$\xi = \frac{\sqrt{2}r^{-1/4}}{2\sqrt{r^{-1/2}}} = 0.707 \quad (\text{D.22})$$

And the natural frequency of the system is a function of the tuning factor

$$\omega_n = \sqrt{\frac{k}{m}} = \sqrt{r^{-1/2}} = r^{-1/4} \quad (\text{D.33})$$

Therefore the selection of the  $r$  determines the bandwidth of the isolation system.

### Case 2: Base acceleration as the white noise disturbance

Instead of treating the base velocity as the process noise one can alternatively treat the base acceleration as the process noise. Using the same 1 d.o.f. model as above and defining the state vector as

$$x = \begin{bmatrix} z_s & -z_u \\ \dot{z}_s & -\dot{z}_u \end{bmatrix} = \begin{bmatrix} z_r \\ \dot{z}_r \end{bmatrix}, \quad (\text{D.23})$$



The state equations can be written as

$$\begin{aligned}\dot{x}_1 &= \dot{\tilde{x}}_s - \dot{\tilde{x}}_u = \dot{\tilde{x}}_r = x_2 \\ \dot{x}_2 &= \ddot{\tilde{x}}_s - \ddot{\tilde{x}}_u = \frac{u}{m} - v\end{aligned}\tag{D.24}$$

State Space Representation can be similarly developed as

$$\dot{x} = \mathbf{A}x + \mathbf{B}u + \mathbf{L}v\tag{D.25}$$

where,

$$\mathbf{A} = \begin{bmatrix} 0 & 1 \\ 0 & 0 \end{bmatrix},\tag{D.26}$$

$$\mathbf{B} = \begin{bmatrix} 0 \\ 1/m \end{bmatrix},\tag{D.27}$$

$$\mathbf{L} = \begin{bmatrix} 0 \\ 1 \end{bmatrix}.\tag{D.28}$$

The performance index is as defined by equation (D.9). If we compare equations (D.26) and (D.27) to equations (D.5) and (D.6), we observe that the  $\mathbf{A}$ ,  $\mathbf{B}$  matrices are the same for both models. Since the solution of the ARE is dependent on only  $\mathbf{A}$ ,  $\mathbf{B}$  matrices, the optimal feedback controller is the same for both model. But in this case,

$$x_2 = \dot{\tilde{x}}_r$$

Therefore the optimal control policy 2 is formulated as

$$u^* = -mr^{-1/2}\ddot{\chi}_r - m\sqrt{2}r^{-1/4}\dot{\chi}_r. \quad (\text{D.29})$$

In this case, the optimal controller is a combination of a passive spring and a passive damper in parallel.

$$u^* = -k_s\ddot{\chi}_r - c_s\dot{\chi}_r \quad (\text{D.30})$$

Therefore depending on the spectral characteristics of the base excitation there are 2 possible optimal control policies. Both involve a passive spring between the sprung mass and the base surface.

## Appendix E

### Derivation of the MPC Controllers

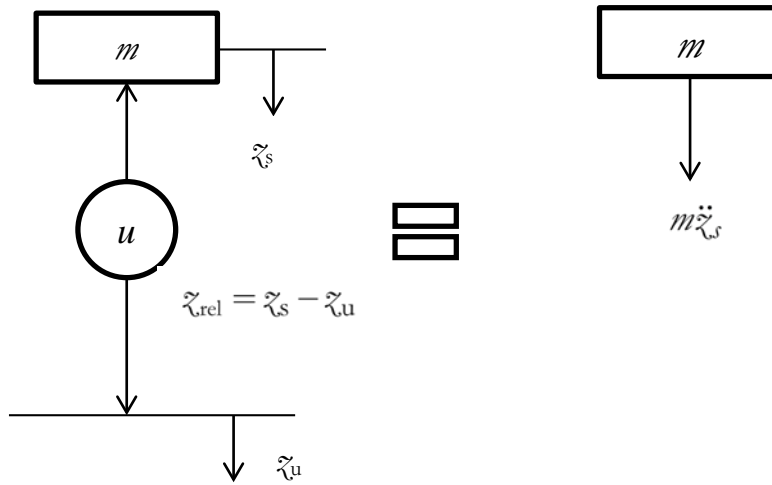


**Figure E.1: Free body diagram of the 1 d.o.f. system used for MPC controller derivation**

The seat was modeled as a base excited linear 1 d.o.f. system. The equation of motion of the system can be represented in the state space form as:

$$\dot{x} = \mathbf{A}x + \mathbf{B}u + \mathbf{B}_m w \quad (\text{E.1})$$

where  $x = [z_{\text{rel}} \quad \dot{z}_{\text{rel}}]'$  is the state vector,  $z_{\text{rel}}$  and  $\dot{z}_{\text{rel}}$  are the relative sprung mass displacement and velocity respectively. The system matrices are

$$\mathbf{A} = \begin{bmatrix} 0 & 1 \\ 0 & 0 \end{bmatrix}, \quad (\text{E.2})$$

$$\mathbf{B} = \begin{bmatrix} 0 \\ -1/m \end{bmatrix}, \quad (\text{E.3})$$

$$\mathbf{B}_w = \begin{bmatrix} 0 \\ -1 \end{bmatrix}. \quad (\text{E.4})$$

The control force  $u$  dictates the sprung mass acceleration based on the equation (E.5)

$$u = \text{force} = m\ddot{z}_s \quad (\text{E.5})$$

Since the control force is realized by a spring and a semi-active damper, the allowable force is described by

$$u = k_s z_{\text{rel}} + c(t)\dot{z}_{\text{rel}} \quad (\text{E.6})$$

The base acceleration is modeled as disturbance to the system. For this study it is assumed that accurate preview of the base acceleration is available. For this study the base acceleration was recorded using the 15 d.o.f model traversing different roads.

$$w = a_{\text{base}} = \ddot{z}_{\text{base}} \quad (\text{E.7})$$

The objective of the controller is to minimize the effects of the disturbance on the dynamic response of the system. The model can be discretized as

$$x(i+1) = \mathbf{A}_d x(i) + \mathbf{B}_d u(i) + \mathbf{B}_{wd} w(i) \quad (\text{E.8})$$

If the discretized version of the model is used let the performance index be

$$J = \sum_{i=1}^{n-1} [a^2(i)] \quad (\text{E.9})$$

where  $n$  is the prediction horizon. For this work the preview horizon and the prediction horizon are assumed to be the same. Equation (E.9) can be written in terms of the state vector and the control input as

$$J = \sum_{i=1}^n [x_i' \mathbf{Q} x_i + u_i' \mathbf{R} u_i] \quad (\text{E.10})$$

where the weight on the control input is  $\mathbf{R} = 1$  and the weight on the state vector is

$$\mathbf{Q} = \begin{bmatrix} 0 & 0 \\ 0 & 0 \end{bmatrix}.$$

If  $c_{\max}$  and  $c_{\min}$  are the limits of the damping rate of the variable semi-active damper, the dissipativity constraints on the control force are

$$\begin{aligned} -|u - k z_{\text{rel}}| + c_{\min} |\dot{z}_{\text{rel}}| &\leq 0 \\ |u - k z_{\text{rel}}| - c_{\max} |\dot{z}_{\text{rel}}| &\leq 0 \\ \text{sign}(u - k z_{\text{rel}}) - \text{sign}(\dot{z}_{\text{rel}}) &= 0 \end{aligned} \quad (\text{E.11})$$

To avoid the suspensions hitting the bump stops, an additional constraint on the relative displacement of the sprung mass is

$$|\tilde{z}_{\text{rel}}| \leq \tilde{z}_{\text{lim}} \quad (\text{E.12})$$

where  $\tilde{x}_{\text{lim}}$  is the maximum allowable relative displacement. The constraints stated in equations (E.11) and (E.12) can be stated in terms of the system states as

$$\begin{aligned}
-|u - kx_1| + c_{\min} |x_2| &\leq 0 \\
|u - kx_1| - c_{\max} |x_2| &\leq 0 \\
\text{sign}(u - kx_1) - \text{sign}(x_2) &= 0 \\
|x_1| &\leq \tilde{x}_{\text{lim}}
\end{aligned} \tag{E.13}$$

Observe that the constraints imposed are non-linear. The problem cannot be reduced to a quadratic programming problem even though the model is linear and the performance index is quadratic.

The control problem is to minimize  $J$  with respect to  $u(i)$  subject to the system dynamics (E.8) and constraints (E.13). The control problem can be rewritten as an optimization problem by developing the prediction model for the system dynamics as

$$X = \Phi x_0 + \Gamma U + \Gamma_w W \tag{E.14}$$

where  $X$  is the matrix by stacking all the future states,  $U$  is formulated by stacking all the future control inputs, and  $W$  is formulated by stacking the preview disturbance.  $x_0$  is the current state vector. It can be shown that the matrices  $\Phi, \Gamma, \Gamma_w$  can be formulated as

$$\Phi = \begin{bmatrix} \mathbf{A}_d \\ \mathbf{A}_d^2 \\ \dots \\ \mathbf{A}_d^n \end{bmatrix} \tag{E.15}$$

$$\mathbf{\Gamma} = \begin{bmatrix} \mathbf{B}_d & & 0 \\ \mathbf{A}_d \mathbf{B}_{nd} & \mathbf{B}_d & \\ \dots & \dots & \\ \mathbf{A}_d^{n-1} \mathbf{B}_{nd} & \mathbf{A}_d^{n-2} \mathbf{B}_d & \dots & \mathbf{B}_d \end{bmatrix} \quad (\text{E.16})$$

$$\mathbf{\Gamma}_W = \begin{bmatrix} \mathbf{B}_{nd} & & 0 \\ \mathbf{A}_d \mathbf{B}_{nd} & \mathbf{B}_{nd} & \\ \dots & \dots & \\ \mathbf{A}_d^{n-1} \mathbf{B}_{nd} & \mathbf{A}_d^{n-2} \mathbf{B}_{nd} & \dots & \mathbf{B}_{nd} \end{bmatrix} \quad (\text{E.17})$$

The performance index can also be written in terms of  $x_0$ ,  $X$  and  $U$ :

$$J = x_0' \mathbf{Q} x_0 + X' \mathbf{\Omega} X + U' \mathbf{\Psi} U \quad (\text{E.18})$$

where

$$\mathbf{\Omega} = \begin{bmatrix} \mathbf{Q} & 0 \\ \dots & \\ 0 & \mathbf{Q} \end{bmatrix}_{2n \times 2n} \quad (\text{E.19})$$

and,

$$\mathbf{\Psi} = \begin{bmatrix} \mathbf{R} & 0 \\ \dots & \\ 0 & \mathbf{R} \end{bmatrix}_{n \times n} \quad (\text{E.20})$$

Substituting equation (E.14) in (E.18)

$$J = x_0' \mathbf{Q} x_0 + [\mathbf{\Phi} x_0 + \mathbf{\Gamma} U + \mathbf{\Gamma}_w W]' \mathbf{\Omega} [\mathbf{\Phi} x_0 + \mathbf{\Gamma} U + \mathbf{\Gamma}_w W] + U' \mathbf{\Psi} U \quad (\text{E.21})$$

$$\begin{aligned}
J(x,U) = & x'_0[\mathbf{Q} + \mathbf{\Phi}'\mathbf{\Omega}\mathbf{\Phi}]x_0 + 2\mathcal{W}'\mathbf{\Gamma}'_m\mathbf{\Omega}\mathbf{\Phi}x_0 + 2U'\mathbf{\Gamma}'\mathbf{\Omega}\mathbf{\Phi}x_0 \\
& + U'[\mathbf{\Gamma}'\mathbf{\Omega}\mathbf{\Gamma} + \mathbf{\Psi}]U + \mathcal{W}'\mathbf{\Gamma}'_m'\mathbf{\Omega}\mathbf{\Gamma}_m\mathcal{W} + 2U'\mathbf{\Gamma}'\mathbf{\Omega}\mathbf{\Gamma}_m\mathcal{W}
\end{aligned} \tag{E.22}$$

Since the objective is to reduce the performance index  $J$  with respect to control input  $U$ , terms which are not a function of  $U$  can be ignored.

$$J(x,U) = 2U'\mathbf{\Gamma}'\mathbf{\Omega}\mathbf{\Phi}x_0 + U'[\mathbf{\Gamma}'\mathbf{\Omega}\mathbf{\Gamma} + \mathbf{\Psi}]U + 2U'\mathbf{\Gamma}'\mathbf{\Omega}\mathbf{\Gamma}_m\mathcal{W} \tag{E.23}$$

The constraints are also be expressed in terms of  $x_0$ ,  $U$  and  $\mathcal{W}$  as

$$\mathbf{D}|x_0| + \mathbf{M}|X| + \mathbf{\Sigma}|U - \mathbf{D}_k x_0 - \mathbf{M}_k X| - \mathbf{C} \leq 0 \tag{E.24}$$

and,

$$\text{sign}(U - \mathbf{D}_k x_0 - \mathbf{M}_k X) - \text{sign}(-\mathbf{D}_{\text{eq}} x_0 - \mathbf{M}_{\text{eq}} X) = 0 \tag{E.25}$$

where  $C$ ,  $D$ ,  $D_k$ ,  $D_{\text{eq}}$ ,  $M$ ,  $M_k$  and  $M_{\text{eq}}$  are defined as:

$$\mathbf{D} = \begin{bmatrix} 0 & c_{\min} \\ 0 & -c_{\max} \\ 1 & 0 \\ 0_{(3N-2) \times 2} \end{bmatrix}_{3N+1 \times 2} ; \mathbf{D}_k = \begin{bmatrix} k & 0 \\ 0_{N \times 2} \end{bmatrix}_{N+1 \times 2} ; \mathbf{D}_{\text{eq}} = \begin{bmatrix} 0 & 1 \\ 0_{N \times 2} \end{bmatrix}_{N+1 \times 2} \tag{E.26}$$



$$\mathbf{M} = \begin{bmatrix} 0_{3 \times 2} & 0_{3 \times 2(N-1)} \\ 0 & c_{\min} \\ 0 & -c_{\max} 0_{3 \times 2(N-1)} \\ 1 & 0 \\ \dots & \dots \end{bmatrix}_{(3N+1) \times 2N} ; \mathbf{M}_{\mathbf{k}} = \begin{bmatrix} 0 \\ k \\ \dots \\ 0 \end{bmatrix}_{(N+1) \times 2N} \quad (\text{E.27})$$

$$\mathbf{M}_{\text{eq}} = \begin{bmatrix} 0 \\ 0 & 1 \\ \dots & \dots \end{bmatrix}_{N+1 \times 2N}$$

$$\mathbf{C} = \begin{bmatrix} 0 \\ 0 \\ \tilde{\zeta}_{\text{lim}} \\ \dots \end{bmatrix}_{3N+1} \quad (\text{E.28})$$

Using equations (E.23) and (E.14), the constraints can be written as

$$\mathbf{D}|x_0| + \mathbf{M}|\Phi x_0 + \Gamma U + \Gamma_{\mathbf{w}} W| + \Sigma|U - \mathbf{D}_{\mathbf{k}} x_0 - \mathbf{M}_{\mathbf{k}}(\Phi x_0 + \Gamma U + \Gamma_{\mathbf{w}} W)| - C \leq 0 \quad (\text{E.29})$$

$$\text{sgn}(U - \mathbf{D}_{\mathbf{k}} x_0 - \mathbf{M}_{\mathbf{k}}(\Phi x_0 + \Gamma U + \Gamma_{\mathbf{w}} W)) - \text{sgn}(-\mathbf{D}_{\text{eq}} x_0 - \mathbf{M}_{\text{eq}}(\Phi x_0 + \Gamma U + \Gamma_{\mathbf{w}} W)) = 0 \quad (\text{E.30})$$

Therefore the objective of the optimization problem is to minimize the performance index as stated in equation (E.23) subject to constraint equations (E.29) and (E.30).

This study also explored the option of using a frequency weighted sprung mass acceleration in place of sprung mass acceleration to develop the performance index. The performance

index can be reformulated from equation (E.19) to include the effect of frequency weighting as:

$$J = x'_0 \mathbf{Q} x_0 + X' \mathbf{\Omega} X + A_w' \mathbf{\Psi} A_w \quad (\text{E.31})$$

where  $A_w$  is the stacked vector of the sprung mass accelerations over the prediction horizon and is defined by equation (E.36)

The transfer function relating the weighted acceleration to the acceleration is defined by ISO [3,54].

$$a_w(s) = W_k(s) a(s) \quad (\text{E.32})$$

The discretized state space form of equation (E.33) is:

$$\begin{aligned} x_a(i+1) &= \mathbf{A}_{Wk} x_a(i) + \mathbf{B}_{Wk} a(i) \\ a_w(i) &= \mathbf{C}_{Wk} x_a(i) \end{aligned} \quad (\text{E.33})$$

where  $x_a$  is the intermediate state vector. Since the initial states of the vector  $x_a$  are zero, and the acceleration  $a$  is proportional to  $u$ , the stacked  $x_a$  vector can be rewritten as

$$X_a = \mathbf{\Gamma}_{Wk} U \quad (\text{E.34})$$

where

$$\mathbf{\Gamma}_{Wk} = \begin{bmatrix} \mathbf{B}_{Wk} & & & 0 \\ \mathbf{A}_{Wk} \mathbf{B}_{Wk} & \mathbf{B}_{Wk} & & \\ \dots & \dots & & \\ \mathbf{A}_{Wk}^{n-1} \mathbf{B}_{Wk} & \mathbf{A}_{Wk}^{n-2} \mathbf{B}_{Wk} & \dots & \mathbf{B}_{Wk} \end{bmatrix} \quad (\text{E.35})$$

The output  $a_w$  is related to the state vector as

$$\begin{aligned}
a_w(1) &= \mathbf{C}_{Wk} x_a(1) \\
a_w(2) &= \mathbf{C}_{Wk} x_a(2) \\
&\dots \\
a_w(n) &= \mathbf{C}_{Wk} x_a(n)
\end{aligned} \tag{E.36}$$

The stacked weighted acceleration vector can therefore be written in terms of  $X_a$

$$A_w = \mathbf{E}_{Wk} X_a \tag{E.37}$$

where

$$\mathbf{E}_{Wk} = \begin{bmatrix} \mathbf{C}_{wk} & & 0 \\ & \dots & \\ 0 & & \mathbf{C}_{wk} \end{bmatrix} \tag{E.38}$$

Combining equations (E.34) and (E.37) we get,

$$A_w = \mathbf{E}_{Wk} \mathbf{\Gamma}_{Wk} U \tag{E.39}$$

The performance index can be reformulated in terms of the control inputs as:

$$\begin{aligned}
J = x_0' \mathbf{Q} x_0 + [\mathbf{\Phi} x_0 + \mathbf{\Gamma} U + \mathbf{\Gamma}_w W]' \Omega [\mathbf{\Phi} x_0 + \mathbf{\Gamma} U + \mathbf{\Gamma}_w W] + \\
[\mathbf{E}_{Wk} \mathbf{\Gamma}_{Wk} U]' \Psi [\mathbf{E}_{Wk} \mathbf{\Gamma}_{Wk} U]
\end{aligned} \tag{E.40}$$

Let us define

$$\Psi_{Wk} = \mathbf{\Gamma}'_{Wk} \mathbf{E}'_{Wk} \Psi \mathbf{E}_{Wk} \mathbf{\Gamma}_{Wk} \tag{E.41}$$

Using equations (E.40) and (E.41) we have

$$\begin{aligned}
J(x, U) = & x'_0 [\mathbf{Q} + \mathbf{\Phi}' \mathbf{\Omega} \mathbf{\Phi}] x_0 + 2\mathcal{W}' \mathbf{\Gamma}_w' \mathbf{\Omega} \mathbf{\Phi} x_0 \\
& + 2U' \mathbf{\Gamma}' \mathbf{\Omega} \mathbf{\Phi} x_0 + U' [\mathbf{\Gamma}' \mathbf{\Omega} \mathbf{\Gamma} + \mathbf{\Psi}_{w_k}] U \\
& + \mathcal{W}' \mathbf{\Gamma}_w' \mathbf{\Omega} \mathbf{\Gamma}_w \mathcal{W} + 2U' \mathbf{\Gamma}' \mathbf{\Omega} \mathbf{\Gamma}_w \mathcal{W}
\end{aligned} \tag{E.42}$$

To simplify, let us define

$$\mathbf{G} = [\mathbf{\Gamma}' \mathbf{\Omega} \mathbf{\Gamma} + \mathbf{\Psi}_{w_k}]$$

$$\mathbf{F} = 2\mathbf{\Phi}' \mathbf{\Omega} \mathbf{\Gamma}$$

$$\mathbf{F}_w = 2\mathbf{\Gamma}_w' \mathbf{\Omega} \mathbf{\Gamma}$$

There the performance index can be expressed in terms of the initial states  $x_0$ , control sequence  $U$  and preview sequence  $\mathcal{W}$  as

$$J = 0.5U' \mathbf{G} U + x'_0 \mathbf{F} U + \mathcal{W}' \mathbf{F}_w U \tag{E.43}$$

The optimization problem minimizes the performance index  $J$  with respect to  $U$  subject to the constraints defined by the equations (E.29) and (E.30)

The control input is initialized based on the current damping level  $c_{\text{prev}}$  as:

$$U_{\text{init}} = \begin{bmatrix} k & c_{\text{prev}} \\ \dots & \dots \\ k & c_{\text{prev}} \end{bmatrix} \begin{bmatrix} x(0) \\ \dots \\ x(n-1) \end{bmatrix} \tag{E.44}$$

## Appendix F

### Derivation of the RLS Estimator

A recursive least square estimator was developed to estimate the seat mass and spring stiffness. The estimation is an offline process. The following model was used for estimating the mass and the stiffness:

$$-c_s \dot{z}_{rel} = m_s \ddot{z}_s + k_s z_{rel} , \quad (F.1)$$

Equation (F.1) can be written as,

$$-F_d = \Phi^T \theta , \quad (F.2)$$

where  $F_d$  is the damping force found from the prescribed damping value and calculated damper velocity. The vector  $\Phi$  is defined as

$$\Phi = [\ddot{z}_s(t) \quad z_{rel}(t)]^T . \quad (F.3)$$

The parameter vector,  $\theta$  is defined as

$$\theta = [m_s \quad k_s] \quad (F.4)$$

For each time step of the estimator, the RLS algorithm can be written as

$$K(t) = P(t-1)\Phi[\lambda + \Phi^T P(t-1)\Phi]^{-1} , \quad (F.5)$$

$$\hat{\theta}(t) = \hat{\theta}(t-1) + K(t) \left[ -F_d - \Phi(t)^T \theta(t-1) \right], \quad (\text{F.6})$$

$$P(t) = \left( \frac{I - K(t)\Phi(t)^T}{\lambda} \right) P(t-1), \quad (\text{F.7})$$

where  $\hat{\theta}$  is the estimated parameter vector,  $K(t)$  is the gain vector,  $P(t)$  is the covariance matrix and  $\lambda$  is the forgetting factor normally defined in the range  $[0.9 \ 1]$ . For estimating the seat parameters the forgetting factor was set to 0.99. The RLS algorithm was initialized as

$$P(0) = \begin{bmatrix} 10000 & 0 \\ 0 & 10000 \end{bmatrix}, \text{ and} \quad (\text{F.8})$$

$$\theta(0) = [0 \ 0]^T. \quad (\text{F.9})$$

## Appendix G

### Model Validation TruckSim and Matlab Parameters

The developed 15 d.o.f model was validated against a commercially available truck dynamics simulator, TruckSim. TruckSim models the tractor sprung mass as a lumped mass. The version of TruckSim available for this research did not have the capability to add cab suspensions or include frame torsion.

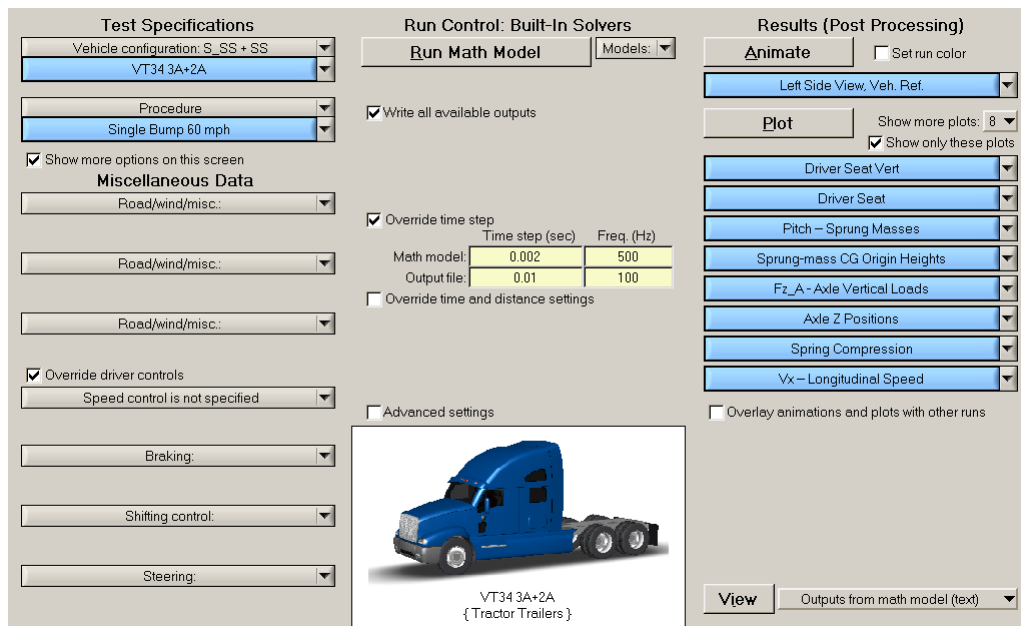


Figure G.1: TruckSim Main Screen

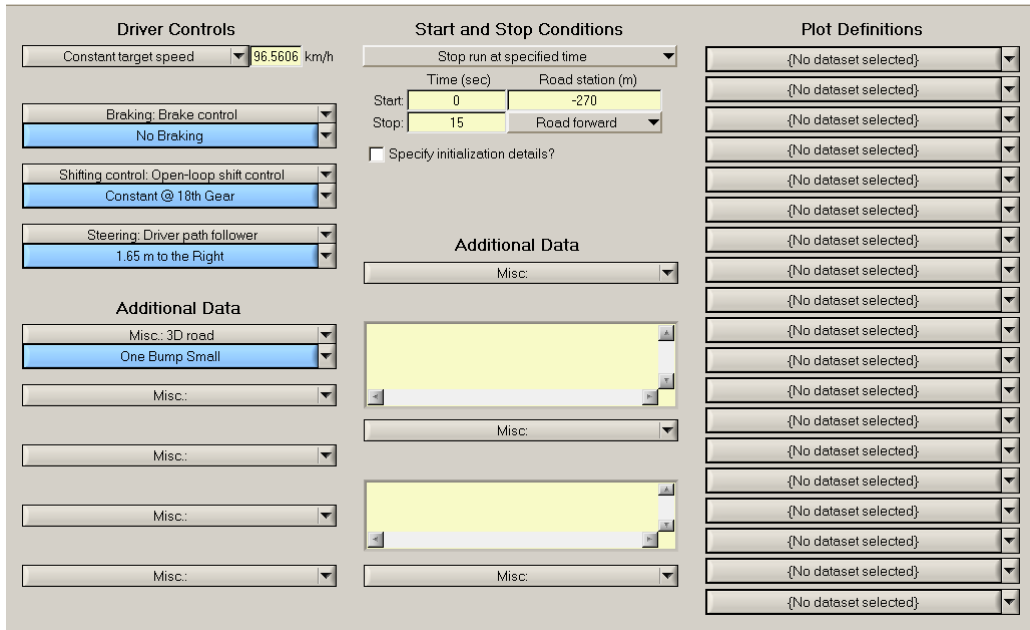


Figure G.2: TruckSim Procedure Screen

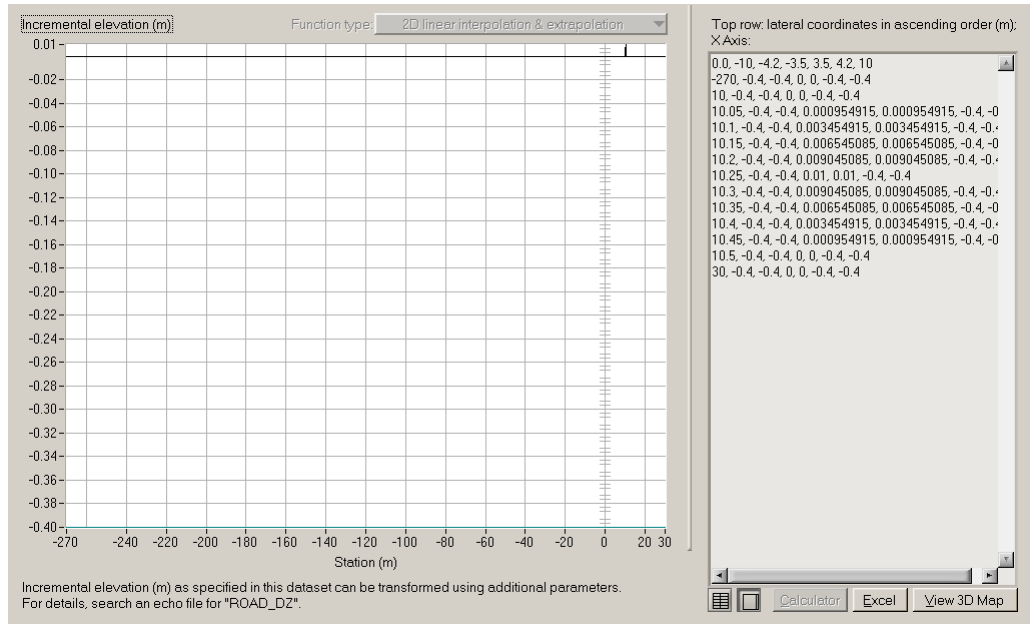


Figure G.3: TruckSim Road Definition



Simulated motion sensors each produce nine output variables related to a point in the sprung mass of a motor vehicle or trailer.

The output variables are X, Y, and Z accelerations (with the effect of gravity, as with real accelerometers); X, Y, and Z components of velocity, and X, Y, and Z components of angular velocity.

You can also specify plot setups to automatically generate plots of the sensor variables when linked to this dataset.

Motion sensor locations (sprung-mass coordinates)

	X	Y	Z	
1	-1623	0	2100	mm
2				mm
3				mm
4				mm
5				mm
6				mm

Motion sensor orientations (relative to sprung-mass axes)

	Roll	Pitch	Yaw	
1	0	0	0	deg
2				deg
3				deg
4				deg
5				deg
6				deg

Specify plot setups: 0

Misc.: Misc.

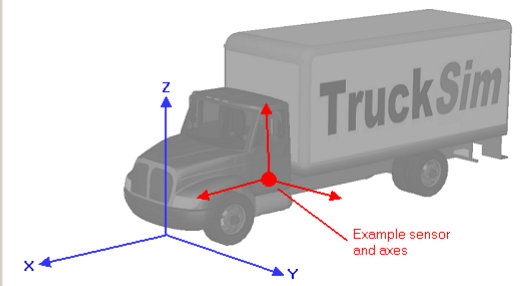


Figure G.4: Driver Seat Sensor Location

3x1 image scale

Dist. back: 5110 Y: 0 Height: 1100 mm  Hitch

Hitch: 5th Wheel (Typical)

Sprung mass: Rigid Sprung Mass VT34

Aerodynamics: No Aerodynamics

Animator shape(s): Vehicle Shape 3A Sleeper VT34

Tires: 3a tire group Michelin X tyres

Steering wheel torque: 1/25 (Typical)

Powertrain: 6x4, axles 2 & 3 Tandem for axles 2 & 3

330 kW, 18 spd. MT, 4WD

Static load for rear axle of tandem: 0.25 -

Dynamic load transfer coefficient: 0 -

Load transfer due to brake torque: 0 1/m

Axle 1 X distance back: 0 mm Axle 2 X distance back: 4650 mm Axle 3 X distance back: 5970 mm

Susp Kin: Steer Kin. 1st Drive 2nd Drive

Comp: Steer Comp. 1st Drive Comp. 2nd Drive Comp.

Brakes: No Brakes No Brakes No Brakes

Steering: Long (6 m) Wheelbase No Steering No Steering

Misc.: Misc. Misc. Misc.

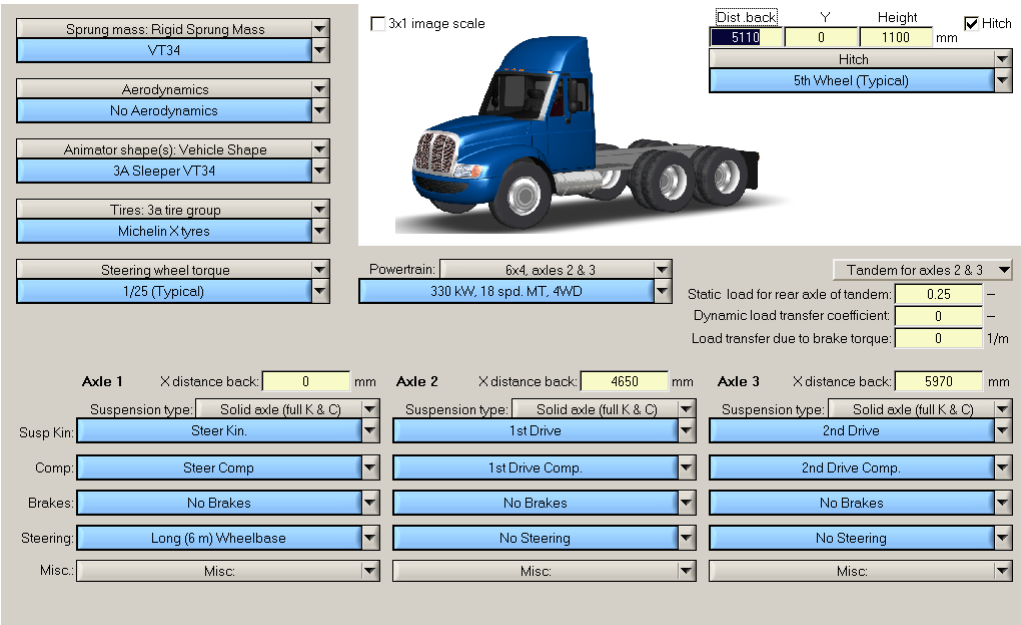


Figure G.5: Tractor Main Screen

Height (for animator): 3200

Width (for animator): 2438

Lateral coordinate of mass center: 0

Mass center of unladen sprung mass: 1000

Origin of sprung mass coordinate system

All dimensions and coordinates are in millimeters

**Frame Torsional Flexibility and Suspended Cab**

Check this box to use optional, more detailed math models. The optional models include the effects of torsional flexibility of the chassis (frame) of the lead unit and all trailers, and a further option to define a suspended cab.

The extended models require a separate license feature.

The inertial properties are for the sprung mass in the design configuration, with no additional loading

Sprung mass:	7390.7	kg	<input type="checkbox"/> Edit radii of gyration	Rx:	0.965	m
Roll inertia (I <sub>xx</sub> ):	6879	kg-m <sup>2</sup>		Ry:	2.638	m
Pitch inertia (I <sub>yy</sub> ):	51449	kg-m <sup>2</sup>		Rz:	1.631	m
Yaw inertia (I <sub>zz</sub> ):	19665	kg-m <sup>2</sup>		Inertia and radius of gyration are related by the equation: I = M*R <sup>2</sup>		
Product (I <sub>xy</sub> ):	0	kg-m <sup>2</sup>				
Product (I <sub>xz</sub> ):	130	kg-m <sup>2</sup>				
Product (I <sub>yz</sub> ):	0	kg-m <sup>2</sup>				

Figure G.6: Tractor Sprung Mass Definition

**Geometry**

Wheel center height (mm): 430

2030

480

Lateral coordinate of axle center: 0

Dimensions are in millimeters

Use linear roll steer coefficient

0 deg / deg

Note:  
No roll center location is specified because the location and movement of the roll center are implied by the kinematic data.

Animator: Shape File

Steer Axle

**Mass and Inertia**

Unsprung mass: 635 kg

Spin inertia for each side:  
Left: 10 kg-m<sup>2</sup>  
Right: 10 kg-m<sup>2</sup>

Axle roll & yaw inertia: 335 kg-m<sup>2</sup>

**Kinematics Based on Jounce**

Specify jounce at design load

Left	Right	mm
0	0	

Jounce for a solid axle is defined at the midpoint of a line between the wheel centers. The value of jounce passed to the kinematic tables is the average of left wheel and right wheel jounce.

**Wheel Toe and Camber**

	Left	Right	
Toe:	0	0	deg
Camber:	0	0	deg

Top View: +Toe

Front End View: +Camber

Figure G.7: Steer Axle Kinematics

**Springs**

Internal springs only

Left: Spring Alone  
270 N/mm, No friction

Right: Spring Alone  
270 N/mm, No friction

Upper spring seat height adjustment: Left: 0 mm, Right: 0 mm

**Shock Absorbers (Dampers)**

Left shock absorber: Shock absorber  
Linear: 6.65 N.s/mm

Right shock absorber: Shock absorber  
Linear: 6.65 N.s/mm

**Jounce / Rebound Stops**

Left jounce / rebound stops: Stroke: +250, -250

Right jounce / rebound stops: Stroke: +250, -250

**Mechanical ratios: component compression / suspension jounce**

	Left	Right
Springs	1	1
Dampers	1	1
Jounce stops	1	1
Rebound stops	1	1

**Lateral spacing between left and right**

Springs	1800 mm
Dampers	1800 mm
Jounce stops	1800 mm
Rebound stops	1800 mm

**Auxiliary Roll Moment**

Roll moment: Aux. Roll Moment  
No Auxiliary Roll Moment

Auxiliary roll damping: 0 N-m sec/deg

**Compliance Coefficients**

	Left	Right	
Toe vs Fx	0	0	deg/N
Steer vs Fy	0	0	deg/N
Steer vs Mz	0	0	deg/(N-m)
Camber vs Fx	0	0	deg/N
Inclination vs Fy	0	0	deg/N
Inclination vs Mz	0	0	deg/(N-m)

Axle longitudinal vs Fx: 0 mm/N  
Axle lateral vs Fy: 0 mm/N

Front End View: +Camber  
Top View: +Toe

When measuring suspension compliance effects, measurements should be made with identical Fx inputs on the left and right wheels (parallel). Measurements are typically made with Fy and Mz on the two sides opposed.

For the right-side wheel, toe = steer and camber = inclination. For the left side, toe = -steer and camber = -inclination.

Figure G.8: Steer Axle Kinematics

**Geometry**

Wheel center height (mm): 480

1863

C.G.

Sprung mass origin: 480

Lateral coordinate of axle center: 0

Dimensions are in millimeters

Use linear roll steer coefficient: 0 deg / deg

Note: No roll center location is specified because the location and movement of the roll center are implied by the kinematic data.

Animator: Shape File  
Rear Drive Axle

**Mass and Inertia**

Unsprung mass: 988 kg

Spin inertia for each side:  
Left: 50 kg-m<sup>2</sup>  
Right: 50 kg-m<sup>2</sup>

Axle roll & yaw inertia: 305 kg-m<sup>2</sup>

**Kinematics Based on Jounce**

Specify jounce at design load

	Left	Right	
	0	0	mm

Jounce for a solid axle is defined at the midpoint of a line between the wheel centers. The value of jounce passed to the kinematic tables is the average of left wheel and right wheel jounce.

Axle dive: Dive table  
No Caster Change

Axle X movement: Longitudinal Movement  
No movement (R = 0)

Axle Y movement - jounce: Lateral Movement  
No movement

Axle Y movement - roll: Lateral Movement  
Roll Center: 195 mm Above Axle

**Wheel Toe and Camber**

	Left	Right	
Toe:	0	0	deg
Camber:	0	0	deg

Top View: +Toe  
Front End View: +Camber

Figure G.9: 1st Drive Axle Kinematics

**Springs**

Internal springs only

Left: Spring Alone  
337.5 N/mm, No friction

Right: Spring Alone  
337.5 N/mm, No friction

Upper spring seat height adjustment: Left 0 Right 0 mm

**Shock Absorbers (Dampers)**

Left shock absorber: Shock absorber  
Linear: 13.75 kN-s/m

Right shock absorber: Shock absorber  
Linear: 13.75 kN-s/m

**Jounce / Rebound Stops**

Left jounce / rebound stops:  
Stroke: +250, -250

Right jounce / rebound stops:  
Stroke: +250, -250

**Mechanical ratios: component compression / suspension jounce**

	Left	Right
Springs	1	1
Dampers	1	1
Jounce stops	1	1
Rebound stops	1	1

**Lateral spacing between left and right**

Springs	1600 mm
Dampers	1600 mm
Jounce stops	1000 mm
Rebound stops	1000 mm

**Auxiliary Roll Moment**

Roll moment: Aux. Roll Moment

No Auxiliary Roll Moment

Auxiliary roll damping: 0 N-m sec/deg

**Compliance Coefficients**

	Left	Right	
Toe vs Fx	0	0	deg/N
Steer vs Fy	0	0	deg/N
Steer vs Mz	0	0	deg/(N-m)
Camber vs Fx	0	0	deg/N
Inclination vs Fy	0	0	deg/N
Inclination vs Mz	0	0	deg/(N-m)

Axle longitudinal vs Fx: 0 mm/N  
Axle lateral vs Fy: 0 mm/N

Front End View + Camber  
Top View + Toe

When measuring suspension compliance effects, measurements should be made with identical Fx inputs on the left and right wheels (parallel). Measurements are typically made with Fy and Mz on the two sides opposed.

For the right-side wheel, toe = steer and camber = inclination. For the left side, toe = -steer and camber = -inclination.

Figure G.10: 1st Drive Compliance

**Geometry**

Wheel center height (mm): 480

1863

C.G.

Sprung mass origin: 480

Lateral coordinate of axle center: 0

Dimensions are in millimeters

Use linear roll steer coefficient: 0 deg / deg

Note:  
No roll center location is specified because the location and movement of the roll center are implied by the kinematic data.

Animator: Shape File  
Rear Drive Axle

**Mass and Inertia**

Unsprung mass: 857 kg

Axle roll & yaw inertia: 305 kg-m<sup>2</sup>

Spin inertia for each side:  
Left: 50 kg-m<sup>2</sup>  
Right: 50 kg-m<sup>2</sup>

**Kinematics Based on Jounce**

Specify jounce at design load

Left	Right	
0	0	mm

Jounce for a solid axle is defined at the midpoint of a line between the wheel centers. The value of jounce passed to the kinematic tables is the average of left wheel and right wheel jounce.

Axle dive: Dive table  
No Caster Change

Axle X movement: Longitudinal Movement  
No movement (R = 0)

Axle Y movement - jounce: Lateral Movement  
No movement

Axle Y movement - roll: Lateral Movement  
Roll Center: 195 mm Above Axle

**Wheel Toe and Camber**

	Left	Right	
Toe:	0	0	deg
Camber:	0	0	deg

Top View + Toe  
Front End View + Camber

Figure G.11: 2nd Drive Axle Kinematics

**Springs**

Internal springs only

Left: Spring Alone  
315 N/mm, No friction

Right: Spring Alone  
315 N/mm, No friction

Upper spring seat height adjustment: Left: 0 mm, Right: 0 mm

**Shock Absorbers (Dampers)**

Left shock absorber: Shock absorber  
Linear: 13.75 kN-s/m

Right shock absorber: Shock absorber  
Linear: 13.75 kN-s/m

**Jounce / Rebound Stops**

Left jounce / rebound stops: Stroke: +250, -250

Right jounce / rebound stops: Stroke: +250, -250

**Mechanical ratios: component compression / suspension jounce**

	Left	Right
Springs	1	1
Dampers	1	1
Jounce stops	1	1
Rebound stops	1	1

**Lateral spacing between left and right**

Springs	1600 mm
Dampers	1600 mm
Jounce stops	1600 mm
Rebound stops	1600 mm

**Auxiliary Roll Moment**

Roll moment Aux. Roll Moment  
No Auxiliary Roll Moment

Auxiliary roll damping: 0 N-m sec/deg

**Compliance Coefficients**

	Left	Right	
Toe vs Fx:	0	0	deg/N
Steer vs Fy:	0	0	deg/N
Steer vs Mz:	0	0	deg/(N-m)
Camber vs Fx:	0	0	deg/N
Inclination vs Fy:	0	0	deg/N
Inclination vs Mz:	0	0	deg/(N-m)

Diagram: Front End View + Camber, Top View + Toe

When measuring suspension compliance effects, measurements should be made with identical Fx inputs on the left and right wheels (parallel). Measurements are typically made with Fy and Mz on the two sides opposed.

For the right-side wheel, toe = steer and camber = inclination. For the left side, toe = -steer and camber = -inclination.

Figure G.12: 2nd Drive Axle Compliance

Spring mass (trailer): 2A Flatbed Trailer JR

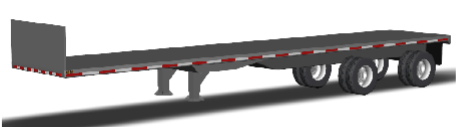
Aerodynamics: No Aerodynamics

Animator shape(s): Vehicle Shape: 2A Flatbed JR

Tires: 2a tire group: Michelin X Tires

No dolly

3x1 image scale



Tandem  Hitch

Fraction of tandem static load carried by rear axle springs: 0.48

Fraction of spring load transferred to other axle (0 - 0.5): 0

Load transfer forward per unit of combined brake torque: 0 1/m

Axle 1 X distance back: 6185 mm Axle 2 X distance back: 7555 mm

Suspension type: Solid axle (full K & C)

Susp Kin: Trailer Kin.

Comp: Trailer Comp.

Brakes: No Brakes

Misc: Misc.

Figure G.13: Semi-Trailer Main Screen

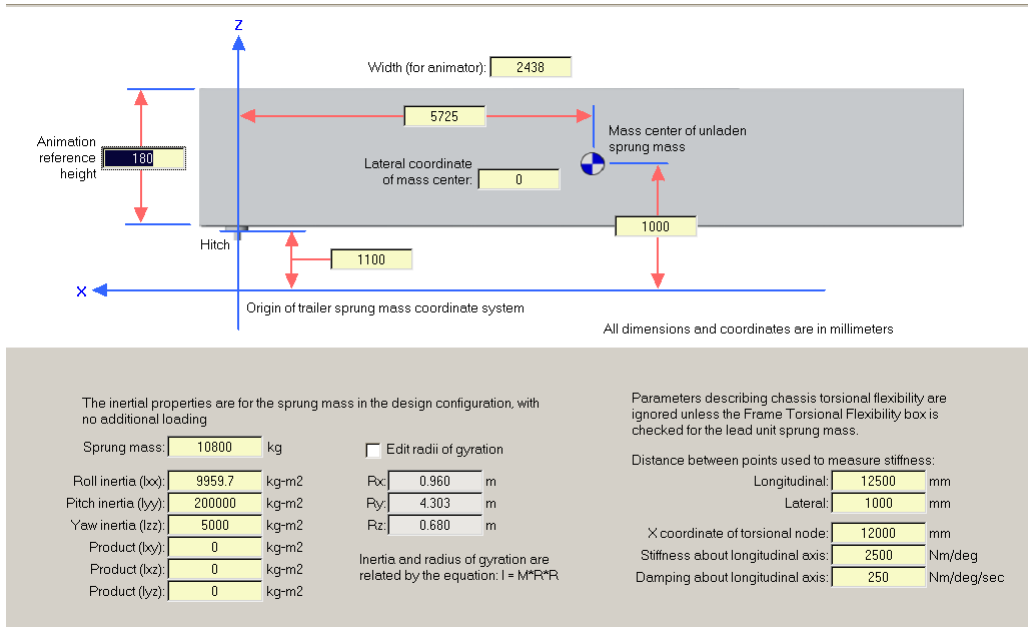


Figure G.14: Semi-Trailer Sprung Mass Definition

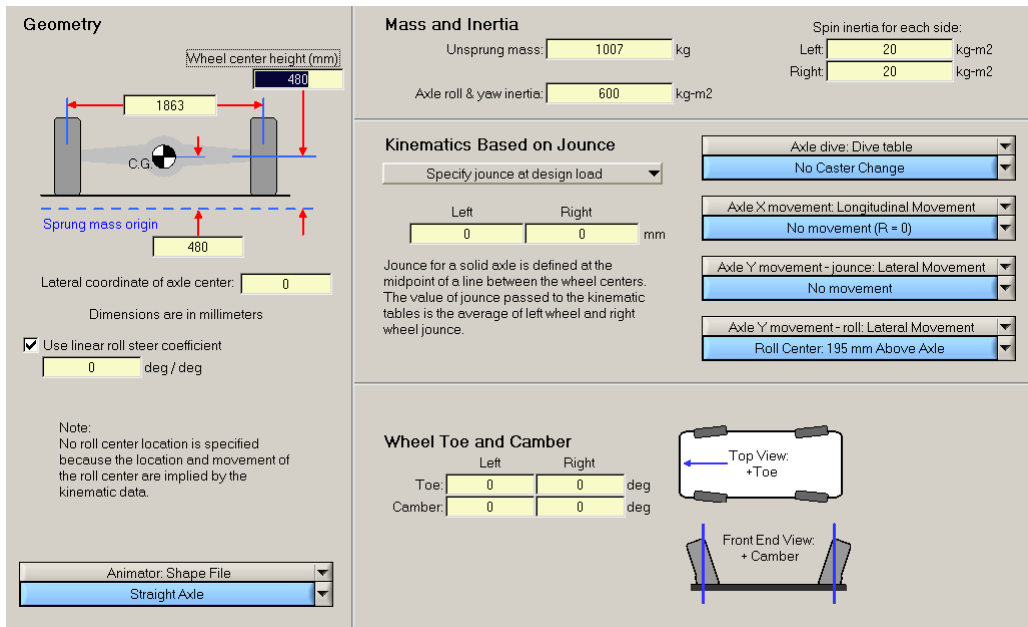


Figure G.15: Trailer Axle Kinematics

**Springs**

Internal springs only

Left: Spring Alone  
1382 N/mm, No friction

Right: Spring Alone  
1382 N/mm, No friction

Upper spring seat height adjustment: Left: 0 mm, Right: 0 mm

**Shock Absorbers (Dampers)**

Left shock absorber: Shock absorber  
Linear: 41.65 kN-s/m

Right shock absorber: Shock absorber  
Linear: 41.65 kN-s/m

**Jounce / Rebound Stops**

Left jounce / rebound stops: Stroke: +250, -250

Right jounce / rebound stops: Stroke: +250, -250

**Mechanical ratios: component compression / suspension jounce**

	Left	Right
Springs	1	1
Dampers	1	1
Jounce stops	1	1
Rebound stops	1	1

**Lateral spacing between left and right**

Springs	1863 mm
Dampers	1863 mm
Jounce stops	1863 mm
Rebound stops	1863 mm

**Auxiliary Roll Moment**

Roll moment: Aux. Roll Moment

No Auxiliary Roll Moment

Auxiliary roll damping: 0 N-m sec/deg

**Compliance Coefficients**

	Left	Right	
Toe vs Fx	0	0	deg/N
Steer vs Fy	0	0	deg/N
Steer vs Mz	0	0	deg/(N-m)
Camber vs Fx	0	0	deg/N
Inclination vs Fy	0	0	deg/N
Inclination vs Mz	0	0	deg/(N-m)

Axle longitudinal vs Fx: 0 mm/N

Axle lateral vs Fy: 0 mm/N

Front End View + Camber

Top View + Toe

When measuring suspension compliance effects, measurements should be made with identical Fx inputs on the left and right wheels (parallel). Measurements are typically made with Fy and Mz on the two sides opposed.

For the right-side wheel, toe = steer and camber = inclination. For the left side, toe = -steer and camber = -inclination.

Figure G.16: Trailer Axle Compliance

Y coordinate of payload center of gravity (positive value is left of vehicle centerline): 0

Mass center of this load

2290

1000

Vehicle Front

Origin of the sprung mass coordinate system

X coordinate of origin:  
At the front axle for motor vehicle,  
At the hitch for trailers

All dimensions and coordinates are in millimeters

Mass of this load: 11367 kg

Roll inertia (Ixx): 0 kg-m<sup>2</sup>

Pitch inertia (Iyy): 0 kg-m<sup>2</sup>

Yaw inertia (Izz): 0 kg-m<sup>2</sup>

Product (Ixy): 0 kg-m<sup>2</sup>

Product (Ixz): 0 kg-m<sup>2</sup>

Product (Iyz): 0 kg-m<sup>2</sup>

Edit radii of gyration

Rx: 0.000 m

Ry: 0.000 m

Rz: 0.000 m

Inertia and radius of gyration are related by the equation:  $I = M \cdot R^2$

Shape file: {No dataset selected}

A payload is a body with mass and inertia that is rigidly attached to a vehicle sprung mass. Use it to represent vehicle options (such as air conditioning), passengers, cargo, and other things that add weight to the sprung mass.

A custom payload can also be given negative mass or rotational inertias.

Figure G.17: Trailer Load Definition

The cab and seat suspension values of the Matlab/Simulink model were increased as shown in Table G.1 to ‘reduce’ the order of the model. Also the frame beaming mode natural frequencies were increased so that the dynamic behavior of the tractor and the semi-trailer frame was closer to that of a rigid body.

**Table G.1: Modified Matlab/Simulink Suspension and Beaming Frequency Values**

Symbol	Description	Generic	Unit
$k_e$	Engine Mount Spring coefficient	1e9	N/m
$c_e$	Engine Mount Damping coefficient	13300	N.s/m
$k_s$	Driver’s seat spring coefficient	250000000	N/m
$c_s$	Driver’s seat damping coefficient	230976	N.s/m
$k_{cf}$	Front Cab spring stiffness	1e9	N/m
$k_{cr}$	Rear Cab spring stiffness	1e9	N/m
$c_{cf}$	Front Cab damping	6430	N.s/m
$c_{cr}$	Rear Cab damping	6430	N.s/m
	Tractor Frame Beaming Natural Frequency	150	Hz
	Tractor Frame Beaming Natural Frequency	150	Hz

For the Matlab model the following equations were used to calculate the static axle loads

1. Summation of forces on the truck frame including unsprung mass

$$f_{z1} + f_{z2} + f_{z3} - f_{FW} = (m_t + m_1 + m_2 + m_3 + m_s + m_c + m_e)g \quad (G.1)$$

2. Summation of moments about truck frame CG including unsprung mass

$$af_{z1} - bf_{z2} - df_{z3} - jf_{FW} = (a m_1 - b m_2 - d m_3 + (w - s)m_s + w m_c - b m_e)g \quad (G.2)$$

3. Summation of forces on the trailer frame including unsprung mass

$$f_{z3} + f_{z4} + f_{FW} = (m_{tr} + m_4 + m_5 + m_{load})g \quad (G.3)$$



4. Summation of moments about trailer frame CG including unsprung mass

$$e \cdot f_{\tilde{z}_4} + f \cdot f_{\tilde{z}_2} - l \cdot f_{FW} = (em_4 + fm_5 + (l - l_2) \cdot m_{\text{load}})g \quad (\text{G.4})$$

5. 1st axle suspension spring in terms of tractor frame heave and pitch

$$\left(1 + \frac{k_1}{k_{t1}}\right) f_{\tilde{z}_1} - k_1 \tilde{z}_t + ak_1 \theta_t = m_1 g \quad (\text{G.5})$$

6. 2nd axle suspension spring in terms of tractor frame heave and pitch

$$\left(1 + \frac{k_2}{k_{t2}}\right) f_{\tilde{z}_2} - k_2 \tilde{z}_t - bk_2 \theta_t = m_2 g \quad (\text{G.6})$$

7. 3rd axle suspension spring in terms of tractor frame heave and pitch

$$\left(1 + \frac{k_3}{k_{t3}}\right) f_{\tilde{z}_3} - k_3 \tilde{z}_t + ak_3 \theta_t = m_3 g \quad (\text{G.7})$$

8. Fifth wheel axle suspension spring in terms of frame heave and pitch and trailer heave and pitch

$$f_{FW} + k_v \tilde{z}_t + jk_v \theta_{\text{tr}} - k_v \tilde{z}_{\text{tr}} - lk_v \theta_{\text{tr}} = 0 \quad (\text{G.8})$$

9. 4th axle suspension spring in terms of trailer frame heave and pitch

$$\left(1 + \frac{k_4}{k_{t4}}\right) f_{\tilde{z}_4} - k_4 \tilde{z}_{\text{tr}} - ek_4 \theta_{\text{tr}} = m_4 g \quad (\text{G.9})$$

10. 5th axle suspension spring in terms of trailer frame heave and pitch

$$\left(1 + \frac{k_5}{k_{t5}}\right) f_{\tilde{z}_5} - k_5 \tilde{z}_{\text{tr}} - fk_5 \theta_{\text{tr}} = m_5 g \quad (\text{G.10})$$

There are 10 unknowns; 4 d.o.f. for the tractor and trailer frame, the 5 axle loads and the fifth wheel load. Since we have 10 equations we can solve the simultaneous equations deterministically.

## BIBLIOGRAPHY

- [1] Federal Motor Carrier Safety Administration, "Report to Congress on the Large Truck Crash Causation Study," **MC-R/MC-RIA**, 2005.
- [2] International Organization for Standardization, "Guide for the evaluation of human exposure to whole-body vibration." **ISO 2631-1974(E)**, 1974.
- [3] International Organization for Standardization, "Mechanical vibration and shock-Evaluation of human exposure to whole-body vibration-Part 1: General requirements," **ISO 2631: 1997**, 1997.
- [4] Paddan G.S. and Griffin M.J., "Evaluation of Whole-Body Vibration in Vehicles," *J.Sound Vibrat.* **253**(1):195-213, 2002, doi:<http://dx.doi.org/10.1006/jsvi.2001.4256>.
- [5] Paddan G.S. and Griffin M.J., "Effect of Seating on Exposures to Whole-Body Vibration in Vehicles," *J.Sound Vibrat.* **253**(1):215-241, 2002, doi:<http://dx.doi.org/10.1006/jsvi.2001.4257>.
- [6] Foster, A.W., "A Heavy Truck Cab Suspension for Improved Ride," *SAE Technical Paper*, 1978, doi:10.4271/780408.
- [7] Flower, W., "Analytical and Subjective Ride Quality Comparison of Front and Rear Cab Isolation Systems on a COE Tractor," *SAE Technical Paper*, 1978, doi:10.4271/780411.
- [8] Gross, A. and Van Wynsberghe, R., "Development of a 4-point-Air Cab Suspension System for Conventional Heavy Trucks," *SAE Technical Paper*, 2001, doi:10.4271/2001-01-2708.
- [9] Field, R.V., Hurtado, J.E., Carne, T., and Dohrmann, C.R., "Structural dynamics modeling and testing of the department of energy tractor/trailer combination," 1994-2000, 1997.
- [10] Field, R.V.J., Hurtado, J.E., and Carne, T.G., "Analytical and experimental assessment of heavy truck ride," *16th International Modal Analysis Conference*, 1998.
- [11] Jain, P., "Design and Analysis of a Tractor-Trailer Cabin Suspension," 2007, doi:10.4271/2007-26-047.
- [12] Rajan, V. and Deshmukh, C., "Cab Suspension Optimization Using Matlab," 2013, doi:10.4271/2013-26-0147.

- [13] Książek M.A. and Iuczek J., "Optimal vibration isolation of a tractor–semi-trailer system," *Veh.Syst.Dyn.* **45**(3):277-289, 2007, doi:10.1080/00423110601140318.
- [14] Gillespie T.D., "Heavy truck ride," 1985.
- [15] Margolis, D. and Edeal, D., "Modeling and Control of Large Flexible Frame Vehicles Using Bond Graphs," *SAE Technical Paper*, 1989, doi:10.4271/892488.
- [16] Cao, C., "Approaches to Reduce Truck Beaming," *SAE Technical Paper*, 2005, doi:10.4271/2005-01-0829.
- [17] Ibrahim I.M., Crolla D.A., and Barton D.C., "Effect of frame flexibility on the ride vibration of trucks," *Comput.Struct.* **58**(4):709-713, 1996, doi:http://dx.doi.org/10.1016/0045-7949(95)00198-P.
- [18] Vaduri S.S.V., "Development of a simulation for preliminary assessment of ride quality of tractor semi-trailers," Clemson University, 1994.
- [19] Law, E.H., Janajreh, I., and Frey, N., "Vehicle Ride Response to New Widebase Tires and Conventional Dual Tires," *SAE Technical Paper*, 2002, doi:10.4271/2002-01-3114.
- [20] Trangsrud C., "Tractor Semi-Trailer Ride Quality Model Development and Simulation Considering the Effects of Frame Beaming and Suspension Friction," M.S., Dept. of Mechanical Engineering, Clemson University, 2004.
- [21] Spivey C.R., "Analysis of ride quality of tractor semi-trailers," M.S., Dept. of Mechanical Engineering, Clemson University, 2007.
- [22] Jiang Z., Streit D.A., and El-Gindy M., "Heavy vehicle ride comfort: literature survey," *International Journal of Heavy Vehicle Systems* **8**(3):258-284, 2001.
- [23] Patricio P.S., "Effects of frame design and cab suspension on the ride quality of heavy trucks," M.S., Virginia Polytechnic Institute and State University, 2002.
- [24] Anderson J., "Development of a Dynamic Vibration Absorber to Reduce Frame Beaming," *SAE Int. J. Commer. Veh.*(2014-01-2315), 2014, doi:10.4271.
- [25] Lord Corp, "MR Seat Suspension," <http://www.lord.com/products-and-solutions/active-vibration-control/industrial-suspension-systems/seat-suspensions>, 5/28 2015.
- [26] Bose Corporation, "Bose Ride Seat Suspension," <http://www.boseride.com/>, 01/15 2015.

- [27] Bender E., "Optimum linear preview control with application to vehicle suspension," *Journal of Fluids Engineering* **90**(2):213-221, 1968.
- [28] Karnopp D., Crosby M.J., and Harwood R.A., "Vibration Control Using Semi-Active Force Generators," *Journal of Engineering for Industry* **96**(2):619-626, 1974, doi:10.1115/1.3438373.
- [29] Alanoly J. and Sankar S., "A new concept in semi-active vibration isolation," *Journal of Mechanical Design* **109**(2):242-247, 1987.
- [30] Jolly M.R. and Miller L.R., "The control of semi-active dampers using relative feedback signals," *SAE Technical Paper*, 1989, doi:892483.
- [31] Margolis D.L., "Semi-Active Heave and Pitch Control for Ground Vehicles," *Veh.Syst.Dyn.* **11**(1):31-42, 1982.
- [32] Song X., "Design of adaptive vibration control systems with application of magneto-rheological dampers," PhD, Virginia Polytechnic Institute and State University, 1999.
- [33] ElMadany M., "Design and optimization of truck suspensions using covariance analysis," *Comput.Struct.* **28**(2):241-246, 1988.
- [34] ElMadany M., "An analytical investigation of isolation systems for cab ride," *Comput.Struct.* **27**(5):679-688, 1987.
- [35] Elmadany M., "Nonlinear ride analysis of heavy trucks," *Comput.Struct.* **25**(1):69-82, 1987.
- [36] ElMadany M., "Design of an active suspension for a heavy duty truck using optimal control theory," *Comput.Struct.* **31**(3):385-393, 1989.
- [37] Moline, D., "Modeling, Simulation and analysis of a Semi-Active cab suspension system for highway tractor semi-trailer," *Clemson University, Dept. of Mechanical Engineering* **TR-94-141-ME-MMS**, 1994.
- [38] van Iersel S., "Passive and semi-active truck cabin suspension systems for driver comfort improvement," .
- [39] Marcu F.M., "Semiactive Cab Suspension Control for Semitruck Applications," Ph.D., Virginia Polytechnic Institute and State University, United States -- Virginia, 2009.
- [40] Kok J.J., Van Heck J.G.A.M., Huisman R.G.M., Muijderman J.H.E.A., et al., "Active and semi-active control of suspension systems for commercial vehicles based on preview," *American Control Conference* **5**:2992-2996, 1997, doi:10.1109/ACC.1997.612006.

- [41] Ieluzzi M., Turco P., and Montiglio M., "Development of a heavy truck semi-active suspension control," *Control Eng.Pract.* **14**(3):305-312, 2006, doi:http://dx.doi.org/10.1016/j.conengprac.2005.03.019.
- [42] Canale M., Milanese M., and Novara C., "Semi-Active Suspension Control Using "Fast" Model-Predictive Techniques," *IEEE Trans.Control Syst.Technol.* **14**(6), 2006.
- [43] Cseko L.H., Kvasnica M., and Lantos B., "Explicit MPC-Based RBF Neural Network Controller Design With Discrete-Time Actual Kalman Filter for Semiactive Suspension,"
- [44] Eslaminasab N., "Development of a semi-active intelligent suspension system for heavy vehicles," PhD, University of Waterloo, 2008.
- [45] Giliomee C.L. and Els P.S., "Semi-active hydropneumatic spring and damper system," *J.Terramech.* **35**(2):109-117, 1998, doi:http://dx.doi.org/10.1016/S0022-4898(98)00016-0.
- [46] Deprez K., Maertens K., and Ramon H., "Comfort improvement by passive and semi-active hydropneumatic suspension using global optimization technique," American Control Conference, 2002. Proceedings of the 2002, 2002, doi:10.1109/ACC.2002.1023233.
- [47] British Standards Institution, "Guide to measurement and evaluation of human exposure to whole-body mechanical vibration and repeated shock," **BS 6841:1987**, 1987.
- [48] Rao S.S., "Mechanical Vibrations, 4/E," Pearson Education India, 2003.
- [49] Meirovitch L. and Parker R., "Fundamentals of vibrations," *Appl.Mech.Rev.* **54**:100, 2001.
- [50] Wong J.Y., "Theory of ground vehicles," Wiley. com, 2001.
- [51] Freightliner Trucks, "Revolution Truck Chassis Bottom," www.freightlinertrucks.com, 5/21 2015.
- [52] Shen Y., Golnaraghi M.F., and Heppler G.R., "Semi-active vibration control schemes for suspension systems using magnetorheological dampers," *JVC/Journal of Vibration and Control* **12**(1):3-24, 2006, doi:10.1177/1077546306059853.
- [53] Ahmadian M. and Blanchard E., "Non-dimensionalised closed-form parametric analysis of semi-active vehicle suspensions using a quarter-car model," *Veh.Syst.Dyn.* **49**(1-3):219-35, 2011, doi:10.1080/00423114.2010.482671.
- [54] International Organization for Standardization, "Human Response to Vibration - Measuring instrumentation," **ISO 8041:2005**, 2005.

- [55] Rimell A.N. and Mansfield N.J., "Design of digital filters for frequency weightings required for risk assessments of workers exposed to vibration," *Ind.Health* **45**(4):512-519, 2007.
- [56] Ahmadian M., Song X., and Southward S.C., "No-jerk skyhook control methods for semiactive suspensions," *Journal of vibration and acoustics* **126**(4):580-584, 2004.
- [57] Song X., Ahmadian M., and Southward S., "Analysis and strategy for superharmonics with semiactive suspension control systems," *Journal of Dynamic Systems, Measurement, and Control* **129**(6):795-803, 2007.
- [58] Rakheja S. and Sankar S., "Vibration and Shock Isolation Performance of a Semi-Active "On-Off" Damper," *Journal of Vibration, Acoustics Stress and Reliability in Design* **107**(4):398-403, 1985, doi:10.1115/1.3269279.
- [59] Kirk D.E., "Optimal control theory: an introduction," Courier Corporation, 2012.
- [60] Åström K.J. and Wittenmark B., "Adaptive control," Addison-Wesley series in electronic engineering (Control engineering), 1989.
- [61] Vahidi A., "Course Notes ME 893: Optimal Control", Fall 2014.
- [62] Law E.H., "Class Notes ME 453/653: Dynamic Performances of Vehicles", Spring 2007.